**UNIVERSIDAD COMPLUTENSE DE MADRID**
FACULTAD DE VETERINARIA


# TESIS DOCTORAL

## Estudio de los mecanismos moleculares que gobiernan la interacción temprana de “Besnoitia besnoiti” con las células diana bovinas

## Study of the molecular mechanisms that govern the early interaction of “Besnoitia besnoiti” with bovine target cells

MEMORIA PARA OPTAR AL GRADO DE DOCTOR

PRESENTADA POR

**María Fernández Álvarez**

DIRIGIDA POR

**Gema Álvarez García**
**Ignacio Ferre Pérez**

Madrid

**UNIVERSIDAD COMPLUTENSE DE MADRID**

FACULTAD DE VETERINARIA


UNIVERSIDAD
COMPLUTENSE
MADRID

**TESIS DOCTORAL**

# Estudio de los mecanismos moleculares que gobiernan la interacción temprana de "*Besnoitia besnoiti*" con las células diana bovinas

# Study of the molecular mechanisms that govern the early interaction of "*Besnoitia besnoiti*" with bovine target cells

MEMORIA PARA OPTAR AL GRADO DE DOCTOR

PRESENTADA POR

María Fernández Álvarez

DIRECTORES

Doctora Gema Álvarez García, Doctor Ignacio Ferre Pérez

2025

**UNIVERSIDAD COMPLUTENSE DE MADRID**
FACULTAD DE VETERINARIA


# TESIS DOCTORAL

## Estudio de los mecanismos moleculares que gobiernan la interacción temprana de “Besnoitia besnoiti” con las células diana bovinas

## Study of the molecular mechanisms that govern the early interaction of “Besnoitia besnoiti” with bovine target cells

MEMORIA PARA OPTAR AL GRADO DE DOCTOR

PRESENTADA POR

**María Fernández Álvarez**

DIRIGIDA POR

**Gema Álvarez García**
**Ignacio Ferre Pérez**

Madrid

# UNIVERSIDAD COMPLUTENSE DE MADRID

FACULTAD DE VETERINARIA

DEPARTAMENTO DE SANIDAD ANIMAL



## TESIS DOCTORAL

# Estudio de los mecanismos moleculares que gobiernan la interacción temprana de "*Besnoitia besnoiti*" con las células diana bovinas

# Study of the molecular mechanisms that govern the early interaction of "*Besnoitia besnoiti*" with bovine target cells

MEMORIA PARA OPTAR AL GRADO DE DOCTOR

PRESENTADA POR


María Fernández Álvarez

DIRECTORES

Doctora Gema Álvarez García, Doctor Ignacio Ferre Pérez


2025

# COMPLUTENSE UNIVERSITY OF MADRID

FACULTY OF VETERINARY MEDICINE

ANIMAL HEALTH DEPARTMENT



# DOCTORAL THESIS

## Estudio de los mecanismos moleculares que gobiernan la interacción temprana de "*Besnoitia besnoiti*" con las células diana bovinas

## Study of the molecular mechanisms that govern the early interaction of "*Besnoitia besnoiti*" with bovine target cells

THESIS SUBMITTED IN FULFILLMENT OF THE REQUIREMENTS FOR THE DEGREE OF DOCTOR

PRESENTED BY


María Fernández Álvarez

SUPERVISORS

Doctor Gema Álvarez García, Doctor Ignacio Ferre Pérez


2025

*Memoria presentada por Dña. María Fernández Álvarez para optar al grado de Doctor por la Universidad Complutense de Madrid.*

*La presente Tesis Doctoral ha sido financiada a través de proyectos de investigación del Ministerio de Ciencia e Innovación de España (Ref. AGL2016-75202-R y Ref. PID2019-103960RB-I00) y de la Comunidad de Madrid (Ref. P2018/BAA-4370 PLATESA2-CM). Dña. María Fernández Álvarez fue apoyada por un Contrato Predoctoral de Personal Investigador en Formación de la Universidad Complutense de Madrid (Ref. UCM 2018).*

Dña. Gema Álvarez-García, Doctora en Veterinaria y Catedrática de Universidad, y D. Ignacio Ferre Pérez, Doctor en Veterinaria y Profesor Titular de Universidad, adscritos al Departamento de Sanidad Animal de la Facultad de Veterinaria de la Universidad Complutense de Madrid,

*CERTIFICAN:*

1) Que la Tesis Doctoral titulada "Estudio de los mecanismos moleculares que gobiernan la interacción temprana de *"Besnoitia besnoiti"* con las células diana bovinas. Study of the molecular mechanisms that govern the early interaction of *"Besnoitia besnoiti"* with bovine target cells" presentada por la Graduada en Veterinaria Dña. María Fernández Álvarez para optar al grado de Doctora por la Universidad Complutense de Madrid ha sido realizada en las dependencias del Departamento de Sanidad Animal de la Facultad de Veterinaria de la Universidad Complutense de Madrid bajo su supervisión.
2) Que la presente Tesis Doctoral cumple con todas las condiciones exigidas para optar al grado de Doctor por la Universidad Complutense de Madrid con Mención Internacional.

De acuerdo con la normativa vigente, y como directora de la mencionada Tesis Doctoral, firmo el presente certificado por el que se autoriza su presentación.

En Madrid, a 13 de noviembre de 2025

Fdo.: Doctora Gema Álvarez García

Fdo.: Doctor Ignacio Ferre Pérez

**DOCTORADO CON MENCIÓN INTERNACIONAL**

La presente Tesis Doctoral cumple con los requisitos exigidos por la Universidad Complutense de Madrid para obtener la mención de Doctor Internacional:

1) Realización de una estancia mínima de tres meses en una institución de enseñanza superior o centro de investigación fuera de España:

- Centro receptor: Facultad de Veterinaria de la Universidad Ludwig Maximilians de Múnich (Alemania).
- Investigador principal: Dra. Elena Jiménez Ruiz.
- Duración de la estancia: 3 meses (15/09/2022-15/12/2022).

2) La Tesis Doctoral ha sido redactada en una de las lenguas habituales para la comunicación científica en su campo de conocimiento, distinta a cualquiera de las lenguas oficiales en España (inglés).

3) La Tesis Doctoral ha sido evaluada por dos expertos pertenecientes a alguna institución de educación superior o instituto de investigación no español.

4) El Tribunal evaluador de la Tesis Doctoral está compuesto por, al menos, un experto perteneciente a alguna institución de educación superior o centro de investigación no español.

**AGRADECIMIENTOS**

Dicen que hacer un Doctorado es un camino largo y arduo, pero yo he tenido la inmensa suerte de estar rodeada de personas que han hecho que este camino no solo sea más fácil, sino también inolvidable. Hoy, al llegar al final de esta etapa, mi corazón está lleno de gratitud y emoción porque no podría haber recorrido este camino sin cada una de las personas que me han acompañado.

A mi querido **grupo SALUVET**, mi hogar académico, muchas gracias por haberme acogido y guiado en este apasionante mundo de la investigación. **Gema**, no tengo palabras suficientes para agradecerte todo lo que me has enseñado. Has sido una directora excepcional, exigente y brillante, que ha sacado lo mejor de mí. Admiro tu inteligencia, tu fuerza y tu capacidad de inspirar a quienes te rodean. **Ignacio**, muchas gracias por ser un gran director, por tu confianza, por tu guía y por tu profesionalidad impecable a lo largo de estos años. **Luis**, todavía recuerdo aquella primera clase de Enfermedades Parasitarias en la que nos ofreciste visitar tu laboratorio; yo me acerqué en el cambio de clase, intrigada, sin saber que años después esta sería mi casa. Muchas gracias por acogerme en tu grupo de investigación. **Rafa Calero**, muchas gracias por tu colaboración y tu constante apoyo, pero también por aportar siempre ese toque de alegría. **Esther**, cuando te conocí empezaste siendo mi profesora de Parasitología y Enfermedades Parasitarias, pero pronto te convertiste en una guía y un apoyo fundamental en el laboratorio, siempre dispuesta a ayudar, muchas gracias por acompañarme con tanta generosidad en este camino. **Pilar**, muchas gracias por ser la persona que me introdujo en el apasionante mundo de la transcriptómica y por enseñarme con tanta claridad que lo que parecía sumamente complicado se volviera comprensible… ¡y hasta divertido! **Javier Regidor**, muchas gracias no solo por tu apoyo técnico durante los experimentos, sino también por tu lado más humano: esas conversaciones espontáneas en los pasillos, en medio de tubos y cultivos celulares, me dieron mucho ánimo estos años. **Iván**, muchas gracias por tu ayuda en cada experimento, por tus protocolos y anotaciones y por tu disposición para resolver cualquier problema con una sonrisa, ha sido un lujo contar contigo. **Lola**, tu bienvenida cada mañana hacía que todo fuera más fácil y tus historias, que nos hacían reír entre experimento y experimento, llenaban el laboratorio de vida. ¡Qué suerte haber coincidido contigo! **Vane**, muchas gracias por tu ayuda en el laboratorio y por hacer que cada jornada fuera más amena. **Daniel Gutiérrez Expósito**, muchas gracias por prestarme tu apoyo siempre que lo he necesitado. **Merche**, gracias por ser ejemplo de profesionalidad y dedicación. **David y Yanina**, aunque hemos coincidido menos de lo que me gustaría, siempre habéis estado dispuestos a ayudarme con los experimentos, os lo agradezco enormemente. **Alejandro**, has sido mi mentor desde el primer día y, además, la primera persona que conocí en el laboratorio. Con infinita paciencia me enseñaste todo desde cero, y, incluso cuando surgía algún problema, siempre supiste mantener la calma y encontrar una solución. Hoy, más allá de maestro, te has convertido en un amigo. Te deseo lo mejor en todo lo que venga, y siempre te estaré profundamente agradecida. **Carlos**, has sido un pilar en el laboratorio, siempre dispuesto a ofrecer tu ayuda. Muchas gracias por ser la persona vitamina del grupo: llenando de

alegría, luz y buenos momentos cada rincón y contagiándonos a todos. **Laura Jiménez,** "la mala", aun no entiendo por qué te presentaste así, pero lo que sí tengo claro es que eres una persona genial. Has pasado de ser una compañera de laboratorio a convertirte en una amiga. **Laura Rico,** "la buena", un verdadero ejemplo de trabajo y constancia, que me ha inspirado profundamente durante todos estos años. Muchas gracias por cada hora compartida, por los experimentos, las risas (¡y hasta los karaokes en el laboratorio!) que han hecho este camino mucho más llevadero y especial. **Marta**, muchas gracias por ser mi mentora en el apasionante mundo de los macrófagos, por enseñarme con tanta generosidad y por tu alegría y energía contagiosa. Hemos vivido muchas aventuras dentro y fuera del laboratorio, y aunque ahora estés por tierras escocesas, te tengo muy presente. **Nadia**, mi querida compañera de esta aventura, muchas gracias por tu apoyo todos estos años que he tenido la suerte de compartir contigo, espero que nos podamos ver pronto. **Nerea**, gracias por tu humor único y por una personalidad que no pasa desapercibida. Has aportado frescura y alegría al laboratorio. **Rafa Amieva**, representante indiscutible de la nueva generación del SALUVET, muchas gracias por tu alegría y por llenar cada rincón con tu estilo y "tus cosas". Sin ti, el laboratorio no habría sido lo mismo. **Darío**, mi compañero de *Besnoitia*, gracias por compartir conmigo tantas horas en el laboratorio y por hacer que cada momento fuera más ameno y llevadero. Tu compañía ha sido clave en esta etapa. **Pablo**, ¡el mejor bioinformático! Muchas gracias por abrirme la puerta a este fascinante mundo. Aunque ahora estés en Italia, espero que volvamos a coincidir muy pronto. **Roberto**, gracias por tu alegría contagiosa y por enseñarme tanto. Compartir contigo los experimentos de ovejas y las necropsias ha sido una experiencia única, quién iba a decir que acabaría disfrutando tanto de algo así. **Ángela, Silvia, Carmen y Andrea**, nuestras amigas de **Saluvet Innova**, muchas gracias por vuestra ayuda incondicional y por esa alegría inagotable que traíais incluso en los ratitos más breves. **Isabel, Chema, Jaime, Cinta, Javier Lobo, Juanjo, Gustavo, Javier, Abel y Alicia**, compañeros del Departamento, muchas gracias por vuestra ayuda, apoyo y disposición siempre. **Manuela**, muchas gracias por hacer que todo fuera más fácil, incluso cuando yo aparecía con mil gestiones y papeles bajo el brazo. Gracias por estar siempre dispuesta a ayudarme, incluso en los momentos más caóticos. No sabes cuánto he valorado tu apoyo en cada paso de este camino.

Al profesor **Markus Meissner**, a la profesora **Elena Jiménez Ruiz** y mis compañeros del laboratorio: **Javier**, **Simon**, **Matthew, Julia, Wei, Vanessa, Peipei y Yuan de Ludwig Maximilian Universität**, muchas gracias por acogerme con los brazos abiertos en Alemania. Nunca olvidaré esos meses en los que me hicisteis sentir en casa y me ayudasteis tanto. A mis queridas **amigas de Múnich, Noela, Julia, Mónica, Bernarda, Stephy, Yana, Amalia, Marie y Mery**, quienes fueron mi familia durante esos meses, siempre estaréis en mi corazón y espero veros muy pronto en España.

A mis **amigas "de siempre"**, **Pati López, Rosamar, Eva, Claudia, Pati Sierra y Cristina**, muchas gracias por haber sido testigos de este viaje desde el primer día, por apoyarme en los momentos duros y por llenar mi vida de risas siempre. Desde luego ya sois familia.

A **mis amigos y profesores del IESE** muchas gracias por ser una red de apoyo increíble en estos 2 años tan intensos, gracias por estar siempre ahí, por ayudarme, por hacer equipo y por enseñarme lo mejor de cada uno de vosotros. Ha sido un privilegio recorrer este camino a vuestro lado.

A **Álvaro**, muchas gracias por tu apoyo incondicional y por todo el cariño que me has dado en estos meses tan intensos. En un año lleno de cambios, retos y aprendizajes, tú has sido, sin duda, uno de los mayores regalos. No sé cómo habría sido esta etapa sin ti, pero sé que contigo ha sido infinitamente mejor, más bonita y feliz.

Pero, sobre todo, **a mi familia**. Sin vosotros, nada de esto habría sido posible. **Mamá**, muchas gracias por ser la mejor madre del mundo, por tu amor inagotable, por tu paciencia sin medida y por tu entrega. Eres mi refugio, mi guía, la persona que con una sola palabra o una mirada es capaz de hacerme sentir que todo estará bien. **Papá**, mi inspiración, mi modelo a seguir, el mejor veterinario y padre del mundo. Gracias por enseñarme que el esfuerzo, la pasión y la dedicación son los pilares de cualquier camino que valga la pena recorrer. Mamá y Papá, todo esto también es vuestro. No hay palabras suficientes para expresar cuánto os admiro y cuánto os debo. Soy inmensamente afortunada de ser vuestra hija. **Alfredo**, mi hermano pequeño (aunque ya no tan pequeño), muchas gracias por tu inmensa bondad, tu alegría contagiosa y esa capacidad única de llenar cada momento de humor. Me has acompañado muchos fines de semana que me tocaba quedarme a escribir la Tesis, tu compañía ha sido un auténtico regalo. **Alejandra**, mi melliza, mi otra mitad, muchas gracias por estar siempre a mi lado, por entenderme sin necesidad de palabras y por ser mi compañera de vida en cada paso y cada aventura; y ahora que **Gonzalo** se ha unido a la familia, gracias a ti también, ya eres uno más. Me alegra profundamente veros tan felices, y os deseo lo mejor a los dos. A mis abuelos **Carmina y Alfredo**, y a mis bisabuelos **Charo y Manolo**, muchas gracias por haber estado siempre a mi lado, desde que era pequeña y hasta hoy, regalándome vuestro amor incondicional y recuerdos que guardo como tesoros. Aunque algunos de vosotros ya no estéis físicamente conmigo, sé que tengo ángeles en el cielo que me cuidan y que también celebran este momento conmigo desde allí. Os llevo siempre en mi corazón. Y a **toda mi familia** y a quienes siempre habéis estado cerca en los pequeños y grandes momentos, gracias por vuestro cariño, también sois parte de este logro.

Con el corazón desbordado de emoción, cierro esta etapa que ha sido una de las más intensas, desafiantes y bonitas de mi vida. No hay palabras suficientes para describir lo afortunada que me siento. A veces, nos empeñamos en pensar que la vida ese compone de grandes momentos, de metas alcanzadas, de logros que podemos medir. Pero cuando miro atrás, me doy cuenta de que lo verdaderamente importante no ha sido el destino, sino el trayecto; no los éxitos, sino las personas con las que he tenido el privilegio de compartir estos años. Este Doctorado ha sido mucho más que investigación, experimentos, horas de escritura y esfuerzo, ha sido una lección de vida. He aprendido que el conocimiento, por valioso que sea, solo cobra sentido cuando se comparte. Que el esfuerzo, por grande que parezca, se hace más ligero cuando se camina en compañía. Y

que lo único que realmente deja huella no es lo que logramos, sino lo que damos. No tengo suficientes líneas para nombrar a todas las personas que me han acompañado todos estos días, pero a cada una de ellas, muchas gracias.

Hoy no termina una etapa académica, sino que nace una versión de mí que no existiría sin cada uno de vosotros, y no es más que el reflejo de todos los que caminaron conmigo. Gracias de corazón…

***" Lo que importa no es cuánto hacemos, sino cuánto amor ponemos en lo que hacemos"*— Madre Teresa de Calcuta**

# Table of contents

# Table of contents

## List of figures

### Chapter II: Introduction



### Chapter IV: Material and methods



### Chapter V: Results

## List of tables

### Chapter II: Introduction



### Chapter IV: Material and methods



### Chapter V: Results

## List of abbreviations

2D: Two-dimensional

3D: Three-dimensional

α-Bz: Polyclonal anti-*B. besnoiti* bradyzoite antiserum

α-NcBSR4: Antibody against *Neospora caninum* BSR4 protein

α-NcROP2: Antibody against *Neospora caninum* rhoptry protein 2

α-NcSAG1: Antibody against *Neospora caninum* surface antigen 1

α-NcSAG4: Antibody against *Neospora caninum* surface antigen 4

α-NcSRS2: Antibody against *Neospora caninum* SRS2 protein

α-NcSRS9: Antibody against *Neospora caninum* SRS9 protein

α-TgBAG1: Antibody against *Toxoplasma gondii* BAG1 protein

α-Tz: Polyclonal anti-*B. besnoiti* tachyzoite antiserum

Ab: Antibody

AGE-RAGE: Advanced Glycation End products–Receptor for Advanced Glycation End products

AIFM1: Apoptosis Inducing Factor Mitochondria Associated 1

AP-2: APETALA2 transcription factors

AREG: Amphiregulin

ATF4: Activating Transcription Factor 4

ATP: Adenosine Triphosphate

BAEC: Bovine Aortic Endothelial Cells

BAG1: Bradyzoite Antigen 1

Bcl-2: B-cell lymphoma 2

BH3: Bcl-2 Homology Domain 3

BHK: Baby Hamster Kidney cells

BKI: Bumped Kinase Inhibitor

BP: Biological Process

BSA: Bovine Serum Albumin

BST2: Bone Marrow Stromal Antigen 2

BUVEC: Bovine Umbilical Vein Endothelial Cells

Bz: Bradyzoite

CASP: Caspase

CC: Cellular Component

CCL: Chemokine (C-C motif) ligand

CDH2: Cadherin-2

CDPK: Calcium-Dependent Protein Kinase

cGAS: Cyclic GMP-AMP Synthase

CHOP-2: C/EBP Homologous Protein 2 (proapoptotic transcription factor)

CLDN15: Claudin 15 (tight junction protein)

CO: Conjunctival

COL13A1: Collagen Type XIII Alpha 1 Chain

COL7A1: Collagen Type VII Alpha 1 Chain

CRFK: Crandell Rees Feline Kidney cells

CoA: Coenzyme A

CSF1R: Colony Stimulating Factor 1 Receptor

Ct: Threshold Cycle

CXCL: Chemokine (C-X-C motif) ligand

DAB: 3,3′-Diaminobenzidine

DAPI: 4′,6-diamidino-2-phenylindole

DBA: Dolichos biflorus Agglutinin

DDIT3: DNA Damage Inducible Transcript 3

DEG: Differentially Expressed Gene

DH: Definitive Host

DIGE: Difference Gel Electrophoresis

DMEM: Dulbecco's Modified Eagle Medium

Dt: Doubling time

DUSP: Dual Specificity Phosphatase

ECM: Extracellular Matrix

EFSA: European Food Safety Agency

EGF: Epidermal Growth Factor

EIF2AK2: Eukaryotic Translation Initiation Factor 2-Alpha Kinase 2

EIF2B3: Eukaryotic Translation Initiation Factor 2B Subunit 3ELISA: Enzyme-Linked Immunosorbent Assay

ELQs: Endochin-Like Quinolones

ENO: Enolase 1

ENO2: Enolase 2

ENSEMBL: European Bioinformatics Institute Genome Browser

ER: Endoplasmic Reticulum

ERN1: Endoplasmic Reticulum to Nucleus Signalling 1

ET: Extracellular Trap

EU: European Union

FAS: Fas Cell Surface Death Receptor

FBS: Fetal Bovine Serum

FC: Fold Change

FDR: False Discovery Rate

FFPE: Formalin-Fixed Paraffin-Embedded

FGF1: Fibroblast Growth Factor 1

FI-Bb: Fibroblasts infected with *B. besnoiti* tachyzoites

FI: Non-infected fibroblasts

FNDC3A: Fibronectin Type III Domain-Containing Protein 3A

FosB: FBJ murine osteosarcoma viral oncogene homolog B

FR235222: Histone deacetylase inhibitor used for inducing differentiation

GAPDH: Glyceraldehyde-3-Phosphate Dehydrogenase

GO: Gene Ontology

GRA: Dense Granule protein

HC: Host Cell

HCFC2: Host Cell Factor C2

HDACi: Histone Deacetylase Inhibitor

HFF: Human Foreskin Fibroblasts

HGF: Hepatocyte Growth Factor

HRP: Horseradish Peroxidase

HSP70: Heat Shock Protein 70

IBVR: Infectious Bovine Rhinotracheitis Virus

IC50: Half Maximal Inhibitory Concentration

ICAM-1: Intracellular Adhesion Molecule 1

ID: intradermal

IF: Immunofluorescence

IFIH1: Interferon Induced with Helicase C Domain 1

IFN-α: Interferon alpha

IFN-β: Interferon beta

IFN-γ: Interferon gamma

IH: Intermediate Host

IHC: Immunohistochemistry

IL: Interleukin

IM: intramuscular

IN: Intranasal

IP: Intraperitoneal

IRAK1: Interleukin-1 Receptor-Associated Kinase 1

IRE1α: Inositol-Requiring Enzyme 1 alpha

ISG: Interferon-Stimulated Gene

ITGA2: Integrin Alpha 2

ITGA5: Integrin Alpha 5

ITGA6: Integrin Alpha 6

ITGA8: Integrin Alpha 8

ITPR1: Inositol 1,4,5-Trisphosphate Receptor Type 1

ITS-1: Internal Transcribed

IU: International Units

IV: Intravenous

IW: Inner Wall

IgG: Immunoglobulin G

IgM: Immunoglobulin M

JAK–STAT: Janus Kinase–Signal Transducer and Activator of Transcription

JNK: c-Jun N-terminal Kinase

KEGG: Kyoto Encyclopedia of Genes and Genomes

LC3B: Microtubule-associated Protein 1A/1B-light Chain 3B (autophagy marker)

LDH: Lactate Dehydrogenase

LRRC4: Leucine Rich Repeat Containing 4

MAPK: Mitogen-Activated Protein Kinase

MARC-145: Monkey Kidney Epithelial Cell Line

Mb: Megabase (million base pairs of DNA)

MCDA: Multi-Criteria Decision Analysis

MDA5: Melanoma Differentiation-Associated protein 5

MF: Molecular Function

MHC-I: Major Histocompatibility Complex Class I

MIC: Microneme protein

MMP9: Matrix Metalloproteinase 9

MMP16: Matrix Metalloproteinase 16

MO-Bb: Macrophage infected with *B. besnoiti* Tachyzoites

MO-hkBb: Macrophage infected with Heat-Killed *B. besnoiti* Tachyzoites

MO: Non-infected macrophage

MOI: Multiplicity of Infection

MP: Micropore

MPO: Myeloperoxidase

MS: Mass Spectrometry

N: Nucleus

NADPH: Nicotinamide Adenine Dinucleotide Phosphate

NCBI: National Center for Biotechnology Information

ND: Not Determined

NETs: Neutrophil Extracellular Traps

NF-κB: Nuclear Factor Kappa-light-chain-enhancer of Activated B Cells

NO: Nitric Oxide

NOTCH1: Neurogenic locus notch homolog protein 1

NRAS: NRAS Proto-Oncogene, GTPase

OAS: Oligoadenylate Synthetase

OCW: Outer Cyst Wall

PBAF: Primary Bovine Aorta Fibroblasts

PBS: Phosphate-Buffered Saline

PCA: Principal Component Analysis

PCR: Polymerase Chain Reaction

PDI: Protein Disulfide Isomerase

PECAM1: Platelet and Endothelial Cell Adhesion molecule 1

PI3K–AKT: Phosphatidylinositol 3-Kinase–AKT signalling pathway

PLA2G4B: Phospholipase A2, Group IVB

PLAUR: Plasminogen Activator, Urokinase Receptor

PLAT: Tissue Plasminogen Activator

PLAUR: Plasminogen Activator, Urokinase Receptor

PLCXD1: Phospholipase C, X Domain Containing 1

PMNs: Polymorphonuclear Neutrophils

PMAIP1: Phorbol-12-Myristate-13-Acetate-Induced Protein 1

PV: Parasitophorous Vacuole

PVM: Parasitophorous Vacuole Membrane

P2X1: Purinergic Receptor P2X, Ligand-gated Ion Channel 1

R: Statistical computing software R

RIN: RNA Integrity Number

RNA-Seq: RNA Sequencing

RON: Rhoptry Neck protein

ROP: Rhoptry protein

ROS: Reactive Oxygen Species

RPMI: Roswell Park Memorial Institute medium

RT: Room Temperature

RT-PCR: Reverse Transcription Polymerase Chain Reaction

SAG: Surface Antigen

SDS: Sodium Dodecyl Sulfate

SMA: Smooth Muscle Actin (α-SMA: alpha-Smooth Muscle Actin)

SC: Subcutaneous

SDC4: Syndecan 4

SELE: Selectin E

SNP: Sodium Nitroprusside

SOD: Superoxide Dismutase

SRS49D: Surface Antigen Related Sequence 49D

SRplot: Statistical Results Plotting (web tool)

T25: 25 $cm^2$ culture flask

TAB1: TGF-beta Activated Kinase 1 Binding Protein 1

TBS: Tris-Buffered Saline

TBS-T: Tris-Buffered Saline with Tween 20

TBS: Tris-Buffered Saline

TEM: Transmission Electron Microscopy

TGFβ1: Transforming Growth Factor beta 1

TGFβ3: Transforming Growth Factor Beta 3

TGFβR2: Transforming Growth Factor Beta Receptor 2

TLN1: Toxolysin 1

TNF: Tumor Necrosis Factor

TUBA1A/B: Tubulin Alpha-1A/B Chain

TUNEL: Terminal deoxynucleotidyl transferase dUTP nick end labeling

TgBAG1: *Toxoplasma gondii* Bradyzoite Antigen 1

TgIST: *Toxoplasma gondii* Interferon Signalling Transducer

ToxoDB: *Toxoplasma gondii* Genomic Database

Tz: Tachyzoite

ULK1: Unc-51 Like Autophagy Activating Kinase 1

UPR: Unfolded Protein Response

VEGF: Vascular Endothelial Growth Factor

VEGFA: Vascular Endothelial Growth Factor A

VEGFC: Vascular Endothelial Growth Factor C

Vero cells: African green monkey kidney epithelial cells

WB: Western Blot

ZNF: Zinc Finger Protein

cGAS: Cyclic GMP–AMP Synthase

h p.i.: Hours Post-Infection

p.i.: Post-Infection

padj: Adjusted p-value

qPCR: Quantitative Polymerase Chain Reaction

α-SMA: Alpha-Smooth Muscle Actin

# Chapter I: Abstract/Resumen

# Chapter I: Abstract/Resumen

## Abstract

Bovine besnoitiosis is a chronic and debilitating cattle disease caused by the cyst-forming apicomplexan parasite *Besnoitia besnoiti*. It significantly impacts animal health and welfare and poses substantial economic challenges to the livestock industry. Since the first description in southern France by Cadéac (1884), bovine besnoitiosis has spread in the Pyrenees and become a re-emerging disease in Europe. In Spain, the disease has been mainly described in cattle in Navarra, Aragón, Castilla y León, Castilla La Mancha, Cataluña, Extremadura, País Vasco, Comunidad Valenciana and Andalucía. The clinical course of bovine besnoitiosis develops in two sequential stages. At an early stage, rapidly replicating tachyzoites may infect target cells such as endothelial cells and macrophages, causing fever, depression, anorexia, subcutaneous oedema, nasal and ocular discharge, respiratory disorders and orchitis. At a later stage, tachyzoites switch into slowly dividing bradyzoites that gather inside tissue cysts in myofibroblasts and fibroblasts, mainly in subcutaneous tissues. Clinical manifestations of chronically infected animals are skin lesions (hyperkeratosis, folding, alopecia, nodules and scars in the udder) and pathognomonic visible tissue cysts in the scleral conjunctive and vestibulum vaginae. Orchitis evolves to scrotal skin thickening and results in testicular atrophy and sterility. Clinical signs and lesion severity are variable. Indeed, most animals remain sub clinically infected, and a small percentage develop visible and severe clinical signs and lesions which sometimes lead them to succumb to the infection. Currently, bovine besnoitiosis is one of the leading causes of reproductive failure in bulls. In this regard, it is a serious health and economic concern for the cattle breeding industry mainly due to permanent sterility of breeding bulls and reduced herd fertility, weight loss, poor body condition and leather depreciation. However, relevant epidemiological aspects of this parasitic disease are still uncertain, including the complete life cycle, the identity of the definitive host and the contribution of the different sources of parasite transmission that hamper disease control. Additionally, the absence of effective drugs and vaccines to combat the parasite, further exacerbates the situation. Accordingly, disease control is highly limited, and biosecurity and management measures

are the only available control options. In this scenario, research on bovine besnoitiosis presents new opportunities related with the development of effective control tools by studying the molecular mechanisms that govern pathogen-host cell interaction to identify novel drug and vaccine targets.

Nowadays, *in vitro* and *in vivo* models for *B. besnoiti* face several limitations that hinder a complete understanding of the parasite's biology and pathogenesis. *In vitro* models are constrained by the lack of primary bovine cells and suitable target cells for the parasite. Additionally, there is no established bradyzoite marker nor system to induce the transformation of tachyzoites into bradyzoites, making it challenging to investigate disease chronification and cyst formation. Bradyzoites can only be obtained from tissue cysts in chronically infected animals, a process that is time-consuming and labour-intensive. Additionally, research relies primarily on cell lines that do not reproduce the structural and functional complexity of tissues, nor the interactions that occur between different cell types within the tissue microenvironments. Moreover, *in vivo* models also present significant challenges. Ethical and regulatory constraints limit large-scale animal studies, requiring strict justifications for experimentation. Moreover, there is no standardized *in vivo* experimental model available. The transition from acute to chronic infection remains poorly understood and cyst formation is not always consistently reproduced in *in vivo* experimental settings. Disease manifestation varies between animals, making it difficult to standardize experimental outcomes. In addition, maintaining infected animals and conducting long-term studies demand substantial financial and logistical resources, making research costly and complex. Despite recent advancements, these limitations continue to restrict progress in understanding *B. besnoiti* pathogenesis. Developing standardized models would be essential for advancing research, vaccine development and therapeutic strategies.

Recent studies have provided valuable insights into host-parasite interactions. During the acute phase, endothelial cells and macrophages play crucial roles in immune response and parasite proliferation. *Besnoitia besnoiti* can invade bovine umbilical vein endothelial cells (BUVEC) and bovine aortic endothelial cells (BAEC), impairing cell cycle progression and triggering endothelial activation with proinflammatory and prothrombotic responses. Macrophages contribute to pathogenesis

by forming extracellular traps (ETs) to limit parasite spread and IFN-γ plays a role in immune priming. In the chronic phase, fibroblasts and myofibroblasts are the primary target cells, driving fibrosis and tissue remodelling. Tissue cysts have been identified in naturally infected bulls, with fibroblasts exhibiting fibrosis-related markers, supporting their role in disease progression. RNA sequencing (RNA-Seq) analysis confirms fibrosis-associated gene expression changes in infected BAEC, reinforcing the significance of fibroblasts and macrophages in *B. besnoiti* pathogenesis.

Our understanding of *B. besnoiti* genes and pathways involved in host cell invasion and lytic cycle progression remains limited as well. The first proteomic study identified tachyzoite proteins linked to energy metabolism, invasion and redox homeostasis. RNA-Seq analysis further revealed the parasite's regulation of endothelial cells through surface (SAG), microneme (MIC) and rhoptry (ROP) genes. Comparative transcriptomics estimated its genome at 58.9 Mb, showing similarities with *Toxoplasma gondii* and *Neospora caninum*. Disease chronification mechanisms, particularly the tachyzoite-to-bradyzoite switch, remain poorly understood. Stage-specific proteins have been identified in bradyzoites (*GAPDH, ENO1, LDH, SOD, RNA polymerase*) and tachyzoites (*ENO2, LDH, ATP synthase, HSP70, PDI*), providing insights for future drug targets. However, the lack of an *in vitro* bradyzoite induction model hinders research, unlike *T. gondii*, where stressors like pH and nutrient deprivation facilitate conversion. Currently, *B. besnoiti* bradyzoites can only be obtained from tissue cysts of chronically infected animals and no specific *B. besnoiti* bradyzoite markers exist apart from the cross-reactive *T. gondii* BAG1 antibody.

Accordingly, the objective of this Doctoral Thesis was to investigate both host- and parasite-dependent factors, as well as the molecular mechanisms governing the interaction of *B. besnoiti* with bovine target cells and the transition toward chronic infection and cyst formation. To achieve this, first a transcriptomic approach using RNA-Seq was performed to study the parasite's interaction with two key cell types: macrophages and fibroblasts and, second, we attempted to develop a tachyzoite-bradyzoite switch *in vitro* model.

In the macrophage model, *B. besnoiti* tachyzoites successfully invaded and proliferated, inducing significant transcriptional and morphological changes. Early macrophage activation was observed as soon as 4 hours post-infection (h p.i.)., with infected cells exhibiting a rounded shape and transcriptional alterations associated with apoptosis and mitogen-activated protein kinase (MAPK) signalling. Apoptosis was confirmed via TUNEL assay, while at 8 h p.i., the *Herpes simplex* virus 1 infection pathway emerged as the most significantly enriched pathway, with key genes such as *IFNα* and *CHOP-2*, also regulated in the testicular parenchyma of naturally infected bulls. In the fibroblast model, *B. besnoiti* efficiently invaded and replicated, triggering a progressive transcriptional response. At 12 h p.i., pathways associated with inflammation, including cytokine–cytokine receptor interaction, TNF signalling and AGE–RAGE signalling, were enriched. As infection progressed to 32 h p.i., fibroblasts exhibited transcriptional changes associated with cell proliferation and extracellular matrix (ECM) remodelling, suggesting an early step of fibroblast-to-myofibroblast transformation. Notably, *TGFβ1*, a key fibrosis regulator, was significantly upregulated along with *VEGFs* and *NOTCH1*, while the absence of α-smooth muscle actin (*α-SMA*) upregulation suggested an early fibrotic stage. Fibroblast transcriptomic data further highlighted parallels with cancer-related pathways, including angiogenesis, apoptosis inhibition and cell migration, supporting the hypothesis that fibrosis in *B. besnoiti* infection shares molecular features with tumour progression. Further transcriptomic analysis identified MAPK signalling as a central regulator in both macrophages and fibroblasts, reinforcing its role in parasite-induced host cell modulation. Moreover, *PLAUR*, *TGFβ1* and *FOSB* emerged as potential biomarkers of *B. besnoiti* infection, providing new targets for future diagnostic and therapeutic strategies. In parallel, the transcriptome of *B. besnoiti* tachyzoites was analysed in both *in vitro* models, revealing distinct host cell–dependent expression patterns. In macrophages, 538 differentially expressed genes (DEGs) were identified between 4 and 8 h p.i. with 537 upregulated—mainly genes involved in invasion (e.g., rhoptry proteins and gliding machinery) and metabolism (e.g., amino acid pathways). In contrast, no transcriptional differences were observed in the fibroblast between 12 and 32 h p.i. However, the analysis of the *B. besnoiti* transcriptome within fibroblasts identified a broad set of genes associated with parasite invasion and intracellular adaptation (SAGs, ROPs, MICs and dense granules (GRAs)).

The tachyzoite-to-bradyzoite conversion in *B. besnoiti* was investigated through a series of *in vitro* assays using stage-specific markers and differentiation protocols adapted from *T. gondii*. α-TgBAG1 was validated as a bradyzoite marker, while none of the antibody tested apart from a polyclonal anti-bradyzoite antibody confirmed bradyzoite detection. Several induction protocols were evaluated to trigger bradyzoite differentiation, including exposure to alkaline pH, heat shock, foetal bovine serum (FBS) deprivation, treatment with sodium nitroprusside (SNP), histone deacetylase inhibitors (HDACi) and bumped kinase inhibitors (BKIs). Among the various stress conditions tested, only three protocols demonstrated partial efficacy in inducing bradyzoite differentiation in *B. besnoiti*: treatment with 70 µM SNP for 7 days, 50 µM apicidin for 15 days and 50 µM FR235222 for 15 days. In contrast, the other protocols, which were effective in *T. gondii*, failed to induce bradyzoite formation in *B. besnoiti*. These findings suggest that *B. besnoiti* follows a distinct differentiation mechanism compared to *T. gondii*. Given their ability to partially induce bradyzoite differentiation, HDACi may represent promising candidates for therapeutic intervention.

This Doctoral Thesis has contributed to the understanding of *B. besnoiti* infection by identifying molecular mechanisms and pathways involved in host-pathogen interactions in macrophages and fibroblasts and potentially relevant biomarkers throughout the course of the disease. In addition, the partial *in vitro* induction of bradyzoite differentiation and the validation of BAG1 as a stage-specific marker provide novel insights into the parasite's chronic stage and open new avenues for studying persistence and latency in bovine besnoitiosis.

## Resumen

La besnoitiosis bovina es una enfermedad crónica y debilitante del ganado vacuno causada por el parásito apicomplejo formador de quistes *Besnoitia besnoiti*. Esta enfermedad afecta de forma significativa a la salud y al bienestar animal, y plantea importantes retos económicos para el sector ganadero. Desde su primera descripción en el sur de Francia por Cadéac (1884), la besnoitiosis bovina se ha propagado por los Pirineos y se ha convertido en una enfermedad reemergente en Europa. En España, la enfermedad ha sido descrita principalmente en ganado bovino de Navarra, Aragón, Castilla y León, Castilla La Mancha, Cataluña, Extremadura, País Vasco, Comunidad Valenciana y Andalucía. El curso clínico de la besnoitiosis bovina se desarrolla en dos fases secuenciales. En una fase temprana, los taquizoítos, que se replican rápidamente, pueden infectar células diana como las células endoteliales y los macrófagos, provocando fiebre, depresión, anorexia, edema subcutáneo, secreción nasal y ocular, trastornos respiratorios y orquitis. En una fase posterior, los taquizoítos se transforman en bradizoítos, que se dividen lentamente y forman quistes tisulares dentro de miofibroblastos y fibroblastos, principalmente en el tejido subcutáneo. Las manifestaciones clínicas en animales crónicamente infectados incluyen lesiones cutáneas (hiperqueratosis, engrosamiento, alopecia, nódulos y cicatrices en la ubre) y quistes tisulares visibles patognomónicos en la conjuntiva escleral y el vestíbulo vaginal. La orquitis evoluciona hacia un engrosamiento del escroto, lo que conlleva atrofia testicular y esterilidad. Los signos clínicos y la gravedad de las lesiones son variables. De hecho, la mayoría de los animales permanecen infectados de forma subclínica, y solo un pequeño porcentaje desarrolla signos clínicos visibles y lesiones graves que, en algunos casos, pueden provocar la muerte del animal. Actualmente, la besnoitiosis bovina es una de las principales causas de fallo reproductivo en toros. En este sentido, constituye una importante preocupación sanitaria y económica para la industria de la cría de ganado bovino, principalmente debido a la esterilidad permanente de los toros reproductores y a la reducción de la fertilidad del rebaño, pérdida de peso, mala condición corporal y depreciación del valor del cuero. Sin embargo, aún existen aspectos epidemiológicos relevantes que no están completamente esclarecidos, como el ciclo biológico completo, la identidad del hospedador definitivo y la contribución relativa de las diferentes fuentes de transmisión del parásito, lo que dificulta el control de la enfermedad. A ello se suma

la ausencia de fármacos y vacunas eficaces contra el parásito, lo que agrava aún más la situación. Como consecuencia, el control de la enfermedad es muy limitado, y las medidas de bioseguridad y manejo son las únicas herramientas disponibles. En este contexto, la investigación sobre la besnoitiosis bovina ofrece nuevas oportunidades para el desarrollo de herramientas de control eficaces, mediante el estudio de los mecanismos moleculares que rigen la interacción parásito-hospedador con el fin de identificar nuevas dianas terapéuticas y vacunales.

Actualmente, los modelos *in vitro* e *in vivo* para *B. besnoiti* presentan varias limitaciones que impiden una comprensión completa de la biología y patogenia del parásito. Los modelos *in vitro* están condicionados por la falta de líneas celulares primarias bovinas y dianas para el parásito. Además, no existe un marcador establecido de bradizoíto ni un sistema para inducir la transformación de taquizoítos a bradizoítos, lo que dificulta el estudio de la cronificación de la enfermedad y la formación de quistes. Los bradizoítos solo pueden obtenerse a partir de quistes tisulares en animales crónicamente infectados, un proceso laborioso y que requiere mucho tiempo. Asimismo, la investigación depende en gran medida de líneas celulares que no reproducen la complejidad estructural y funcional de los tejidos, ni las interacciones que se establecen entre los diferentes tipos celulares dentro del microambiente tisular. Por otra parte, los modelos *in vivo* también presentan retos importantes. Las restricciones éticas y normativas limitan la realización de estudios a gran escala en animales, requiriendo justificaciones estrictas para su ejecución. Además, no existe un modelo experimental *in vivo* estandarizado. La transición de la infección aguda a la crónica sigue siendo poco conocida y la formación de quistes no siempre se reproduce de manera consistente en los modelos experimentales. La manifestación clínica varía entre animales, lo que dificulta la estandarización de los resultados. Además, el mantenimiento de animales infectados y la realización de estudios a largo plazo requieren importantes recursos económicos y logísticos, lo que encarece y complica la investigación. A pesar de los avances recientes, estas limitaciones continúan dificultando el progreso en la comprensión de la patogenia de *B. besnoiti*. El desarrollo de modelos estandarizados es fundamental para avanzar en la investigación, el desarrollo de vacunas y nuevas estrategias terapéuticas.

Estudios recientes han aportado información valiosa sobre las interacciones hospedador-parásito. Durante la fase aguda, las células endoteliales y los macrófagos desempeñan un papel crucial en la respuesta inmunitaria y en la proliferación del parásito. *Besnoitia besnoiti* puede invadir células endoteliales de vena umbilical bovina (BUVEC) y células endoteliales aórticas bovinas (BAEC), interfiriendo en la progresión del ciclo celular y desencadenando una activación endotelial con respuestas proinflamatorias y protrombóticas. Los macrófagos contribuyen a la patogenia mediante la formación de trampas extracelulares que limitan la diseminación del parásito, y el IFN-γ participa en la activación de la respuesta inmunitaria. En la fase crónica, los fibroblastos y miofibroblastos son las principales células diana, promoviendo la fibrosis y la remodelación tisular. Además, se han identificado quistes tisulares en toros infectados de forma natural, cuyos fibroblastos muestran expresión de marcadores relacionados con la fibrosis, lo que apoya su papel en la progresión de la enfermedad. El análisis mediante secuenciación de ARN (RNA-Seq) confirma la expresión diferencial de genes asociados a fibrosis en BAEC infectadas, lo que refuerza la relevancia de fibroblastos y macrófagos en la patogenia de *B. besnoiti*.

El conocimiento actual sobre los genes y rutas moleculares implicadas en la invasión y la progresión del ciclo lítico de *B. besnoiti* sigue siendo limitado. El primer estudio proteómico identificó proteínas de taquizoíto relacionadas con el metabolismo energético, la invasión y la homeostasis redox. El análisis transcriptómico mediante RNA-Seq reveló también la regulación del endotelio por parte del parásito a través de genes de superficie (SAG), micronemas (MIC) y roptrias (ROP). La transcriptómica comparativa estimó el genoma de *B. besnoiti* en 58,9 Mb, mostrando similitudes con *Toxoplasma gondii* y *Neospora caninum*. Los mecanismos de cronificación de la enfermedad, en particular la conversión de taquizoíto a bradizoíto, aún no se comprenden bien. Se han identificado proteínas específicas de estadio en bradizoítos (*GAPDH, ENO1, LDH, SOD, ARN polimerasa*) y en taquizoítos (*ENO2, LDH, ATP sintasa, HSP70, PDI*), lo que ofrece perspectivas prometedoras para el desarrollo de nuevas dianas terapéuticas. No obstante, la falta de un modelo *in vitro* de inducción de bradizoítos limita el avance en este campo, a diferencia de *T. gondii*, donde factores de estrés como el pH o la privación de nutrientes facilitan dicha conversión. Actualmente, los bradizoítos de *B. besnoiti* solo pueden obtenerse a partir de quistes tisulares de

animales infectados crónicamente, y no existen marcadores específicos de bradizoíto, aparte del anticuerpo BAG1 de *T. gondii*, que presenta reactividad cruzada.

En consecuencia, el objetivo de esta Tesis Doctoral fue investigar los factores dependientes tanto del parásito como del hospedador, así como los mecanismos moleculares que regulan la interacción de *B. besnoiti* con las células diana bovinas y la transición hacia la infección crónica y la formación de quistes. Para ello, se aplicó un enfoque transcriptómico mediante RNA-Seq para estudiar la interacción del parásito con dos tipos celulares clave: macrófagos y fibroblastos. Además, se intentó desarrollar un modelo *in vitro* de conversión taquizoíto-bradizoíto.

En el modelo de macrófago, los taquizoítos de *B. besnoiti* invadieron y proliferaron eficazmente, induciendo cambios morfológicos y transcripcionales significativos en los macrófagos. Se observó una activación temprana de los macrófagos a las 4 h p.i., con células infectadas que adoptaban una morfología redondeada y presentaban alteraciones transcriptómicas asociadas con la apoptosis y la señalización mediante la proteína quinasa activada por mitógenos (MAPK). La apoptosis se confirmó mediante el ensayo TUNEL, y a las 8 h p.i. se identificó la vía de infección por el virus *Herpes simplex* tipo 1 como la más enriquecida, con genes clave como *IFNα* y *CHOP-2*, también regulados en el parénquima testicular de toros infectados de forma natural. En el modelo de fibroblasto, *B. besnoiti* invadió y se replicó con eficacia, desencadenando una respuesta transcriptómica progresiva. A las 12 h p.i. se enriquecieron rutas asociadas con la inflamación, incluyendo la interacción citoquina–receptor, la señalización TNF y la señalización AGE–RAGE. Conforme la infección progresaba hasta las 32 h p.i., los fibroblastos presentaron cambios transcriptómicos asociados con la proliferación celular y la remodelación de la matriz extracelular (MEC), lo que sugiere un paso temprano en la transformación de fibroblasto a miofibroblasto. Destaca la sobreexpresión significativa de *TGFβ1*, regulador clave de la fibrosis, junto con *VEGFs* y *NOTCH1*, mientras que la ausencia de sobreexpresión de la actina de músculo liso α (*α-SMA*) sugiere un estadio fibrótico incipiente. Los datos transcriptómicos de fibroblastos revelaron además similitudes con rutas moleculares asociadas al cáncer, incluyendo angiogénesis, inhibición de la apoptosis y migración celular, lo que respalda la hipótesis de que la fibrosis inducida por *B. besnoiti* comparte mecanismos con la progresión tumoral.

Análisis transcriptómicos adicionales identificaron la señalización MAPK como regulador central tanto en macrófagos como en fibroblastos, lo que refuerza su papel en la modulación celular inducida por el parásito. Además, *PLAUR*, *TGFβ1* y *FOSB* surgieron como posibles biomarcadores de la infección por *B. besnoiti*, lo que ofrece nuevas dianas para estrategias diagnósticas y terapéuticas futuras.

Paralelamente, se analizó el transcriptoma de los taquizoítos de *B. besnoiti* en ambos modelos *in vitro*, revelando patrones de expresión diferencial dependientes de la célula hospedadora. En macrófagos, se identificaron 538 genes diferencialmente expresados (DEGs) entre las 4 y 8 h p.i., de los cuales 537 estaban sobreexpresados, principalmente genes implicados en la invasión (por ejemplo, proteínas de los roptrias y maquinaria de deslizamiento) y el metabolismo (por ejemplo, rutas de aminoácidos). En contraste, no se observaron diferencias transcriptómicas en la expresión de genes del parásito entre las 12 y 32 h p.i. en fibroblastos. Sin embargo, el análisis del transcriptoma de *B. besnoiti* en fibroblastos permitió identificar un amplio conjunto de genes asociados a la invasión del parásito y a su adaptación intracelular (SAGs, ROPs, MICs, gránulos densos (GRAs)).

La conversión de taquizoíto a bradizoíto en *B. besnoiti* se investigó mediante una serie de ensayos *in vitro* utilizando marcadores específicos de estadio y protocolos de diferenciación adaptados de *T. gondii*. BAG1 fue validado como marcador de bradizoíto, mientras que ninguno de los anticuerpos evaluados, salvo un anticuerpo policlonal anti-bradizoíto, confirmó la detección de bradizoítos. Se evaluaron diversos protocolos de inducción para promover la diferenciación a bradizoíto, incluyendo la exposición a pH alcalino, choque térmico, privación de suero fetal bovino (SFB), y el tratamiento con nitroprusiato sódico (NPS), inhibidores de histona desacetilasa (HDACi) e inhibidores de cinasas (BKIs). Entre las distintas condiciones de estrés analizadas, solo tres protocolos mostraron eficacia parcial para inducir la diferenciación a bradizoíto en *B. besnoiti*: exposición a 70 µM de SNP durante 7 días, 50 µM de apicidina durante 15 días y 50 µM de FR235222 durante 15 días. Los demás protocolos, que resultaron eficaces en *T. gondii*, no lograron inducir la formación de bradizoítos en *B. besnoiti*. Estos hallazgos sugieren que *B. besnoiti* sigue un mecanismo de diferenciación distinto al de *T.*

*gondii*. Dada su capacidad para inducir parcialmente la diferenciación a bradizoíto, los HDACi podrían representar candidatos prometedores para una intervención terapéutica.

Por tanto, esta Tesis Doctoral ha contribuido al conocimiento sobre la infección por *B. besnoiti*, identificando mecanismos y rutas moleculares implicados en la interacción patógeno-hospedador en el macrófago y el fibroblasto y posibles biomarcadores relevantes a lo largo del desarrollo de la enfermedad. Además, la inducción parcial *in vitro* de la diferenciación a bradizoíto y la validación de BAG1 como marcador específico de estadio aportan nuevos conocimientos sobre la fase crónica del parásito y abren nuevas vías para el estudio de la persistencia y la latencia en la besnoitiosis bovina.

# Chapter II: Introduction

# Chapter II: Introduction

## 2.1 Brief historical review of bovine besnoitiosis

Bovine besnoitiosis is a chronic and debilitating cattle disease, caused by the cyst-forming apicomplexan parasite *Besnoitia besnoiti* (Besnoit and Robin, 1912). The disease can be severe and even fatal during both the acute and chronic phases of infection. Despite its relatively low mortality rate, the disease poses a severe economic challenge due to its high morbidity (up to 90%) within affected herds (Bigalke, 1968; Pols, 1960; Coelho et al., 2023). The disease relevance relies not only on the significant financial hardship inflicted through cattle raised under extensive husbandry systems but also on the serious concerns for animal health and welfare. Conditions such as bull sterility, deterioration of body condition and skin lesions impair production and reproduction parameters, with fertility particularly affected in herds relying on natural breeding (Álvarez-García et al., 2013).

Throughout its history, besnoitiosis has been identified under various names. Originally it was reported in Europe in 1884, when the French researcher Cadéac first reported a skin condition in cattle in southern France. He named this novel disease as "*l'élephantiasis et l'anasarque du boeuf*" (Cadéac, 1884). Almost three decades later, in 1912, French parasitologists Besnoit and Robin found cases of the disease in the French Pyrenees, and they were initially attributed it to a *Sarcocystis* species (Besnoit and Robin, 1912). In that same year, Marotel suggested the term *Sarcocystis besnoiti* for this parasite (Marotel, 1912). In 1915, Franco and Borges conducted clinical studies in the Alentejo region of Portugal, giving a formal name to the responsible pathogen -*Besnoitia besnoiti*- and introducing the term "besnoitiosis" for the disease itself (Franco and Borges, 1915).

In 1945, besnoitiosis was described in South Africa (Hofmeyr, 1945). Four years later, it was discovered that cattle imported from Angola to Portugal were affected by the disease (Leitao, 1949), suggesting a possible African origin of this

parasitic disease. From the late 1940s to the 1970s, there were key developments in the knowledge of bovine besnoitiosis in the African continent. Researchers isolated *B. besnoiti* from naturally infected ungulates like cattle, impala and wildebeest (Pols, 1960; Bigalke et al., 1967; Bigalke, 1968; Basson et al., 1970). These *Besnoitia* isolates, which were maintained in rabbits, enabled the first experimental infections in cattle, opening research avenues into transmission routes of the parasite, chronobiology of the disease and the lesions in different tissues (Basson et al., 1965, 1970; McCully et al., 1966). It was observed that isolates of *B. besnoiti* obtained from wildebeests exhibited lower virulence in cattle compared to isolates of bovine origin (Bigalke et al., 1974). This difference in virulence led to the development of a live vaccine in South Africa, derived from a low-virulence isolate obtained from wildebeests. This vaccine demonstrated effectiveness in preventing the onset of clinical signs in vaccinated animals for up to four years (Shkap, 1986; Shkap et al., 1987). Similarly, another live vaccine was developed in Israel; however, its safety profile remains uncertain. Despite this, it is routinely administered in Israel to reduce the risk of clinical symptoms in imported breeding bulls (Gutiérrez-Expósito et al., 2017).

Bovine besnoitiosis is endemic in several Sub-Saharan African countries and has also been reported outside of Africa in Israel, Russia, South Korea and Venezuela (Coelho et al., 2023). By the late 20th century, Europe experienced a resurgence of bovine besnoitiosis, particularly in southern regions of Spain, Portugal and France. This prompted the European Food Safety Authority to classify it as a re-emerging disease in 2010 (EFSA, 2010). In the Iberian Peninsula, the disease initially was detected in the cattle of the Pyrenees and subsequently spread to both central and southern areas of Spain where extensive cattle farming is common in mountain regions and Dehesa systems, except for the Cantabrian coast and the islands. In Portugal, the disease is endemic in the Alentejo region and cases have also been reported in other areas of the country, mainly in beef cattle (Coelho et al., 2023). France also reported multiple outbreaks, notably in the French Pyrenees and the Massif Central but cases are now present throughout the country in both dairy and beef cattle (Álvarez-García et al., 2013). Although Italy confirmed bovine besnoitiosis as endemic in the Northern Apennine Mountains in both dairy and beef cattle by 2009, it is not yet considered endemic across the entire country, with independent infection foci recorded only in the Lombardy region

(Gazzonis et al., 2014). In Germany, a specific outbreak occurred in a beef cattle herd in Bavaria, strongly suspected to be linked to imported Charolais or Limousin cattle from France. However, cases are now present throughout the country in both dairy and beef cattle. Additionally, infected cattle transported from endemic areas have introduced the disease into previously unaffected regions, including Germany, Switzerland and Croatia (Majzoub et al., 2010; Rostaher et al., 2010; Lesser et al., 2012). In Hungary, clinical cases emerged after 178 imported cattle -originally thought to be healthy- spread the disease to both local and imported populations (Hornok et al., 2014). In Mediterranean countries such as Greece, the presence of seropositive cattle in herds receiving animals from Germany, France and the Netherlands suggests the disease may already be present (Papadopoulos et al., 2014). Recently, bovine besnoitiosis was detected in Irish dairy herds, extending the disease's known range to the British Isles (Ryan et al., 2016).

Over the past three decades, alongside the increasing number of reported outbreaks, various serological and molecular diagnostic techniques have been developed and validated. These tools now play a crucial role in disease control, which relies solely on diagnosis and management measures due to the absence of effective drugs and vaccines (Gutiérrez-Expósito et al., 2017). Despite bovine besnoitiosis being known for over a century, significant knowledge gaps remain, including its pathogenesis, the host immune response, the complete life cycle of the parasite and the molecular mechanisms governing parasite-host interactions. The challenge of controlling this disease is further compounded by the lack of approved treatments or vaccines in Europe (Álvarez-García et al., 2013).

## 2.2 Taxonomy, aetiology and life cycle

*Besnoitia besnoiti* is a protozoan parasite classified within the phylum Apicomplexa and the infraphylum Sporae. It belongs to the class Conoidasida, subclass Coccidia and suborder Eimeriorina, within the order Eucoccidiorida. As a member of the family Sarcocystidae, it shares evolutionary relationships with other tissue cyst-forming apicomplexan parasites such as *T. gondii* and *Neospora caninum* (Adl et al., 2019).

The genus *Besnoitia* comprises ten diverse species, divided into two groups based on their primary hosts (**Table 1**). The first group infects small mammals, including *B. akodoni, B. jellisoni, B. darlingi, B. neotomofelis, B. oryctofelisi* and *B. wallacei*. The second group targets large mammals, with species such as *B. besnoiti, B. bennetti, B. caprae* and *B. tarandi*. Within this classification, *B. besnoiti* is responsible for bovine besnoitiosis and all the species that infect large mammal hosts produce similar clinical symptoms (Olias et al., 2011). However, their differentiation has been a subject of debate due to the absence of an identified definitive host, lack of ultrastructural differences and observed serological cross-reactivity, such as between *B. besnoiti* and *B. tarandi* or *B. besnoiti* and *B. bennetti* (Dubey et al., 2003; Gutiérrez-Expósito et al., 2012; Ness et al., 2012). Molecular studies further demonstrated close genetic relationships among these species, with identical ITS-1, 18S and 5.8S ribosomal RNA sequences (Ellis et al., 2000; Schares et al., 2009; Olias et al., 2011). Despite these similarities, microsatellite analysis allowed for differentiation between species and among isolates of *B. besnoiti* (Madubata et al., 2012; Gutiérrez-Expósito et al., 2016; Diezma-Díaz et al., 2019).

**Table 1**. **Natural hosts, geographical distribution and first description of *Besnoitia* species**.

| Species | Intermediate host | Final host | Geographical distribution | First description |
|---|---|---|---|---|
| ***B. besnoiti*** | Bovine, antelope, impala and blue wildebeest (*Connochaetes taurinus*) | Unknown * | Africa, Asia, Europe and Venezuela | Besnoit and Robin., 1912 |
| ***B. bennetti*** | Donkey (*Equus africanus asinus*), horse (*Equus ferus caballus*) and zebra (*Equus zebra, Equus quagga, Equus grevyi*) | Unknown * | Africa, Asia, USA and France | Bennett., 1927 |
| ***B. caprae*** | Goat (*Capra aegagrus hircus*) | Unknown * | Iran and Kenya | Cheema and Toofanian., 1979 |
| ***B. tarandi*** | Muskox (*Ovibos moschatus*), reindeer (*Rangifer tarandus*), mule deer (*Odocoileus hemionus*) | Unknown * | Canada, USA, Finland, Russia and Sweden | Hadween., 1922 |
| ***B. akodoni*** | *Akodon montensis* [1] | Unknown | USA | Dubey et al., 2003 |
| ***B. jellisoni*** | *Dipodomys* spp. [1] *Peromyscus maniculatus* [1] | Unknown | USA | Frenkel and Wilson.; 1972 |
| ***B. darlingi*** | *Ameiva* [2], *Basiliscus* [2] y *Didelphis marsupialis* [3] | Cat (*Felis catus*) | USA and Panama | Carboni and Tully., 2009 |
| ***B. neotomofelis*** | *Neotoma microptus* [1] | Cat (*Felis catus*) | USA | Dubey and Yabsley., 2010 |
| ***B. oryctofelisi*** | *Oryctolagus cuniculus* [4] | Cat (*Felis catus*) | Argentina and USA | Dubey and Lindsay., 2003 |
| ***B. wallacei*** | *Rattus exulans* [1] | Cat (*Felis catus*) | Australia, Hawaii, Japan and Kenya | Wallace and Frenkel., 1975 |

[1] Rodent; [2] Reptile; [3] Marsupial; [4] Lagomorph

* A carnivorous definitive host is suspected for *B. besnoiti.* Peteshev *et al*. (1974) suggested the role of felids as definitive hosts. However, extensive studies carried out by other authors have been inconclusive.

A recent study reported *Besnoitia* infection in a road-killed southern black-eared opossum (*Didelphis aurita*) in Argentina, with histopathological and molecular analyses indicating a species closely related to *B. oryctofelisi*, distinct from *B. darlingi* (Arrabal et al., 2024).

An unidentified *Besnoitia* species has been detected in Namibian cheetahs (*Acinonyx jubatus*), closely related to *B. darlingi, B. neotomofelis, B. oryctofelisi, B. akodoni* and *B. jellisoni*. Evidence suggests that cheetahs act as definitive hosts, while their prey may serve as intermediate hosts (Schares et al., 2021).

The first *B. besnoiti* isolates were obtained from naturally infected ungulates in South Africa in the 1960s and 1980s (Bigalke, 1967; 1968; Basson et al., 1970). More recently, numerous isolates from chronically infected cattle have been

characterized, including *Bb-Israel, Bb1-Evora 03, Bb2-Evora 03, Bb-Spain 1, Bb-Spain 2, Bb-GER 1, Bb-Italy 1, Bb-IPZ-1-CH, Bb-IPZ-2-CH, Bb-IPZ-3-CH* and *Bb-French* (Dubey et al., 2003; Cortes et al., 2006; Schares et al., 2009; Fernández-García et al., 2009a; Gentile et al., 2012; Basso et al., 2013; Frey et al., 2016). Despite genetic similarities, recent studies have revealed significant intraspecific variation in *B. besnoiti* isolates, particularly in their invasion rates and intracellular proliferation dynamics. *In vitro* analyses categorized isolates into high, medium and low invaders, with high-invading isolates (e.g., Bb-France, Bb-Evora03, Bb-Israel) demonstrating prolonged extracellular survival. Additionally, *B. besnoiti* exhibits a notably slower proliferation rate compared to related parasites such as *N. caninum* and *T. gondii* (Frey et al., 2016).

*Besnoitia besnoiti* presents two parasitic stages: the rapid-replicating tachyzoite, responsible for the acute phase of the disease and the slow-replicating bradyzoite, which is responsible for the chronic phase. Both parasite stages share similar morphological characteristics, appearing as ovoid or crescent-shaped bodies with pointed anterior and rounded posterior ends. Their ultrastructure aligns with that of other apicomplexan protozoa (Dubey, 1998; Speer et al., 1999). Langenmayer et al. (2015) provided an in-depth analysis of *B. besnoiti* tachyzoites, which reside within the host cell cytoplasm or in parasitophorous vacuoles, often forming botryoid conglomerates. Structurally, tachyzoites possess a three-layered pellicle, consisting of an outer plasmalemma and a double-layered inner membrane complex (IMC) that forms polar rings at both ends. Internally, they contain a centrally or posteriorly located nucleus, a Golgi complex and an apicoplast. Between the nucleus and the apical conoid, club-shaped ROPs are present, distinguished by a narrow neck and bulbous end. Notably, as tachyzoites infiltrate host cells, they exhibit an "hourglass-like" constriction marked by an electron-dense collar, possibly linked to their invasion mechanisms. Langenmayer et al. (2015) also observed a distended endoplasmic reticulum (ER) in some tachyzoites and described their reproductive method, known as endodyogeny (**Figures 1, 2 and 3**).

On the other hand, bradyzoites within tissue cysts exhibit distinct ultrastructural features. Fernández-García et al. (2009a) demonstrated that cysts possess

a double-layered wall that envelops the host cell nucleus, while bradyzoites are housed in parasitophorous vacuoles, encased by an electron-dense granular layer. Unlike tachyzoites, bradyzoites typically exhibit a nucleus positioned in the posterior half of the cell, accompanied by amylopectin granules. Additionally, a micropore has been observed at the posterior end of individual bradyzoites. Further insights into tissue cyst architecture were provided by Langenmayer et al. (2015) who described the outer cyst wall (OCW) as a structure composed of multiple layers of tightly interlocked fibrils, some of which extend outward to form connections between different layers. A gap between the OCW and the host cell membrane contains fibrillary and membrane protrusions, giving the host cell surface a ruffled appearance. Inside the parasitophorous vacuole, bradyzoites are tightly packed, often exhibiting a granular substance on their outer membrane, which sometimes aggregates into larger clusters.

Despite significant advancements, the complete life cycle of *Besnoitia* species remains poorly understood. Current evidence suggests a heteroxenous transmission cycle, with bovids (Pols, 1960) or antelopes (Basson et al., 1965) acting as intermediate hosts (IH), where both tachyzoites and bradyzoites develop. The cycle is presumed to involve a definitive host (DH) in which sexual reproduction occurs, leading to the production of oocysts. However, the DH of *B. besnoiti* and the epidemiological significance of oocyst shedding remain unknown. It is hypothesized that an as-yet unidentified DH excretes unsporulated oocysts in faeces, which subsequently sporulate under optimal environmental conditions, as observed in other *Besnoitia* species (**Figure 4**). Supporting this hypothesis, Ramakrishnan et al. (2022) conducted a comprehensive genomic analysis of *B. besnoiti*, revealing that its genome retains the capacity to encode most of the factors essential for completing a sexual cycle in a yet unidentified DH. These findings suggest that *B. besnoiti* may still rely on a DH for sexual reproduction, reinforcing the need for further studies to identify this host and clarify its role in transmission. In addition, a study by Peteshev et al. (1974) cited by the EFSA (2010), suggested that both domestic and wild cats could shed oocysts after ingesting cyst-containing tissues. Yet, subsequent studies have yielded contradictory results. For instance, Diesing et al. (1988) observed no oocyst shedding in the faeces of 23 wild carnivores—including cats and dogs—after they were fed cyst-containing tissue.

Similarly, Basso et al. (2011) found that dogs and cats did not produce antibodies when fed *B. besnoiti* tachyzoites, although cats did develop antibodies when exposed to cyst-containing tissues. Conversely, serological studies on wild carnivores, including wolves, red foxes, pine martens, stone martens, Eurasian badgers and European wildcats, found no serological evidence of their involvement in *B. besnoiti* transmission (Millán et al., 2012). Interestingly, *Besnoitia* spp. DNA has been detected in red fox faeces in western Spain, marking the first report of a *B. besnoiti*-like sequence in carnivore faeces worldwide (González-Barrio et al., 2021a). This discovery suggests a potential role for wild carnivores in the parasite's transmission, although its significance remains unclear.

In addition, other potential IH have been identified. *Capreolus capreolus* and *Cervus elaphus* appear to be susceptible to infection (Gutiérrez-Expósito et al., 2016), while *Ovis aries* and *Capra hircus* seem to play a minimal role in the parasite's life cycle (Gutiérrez-Expósito et al., 2017).

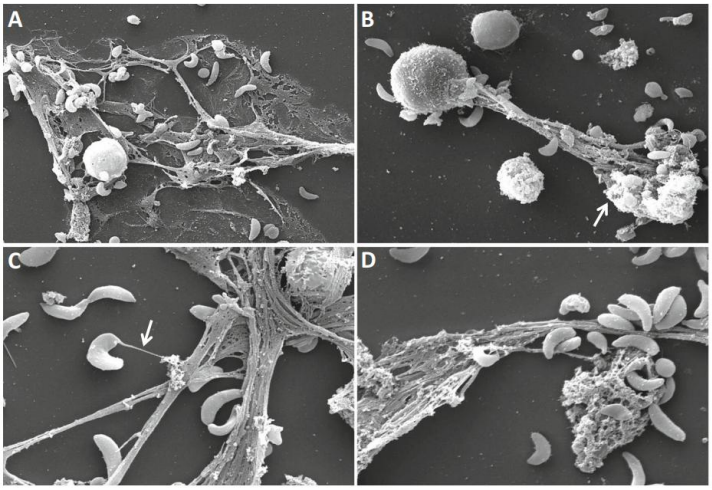


**Figure 1. Scanning electron microscopy of *B. besnoiti* tachyzoites and ETs formation in bovine monocytes. Scanning electron microscopy analysis revealed ETs being formed by bovine monocytes exposed to viable *B. besnoiti* tachyzoites in the absence of serum (A–D). (A) Overview of streets of fibres composed of monocyte-derived ETs showing attached *B. besnoiti* tachyzoites to them and one intact monocyte, (B) moment of strong ETs release by a single dead monocyte (indicated by white arrow) with entrapped *B. besnoiti* tachyzoites, (C) captured *B. besnoiti* tachyzoites in a massive network of long drawn-out fibres originating from dead monocytes and one tachyzoite being attached to a thin ET fibre (indicated by white arrow) and (D) detailed view of thick bundles of monocyte-ETs fibres as well as a meshwork capturing a conglomerate of *B. besnoiti* tachyzoites.**

* Source: Muñoz-Caro, T., Silva, L. M. R., Ritter, C., Taubert, A., and Hermosilla, C. (2014). *Besnoitia besnoiti* tachyzoites induce monocyte extracellular trap formation. Parasitology Research, 113(11), 4189–4197. https://doi.org/10.1007/s00436-014-4094-3.

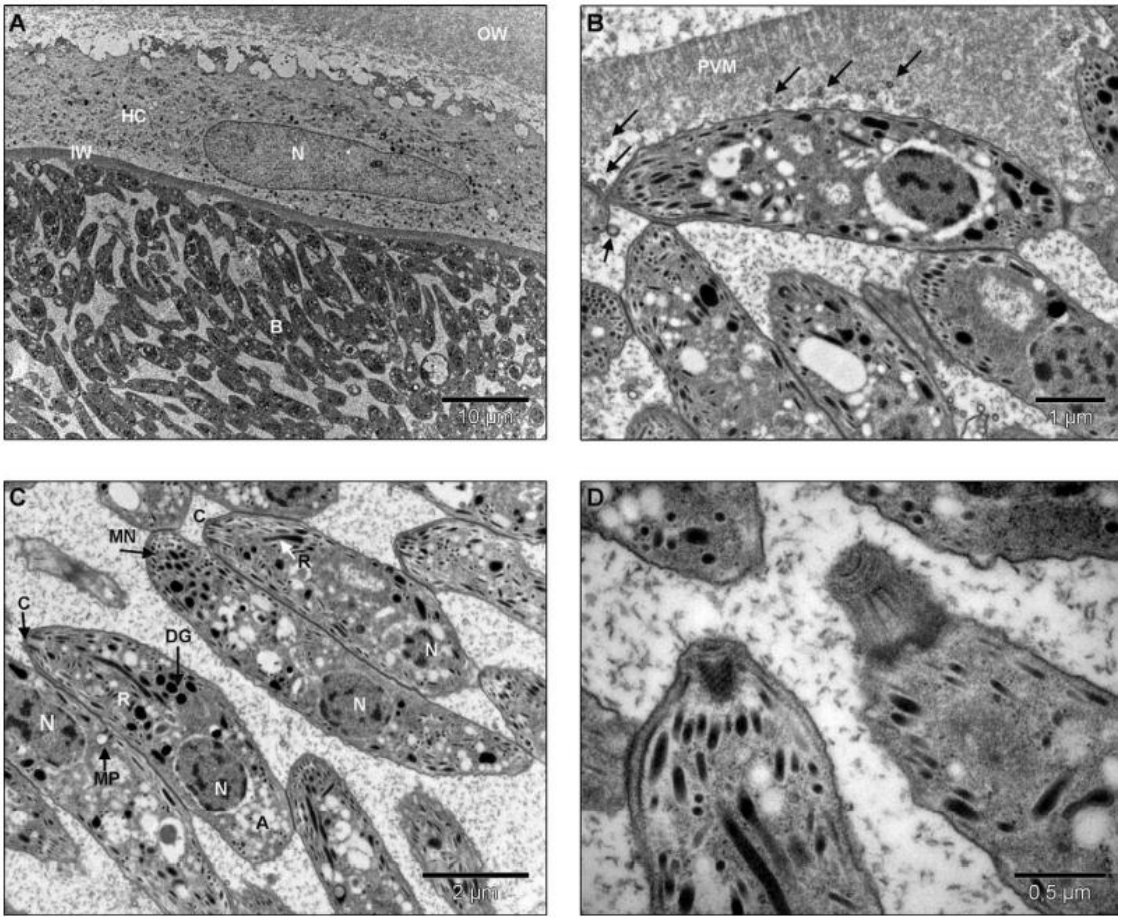


**Figure 2. Transmission electron micrograph (TEM) of *B. besnoiti* BbSpain-1 bradyzoites. (A) Tissue cyst of *B. besnoiti* (2.5K); note the outer cyst wall (OCW) enclosing a host cell (HC), host cell nucleus (N), the inner wall (IW) and numerous bradyzoites (B). (B) Inner cyst wall (20K), including a parasitophorous vacuole membrane (PVM) and an electron dense granular layer with small vesiculated structures released from adjacent bradyzoites (arrows). (C) TEM of *B. besnoiti* bradyzoites (15K); note characteristic organelles of the apical complex: conoid (C), rhoptries (ROPs), numerous micronemes (MICs) and dense granules (GRAs), plus a cell nucleus located at the posterior end (N) and amylopectin granules (A). A micropore (MP) can be seen in a parasite. (D) TEM of the conoid of tachyzoites in detail (50K); note the morphology of the conoid, a small cone-shaped spiral of filaments that can be protruded beyond the apical polar ring.**

* Source: Fernández-García, A., Risco-Castillo, V., Pedraza-Díaz, S., Aguado-Martínez, A., Álvarez-García, G., Gómez-Bautista, M., Collantes-Fernández, E. and Ortega-Mora, L. M. (2009a). First isolation of *Besnoitia besnoiti* from a chronically infected cow in Spain. *Veterinary Parasitology, 164*(2-4), 277–281. https://doi.org/10.1016/j.vetpar.2009.06.007.

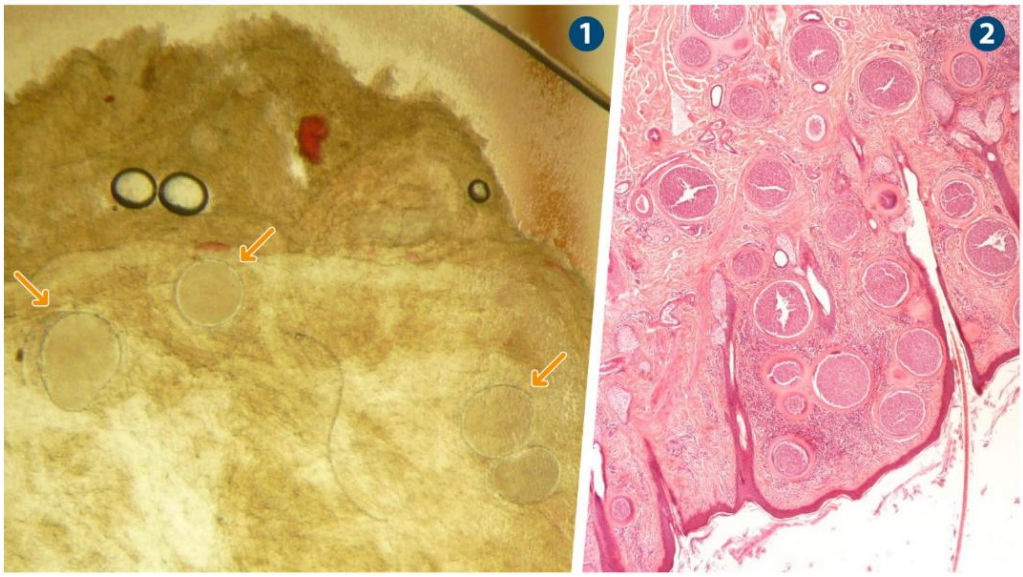


**Figure 3. Tissue cysts of *B. besnoiti*. (1) Cysts in a skin biopsy after compression on a slide; (2) Histological section of skin stained with hematoxylin-eosin (x100).**

* Source: ParasitXpert. *El parásito del mes: Besnoitia besnoiti y la besnoitiosis bovina*. https://parasitxpert.es/el-parasito-del-mes-besnoitia-besnoiti-y-la-besnoitiosis-bovina/

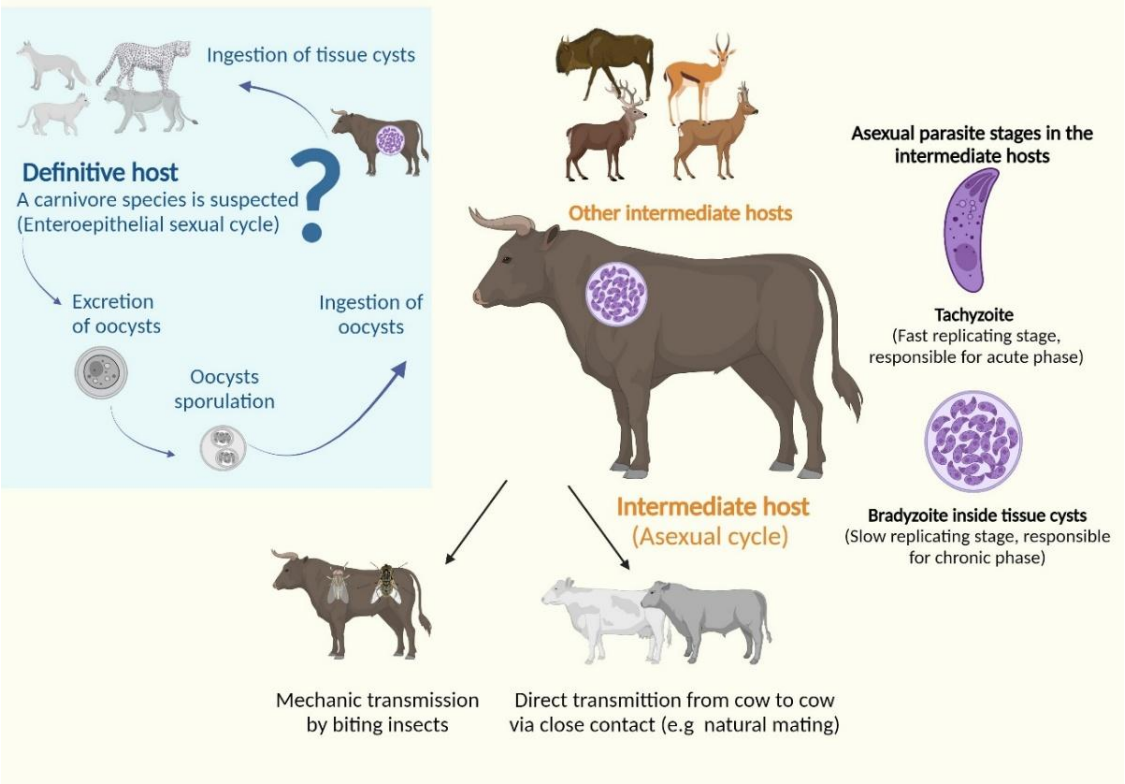


**Figure 4. Biological cycle and transmission of *B. besnoiti*.**

*Source: In M. Florin-Christensen & L. Schnittger (Eds.), *Parasitic protozoa of farm animals and pets* (2018). Springer.

## 2.3 Pathogenesis and clinical signs

### 2.3.1 Pathogenesis

The acute stage of *B. besnoiti* infection is driven by the rapid proliferation of tachyzoites, which invade target cells, particularly endothelial cells and macrophages, through a lytic cycle (**Figure 5**). This cycle begins with adhesion, where tachyzoites attach to the host cell surface using specialized adhesins, including MICs and SAGs. Once attached, the parasite actively invades the host cell by utilizing the glideosome motility system and ROPs, which facilitate the formation of a parasitophorous vacuole (PV) that allows the parasite to evade immune detection. Within the PV, tachyzoites undergo repeated rounds of endodyogeny, leading to exponential intracellular replication. As the infection progresses, the host cell ultimately ruptures, releasing mature tachyzoites, which are then free to invade new cells and perpetuate the infection cycle (García-Sánchez et al., 2019; Jiménez-Meléndez et al., 2019; Black and Boothroyd, 2000).

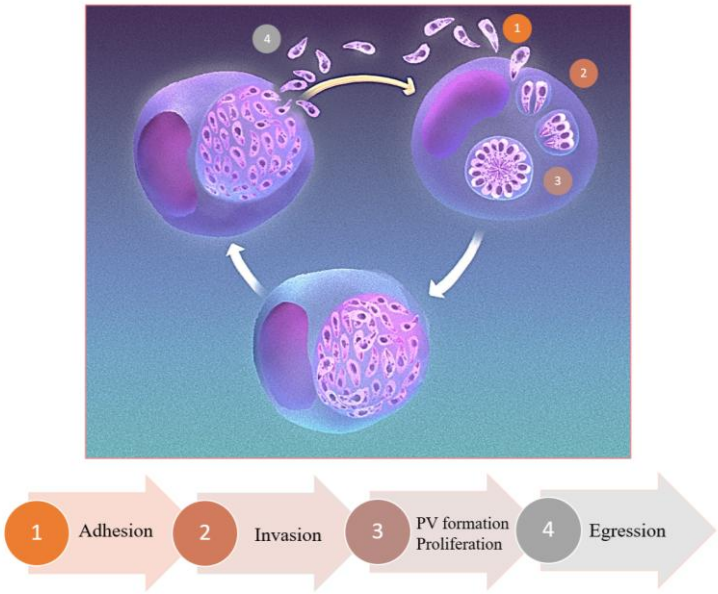


**Figure 5. Lytic cycle of *B. besnoiti* within the host cell.**

* Source: García-Sánchez, M. (2019). *Interacciones entre aislados de alta y baja virulencia de Neospora caninum y células diana de la respuesta inmunitaria innata bovina*. Doctoral Thesis, Complutense University of Madrid.

Experimental *in vitro* studies have demonstrated that *B. besnoiti* is capable of efficiently invading and proliferating within bovine endothelial cells, particularly BUVEC and BAEC (Muñoz-Caro et al., 2014; Maksimov et al., 2016; Jiménez-Meléndez et al., 2019). Once inside endothelial cells, tachyzoite replication leads to a cascade of vascular alterations, including loss of endothelial integrity, upregulation of leukocyte adhesion molecules and the development of a proinflammatory, prothrombotic and profibrotic phenotype. These pathological changes are driven by the parasite's regulation of key virulence genes, such as SAG, MIC and ROP genes, as well as apetala-2 (AP-2) transcription factors, all of which are crucial for host cell invasion and the progression of the lytic cycle (Jiménez-Meléndez et al., 2020).

As the parasite spreads, macrophages play a pivotal role in the pathogenesis of acute bovine besnoitiosis, as demonstrated by both *in vitro* and *in vivo* studies. *In vitro* experiments have revealed that upon encountering viable tachyzoites, macrophages release ETs, which serve to immobilize parasites and limit further invasion. This mechanism represents a crucial innate immune defence, attempting to contain the infection before adaptive immunity is established (Muñoz-Caro et al., 2014). Beyond *in vitro* observations, histopathological analyses of naturally infected bulls have provided *in vivo* evidence of a strong macrophage-driven inflammatory response, with intense macrophage-dominated infiltrates in the testicular parenchyma (González-Barrio et al., 2020). This macrophage response is further reinforced by a robust IFN-γ-mediated immune reaction, which enhances macrophage antimicrobial activity and amplifies the proinflammatory environment characteristic of acute infection (Su et al., 2015). Notably, innate immune activation precedes the onset of adaptive immunity, as evidenced in *in vivo* studies, by seroconversion occurring within 2–3 weeks post-infection (p.i.) (Diezma-Díaz et al., 2018). This sequential activation of immune responses underscores the dynamic nature of host defences. On the other hand, during chronic infection, *B. besnoiti* cysts primarily form within fibroblasts, which play a central role in ECM remodelling by producing collagen, laminins and proteoglycans (Pakshir et al., 2019; Tracy et al., 2016; Xuan et al., 2022). Fibrosis, a hallmark of chronic besnoitiosis, is driven by activated fibroblasts (myofibroblasts), which contribute to ECM deposition and the release of profibrotic factors, leading to tissue dysfunction and impaired thermoregulation (McAnulty et al., 2007; Yao et al., 2022).

### 2.3.2 Clinical signs

The acute stage of bovine besnoitiosis typically develops within two months p.i. and is associated with both systemic and localized clinical signs. Systemically, infected animals exhibit hyperthermia (lasting 3–10 days), depression, anorexia, tachycardia and congested mucous membranes (Álvarez-García et al., 2013). Locally, subcutaneous oedema, orchitis and hydrocele are observed, correlating with tachyzoite-induced endothelial activation, vascular injury and inflammatory responses (González-Barrio et al., 2020). In breeding bulls, testicular degeneration is a hallmark of the acute stage, manifesting as germline atrophy, fibrosis and disrupted spermatogenesis due to vascular lesions and macrophage-driven inflammation in the seminiferous tubules. These pathological alterations ultimately compromise reproductive performance and may lead to azoospermia and infertility (González-Barrio et al., 2020).

As the infection progresses, *B. besnoiti* transitions to its chronic stage, which is primarily characterized by the transformation of tachyzoites into bradyzoites and the formation of bradyzoite-containing tissue cysts. These cysts persist within the connective tissue of intermediate hosts, particularly in the skin and mucous membranes (Kumi-Diaka et al., 1981; Basso et al., 2013; Frey et al., 2013; Langenmayer et al., 2015). Their development is asynchronous, varying in size depending on the duration of infection (Bigalke, 1968) and they can even be detected during the acute phase (Basson et al., 1970; Gollnick et al., 2015). Mature cysts can contain up to 200,000 bradyzoites (Bigalke, 1968), whereas degenerated cysts, identified by a disrupted outer wall and loss of spherical morphology, have been observed as early as 30 days p.i. (Basson et al., 1970; Frey et al., 2013) (**Figure 6)**.

The clinical manifestations of chronic infection include progressive skin lesions, such as hyperkeratosis, alopecia, nodule formation and thickened skin, as well as reproductive impairments, including orchitis, scrotal thickening, testicular atrophy and sterility (Álvarez-García et al., 2013; Gollnick et al., 2015). Additionally, milk production declines in seropositive cows, with increased somatic cell counts, suggesting mammary gland involvement in chronic infection (Anastácio et al., 2022; Sambo et al., 2014).

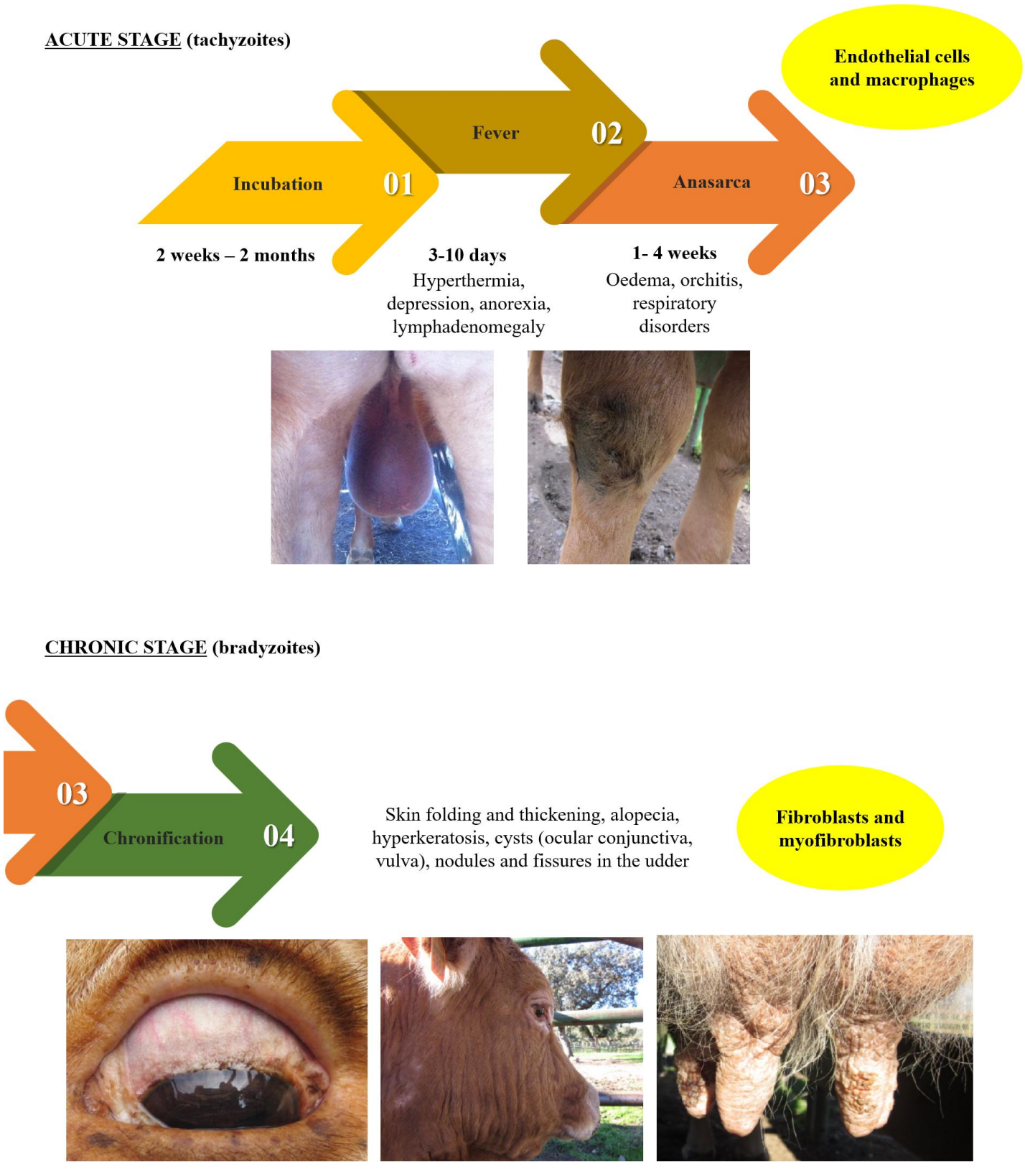


**Figure 6. Clinical signs associated with acute and chronic stages of *B. besnoiti* infection.**

* Source: ParasitXpert. *El parásito del mes: Besnoitia besnoiti y la besnoitiosis bovina*. https://parasitxpert.es/el-parasito-del-mes-besnoitia-besnoiti-y-la-besnoitiosis-bovina/

## 2.4 Epidemiology

### 2.4.1 Transmission and risk factors

Epidemiological data indicate that the primary mode of *B. besnoiti* transmission is horizontal. This transmission occurs either through direct contact—such as natural mating and skin lacerations—or via mechanical transmission facilitated by arthropod vectors from the Tabanidae and Muscidae families (Álvarez-García et al., 2013). Horizontal transmission through oocyst ingestion has not been documented, as the definitive host of the parasite remains unidentified and venereal transmission appears improbable (Esteban-Gil et al., 2014). Nonetheless, bradyzoites are known to possess the ability to cross mucosal barriers (Bigalke, 1968). Tissue cysts are often located superficially in the mucosa of both male and female reproductive tracts (Nobel et al., 1981; Kumi-Diaka et al., 1981). These cysts may rupture during natural mating, thereby releasing bradyzoites that can infect a new host. Consequently, infected bulls may pose a risk to females during mating and infected females may reciprocally infect bulls.

The predominant localization of cysts in the papillary dermis also facilitates the release of bradyzoites into the external environment following cyst rupture due to wounds or excoriations (McCully et al., 1966; Dubey et al., 2013; Langenmayer et al., 2015). The ingestion of oocysts has been investigated as a potential route of transmission, particularly in attempts to elucidate the complete life cycle of *B. besnoiti*. While early studies identified cats as potential definitive hosts (Peteshev et al., 1974), these findings were not reproduced in later studies (Diesing et al., 1988; Basso et al., 2011). Despite the parasite's known tropism for the male reproductive tract (Kumi-Diaka et al., 1981), *B. besnoiti* DNA has not been detected in the semen of seropositive bulls, regardless of whether they exhibited clinical signs of chronic besnoitiosis (Esteban-Gil et al., 2014). Thus, venereal transmission appears unlikely. Even if parasite DNA were to be detected in semen, viability of the organism would still be a critical factor for successful infection establishment.

Vertical transmission, either transplacental or via colostrum ingestion, also appears improbable. Hornok et al. (2014) found no evidence of vertical transmission,

as precolostral antibodies were absent in calves born to seropositive mothers and *B. besnoiti* DNA was not detected in colostrum. Similarly, Shkap et al. (1994) reported an absence of precolostral antibodies in calves from chronically infected mothers.

Host-specific susceptibility plays a crucial role in the transmission dynamics of *B. besnoiti*, particularly concerning age and breed. Studies indicate that cattle show a higher seroprevalence as age increases. This is most likely due to their prolonged exposure to arthropod vectors and repeated contact with infected individuals (Coelho et al., 2023). In contrast, younger animals, particularly those under one year of age, tend to show lower seroprevalence. This is primarily attributed to their limited exposure to vectors and the transient protective effect of maternally derived antibodies. However, as maternal immunity wanes over time, calves become increasingly susceptible, especially when exposed to high vector densities during warm seasons (Coelho et al., 2023; Gazzonis et al., 2017). This interaction between declining maternal immunity and seasonal vector activity may help explain why infection rates increase as calves mature.

Breed might also influence on cattle susceptibility on the disease. Studies have identified Salers and Charolais cattle as particularly vulnerable to *B. besnoiti*, while crossbred animals appear to exhibit greater resistance (Coelho et al., 2023; Gazzonis et al., 2017). The greater resistance seen in crossbreeds may be attributed to enhanced genetic diversity, which could either reduce the severity of infection or improve immune responsiveness. Furthermore, crossbred cattle raised in endemic regions may develop partial acquired immunity through natural exposure, making them less susceptible than purebred animals. However, there is not enough scientific evidence regarding breeding associated resistance or susceptibility.

Mechanical transmission of *B. besnoiti* by hematophagous arthropods plays a significant role in both acutely infected animals (which carry tachyzoites in circulating blood) and chronically infected animals (which harbour tissue cysts in the skin). Several species of horseflies (Tabanidae) and stable flies (*Stomoxys calcitrans*) have been implicated in mechanical transmission. *Stomoxys calcitrans* that had been in contact with chronically infected cows were shown to transmit the parasite to a rabbit, which subsequently developed clinical signs characteristic of acute besnoitiosis (Sharif et

al., 2019). However, successful transmission appears to require a high number of insect bites. Additionally, the limited survival time of the parasite within insect vectors suggests that long-distance transmission is unlikely (Bigalke, 1968). Further studies have detected *Besnoitia* spp. DNA in *S. calcitrans* after exposure to infected skin (Liénard et al., 2013) or during cohabitation of infected and uninfected animals (Gollnick et al., 2015). Quantitative PCR has confirmed the presence of parasite DNA in the intestinal contents of *Stomoxys* spp. up to 24 hours after ingestion of infected blood (Liénard et al., 2013), although these studies did not confirm the viability of the parasites. Transmission rates peak during warm seasons when hematophagous arthropods are most active, and cattle are typically grazing in shared pastures. This seasonal pattern has been consistently documented in both field and experimental studies (Bigalke, 1968; Gutiérrez-Expósito et al., 2017; Fernández-García et al., 2010; Alzieu, 2007). Moreover, secretophagous flies may act as potential vectors, particularly during lactation, when calves remain in close and prolonged contact with infected mothers (Hornok et al., 2015).

The transmission dynamics of *B. besnoiti* in Europe are influenced by a complex interplay of factors related to management practices, vector ecology, cattle movement, diagnostic limitations and host susceptibility. Saegerman et al. (2022) identified seven major drivers that significantly influence the emergence, transmission and spread of bovine besnoitiosis, especially in the context of Europe:

1. **Regulated and unregulated cattle movements**, both within the European Union (EU) and between the EU and third countries, are considered the most critical drivers of disease introduction and dissemination. The movement of asymptomatic but infected animals from endemic to disease-free areas facilitates the silent spread of *B. besnoiti*. Many subclinically or chronically infected cattle show no overt signs, making visual inspection ineffective. The lack of mandatory testing before trade further exacerbates the risk, allowing infected individuals to be introduced into naïve herds. Implementing routine serological screening before animal movements could significantly reduce this risk.
2. **Silent transmission and early diagnostic difficulties** represent another major challenge. The absence of reliable early diagnostic tools makes it difficult to identify infected animals during the incubation or subclinical phases. This

contributes to the unintentional spread of the parasite by apparently healthy animals.

3. **Presence and spread potential of mechanical vectors** also plays a critical role. While the infectivity window of vectors is limited to a few hours, high vector densities—especially in warm and humid climates—amplify local transmission. The involvement of mechanical rather than biological vectors complicate control measures, as the parasite does not require development within the insect to become infectious.
4. **Geographical proximity of affected regions** increases the probability of cross-border disease transmission, especially in regions with dense agricultural activity and shared pastures. Clusters of high cattle density further enhance this risk by increasing animal contact rates.
5. **Density of cattle farms** is another crucial factor, as regions with high farm densities inherently have more frequent cattle movement and greater risk of cross-infection, particularly when vector activity is intense.
6. **Farm management practices**, especially extensive systems where natural mating and co-grazing occur, enhance both direct and indirect contact among animals. These conditions are favourable for disease spread, particularly in the presence of vectors like *S. calcitrans* and horseflies.
7. **Vector ecology and seasonal climatic factors** are tightly linked to transmission peaks. Since vector activity increases during warmer months, the risk of transmission also rises during this period. This coincides with cattle reproductive seasons, compounding the risk when susceptible animals are co-grazing.

To address these complex dynamics, Saegerman et al. (2022) propose the use of multi-criteria decision analysis (MCDA) to guide future research priorities and policy development. These methods can help quantify the importation risk of *B. besnoiti*, estimate the potential economic burden of the disease and support evidence-based decisions on whether bovine besnoitiosis should be designated as a reportable disease within the EU. A formal designation could trigger stricter prevention and control measures, including biosecurity enhancements, mandatory testing and vector control strategies tailored to the key risk factors identified.

### 2.4.2 Geographic distribution

Historically, *B. besnoiti* was considered a disease restricted to parts of sub-Saharan Africa and certain Middle Eastern countries. The first descriptions of besnoitiosis date back to the early 20$^{th}$ century in South Africa (Bigalke, 1968), where the disease remains endemic, particularly in cattle and antelope species such as *Tragelaphus strepsiceros*. The disease has also been reported in Namibia, Botswana, Zimbabwe and Kenya (Njenga et al., 1993). Sporadic detections have also been published from Asia and South America, whereas none have been documented from North America or Australia (Álvarez-García et al., 2013). Cases in Turkey and Israel indicate a broader Middle Eastern distribution than previously assumed (Shkap et al., 2002). More recently, autochthonous infections have been identified in Europe, including Belgium (Delooz et al., 2021) and Ireland (Ryan et al., 2016).

Despite these reports, the global distribution of *B. besnoiti* remains poorly defined due to a lack of systematic surveillance, limited diagnostic tools in low-resource settings and the frequent confusion with other similar diseases such as lumpy skin disease or cutaneous tuberculosis. The situation is further complicated by the existence of closely related species such as *B. tarandi* (in reindeer) and *B. bennetti* (in donkeys), which may confound diagnostic results in wildlife and mixed-species livestock systems (Dubey et al., 2005). In recent decades, *B. besnoiti* has emerged as a significant veterinary problem in Europe, where it is now classified as an emerging disease of cattle (EFSA, 2010). The first confirmed cases on the continent were reported in the 1990s in the south of France but retrospective serological studies suggest that the parasite may have been present in isolated pockets well before its official recognition (Jacquiet et al., 2010). The expansion of besnoitiosis in Europe has followed a concerning trend, with cases now reported in Portugal (Cortes et al., 2006), Italy (Rinaldi et al., 2013), Germany (Rostaher et al., 2010), Switzerland (Basso et al., 2011) and Hungary (Hornok et al., 2014). Spain represents one of the most affected countries in Europe regarding bovine besnoitiosis and it plays a central role in the epidemiology of the disease on the continent. The first cases were described in the 1990s in Cataluña, but like in France, serological evidence suggests the parasite may have been present earlier (Fernández-García et al., 2009a). Today, *B. besnoiti* is considered endemic in several autonomous communities, including Castilla-La Mancha, Castilla y León, Andalucía, Aragón, Comunidad

Valenciana, Extremadura, Cataluña, Navarra y País Vasco (Diezma-Díaz et al., 2020; García-Lunar et al., 2013b). Prevalence rates vary widely between regions and even within provinces, ranging from 5% to over 60% in some localized cattle populations. Analyses conducted in Spain have identified several risk factors of infection, including herd size, proximity to other infected farms, the presence of wildlife reservoirs and participation in transhumance or livestock fairs (Gutiérrez-Expósito et al., 2017). Additionally, the importation of infected cattle from France, Portugal and Latin America is believed to have contributed to the introduction and perpetuation of the disease in the Iberian Peninsula (Cortes et al., 2006; Fernández-García et al., 2010).

### 2.4.3 Prevalence and incidence

The first studies on the prevalence of bovine besnoitiosis were conducted in South Africa, where prevalence rates ranging from 10% to 50% were reported based on the detection of ocular conjunctival cysts and skin lesions (Bigalke, 1968). Later, with the implementation of serological techniques, higher prevalence rates were observed. In Israel, seroprevalence in beef cattle ranged between 64.4% and 66.9% (Neuman, 1972; Frank et al., 1977), while in South Africa, 50% of asymptomatic cattle tested seropositive (Janitschke et al., 1984). More recent studies have also reported seroprevalence rates such as 13.5% in Egyptian cattle, based on enzyme-linked immunosorbent assay (ELISA) testing (Ashmawy and Abu-Akkada, 2014). In Jordan, seroprevalence rates of 6% at the individual level and 28.7% at the herd level were detected in dairy cattle, despite the absence of clinical signs (Talafha et al., 2015).

In Europe, the first reported case dates to the 1990s, when an outbreak was identified in a northwestern Italian farm housing cattle imported from France (Agosti et al., 1994). Subsequent surveillance in Italy by Gentile et al. (2012) confirmed autochthonous cases, with 41.2% of animals testing seropositive and 23.4% displaying clinical signs. However, a later study found lower seroprevalence rates in northwestern regions, including Lombardy, Piedmont, Liguria and Sardinia, where individual seroprevalence was 0.3% and intra-herd prevalence reached 3.9% (Gazzonis et al., 2014). In France, a dairy farm in a non-endemic area recorded an intra-herd seroprevalence of 50% (Genest, 2008). Another northwestern French farm, located in an endemic region,

reported an individual seroprevalence of 33.8%, with 10% of cattle exhibiting clinical signs. A 14-month follow-up study on the same farm revealed a rise in seroprevalence to 89.5%, while the proportion of cattle with clinical signs remained stable (12.3%) (Liénard et al., 2013).

In Portugal, a study in southern regions found that 42% of clinically healthy breeding bulls carried *B. besnoiti* cysts detectable via histopathology (Cortes et al., 2005). Within the Alentejo region, a known endemic area, seroprevalence reached 5.1% at the individual level and 33% within herds (Waap et al., 2014). In Germany, bovine besnoitiosis was first identified in Bavaria, where a naturally infected beef herd exhibited seroprevalence rates between 89.4% and 100%, with clinical prevalence ranging from 23.5% to 36.6% (Gollnick et al., 2018). Similarly, in Croatia, an outbreak affected 42% of cattle in a herd, with 37% showing clinical symptoms (Beck et al., 2013). In Hungary, 12 infected cattle were detected, 10 of which displayed clinical signs, though the rest of the herd was not tested (Hornok et al., 2014). The disease has also been reported in Ireland, where a case report in a dairy farm was confirmed. The study found a seroprevalence of 68%, with ocular conjunctival cysts observed in 50% of infected cattle and vulvar mucosal cysts detected in 68% of females (Ryan et al., 2016). Besnoitiosis has also been identified in Greece, where seroprevalence rates of up to 22% have been detected, although no clinical signs were reported (Papadopoulos et al., 2014). In studies where high seroprevalence is detected in the absence of clinical symptoms, a combination of serological techniques is recommended to provide an accurate estimate of the true disease prevalence.

In Spain, several studies indicate that bovine besnoitiosis is widely distributed across endemic regions. In a cross-sectional study on beef cattle in Navarra, seroprevalence was estimated at 16%, with positive cases concentrated in mountain areas, particularly the Urbasa and Andía mountain ranges and the Pyrenees, where clinical cases had been reported previously (Álvarez-García et al., 2014a). A large-scale analysis of 3,211 cows from 63 herds, along with 587 breeding bulls from the Huesca Pyrenees, revealed seroprevalence rates of 48.7% in males, 51.9% in females and a herd-level prevalence of 87.3% (Gutiérrez-Expósito et al., 2017). A recent study in the Catalan Pyrenees found an individual seroprevalence rate of 25.1% and a herd-level prevalence

of 46% in extensively farmed cattle (Garrido-Castañé et al., 2019). Additionally, in the Sierra de Guadalajara, a study documented seropositivity in 90.8% of females and 71.4% of males, with 43.2% of animals exhibiting clinical signs of either acute or chronic besnoitiosis (Fernández-García et al., 2010). Another outbreak in southwestern Spain found an individual seroprevalence of 40% (Nieto-Rodríguez et al., 2016). With respect to disease incidence, two longitudinal studies have been conducted in endemic areas, each with a four-year observation period, to evaluate the transmission of bovine besnoitiosis in the absence of specific control programs. In Spain, a study in the Urbasa and Andía mountain ranges reported a serological incidence of 23.5 cases per 100 animal-years, with an incidence of clinical signs ranging between 12.5 and 16.7 per 100 animal-years (Gutiérrez-Expósito et al., 2017). A similar study conducted in Bavaria, Germany, documented a higher serological incidence rate (40.5 per 100 animal-years), while the clinical incidence rate remained comparable (16.7 per 100 animal-years) (Gollnick et al., 2018). Both studies highlighted the significant increase in disease transmission in the absence of control strategies.

### 2.5 Diagnosis

Diagnosis of bovine besnoitiosis requires integrating epidemiological data, clinical inspection and laboratory analysis. Characteristic signs of the acute or chronic phases should be identified, keeping in mind that these signs may overlap with other diseases. A differential diagnosis is essential, as acute-phase signs may resemble viral infections (e.g., bluetongue, mucosal disease), allergies or photosensitivity. Chronic-phase signs, meanwhile, may be attributed to fungal (dermatophytosis), viral (lumping skin disease) and parasitic infections (sarcoptic or psoroptic mange), mineral deficiencies, cutaneous lymphoma or benign nodular dermatitis, among others. However, macroscopic cysts in the sclera and vulvar mucosa are pathognomonic of the chronic phase of the disease. For laboratory diagnosis, a skin biopsy from lesion sites (preferably from the perineal region) is recommended to identify tissue cysts via trichinoscopy plates (direct diagnosis). However, this technique has low sensitivity, and a negative result does not rule out infection. A blood sample should also be taken to detect antibodies against *B. besnoiti* (indirect diagnosis). Serological tests can confirm direct diagnostic results and identify subclinically infected animals that lack visible signs and may have low cyst

counts (Florin-Christensen and L. Schnittger, 2018). Among serological tests, ELISAs are widely used for routine diagnosis due to their high sensitivity and specificity, quick turnaround and cost-effectiveness for processing large sample volumes. However, current commercial serological tests, which detect specific IgG antibodies, have limitations because seroconversion in infected animals does not occur until three weeks p.i., hindering acute-phase detection. To address this, an ELISA targeting specific IgM antibodies should be performed, enabling the detection of acute phase besnoitiosis. Paired IgM and IgG detection is recommended for acute-phase diagnosis, as clinical signs in this phase correspond with high IgM levels in the absence of IgG. Conversely, simultaneous detection of both immunoglobulins does not confirm recent infection, as IgM levels persist for years in chronically infected animals. In such cases, an avidity ELISA test, developed by SALUVET (Diezma-Díaz et al., 2020) but not commercially available, can differentiate recent infections based on low IgG avidity. If the ELISA test yields a positive result, management measures should be implemented to prevent disease spread. If the result is negative, it is advisable to confirm the diagnosis using Western blot (WB) analysis. Animals testing negative on both ELISA and WB are considered uninfected. However, discrepancies between serological tests and clinical findings may necessitate retesting three weeks later using WB (**Figure 7**).

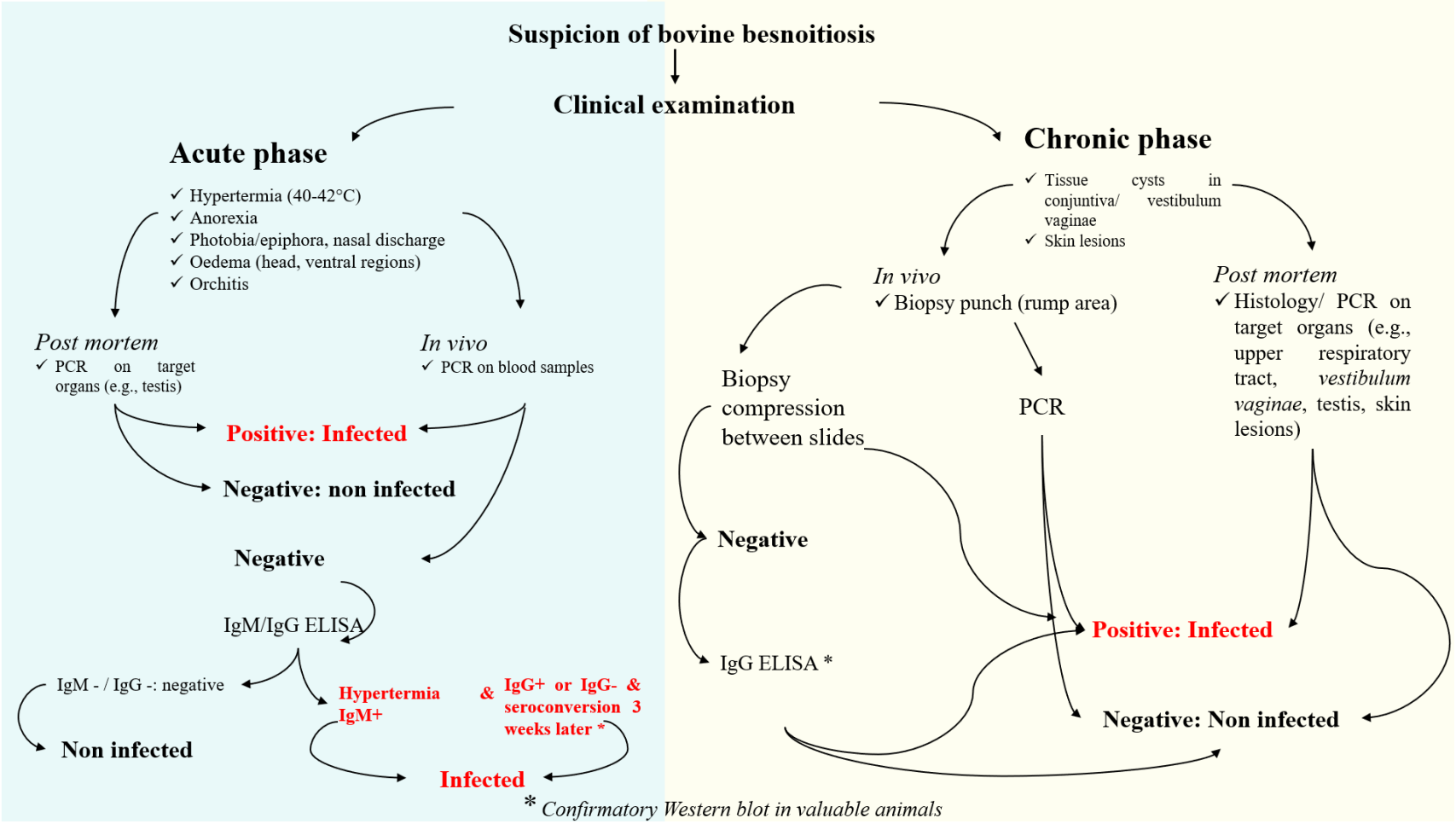


**Figure 7. Diagnosis workflow for bovine besnoitiosis.**

* Source: In M. Florin-Christensen & L. Schnittger (Eds.), *Parasitic protozoa of farm animals and pets* (2018). Springer.

## 2.6 Treatment and control strategies

Currently, no commercial drugs are available for the effective treatment of bovine besnoitiosis. While various compounds have been tested, their effectiveness remains limited, particularly for chronic infections. Experimental studies have primarily focused on antibiotics, antiparasitic drugs and natural compounds, but no therapy has demonstrated consistent efficacy in eliminating the parasite. Research has explored repurposing drugs approved for other protozoan diseases and evaluating new-generation molecules, including calcium-dependent protein kinase (CDPK) inhibitors, nitro-thiazolides and bifenylimidazoazines. Despite promising *in vitro* results, many tested compounds have shown only parasitostatic effects, meaning that they halt parasite replication without eradicating it. The lack of an effective treatment, especially for the chronic stage characterized by bradyzoite-containing tissue cysts, underscores the urgent need for new therapeutic approaches. A summary table of the main treatments evaluated is presented below (**Table 2**).

**Table 2. Experimental treatments for bovine besnoitiosis.**

| Category | Drug/Compound | Test model | Parasite stage targeted | Efficacy | Reference |
|---|---|---|---|---|---|
| **Early treatments** | **Formalin** | *In vivo* (cattle) | Bradyzoites | Partial efficacy, inconsistent results | Franc and Cardiegues, 1999 |
| | **Sulfamethazine** | *In vivo* (cattle) | Tachyzoites | Partial efficacy, inconsistent results | Franc and Cardiegues, 1999 |
| | **Toltrazuril** | *In vivo* (cattle) | Tachyzoites | No proven efficacy | Franc and Cardiegues, 1999 |
| | **Organochlorine compounds** | *In vivo* (cattle) | Bradyzoites | No proven efficacy | Schulz, 1960 |
| **Repurposing drugs** | **Buparvaquone** | *In vitro* (Vero81) | Tachyzoites | Promising activity but no *in vivo* testing; unauthorized for food animals in Europe | Müller et al., 2018 |
| | **Oxytetracycline** | *In vivo* (rabbits, gerbils) | Tachyzoites | Effective at 30 mg/kg (rabbits) and 200 mg/kg (gerbils) but no *in vitro* efficacy | Shkap et al., 1985; 1987 |
| | **Sulfonamides** | *In vivo* (cattle) | Tachyzoites | Temporary clinical improvement, but frequent relapses | Jacquiet et al., 2010 |

| | | | | | |
|---|---|---|---|---|---|
| | **Diclazuril, toltrazuril, decoquinate, imidocarb, sulfadiazine, trimethoprim** | *In vitro* (MARC-145) | Tachyzoites | Dilclazuril and decoquinate showed significant inhibitory effects on the proliferation | Jiménez-Meléndez et al., 2018 |
| | **Turmeric (*Curcuma longa*) extracts** | *In vitro* (BUVEC) | Tachyzoites | IC50 of 5.93 µM, reduced viability and motility | Cervantes-Valencia et al., 2018 |
| **New-generation drugs** | **Arylimidamides** | *In vitro* (Vero81) | Tachyzoites | DB811 and DB750 showed the highest activity | Cortes et al., 2011 |
| | **Nitro-thiazolides (nitazoxanide, brominated derivatives)** | *In vitro* (Vero81) | Tachyzoites | Inhibited proliferation but did not prevent invasion | Moine et al., 2015 |
| | **Bifenylimidazoazines (Compound 8e)** | *In vitro* (Human fibroblasts) | Tachyzoites | IC50 of 0.37 µM, effective at low concentrations | Moine et al., 2015 |
| | **CDPK Inhibitors (1294, 1517, 1553, 1571)** | *In vitro* (MARC-145) | Tachyzoites | Inhibited >90% of invasion and proliferation, but parasitostatic | Jiménez-Meléndez et al., 2017 |
| | **Endochin-like quinolones (ELQs)** | *In vitro* (HFF) | Tachyzoites | Substantial delay in parasite proliferation | Eberhard et al., 2020 |

## 2.7 Experimental models for *B. besnoiti* infection

Experimental models, both *in vitro* and *in vivo*, are essential for understanding the biology, pathogenesis and potential treatment strategies for intracellular protozoan parasites. These models provide controlled environments that allow researchers to study parasite replication and host-parasite interactions. Furthermore, experimental models play a crucial role in identifying and evaluating new diagnostic tools, therapeutic compounds and disease control strategies, accelerating the development of effective intervention measures for parasitic infections.

As an obligate intracellular parasite, *B. besnoiti* requires host cells for survival and replication, making *in vitro* models indispensable for its study. Primary and immortalized cell cultures have proven to be powerful tools for investigating the parasite's growth, invasion mechanisms and interaction with host cells. Extensive research on *T. gondii* has provided key insights into the biology of cyst-forming protozoa, helping to decipher host-parasite interactions and immune evasion strategies and has thus served as a model for studying related apicomplexan parasites (Kim and Weiss, 2004).

While *in vitro* models have been instrumental in elucidating *B. besnoiti* biology, *in vivo* models remain necessary for studying disease progression, immune responses and treatment efficacy in a whole-organism context. Animal models allow researchers to reproduce the natural infection dynamics, providing valuable information on parasite dissemination, tissue tropism and immune modulation. They also serve as critical platforms for evaluating drug efficacy and vaccine candidates under conditions that closely resemble those found in naturally infected cattle. Together, *in vitro* and *in vivo* models offer complementary approaches to studying *B. besnoiti*, each contributing to a comprehensive understanding of the parasite's biology and pathogenesis.

## *In vitro* models

### Cell-based models

*In vitro* models are based on two-dimension (2D) or three-dimension (3D) cultures of primary or immortalized cells and tissues. *In vitro* research has many advantages over *in vivo* research. Well-established cell culture models provide a valuable tool because they are inexpensive, highly scalable and allow for the study of specific cellular targets (Rosa et al., 2021). Moreover, they represent an alternative to *in vivo* models, avoiding the ethical issues of laboratory animal use. In spite of this, they also have some limitations directly associated with the study of Toxoplasmatinae: i) inability to reproduce the complete biological cycle of the parasite; ii) there is no standardised cell culture model or reference parasite isolates to make the different studies comparable; iii) there is no uniform methodology for quality control of cell cultures; and iv) immortalised cell lines have generally been used from tissues other than the parasite target tissues (Diezma-Díaz et al., 2019).

In this sense, several *in vitro* models have been developed obtaining *B. besnoiti* isolates from clinical cases to study the essential processes in the lytic cycle of the parasite in non-bovine and bovine cell lines. *Besnoitia besnoiti in vitro* cell-based models are summarised in **Table 3**.

**Table 3. *In vitro* cell-based models for *B. besnoiti.***

| Cell type | Cell line | Animal origin | Tissue | Cell type | Reference |
|---|---|---|---|---|---|
| **Immortalized** | **BHK** | Hamster | Kidney | Fibroblast | Neuman, 1974 |
| | **HeLa** | Human | Cervix | Epithelial | Neuman, 1974 |
| | **BHK (21)** | Hamster | Kidney | Fibroblast | Schares et al., 2009 |
| | **NA42/13** | Bovine | Endothelium | Endothelial cells | Schares et al., 2009 |
| | **KH-R** | Bovine | Embryonic heart | Fibroblast | Schares et al., 2009 |
| | **Vero81** | African green monkey | Kidney | Epithelial cells | Schares et al., 2009 |
| | **MARC-145** | Monkey | Kidney | Epithelial cells | Fernández-García et al., 2009b |
| | **CRFK** | Cat | Kidney | Epithelial | Gobel et al., 1985 |
| | **RML-15** | Tick | Embryonic/adult cells | Embryonic/ adult cells | Samish et al., 1988 |
| | **L929** | Mouse | Subcutaneous connective tissue | Fibroblast | Shkap et al., 1987 |
| | **BEK** | Bovine | Embryo kidney | Epithelial | Shkap et al., 1987 |
| | **MDBK (Madin-darby bovine kidney)** | Bovine | Kidney | Epithelial | Shkap et al., 1987 |
| | **Bovine lymphoblastoid cells (co-infected with *Theileria annulata*)** | Bovine | Lymphoid tissue | Lymphocytes | Shkap et al., 1987 |
| **Primary** | **HFF** | Human | Prepuce | Fibroblast | Frey et al., 2016 |
| | **HFF** | Human | Prepuce | Fibroblast | Jiménez-Meléndez et al., 2017 |
| | **FLK (Foetal lamb kidney)** | Ovine | Kidney | Epithelioid | Bigalke and Naude, 1962 |
| | **BL (Thyroid cultures)** | Ovine | Thyroid | Epithelial | Neuman, 1974 |
| | **BAEC** | Bovine | Aorta | Endothelial | Jiménez-Meléndez et al., 2019 |
| | **Primary bovine aorta fibroblasts (PBAF)** | Bovine | Aorta | Fibroblast | Jiménez-Meléndez et al., 2019 |
| | **BUVEC** | Bovine | Umbilical cord | Endothelial | Maksimov et al., 2016 |

In addition, *in vitro* models play a fundamental role in parasitology by enabling the isolation, culture and long-term propagation of parasite strains or isolates from infected animals. They are essential for studying parasite biology, life cycle progression, host–parasite interactions, virulence mechanisms and immune evasion

strategies. Moreover, *in vitro* systems provide a controlled platform for evaluating drug efficacy, assessing cytotoxicity and screening potential therapeutic compounds, thereby contributing significantly to the development of novel control strategies.

For *B. besnoiti*, *in vitro* isolation has been performed using bradyzoites from mature tissue cysts extracted from skin or vaginal biopsies of chronically infected animals. These bradyzoites are liberated through mechanical (Potter-Elvehjem tissue homogenizer) or enzymatic (trypsin) disruption before inoculation onto cell monolayers, such as MARC-145 (Fernández-García et al., 2009b; Gentile et al., 2012; Frey et al., 2016) or Vero81 cells (Schares et al., 2009). An alternative approach, like that used for *N. caninum* and *T. gondii*, involves pre-inoculating IFN-γ knockout mice (e.g., *B6.129S7-Ifngtm1Ts/J* strain, Jackson Laboratories) with tissue cyst contents, typically via intraperitoneal injection, before transferring the parasite to cell culture (Schares et al., 2009; Gentile et al., 2012). This method enhances the chances of successful parasite propagation and has been instrumental in advancing *B. besnoiti* research. *Besnoitia besnoiti* isolates are summarised in **Table 4**.

**Table 4. *Besnoitia besnoiti* isolates.**

| Isolate | Country | Animal | Type of infection | *In vitro* culture | Use in experimental infections | Reference |
|---|---|---|---|---|---|---|
| Impala strain | South Africa | Antelope | Chronic | No | Rabbit | Bigalke, 1968 |
| Bb-Fuls strain | South Africa | Cattle | Acute | Yes | Cattle, rabbit, mouse | Shkap et al., 1987 |
| Bb-Schoeman strain | South Africa | Cattle | Acute | No | Rabbit, mouse | Bigalke, 1968 |
| Bb-Lamprechts A strain | South Africa | Cattle | Acute | No | Cattle, rabbit, mouse | Shkap et al., 1987 |
| Bb-Lamprechts B strain | South Africa | Cattle | Chronic | No | Cattle, rabbit, mouse | Shkap et al., 1987 |
| Bb-Wildebeest | South Africa | Antelope | Chronic | Yes | Cattle, rabbit, mouse | Shkap et al., 1987 |
| Bb-Israel | Israel | Cattle | Chronic | Yes | Cattle, mouse | Shkap et al., 1987 |
| Bb1-Evora03 | Portugal | Cattle | Chronic | Yes | No | Cortes et al., 2006 |
| Bb1-Evora04 | Portugal | Cattle | Chronic | Yes | No | Muñóz-Caro et al., 2014 |
| Bb-Lisbon14 | Portugal | Cattle | Chronic | Yes | No | Ramakrishnan et al., 2022 |
| Bb-Spain1 | Spain | Cattle | Chronic | Yes | No | Fernández-García et al., 2009b |
| Bb-Spain2 | Spain | Cattle | Chronic | Yes | No | Unpublished |
| Bb-Spain3 | Spain | Cattle | Chronic | Yes | Cattle | Diezma-Díaz et al., 2017 |
| Bb-Ger1 | Germany | Cattle | Chronic | Yes | Guinea pig, cat, dog, mouse | Schares et al., 2009 |
| Bb-IPZ-2-G CH | Germany | Cattle | Chronic | Yes | mouse | Basso et al., 2013 |
| Bb-France | France | Cattle | Chronic | Yes | mouse | Liénard et al., 2015 |
| Bb-IPZ-1-G CH | France | Cattle | Chronic | Yes | No | Basso et al., 2013 |
| Bb-Italy1 | Italy | Cattle | Chronic | Yes | No | Gentile et al., 2012 |
| Bb-Italy2 | Italy | Cattle | Chronic | Yes | No | Frey et al., 2016 |
| Bb-IPZ-3-G CH | Switzerland | Cattle | Chronic | Yes | No | Basso et al., 2013 |

Significant progress has been made in understanding *B. besnoiti* biology; however, many challenges persist in achieving a comprehensive understanding of host-pathogen interactions. One major limitation is that the existing *in vitro* models are predominantly based on 2D cell culture systems. It is known that these models modify the tissue-specific architecture (forced polarity, flattened cell shape), mechanical/biochemical signals and subsequent cell-to-cell communication and therefore do not fully reflect the essential physiology of natural infections (Hoarau-Véchot et al., 2018). There is a need to implement new technologies such as 3D tissue and organoid models, 3D tissue printing, *ex vivo* models (bovine skin) and other novel technology approaches that may provide tools to develop successful and correlating *in vitro* systems that are of particular interest for apicomplexan research.

In addition, the *in vitro* transformation of *B. besnoiti* from the tachyzoite to the bradyzoite stage has not yet been achieved, unlike in other apicomplexan parasites such as *T. gondii* (Mayoral et al., 2020; Christiansen et al., 2022) and *N. caninum* (Risco-Castillo et al., 2004). This limitation hinders the study of the chronic phase of the disease, preventing researchers from fully understanding bradyzoite development, persistence and reactivation mechanisms.

### *In vivo* models

*In vitro* models limitations led to a rapid development of multiple *in vivo* models. *In vivo* models closely resemble the parasite natural infection and represent a good alternative to carry out vaccine and therapeutic trials, as well as to study chronic infection and cyst burden, pathophysiological processes, early-stage biomarkers and immune response (Sitali et al., 2022). Currently, no established or widely accepted animal infection model for *B. besnoiti* exists that accurately reproduces both the acute and chronic phases of the disease while adhering to the necessary standards for an animal model. Despite these limitations, many experimental infections have provided valuable insights into key factors related to both the parasite and the host.

Between the 1960s and 1980s, several experimental infections were conducted, though these studies were carried out under highly variable conditions, making comparisons difficult. The lack of standardized experimental designs -such as varying parameters, sampling frequency, animal group sizes (often consisting of just one animal per group) and durations- and the reliance on clinical inspections and histopathological methods (without the availability of serological and molecular techniques) significantly hampered the reproducibility of their results. Nonetheless, the researchers offered detailed descriptions of their findings, noting challenges in reproducing besnoitiosis (Bigalke, 1968; Basson et al., 1970; Diesing et al., 1988; Shkap and Pipano, 1993).

### *In vivo* models in laboratory animals

An ideal infection model for *B. besnoiti* in experimental animals would replicate both the acute and chronic phases of infection, making it valuable for preliminary drug and vaccine testing. Such a model would be easier to handle, have shorter study durations and incur lower costs. However, while various laboratory rodent species (gerbils, rats, hamsters, different strains of mice) have been used in experimental infections, they have not successfully reproduced the chronic phase of the disease. Only gerbils (*Meriones tristami*) have shown some susceptibility and have been used in immunization trials (Shkap, 1986; Shkap and Pipano, 1993). IFN-γ-deficient mice, which exhibit an acute disease course due to the critical role of cellular immunity in protection against these parasites, have been used for parasite isolation studies from chronically infected cattle (Schares et al., 2009; Gentile et al., 2012), though their utility as a model is limited (Diezma-Díaz et al., 2019).

Rabbits, in contrast, have exhibited higher susceptibility to *B. besnoiti* infection. Inoculating both tachyzoites and bradyzoites has successfully induced signs consistent with the acute phase of the disease, such as fever, lymphadenitis, oedema in the limbs or scrotum, conjunctivitis and photophobia in severe cases (Bigalke, 1967; 1968; Basson et al., 1970; Bigalke et al., 1974; Shkap, 1986; Basso et al., 2011; Liénard et al., 2015).

Notably, bradyzoite inoculation has provided the most promising results in replicating the chronic phase of the disease in rabbits, marked by the detection of cysts in histology, parasite DNA presence in various tissues and seroconversion around 2-3 weeks post-inoculation (Basso et al., 2011; Liénard et al., 2015; Sharif et al., 2019). However, the variability in the inoculum used and the lack of consistent experimental methods have hindered the development of a standardized experimental model in rabbits, preventing its use as a preliminary step before studies in the target species, cattle. **Table 5** summarizes experimental infections of *B. besnoiti* in laboratory mice and **Table 6** summarizes experimental infections of *B. besnoiti* in rabbits.

## Table 5. Experimental infections of *B. besnoiti* in laboratory mice.

| Animal | Nª | Inoculated stage | Inoculum origin | Dose | Route | Acute phase | Chronic phase | Parasite detection (Technique) | Survival (%) | Observations | Reference |
|---|---|---|---|---|---|---|---|---|---|---|---|
| Gerbil (*Meriones tristrami*) | 6 | Tz | Cell culture | $10^7$ | IP | Anorexia, cachexia and death (6-8 days p.i.) | - | +, Peritoneal fluid (Smear) | 0 | - | Shakp, 1986 |
| Gerbil (*M. tristrami*) | 84 | Tz | Cell culture | 10-$10^7$ | IP | ND | - | - | 56 | Immunization assays | Shakp and Pipano, 1993 |
| Gerbil (*M. tristrami*) | 84 | Tz | Cell culture | 10-$10^7$ | SC | Palpable nodules (Injection site) | - | ND | 100 | - | Shakp and Pipano, 1993 |
| Gerbil (*Meriones unguiculatus*) | 3 | Tz | Cell culture | 5 x $10^5$ | SC | - | - | +, Parasitaemia (ITS1-PCR) | 100 | Seroconversion (3 weeks p.i.) | Basso et al., 2011 |
| Gerbil (*M. unguiculatus*) | 3 | Bz | Bovine | 5 x $10^5$ | SC | - | - | - | 100 | - | Basso et al., 2011 |
| Hamster (*Cricetus auratus*) | 3 | Tz | Cell culture | $10^7$ | OIP | - | - | - | 100 | - | Shkap, 1986 |
| Hamster (*C. auratus*) | 3 | ND | Rabbit/ Hamsters | ND | oral | Diarrhea and weakness | - | +, Peritoneum and lung (ND) | S | Immunosuppression (cortisone) | Bigalke, 1968 |
| Hamster (*C. auratus*) | 2 | Tz | Rabbit blood | 20 ml | IP | - | - | - | 100 | - | Pols, 1960 |
| Guinea pig (*Cavia porcellus*) | 5 | Tz | Cell culture | $10^7$ | IP | - | - | - | 100 | - | Shkap, 1986 |
| Guinea pig (*C. porcellus*) | 16 | Tz | Rabbit blood | 20-30 ml | IP/SC | Intermittent fever | - | +, Parasitaemia (Smear) | 100 | - | Pols, 1960 |
| Guinea pig (*C. porcellus*) | 3 | Tz | Cell culture | 5 x $10^5$ | SC | - | - | - | 100 | - | Basso et al., 2011 |
| Guinea pig (*C. porcellus*) | 3 | Bz | Bovine | 5 x $10^5$ | SC | - | - | - | 100 | - | Basso et al., 2011 |
| Mouse (*Mus musculus*) | 6 | ND | Bovine blood | 10-20 ml | IP/SC | - | - | - | 100 | - | Pols, 1960 |
| Mouse (*M. musculus*) | 16 | Tz | Rabbit blood | 10-20 ml | IP/SC | - | - | - | 100 | - | Pols, 1960 |
| Mouse (*M. musculus*) | 6 | Tz | Cell culture | $10^7$ | IP | - | - | - | 100 | - | Shkap, 1986 |
| Mouse BALB/C | 6 | Tz | Cell culture | $10^7$ | IP | - | - | - | 100 | - | Shkap, 1986 |
| Mouse C57BL/6 | 6 | Tz | Cell culture | $10^7$ | IP | - | - | - | 100 | - | Shkap, 1986 |

| | | | | | | | | | | | |
|---|---|---|---|---|---|---|---|---|---|---|---|
| Mouse IFN-γ knockout | 2 | Bz | Bovine | $10^8$ | IP | Apathy and ruffled fur | - | +, Peritoneal fluid, skin and tissues (qPCR) | 0 | Isolation assays | Gentile et al., 2012 |
| Mouse IFN-γ knockout | 6 | Tz/ Bz | Bovine/Rat | ND | IP | Apathy and ruffled fur | - | +, Peritoneal fluid, skin and tissues (Histology, PCR) | 0 | - | Schares et al., 2009 |
| Rat (*Rattus rattus*) | 6 | Tz | Rabbit blood | 20 ml | IP/SC | - | - | - | 100 | - | Pols, 1960 |
| Rat (*R. rattus*) | 8 | Tz | Cell culture | $10^7$ | IP | - | - | - | 100 | - | Shkap, 1986 |

**a:** N: Total number of inoculated animals.

**Tz**: Tachyzoite

**Bz**: Bradyzoite

**IP:** Intraperitoneal.

**SC:** Subcutaneous.

**OIP:** Oculo-Intranasal-Pharyngeal

**ND:** Not determined.

**p.i.:** Post-infection.

**mL:** Millilitres.

**S:** Sacrificed.

**- :** Absent.

**+ :** Positive

## Table 6. Experimental infections of *B. besnoiti* in laboratory rabbits.

| | Inoculum source | Dose | Route | N[a] | Days[b] | Acute phase | Chronic phase | Parasite detection (technique) | Survival (%) | Observations | Reference |
|---|---|---|---|---|---|---|---|---|---|---|---|
| Tz | Rabbit blood | 20 ml | IP | 3 | ND | - | - | - | 100 | - | Bigalke, 1967 |
| | Bovine blood | 25 ml | IP | 2 | ND | - | - | - | 100 | - | Bigalke, 1967 |
| | Antelope isolate | ND | IP | 8 | 14-40 | Lymphadenitis and epididymitis | Skin lesions | +, Reproductive system, myocardium, spleen (Histology) | 87,5 | - | Basson et al., 1970 |
| | Cell culture | ND | IP | 8 | 7-39 | Lymphadenitis and epididymitis | Skin lesions | +, Reproductive system, myocardium, veins, spleen, lung (Histology) | 100 | - | Basson et al., 1970 |
| | Cell culture | $10^7$ | IP | 6 | 90 | Fever, conjunctivitis, testicular swelling | - | - | 100 | - | Shakp, 1986 |
| | Cell culture | $10^4$ | SC | 5 | 60 | High fever († 11 days p.i.) | - | - | 80 | - | Bigalke et al., 1974 |
| | Cell culture | $10^3$-$10^7$ | SC | 26 | 60-180 | † (10-25 days p.i.) | - | - | 38,4 | Immunization trials | Bigalke et al., 1974 |
| | Cell culture | $2\times10^5$ | SC | 10 | 30 | - | - | - | 90 | - | Bigalke et al., 1974 |
| | Cell culture | $10^5$ | SC | 10 | 90 | High fever († 14 days p.i.) | - | - | 70 | - | Bigalke et al., 1974 |
| | Cell culture | 10-$10^5$ | SC | 25 | 60 | † (21-30 days p.i.) | - | +, Spleen (ND) | 68 | - | Bigalke et al., 1974 |
| | Cell culture | $5\times10^6$ | SC | 3 | 21 | Fever, conjunctivitis, testicular oedema | - | +, Parasitaemia (ITS1-PCR) | 100 | Seroconversion (3 weeks pi) | Basso et al., 2011 |
| | Cell culture | $6\times10^6$ | SC | 6 | 70 | - | - | +, Parasitaemia (qPCR) | 100 | Seroconversion (21 days pi) | Liénard et al., 2015 |
| Bz | Bovine | 3-10 ml | SC | 7 | 9-13* | Fever, oedema in scrotum, prepuce and limbs | Skin cysts, necrosis in scrotum | +, Parasitaemia (ND) | 85,7 | - | Bigalke, 1967 |
| | Bovine | 7-10 ml | IP | 4 | 9-20* | Fever, oedema in scrotum, prepuce and limbs | Skin cyst | +, Parasitaemia (ND) | 100 | - | Bigalke, 1967 |
| | Bovine | ND | CO | 3 | 13* | - | Skin cyst | - | 100 | - | Bigalke, 1968 |
| | Bovine | ND | IN | 2 | 10* | - | - | +, (ND) | 100 | - | Bigalke, 1968 |
| | Bovine | ND | SC | 1 | 20 | Lymphadenitis, epididymitis | Skin lesions | (**) | 100 | - | Basson et al., 1970 |
| | Antelope isolate | ND | SC | 6 | 24-100 | Lymphadenitis | Skin lesions | (**) | 100 | - | Basson et al., 1970 |

| | | | | | | | | | | | |
|---|---|---|---|---|---|---|---|---|---|---|---|
| | Bovine | $5\times10^{5}$ | SC | 3 | 21* | Fever, conjunctivitis and testicular oedema | - | +, Parasitaemia (ITS1-PCR) | 100 | Seroconversion (3 weeks pi) | Basso et al., 2011 |
| | Bovine | $6\times10^{6}$ | SC | 6 | 70 | Fever, photophobia, nasal discharge | Skin cysts and other tissues | +, Parasitaemia and cysts (Histology, qPCR) | 100 | Seroconversion (14 days pi) | Liénard et al., 2015 |
| | *Stomoxys calcitrans* | - | B | 3 | 152 | Fever (7-12 days p.i.) | - | +, Parasitaemia (qPCR) | 100 | Seroconversion (14 days pi) | Sharif et al., 2019 |
| **Tz/Bz** | Tachyzoite/bradzyzoite | 10-18 ml | IP | 5 | ND | Fever, oedema in scrotum and prepuce | Cysts | +, Parasitaemia (ND) | 60[h] | - | - |
| | Bovine/Rabbit | 10 ml | IV | 1 | ND | - | - | - | 100 | - | Bigalke, 1967 |
| | Bovine/Rabbit | 10 ml | SC | 5 | 11-12* | - | - | - | 60[h] | - | - |
| **ND** | Infected bovine blood | 30 ml | IV | 1 | 11* | † | - | 0 | - | - | |
| | Infected bovine blood | 50 ml | IP | 1 | 11* | Oedema in limbs, base of ears and scrotum | - | +, Parasitaemia (Frotis) | 0 | - | Pols, 1960 |
| | Infected bovine blood | 100 ml | SC | 1 | 14* | - | - | ND | - | - | |

**a**. Total number of inoculated animals.

**b**. Duration of the trial (days).

***** : Incubation period.

**Tz**: Tachyzoite

**Bz**: Bradyzoite

**IP**: Intraperitoneal.

**SC**: Subcutaneous.

**CO**: Cutaneous

**IV**: Intravenous.

**B**: Bites.

**ND**: Not determined.

**p.i.**: Post-infection.

**-** : Absent.

**+** : Positive.

**mL**: Millilitres.

†: Death.

**(**) :** Reproductive system, myocardium, veins, spleen and lung (Histology)

### *In vivo* models in cattle

An animal model of *B. besnoiti* infection in cattle, or at least in another ruminant host, which replicates both acute and chronic besnoitiosis clinical signs, would be ideal for testing therapeutic candidates that have already been analysed in laboratory animals or *in vitro* systems. As previously mentioned, findings from *in vitro* studies or laboratory animal models are not always directly applicable to the target species. In many cases, the immune response to the pathogen differs significantly across species. Therefore, while laboratory models are valuable for preliminary drug screenings, these results must be validated in the target species as a final step.

Between the 1960s and 1980s, multiple experimental infections in cattle were conducted. However, the outcomes were highly variable and difficult to compare, primarily due to differing inoculum and experimental designs (often involving only one animal per experimental group). Furthermore, issues such as lack of inoculum quality control, potential contamination with other bovine pathogens, unknown animal health status and varying ages of inoculated animals complicated the standardization of the infection model. The acute phase of the disease was repeatedly induced with various inoculum (Bigalke, 1968; Basson et al., 1970; Janitschke et al., 1984; Shkap, 1986; Diesing et al., 1988). However, to induce the chronic phase with moderate severity, immunosuppressive treatments (such as splenectomy or corticosteroid administration) were necessary (Bigalke, 1968; Basson et al., 1970). In contrast, inoculating bradyzoites successfully induced the chronic phase in some trials. Bigalke et al. (1968) reported the presence of cysts in the ocular conjunctiva following intranasal or vector-borne bradyzoite inoculations. Later, Diesing et al. (1988) demonstrated the chronic phase in animals treated with corticosteroids prior to bradyzoite inoculation. Immunosuppressing animals induced clinical signs, but this approach may not be ideal for developing an animal model due to the increased risk of environmental infections in immunocompromised animals.

In addition, recent studies have investigated the effects of parasite dose and host age on the infection dynamics of *B. besnoiti* tachyzoites in cattle. In two independent experiments, calves and bulls were inoculated intravenously with varying doses of tachyzoites and clinical signs of both acute and chronic besnoitiosis were

monitored. While infected animals developed mild to moderate signs of acute besnoitiosis, including lymphadenopathy and fever, they did not show typical signs or macroscopic lesions of chronic besnoitiosis. However, parasite DNA was detected in select tissues, such as the conjunctiva, ocular sclera, epididymis and skin and a tissue cyst along with mild microscopic lesions were observed in some cases (Diezma-Díaz et al., 2018). Building on this, another study tested subcutaneous and intradermal inoculation routes with the aim of inducing macroscopic lesions associated with the chronic stage. Calves infected via these routes displayed mild to moderate acute disease, including lymphadenopathy and sporadic fever, but no characteristic chronic macroscopic lesions. Moreover, the study revealed subtle differences in immune response kinetics based on inoculation route, suggesting that early innate immune mechanisms play a role in shaping disease outcomes (Diezma-Díaz et al., 2019). To further refine the model, a more recent study explored the effects of the parasite stage (bradyzoite) and inoculation route on the clinical and pathological outcomes. In this study, calves were inoculated with *B. besnoiti* bradyzoites via intravenous, subcutaneous or intradermal routes. While the acute stage was mild to moderate across all groups, the chronic stage showed notable differences. Pathognomonic conjunctival cysts appeared in all infected calves after 40 days p.i., with the intradermal group exhibiting more severe clinical signs, including skin lesions and a higher parasite load in tissues. These findings highlight that both the parasite stage and the inoculation route are critical variables influencing the progression of chronic besnoitiosis, with the intradermal route producing the most severe manifestations (Diezma-Díaz et al., 2020).

Additionally, the histological findings associated with *B. besnoiti* infection were exhaustively studied in target tissues from experimentally and chronically infected calves, providing new insights into the disease's pathology. Tissue cysts, which were most abundant in the intradermal group, were primarily observed in the skin (including the scrotum, nostrils and nasal turbinates) and measured an average diameter of 181.2 µm. Lesions associated with both acute (e.g., thrombi, oedema and inflammation) and chronic besnoitiosis (e.g., hyperkeratosis, dilated sweat glands and vascular damage) coexisted. Vascular damage and inflammation were most frequently detected in the skin, followed by reproductive tissues, such as the testicular parenchyma, epididymis and pampiniform plexus. Importantly, while lesions indicated subclinical chronic besnoitiosis, they were not expected to impair fertility, as the seminiferous

epithelium remained unaffected (Diezma-Díaz et al., 2020). A summary of experimental infections with *B. besnoiti* in cattle is presented in **Table 7**.

**Table 7. Experimental infections of *B. besnoiti* in cattle.**

| Isolate | Inoculum source | Inoculum | Dose | Route | Sex | Breed | Age | Immune suppression | Acute | Chronic | Parasite detection | Reference |
|---|---|---|---|---|---|---|---|---|---|---|---|---|
| Lamprechts A and B | Rabbit | Tz | ND | Oral | Male | Holstein | 2-3 years | No | Mild | Mild | +, Cysts in conjunctiva | Bigalke, 1968 |
| Lamprechts A and B | Rabbit | Tz | 2.7-14 x $10^7$ | IV | Male | ND | 3 years | No | Mild | Mild | - | Bigalke, 1968 |
| Lamprechts A and B | Rabbit | Tz | ND | IV | Female | Hereford | ND | No | Moderate | Severe | +, Parasitaemia, cysts in the sclera, skin and veins | Bigalke, 1968 |
| Fuls strain (Low passage) | Cell culture | Tz | $10^4$ - $10^7$ | IV | Female | Hereford | 7 years | Yes | Severe | - | ND | Basson et al., 1970 |
| Fuls strain (Low passage) | Cell culture | Tz | 984.9 x $10^6$ | IV | Male | South Devon Afrikaner | 1 year | No | Mild | Mild | +, Parasitaemia, cysts in the sclera, skin and veins | Basson et al., 1970 |
| Fuls strain (Low passage) | Cell culture | Tz | 1068 x $10^6$ | IV | Male | Hereford | 3 years | Yes | Moderate | Severe | +, Parasitaemia, cysts in the sclera, skin and veins | Bigalke, 1968 |
| Fuls strain (Low passage) | Bovine blood | Tz | 3.5-41 | IV | Male | Hereford | 2-3 years | No | Moderate | Moderate | +, Parasitaemia, cysts in the sclera, skin and veins | Basson et al., 1970 |
| Fuls strain (High passage) | Cell culture | Tz | 46.75-66.4 x $10^6$ | IV | Male | ND | 2 years | No | Mild | - | ND | Bigalke, 1968 |
| Fuls strain (High passage) | Cell culture | Tz | 106.56 x $10^6$ | SC | Male | ND | 3 years | No | Mild | - | ND | Bigalke, 1968 |
| Fuls strain (High passage) | Rabbit | Tz | 141.75 x $10^6$ | IV | Male | Hereford | 3 years | No | Severe | - | +, Parasitaemia | Bigalke, 1968 |
| Fuls strain (High passage) | Bovine blood | Tz | 41 | IV | Male | ND | ND | No | Mild | - | +, Cysts in skin and veins | Basson et al., 1970 |
| Bb-Israel | Cell culture (Vero81) | Tz | $10^6$- 7.6 x $10^6$ | IV, IM, SC | Male | Holstein | >1 year | No | Mild | - | +, (IF) | Shkap, 1986 |
| Bb-Israel | Bovine blood | Tz | 1L | IV | Male | Holstein | >1 year | Yes | Mild | - | +, (IF) | Shkap, 1986 |
| Niu strain | Rabbit blood | Tz | 50 ml | IV | Male | Hereford | 3-6 years | No | - | - | ND | Bigalke, 1967 |
| Niu strain | Rabbit blood | Tz | 40-80 ml | SC, IV | Male | Hereford | 3-6 years | No | - | - | ND | Bigalke, 1967 |
| ND | Cell culture (MDBK) | Tz | 3.7 x $10^8$ | SC | ND | Holstein | 3-6 months | Yes | Mild | - | ND | Diesing et al., 1988 |
| ND | Hamsters | Tz | 4 x $10^7$ | IP | ND | ND | >1 year | Yes | Severe | - | +, Parasitaemia | Diesing et al., 1988 |
| Bb-Spain3 | Cattle | Tz | $10^6$, $10^7$, $10^8$ | IV | Male | Holstein | 2 months | No | Mild | - | +, Parasitaemia | Diezma-Díaz et al., 2018 |
| Bb-Spain3 | Cattle | Tz | $10^6$ | SC, ID | Male | Holstein | 3 months | No | Mild | | +, Tissue samples | Diezma-Díaz et al., 2019 |

| | | | | | | | | | | | | |
|---|---|---|---|---|---|---|---|---|---|---|---|---|
| Nu/Impala | Tissue cysts | Bz | 1.8-5.4 x $10^7$ | SC, IV | ND | Crossbreed | <1 year | No | Mild | - | +, Parasitaemia | Bigalke, 1967 |
| Nu/Impala | Tissue cysts | Bz | ND | SC, IV | Female | ND | ND | No | - | - | ND | Besnoit and Robin, 1912 |
| Nu/Impala | Tissue cysts | Bz | ND | Oral | Male and female | ND | ND | No | - | - | ND | Bigalke, 1968 |
| Nu/Impala | Tissue cysts | Bz | 2.2-4.2 x $10^6$ | IN | Male | ND | 2-3 years | No | Mild | Mild | +, Cysts in conjunctiva and veins | Bigalke, 1968 |
| Nu/Impala | Tissue cysts | Bz | 2.3 x $10^6$ | SC, IV | ND | ND | 2 years | No | Mild | - | - | Bigalke, 1968 |
| Nu/Impala | *Glossina* bites | Bz | ND | SC | Male | ND | ND | No | Mild | Mild | +, Cysts in conjunctiva | Bigalke, 1968 |
| Nu/Impala | *Stomoxys* bites | Bz | ND | SC | Male | ND | ND | No | Moderate | - | - | Bigalke, 1968 |
| Nu/Impala | 2 *Tabanus* bites | Bz | ND | SC | Male | ND | 2 years | No | Mild | Mild | +, Cysts in conjunctiva | Bigalke, 1968 |
| Nu/Impala | 6 *Tabanus* bites | Bz | ND | SC | Male | ND | 3 years | No | - | - | - | Bigalke, 1968 |
| Bovine | 6 *Tabanus* bites | Bz | ND | SC | ND | ND | ND | No | Moderate | Mild | +, Cysts in conjunctiva and skin | Bigalke, 1968 |
| Bovine | ND | Bz | ND | IP | ND | Holstein | 3-6 months | Yes | Moderate | Moderate | +, Connective tissue | Diesing et al., 1988 |
| Bovine | ND | Bz | ND | IP | ND | Holstein | 3-6 months | No | Mild | - | - | Diesing et al., 1988 |
| Bovine | ND | Bz | ND | SC, IV | ND | Holstein | 3-6 months | Yes | Moderate | Moderate | +, Connective tissue | Diesing et al., 1988 |
| Bovine | ND | Bz | ND | IP | ND | Holstein | 3-6 months | No | - | - | - | Diesing et al., 1988 |
| Bovine | Tissue cysts | Bz | ND | SC, IV | ND | ND | Adult | Yes | Severe | - | +, Parasitaemia | Diesing et al., 1988 |
| Bovine | Tissue cysts | Bz | ND | IV | ND | ND | Adult | Yes | Moderate/ Severe | - | +, Parasitaemia | Diesing et al., 1988 |
| Bovine | Tissue cysts | Bz | ND | IV | ND | ND | Adult | Yes | Severe | - | +, Parasitaemia | Diesing et al., 1988 |
| Bovine | Tissue cysts | Bz | ND | IV | ND | ND | Adult | Yes | Moderate/ Severe | - | +, Parasitaemia | Diesing et al., 1988 |
| Bovine | Tissue cysts | Bz | ND | IP | Male | Holstein | >1 year | No | Mild | - | +, (IF) | Diesing et al., 1988 |
| Bovine | Tissue cysts | Bz | 10^6 | SC, ID, IV | Male | Holstein | 3 months | No | - | Mild | +, Parasitaemia, cysts in the conjunctive and histology | Diezma-Díaz et al., 2017 |

**Tz:** Tachyzoite

**Bz:** Bradyzoite

**SC:** Subcutaneous

**IP:** Intraperitoneal

**ID:** intradermal

**IN**: intranasal

**IV:** Intravenous

**IF**: Immunofluorescence

**ND:** Not determined

**+** : positive

**-** : negative

## 2.8 Host-pathogen interactions

Understanding the host–pathogen interaction mechanisms of *B. besnoiti* is essential to decipher its pathogenesis, persistence and tissue tropism. The first standardized study of the *B. besnoiti* lytic cycle was conducted by Frey et al. (2016) using MARC-145 cells, a non-bovine monkey kidney epithelial cell line. This work evaluated seven *B. besnoiti* isolates and one *B. tarandi* isolate. Unlike its closely related apicomplexan parasites *T. gondii* and *N. caninum*, *B. besnoiti* displays notably slow and asynchronous invasion and proliferation dynamics. During the invasion phase, approximately 50% of tachyzoites entered host cells within 3–6 h p.i. although invasion continued up to 24 h p.i. Intracellular replication by endodyogeny ranged from 18 to 35 hours and was isolate-dependent. The Bb-Israel and *B. tarandi* isolates showed the highest replication capacity, while Bb-France and Bb-Evora03 were most efficient in invasion. Within the same culture, heterogeneous plaque morphologies and variable PV sizes reflected the asynchronous nature of the tachyzoite life cycle, emphasizing the complexity of *B. besnoiti*–host cell interactions.

Subsequent research focused on the parasite's interaction with the bovine innate immune system. Muñoz-Caro et al. (2014) were the first to show that *B. besnoiti* tachyzoites trigger the formation of neutrophil extracellular traps (NETs) in bovine polymorphonuclear neutrophils (PMNs). These NETs, composed of DNA fibres decorated with histones, neutrophil elastase (NE) and myeloperoxidase (MPO), entrapped approximately one-third of tachyzoites and significantly impaired their invasion capability. NET formation was shown to be reactive oxygen species (ROS)-dependent, as pharmacological inhibition of nicotinamide adenine dinucleotide phosphate (NADPH) oxidase, NE and MPO suppressed this response.

Conejeros et al. (2019) further investigated the downstream effects of NETs on infected host cells, revealing that NET-derived histone H2A and NET structures exerted cytotoxic effects on BUVEC. Despite disruption of PV architecture, parasite replication remained unaffected, suggesting that NETs contribute to host tissue damage more than to parasite clearance.

Zhou et al. (2020) elucidated the metabolic demands of NET formation in response to *B. besnoiti* by showing that glycolysis, mitochondrial adenosine triphosphate (ATP) production, pyruvate metabolism and oxidative phosphorylation are all required. Inhibitors of lactate production (e.g., oxamate) and mitochondrial ATP synthesis (e.g., oligomycin A) significantly impaired NETosis, confirming the energy-intensive nature of this innate response. Complementarily, Espinosa et al. (2023) identified purinergic P2X1 receptor signalling as a central mediator of tachyzoite-triggered NETosis and neutrophil clustering. Using the selective P2X1 antagonist NF449, they demonstrated a reduction in anchored NETs and neutrophil clustering upon tachyzoite exposure, highlighting ATP-mediated signalling as a key innate immune activator during early infection.

Zhou et al. (2019) also demonstrated that *B. besnoiti* bradyzoites—traditionally considered less immunogenic—can induce both suicidal and vital NETosis. These NET responses were associated with autophagosome (LC3B-positive) formation, indicating a functional link between autophagy and NETosis. The observed positive correlation suggests a synergistic mechanism that enhances host defence against the chronic cystic stage. Macrophages are also implicated in the early immune response. Muñoz-Caro et al. (2014) observed that exposure to *B. besnoiti* tachyzoites triggers the release of ETs from bovine macrophages, like neutrophils. *In vivo*, González-Barrio et al. (2020; 2021b) described intense macrophage infiltration in the testicular parenchyma of naturally infected bulls, both in acute and chronic stages. These findings suggest that macrophages play a central role in immunopathology and parasite containment. Supporting this, Diezma-Díaz et al. (2018) reported that experimental infection in calves induced an early innate IFN-γ response followed by seroconversion within 2–3 weeks post-infection, in line with IFN-γ's known role in macrophage activation (Su et al., 2015). *In vitro* models based on monocyte-derived macrophages have provided valuable insights into the dissection of host–parasite interactions in other apicomplexan parasites (García-Sánchez et al., 2019; Jiménez-Pelayo et al., 2020).

Endothelial cells are central to parasite dissemination and chronic vascular pathology. *Besnoitia besnoiti* is capable of infecting and modulating both BUVEC and BAEC (Muñoz Caro et al., 2014; Maksimov et al., 2016; Jiménez-Meléndez

et al., 2019). Infection of BUVEC impairs G1-phase progression in a species-specific manner (Velásquez et al., 2020), consistent with lipidomic and metabolomic remodelling (Kadesch et al., 2020). In BAEC, tachyzoite infection induces a sequential loss of vascular integrity, upregulation of leukocyte adhesion molecules (e.g., *SELE*, *ICAM-1*) and the emergence of a proinflammatory, profibrotic and prothrombotic phenotype (Jiménez-Meléndez et al., 2020). These *in vitro* findings are consistent with the fibrosis and chronic inflammation observed *in vivo*, particularly in testicular and scrotal tissues of chronically infected bulls. Fibroblasts also play a key role in this context, as the main ECM-producing cells and drivers of fibrosis. During infection, they may become activated into myofibroblasts, enhancing ECM production and profibrotic signalling. *ICAM-1* and *PLAT*, two markers of fibrosis, were upregulated in testicular and scrotal tissues of infected bulls, underscoring the relevance of fibroblast-driven pathology (González-Barrio et al., 2020; 2021b).

To further dissect the molecular mechanisms underlying these host–parasite interactions, omics-based approaches have been applied. Schares et al. (2017) published the first annotated *B. besnoiti* genome, revealing high synteny with *T. gondii* and *N. caninum*. Ramakrishnan et al. (2022) conducted a comparative transcriptomic analysis of tachyzoites and bradyzoites, identifying stage-specific markers and gene families involved in invasion (MICs), immune modulation (GRAs) and intracellular survival (ROPs). Many of these genes were upregulated in bradyzoites, supporting their role in tissue cyst persistence and immune evasion. Although genes associated with sexual development were also detected, the definitive host and sexual cycle remain unknown.

Regarding host cell responses, Jiménez-Meléndez et al. (2020) performed the only RNA-Seq study to date in primary BAEC infected with tachyzoites. At 12 h p.i. (early invasion), endothelial cells upregulated proinflammatory mediators (*IL-6, CXCL2, CCL2*) and adhesion molecules (*SELE, ICAM-1*). By 32 h p.i. (active proliferation), a shift toward a profibrotic and prothrombotic transcriptional profile occurred, with increased expression of *MMP14*, *ITGA5*, *ITGB8* and *vasohibin-1*. Enrichment of NF-κB and TNF-α signalling pathways was evident throughout infection.

Concurrently, the parasite upregulated invasion-related genes (*ROP5B, ROP40, MIC10, AMA1*), suggesting preparation for continued replication and reinvasion.

# Chapter III: Justification and objectives

# Chapter III: Justification and objectives

Bovine besnoitiosis is a chronic and debilitating cattle disease caused by the cyst-forming apicomplexan parasite *B. besnoiti*. Since the first description by Cadéac (1884), bovine besnoitiosis spread in the Pyrenees and become a re-emerging disease in Europe in the last two decades, including Spain, (EFSA, 2010, Álvarez-García et al., 2016). Currently, it is one of the leading causes of reproductive failure in bulls. In this regard, it is a serious health and economic concern for the cattle breeding industry mainly due to permanent sterility of breeding bulls and reduced herd fertility, weight loss, poor body condition and leather depreciation. However, relevant epidemiological aspects of this parasitic disease are still uncertain, including the identity of the definitive host and the contribution of the different sources of parasite transmission that hamper disease control. Additionally, the absence of effective drugs and vaccines to combat the parasite, further exacerbates the situation. Accordingly, disease control is highly limited, and biosecurity and management measures are the only available control options. In this scenario, research on bovine besnoitiosis presents new opportunities related with the development of effective control tools by studying the molecular mechanisms that govern pathogen-host cell interaction to identify novel drug and vaccine targets.

In recent years, novel *in vitro* and *in vivo* models have played a crucial role in enhancing our understanding of the parasite biology. To decipher the intricate interplay between the parasite and the host, it is essential to focus on bovine target cells involved in the early steps of the infection. Endothelial cells and macrophages are key players of the innate immune system that might be crucial during the acute phase (Pols, 1960, McCully et al., 1966, Schares et al., 2009, Álvarez-García et al., 2013). In addition, fibroblasts and myofibroblasts serve as the primary target cells during the chronic phase (Álvarez-García et al., 2013) and play a significant role as the main drivers of fibrosis in collaboration with immune cells (McAnulty, 2007; Yao et al., 2022).

Previous research has demonstrated that *B. besnoiti* is capable of invading and proliferating in BUVEC (Muñoz-Caro et al., 2014, Maksimov et al., 2016),

BAEC and fibroblasts (Jiménez-Meléndez et al., 2019). In the case of BUVEC, *B. besnoiti* tachyzoite infection specifically affects the progression of the cell cycle, impairing G1-phase progression in a species-specific manner (Velásquez et al., 2020). Furthermore, RNA-Seq analysis revealed that BAEC infected with *B. besnoiti* tachyzoites experience an endothelial activation characterized by a sequential disruption of vascular integrity and the development of a proinflammatory, prothrombotic and profibrotic phenotype, evidenced by the upregulation of adhesion molecules (*SELE, SELP, VCAM* and *ICAM1*) and cytokines (*IL-1, IL-6, CCL2,* and *CXCL-1*), among others (Jiménez-Meléndez et al., 2020). These *in vitro* observations align with histopathological findings in the testes of acutely infected breeding bulls, which exhibited significant endothelial damage (vasculitis) in the pampiniform plexus. Furthermore, a pronounced inflammatory infiltrate was found in the testicular parenchyma, where macrophages were the predominant immune cell population (González-Barrio et al., 2020; 2021b). In this context, macrophages are believed to play a significant role in the disease pathogenesis, as indicated by the scarce number of studies carried out in *in vitro* and *in vivo* experimental models. Muñoz-Caro et al. (2014) reported that viable tachyzoites induced the formation of ETs in macrophages, aiming to entrap the parasites and block their invasion. Moreover, the role of IFN-γ in macrophage priming and activation of the inflammatory response has been reported in the infections caused by the closely related apicomplexan parasites *T. gondii* and *N. caninum*. In this regard, an experimental model of bovine besnoitiosis revealed an early innate IFN-γ response after infection, followed by an acquired immune response demonstrated by seroconversion at 2-3 weeks p.i. (Diezma-Díaz et al., 2018).

Likewise, fibroblasts have gained considerable attention as key target cells during *B. besnoiti* chronic infection, as highlighted in a study by Dubey et al. (2013) reported the development of early *B. besnoiti* tissue cysts in a naturally infected bull from South Africa. The host cells involved in tissue cyst formation were likely identified as myofibroblasts, as indicated by immunohistochemical analysis. These myofibroblasts exhibited negative staining for two macrophage markers and Von Willebrand factor, ruling out an endothelial cell origin. However, positive cytoplasmic vimentin staining confirmed their mesodermal origin, most likely as fibroblasts. The staining patterns of smooth muscle actin within the cyst cytoplasm varied in intensity and distribution, characteristic of myofibroblasts.

Furthermore, fibroblasts are well-known for their roles in tissue repair, remodelling and immune responses (Pakshir et al., 2019; Xuan et al., 2022). Specifically, activated fibroblasts, also referred to as myofibroblasts, play a critical role in fibrosis. Notably, fibrosis is a prominent pathological feature observed in the scrotal skin of both acutely and chronically naturally infected bulls (González-Barrio et al., 2020; 2021b) and two fibrosis biomarkers (*ICAM-1, PLAT*) were found to be upregulated in the testicular parenchyma, pampiniform plexus and scrotal skin of naturally chronically infected bulls (González-Barrio et al., 2021b). Additionally, evidence of fibrosis occurrence has been demonstrated in BAEC during *B. besnoiti* infection through *in vitro* RNA-Seq analysis. Several fibrosis markers, including chemokines responsible for monocyte and macrophage recruitment, as well as mediators of macrophage differentiation, were upregulated in BAEC infected with *B. besnoiti* tachyzoites (*CCL2, IL-6, IL-1A, MCSF-1, proheparin-binding EGF-like growth factor, fibronectin* and *collagen*, among others.) (Jiménez-Meléndez et al., 2020). This suggests that fibroblasts/myofibroblasts may play a significant role in the context of fibrosis associated with *B. besnoiti* infection.

Regarding the parasite-dependent factors, our knowledge of the specific *B. besnoiti* genes and pathways involved in host cell invasion and lytic cycle progression remains limited and it holds significance as these events take place during the intra-organ spread of the parasite. The first proteomic approach conducted in *B. besnoiti* was performed by García-Lunar et al. (2013a) and identified tachyzoite proteins primarily involved in energy metabolism (heat shock protein 60 (HSP60), HSPP70, HSP90), as well as proteins associated with metabolism (fructose-1,6-bisphosphate aldolase, phosphoglycerate kinase, lactate dehydrogenase), host cell invasion processes (actin, actin depolymerising factor, tubulin-β chain) and cellular redox homeostasis (thioredoxin-dependent peroxide reductase mitochondrial, protein disulphide isomerase). Additionally, a previous RNA-Seq analysis conducted in BAEC revealed that *B. besnoiti* regulates various functions within bovine endothelial cells through the modulation of several surface SAGs, MICs, AP-2 transcription factors and ROPs (Jiménez-Meléndez et al., 2020). Moreover, a recent comparative transcriptomics investigation estimated the total genome size of the parasite to be 58.9 Mb, highlighting a substantial preservation of synteny and genomic rearrangements like other members of Sarcocystidae such as *T.*

*gondii* and *N. caninum* (Ramakrishnan et al., 2022). The study identified several stage-specific markers and metabolic pathways within the parasite genome. In addition, the process of disease chronification remains poorly understood, including the specific determinants that trigger the transformation of the rapidly multiplying tachyzoite form into the slow multiplying bradyzoite form. These bradyzoites form cysts within the mucous membranes and subcutaneous tissue, as a mechanism of immune system evasion and limiting drug accessibility due to the presence of a thick wall. In a previous study conducted by Fernández-García et al. (2013), stage-specific proteins were identified using a combination of difference gel electrophoresis (DIGE) and mass spectrometry (MS) analysis. Analysis of tachyzoite and bradyzoite extracts revealed 130 differentially expressed spots in bradyzoites and 132 in tachyzoites. Subsequent MALDI-TOF/MS analysis identified five upregulated proteins in bradyzoites (GAPDH, ENO1, LDH, SOD and RNA polymerase) and five upregulated proteins in tachyzoites (ENO2, LDH, ATP synthase, HSP70 and PDI). These findings, offer valuable insights into the stage-specific protein expression patterns of *B. besnoiti*, paving the way for future research to explore these proteins as potential drug targets. However, to investigate the process of disease chronification and develop effective therapies against *B. besnoiti*, it is crucial to establish a standardized *in vitro* model of tachyzoite-bradyzoite switch. Currently, the only method to obtain *B. besnoiti* bradyzoites is by isolating them from tissues cysts of chronically infected animals and is time-consuming and labour-intensive. Extensive research has focused on the conversion from tachyzoites to bradyzoites in *T. gondii* (Skariah et al., 2010, Sokol-Borrelli et al., 2020; Cerutti et al., 2020). Various stressors such as alkaline pH, heat shock, nutrient starvation and specific drugs have been effectively used to induce this transformation *in vitro*. However, unlike *T. gondii*, there is currently no available *in vitro* model for inducing the conversion of *B. besnoiti* tachyzoites into bradyzoites, nor is there a specific molecular marker for *B. besnoiti* bradyzoites, which precludes further research in genetic characterization, drug efficacy studies and bradyzoite obtaining for *in vivo* assays, among others. In addition, there are not available *B. besnoiti* bradyzoite specific markers apart from the antibody directed against the *T. gondii* bradyzoite antigen 1 named as α-TgBAG1. α-TgBAG1 is also known as HSP30, belongs to the small heat-shock protein (sHSP) family and plays a crucial role in stress response. Although it is non-essential for cyst formation it is an early marker of tachyzoite-bradyzoite switch (Colos-Arango et al., 2023; Wu et al., 2024). Moreover, it was reported that the antibody

directed against α-TgBAG1 labelled *B. besnoiti* bradyzoites inside tissue cysts (Dubey et al., 2013).

Accordingly, the general objective of the present Doctoral Thesis was to investigate the host and parasite dependent factors and molecular mechanisms governing the early interaction of *B. besnoiti* with bovine target cells and the chronification process with the subsequent cyst formation. The general objective comprised two specific objectives:

## Objective 1: Study of host cell-dependent factors involved in the parasite-host cell interaction

### Sub-objective 1.1: Characterization of the lytic cycle of *B. besnoiti* tachyzoites in primary bovine monocyte-derived macrophages

The lytic cycle of *B. besnoiti* tachyzoites has been characterized in terms of invasion and proliferation. Furthermore, the morphological changes of macrophages during the development of the lytic cycle have been studied.

### Sub-objective 1.2: Analysis of the transcriptome of *B. besnoiti*-infected primary bovine monocyte-derived macrophages and PBAF

A transcriptomic approach using RNA-Seq was performed to study the parasite interaction with two target cells: macrophages as the target cell during the acute phase and fibroblasts as the target cell during the chronic phase of infection. For macrophages, the transcriptome was analysed at two time points: 4 h p.i., as a representative time of early interaction and 8 h p.i., as a representative time of early invasion stage. On the other hand, in the case of fibroblasts, the transcriptome was analysed at two time points: 12 h p.i., as a representative time of early invasion and 32 h p.i., as a representative time of initial proliferation. Furthermore, the transcriptomics results were subsequently validated *in vitro* by TUNEL assay in the macrophage model.

In addition, samples from testicular parenchyma and scrotal skin of naturally infected bulls were employed to analyse the expression of a panel of DEGs selected from the transcriptomic data. Genes were selected based on the most significant changes in the differential expression and KEGG enrichment analysis.

## Objective 2: Study of parasite-dependent factors involved in the parasite-host cell interaction

### Sub-objective 2:1: Analysis of the transcriptome of *B. besnoiti* tachyzoites during infection in primary bovine monocyte-derived macrophages and PBAF

The transcriptome of *B. besnoiti* tachyzoites was studied in both *in vitro* models (macrophages and fibroblasts) at the time points p.i. previously described, to identify *B. besnoiti* tachyzoite specific genes that may be relevant during the host cell modulation.

### Sub-objective 2.2: Development of an *in vitro* tachyzoite-to-bradyzoite switch model

To study the tachyzoite-to-bradyzoite conversion, a screening of different markers for tachyzoite and bradyzoite stages was performed by employing Western-blot (WB), immunofluorescence (IF) and immunohistochemistry assays (IHC). Subsequently, a series of conversion protocols were applied, adapted from those previously described for the closely related parasite *T. gondii*. These included exposure to alkaline pH, heat shocks at 40.5 °C and 43 °C, deprivation of foetal bovine serum (FBS), and treatment with HDACi, such as apicidine and FR235222, as well as treatment with BKIs. Two isolates of *T. gondii* (TgME49 and TgSpain3) were used as controls for all conversion experiments.

# Chapter IV: Material and methods

# Chapter IV: Material and methods

## 4.1 Ethics statement

Animal welfare was considered to carry out these experiments. Protocols were approved by the Animal Welfare Committee of the Community of Madrid, Spain (permit number PROEX 236/17). In addition, all procedures were performed following current Spanish and European legislation and good practices were in accordance with the European Directive 2010/63/EU, which is transposed into national legislation through the Spanish Royal Decree (RD) 53/2013 for the protection of animals used for research experimentation and other scientific purposes.

## 4.2 Cell lines

Primary bovine monocyte-derived macrophages and PBAF were employed to address Objectives 1 (Subobjectives 1.1 and 1.2) and 2 (specifically Subobjective 2.1). These objectives focused on investigating host cell-dependent factors of primary bovine cells and parasite-specific factors during *B. besnoiti* infection.

For bovine monocyte isolation and *in vitro* macrophage differentiation, heparinized peripheral blood was obtained from a healthy adult *Bos taurus* (Holstein-Friesian) who tested negative for infectious bovine rinotracheitis virus (IBRV) by ELISA-IBR-gE Ab (Idexx, Netherlands), bovine viral diarrhoea virus (BVDV) by ELISA-BDV-p80 (Idexx, Netherlands), Pestivirus by RT–PCR (Hoffman et al., 2006) and *B. besnoiti* and *N. caninum* by WB (García-Lunar et al., 2013a). Bovine monocyte isolation was carried out by immunomagnetic separation using anti-human CD14–conjugated magnetic microbeads (Miltenyi Biotec, Germany) following the protocol previously described by García-Sánchez et al. (2019). Briefly, immunomagnetic purified monocytes were incubated in 6-well culture plates at a density of 3 x $10^6$ cells/well at 37 °C and 5% $CO_2$ in Roswell Park Memorial Institute medium (RPMI) 1640 medium (GE Healthcare, USA) containing 10% heat-inactivated FBS, 50 µM 2-beta-mercaptoethanol, 100 IU $mL^{-1}$ penicillin, 100 µg $mL^{-1}$ streptomycin and 100 ng $mL^{-1}$ recombinant bovine GM-CSF

(Kingfisher Biotech, USA). After 3 days of culture, 1 mL of the culture medium from each well was replaced with 1 mL of fresh medium. Two days later, the monocytes which differentiated into macrophages were reseeded in 24-well and 6-well culture plates at the density of viable cells indicated for each assay. The plates were incubated at 37 °C in a 5% $CO_2$ atmosphere for 24 hours before parasite infection.

On the other hand, PBAF (Jiménez-Meléndez et al., 2019) were cultured in T25 culture flasks with Dulbecco's modified Eagle Medium (DMEM) (Sigma-Aldrich, Germany) containing 15% FBS and 100 IU/mL of penicillin, 100 mg/mL of streptomycin and 0.25 µg/mL of amphotericin B. Low passage fibroblasts (up to passage 10) were passaged once a week using pre-mix trypsin EDTA (TrypLE Gibco, Thermo Fisher Scientific, Waltham, MA, USA), following the protocol previously described by Jiménez-Meléndez et al. (2019).

For Objective 2, specifically Subobjective 2.2, which aimed to develop an *in vitro* tachyzoite-to-bradyzoite differentiation model, four cell lines were employed: MARC-145, Vero81, primary human foreskin fibroblasts (HFF) and PBAF.

MARC-145 cells were cultured for 24 hours in DMEM (Sigma-Aldrich, Germany) supplemented with 10% FBS, 2 mM glutamine, 100 U/mL penicillin and 100 µg/mL streptomycin, in a 5% $CO_2$ atmosphere at 37 °C. Cells were passaged twice weekly.

Vero81 cells were cultured under similar conditions, using DMEM (Sigma-Aldrich, Germany) supplemented with 10% FBS, 2 mM glutamine, 100 U/mL penicillin and 100 µg/mL streptomycin in a 5% $CO_2$ atmosphere at 37 °C. These cells were also passaged twice weekly.

HFF were maintained in DMEM (Sigma-Aldrich, Germany) supplemented with 10% FBS, 2 mM glutamine, 100 U/mL penicillin and 100 µg/mL streptomycin in a 5% $CO_2$ atmosphere at 37 °C. Passaging was performed twice weekly.

Primary bovine aorta fibroblasts (PBAF) were cultured in DMEM (Sigma-Aldrich, Germany) supplemented with 15% FBS, 2 mM glutamine, 100 U/mL penicillin and 100 µg/mL streptomycin in a 5% $CO_2$ atmosphere at 37 °C. Cells were passaged weekly using pre-mixed Trypsin EDTA (Sigma-Aldrich, Germany), as previously described by Jiménez-Meléndez et al. (2019).

## 4.3 Parasite culture

To address Objectives 1 (Subobjectives 1.1 and 1.2) and 2 (specifically Subobjective 2.1), *B. besnoiti* tachyzoites of BbSpain-1 isolate were employed. These tachyzoites were maintained in monolayer cultures of MARC-145 at a multiplicity of infection (MOI) of 2:1 (parasite:host cell) following previously published procedures (Jiménez-Meléndez et al., 2017). To minimize parasite adaptation to cell culture, only low-passage tachyzoites (passage numbers 10 to 21) were employed.

For Objective 2 (specifically Subobjective 2.2), both *B. besnoiti* BbSpain-1 and *T. gondii* isolates TgME49 and TgSp3 were employed. *B. besnoiti* tachyzoites were cultured as described above, while *T. gondii* tachyzoites were maintained in monolayer cultures of Vero81 cells at a MOI (parasite:host cell) of 0.25:1 in the case of TgME49 and 0.5:1 in the case of TgSp3. Similar to *B. besnoiti*, only low-passage *T. gondii* tachyzoites (up to passage 20) were used to avoid adaptation to cell culture.

For infection, tachyzoites of *B. besnoiti* BbSpain-1 isolate and *T. gondii* TgME49 and TgSp3 isolates were harvested three days p.i., when most tachyzoites remained intracellular. Parasites were released from their host cells by repeated passage through a G25 needle and subsequently purified using disposable PD-10 columns (Sephadex G-25; GE-Healthcare, USA). Tachyzoite viability was assessed using trypan blue exclusion and parasite counts were determined with a Neubauer chamber. For all experiments, infections of cell lines were performed within one hour of tachyzoite purification to ensure optimal viability.

## 4.4 Primary bovine monocyte-derived macrophages IF assays

As shown in **Figure 8**, IF assays were performed as part of Objective 1, specifically Subobjective 1.1, using primary bovine monocyte-derived macrophages. Macrophages were seeded onto sterile coverslips in 24-well plates at a density of 2.5 × $10^5$ cells per well and inoculated with live *B. besnoiti* BbSpain-1 tachyzoites (MO-Bb) at a MOI of 5:1. The cultures were incubated at 37 °C to allow parasite-host cell interactions. As a control for phagocytosis, macrophages were also inoculated with heat-killed *B. besnoiti* BbSpain-1 tachyzoites (MO-hkBb) at the same MOI. Tachyzoites were killed by incubation at 56 °C for 30 minutes as previously described by García-Sánchez et al. (2020). The trypan blue dye exclusion test indicated that 100% of the heat-treated tachyzoites were dead. In addition, heat-treated tachyzoites were inoculated into MARC-145 cell cultures and it was confirmed that there was no parasite growth after 7 days. Inoculated macrophages (MO-Bb and MO-hkBb) were fixed with 0.05% glutaraldehyde and 3% paraformaldehyde at 4, 8, 12, 24 and 36 h p.i.. Afterwards, a double IF probe was performed (Jiménez-Pelayo et al., 2017). Briefly, after fixation, hyperimmune rabbit antiserum directed against *B. besnoiti* tachyzoites (1:500) was employed as the primary antibody (Gutiérrez-Expósito et al., 2012) and Alexa Fluor-488-labelled secondary antibody (Thermo Fisher Scientific, USA) was employed. Afterwards, the cells were permeabilized with 0.25% Triton X-100 (Thermo Fisher Scientific, USA). Subsequently, extracellular and intracellular parasites were stained using hyperimmune rabbit antiserum directed against *B. besnoiti* tachyzoites (1:500) as the primary antibody and Alexa Fluor-594-labelled secondary antibody (Thermo Fisher Scientific, USA). The nuclei were stained by washing the cells with a solution of 1:5,000 4′,6-diamidino-2-phenylindole (DAPI) (Thermo Fisher Scientific, USA) in 1x phosphate-buffered saline (PBS) and the coverslips were embedded in Prolong (Thermo Fisher Scientific, USA). Intracellular tachyzoites were stained red, while extracellular tachyzoites were stained green and red. The number of cells containing at least one tachyzoite was determined by counting in 10 arbitrarily selected fields using an inverted fluorescence microscope (Nikon Eclipse TE 200, Japan) at a magnification of 200x. A mean value of 50 cells was counted in each field by a single operator. Three independent assays were performed, each with 3 different replicates.

In addition, macrophage morphology was assessed microscopically by staining the cells with fluorescently labelled phalloidin (Thermo Fisher Scientific, USA). Macrophages were seeded on sterile coverslips in 24-well plates at a density of 2.5 x $10^5$ cells/well and inoculated with live BbSpain-1 tachyzoites (MO-Bb) and heat-killed tachyzoites (MO-hkBb) at an MOI of 5:1, followed by incubation at 37 °C. Cultures were fixed at 4, 8, 12 and 36 h p.i. with 0.05% glutaraldehyde and 3% paraformaldehyde. Afterwards, the cells were permeabilized with 0.25% Triton X-100 (Thermo Fisher Scientific, USA). Parasites were stained using hyperimmune rabbit antiserum directed against *B. besnoiti* tachyzoites (1:500) as the primary antibody and Alexa Fluor-488-labelled secondary antibody (Thermo Fisher Scientific, USA). In addition, Alexa Fluor-594-labelled phalloidin (Thermo Fisher Scientific, USA) was used for the staining of F-actin. The nuclei were stained by washing the cells with a solution of 1:5,000 DAPI (Thermo Fisher Scientific, USA) in 1x PBS and the coverslips were embedded in Prolong (Thermo Fisher Scientific, USA). Based on microscopic analysis of cells in different experimental conditions, macrophages were classified according to two distinct morphologies: 1) small and rounded with short and irregular filopodia and 2) large and elongated with long filopodia.

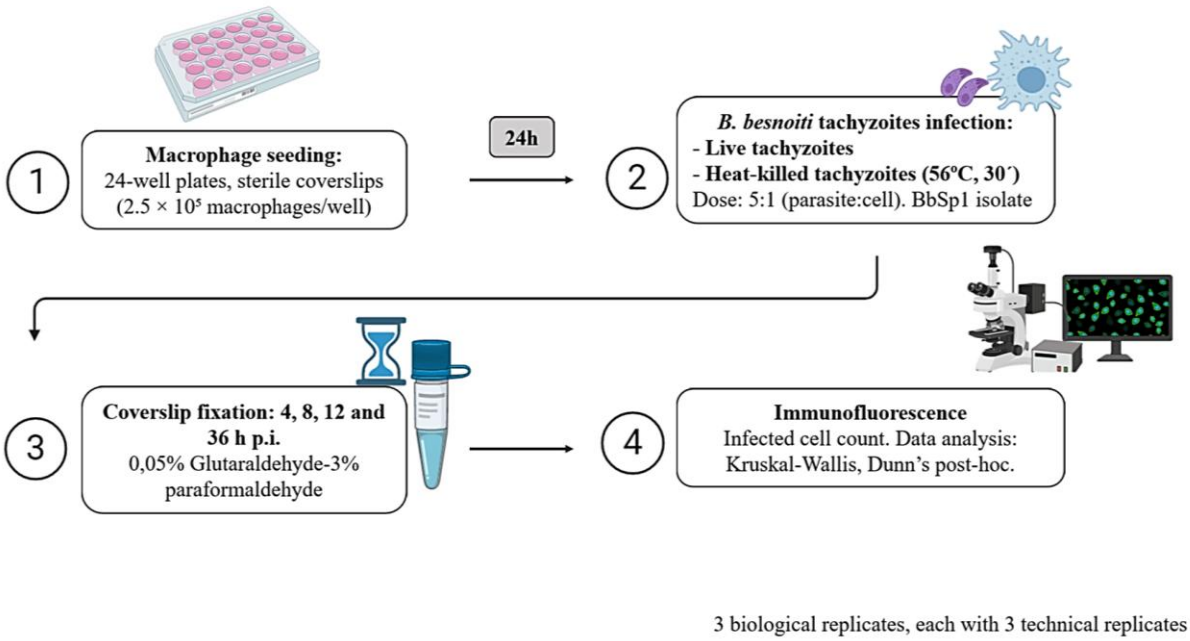


**Figure 8. Graphical abstract of *B. besnoiti* tachyzoite invasion in primary bovine monocyte-derived macrophages assay.**

## 4.5 Primary bovine monocyte-derived macrophages proliferation assays

As shown in **Figure 9,** for Objective 1, specifically Subobjective 1.1, macrophages proliferation assays were performed in 6-well plates, with macrophages seeded at a density of 3 x $10^6$ cells/well and infected with live tachyzoites (MO-Bb) at an MOI of 5:1, followed by incubation at 37ºC. In parallel, MO-hkBb was used as a control. DNA was extracted according to Jiménez-Meléndez et al. (2019) at different times p.i. (4, 8, 12, 24, 32, 48 and 72 h p.i.). DNA concentration and quality were measured by UV spectrometry using a Biotek Multiplate Reader (Agilent Biotek, USA). Quantification of *B. besnoiti* was performed by quantitative PCR (qPCR) and the proliferation kinetics were displayed by plotting the parasite loads against their respective time points of collection (4, 8, 12, 24, 32, 48 and 72 h p.i.) following the indications previously described by Jiménez-Meléndez et al. (2019). Proliferation was also monitored by IF staining using hyperimmune rabbit antiserum directed against *B. besnoiti* tachyzoites, as described above. Assays were carried out in triplicate, each with 3 different replicates.

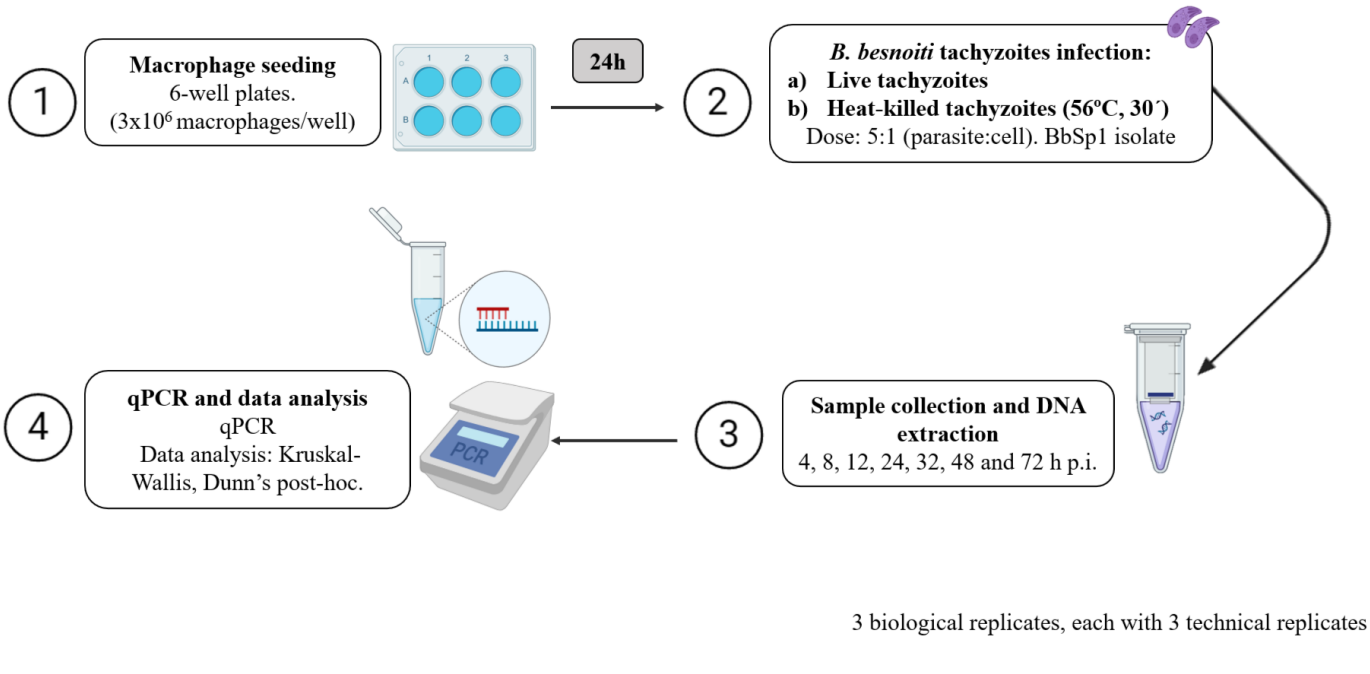


**Figure 9. Graphical abstract of *B. besnoiti* tachyzoite proliferation in primary bovine monocyte-derived macrophages assay.**

## 4.6 Primary bovine monocyte-derived macrophages and fibroblasts transcriptome analyses

As shown in **Figure 10,** for Objective 1, specifically Subobjective 1.2, the transcriptomic analysis of *B. besnoiti*-infected primary bovine monocyte-derived macrophages (A) and PBAF (B) was conducted under controlled conditions. Macrophages were seeded in 6-well plates at a density of 3 x $10^6$ cells/well, infected with live tachyzoites (MO-Bb) at a MOI of 5:1 and inoculated with heat-killed tachyzoites (MO-hkBb) at the same MOI. Non-infected macrophages (MO) were used as a control. On the other hand, primary bovine fibroblasts were seeded in T25 flasks with confluent fibroblasts monolayers at a density of 2 × $10^6$ cells and infected with live tachyzoites (FI-Bb) at a MOI of 10:1. Non-infected fibroblasts (FI) were used as a control.

Total RNA from three independent biological replicates was purified from the pellet of inoculated macrophages at 4 and 8 h p.i. and inoculated fibroblasts at 12 and 32 h p.i.. In the case of fibroblasts, extracellular parasites were eliminated by washing infected flasks with 1x PBS before the cells were recovered at both time points. Primary bovine cells were recovered by gentle scraping, centrifuged at 1350 × g for 10 min at 4 ◦C and, once the supernatant was discharged, the pelleted cells were stored at −80 ◦C until RNA extraction. All the analyses were performed with three biological replicates. Total RNA from the three independent biological replicates was purified by using a QIAGEN RNeasy Mini Kit (Qiagen, Germany) following QIAshredder (Qiagen, Germany) homogenization according to the manufacturer's instructions. RNA integrity was evaluated by 1% agarose gel electrophoresis with GelRed staining (Biotium, USA).

The quality and quantity of the total RNA was determined with a Bioanalyzer 2100 (Agilent Biotek, USA) and a Qubit 2.0. B (Invitrogen, USA). The poly(A)+ mRNA fraction was isolated from the total RNA and cDNA libraries were obtained following Illumina's recommendations. Briefly, poly(A)+ mRNA was isolated on poly-T oligo-attached magnetic beads and chemically fragmented prior to reverse transcription and cDNA generation. The cDNA fragments were then subjected to a repair process, addition of a single 'A' base to the 3' end and ligation of the adapters. The products were purified and enriched with PCR to create the indexed final double-stranded cDNA library. The quantity of the libraries was determined by qPCR with a LightCycler

480 (Roche, Switzerland) and quality was analysed with a Bioanalyzer 2100 (Agilent Biotek, USA) high sensitivity assay. Prior to cluster generation in cBot (Illumina, USA), equimolar pooling of the libraries was performed. The pool of the cDNA libraries was sequenced by paired-end sequencing (100 bp × 2) with an Illumina HiSeq 2000 sequencer (Illumina, USA).

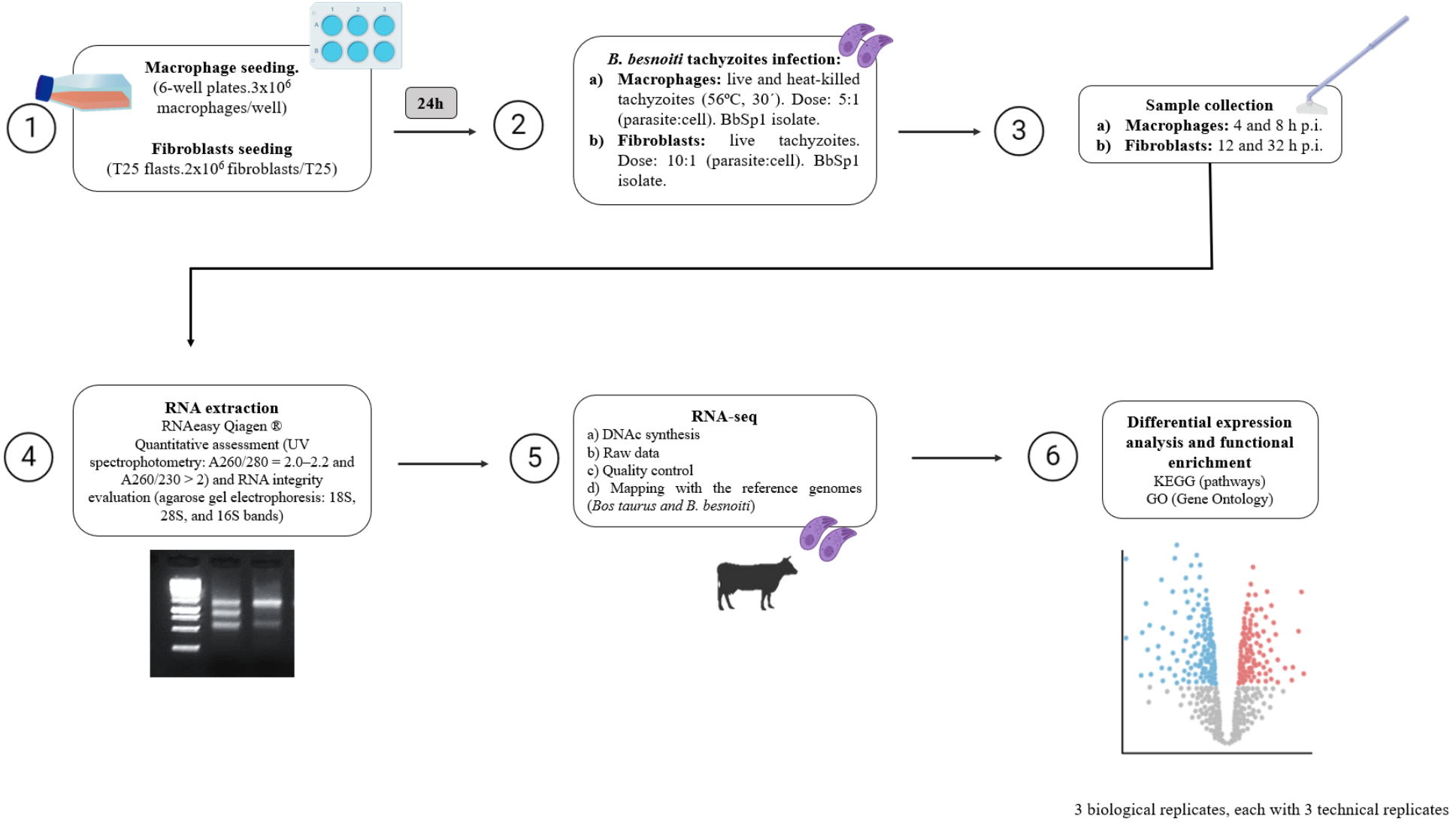


**Figure 10. Graphical abstract of primary bovine monocyte-derived macrophages and fibroblasts transcriptome assays.**

## 4.7 Primary bovine monocyte-derived macrophages terminal deoxynucleotidyl transferase-mediated dUTP nick-end labelling (TUNEL) assay

For Objective 1, specifically Subobjective 1.2, TUNEL assays were conducted to verify and quantify apoptosis, identified as a highly enriched pathway in the transcriptomic analysis of primary bovine monocyte-derived macrophages. The assay was performed using the *In Situ Cell Detection Kit TMR Red* (Roche, Switzerland) following the manufacturer's instructions. Briefly, macrophages were cultured on sterile coverslips in 24-well plates at a density of 2.5 x $10^5$ cells/well and inoculated with live tachyzoites (MO-Bb) and heat-killed tachyzoites (MO-hkBb) at a MOI of 5:1, followed by incubation at 37 °C. Cultures were fixed at 4 and 8 h p.i. with 4% paraformaldehyde. Apoptotic cells were visualized by fluorescence microscopy (Nikon Eclipse TE 200, Japan) (**Figure 11**).

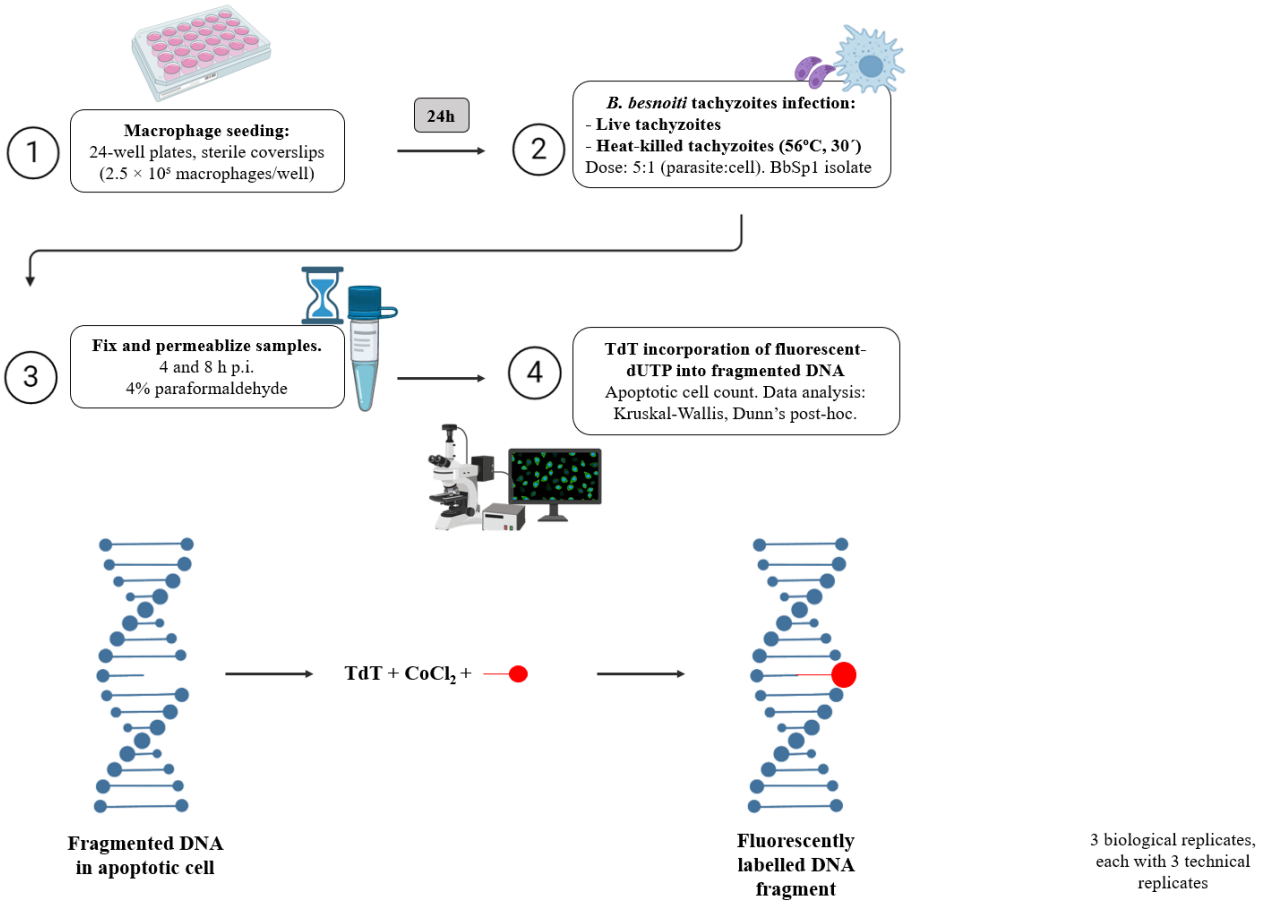


**Figure 11. Graphical abstract of primary bovine monocyte-derived macrophages TUNEL assay.**

## 4.8. Analysis of gene expression in target tissues of naturally infected bulls

As part of Objective 1, Subobjective 1.2, the expression of a panel of DEGs identified in the transcriptomic analyses of primary bovine monocyte-derived macrophages and PBAF was examined (**Table 8)**. Tissue samples from the testicular parenchyma and scrotal skin of naturally infected bulls were analysed to investigate the expression patterns of these DEGs. This study included fifteen naturally infected breeding bulls from extensive beef herds (acute infection: n = 5; chronic infection: n = 10; negative controls: n = 9). Acutely infected animals showed signs compatible with acute besnoitiosis, mainly fever and orchitis and only 1 presented 2–3 tissue cysts per section (González-Barrio et al., 2020). Chronically infected animals were sterile bulls that presented skin lesions and testis atrophy with azoospermia (González-Barrio et al., 2021b). Testicular parenchyma and scrotal skin tissue samples were collected from each bull and samples were frozen at −80 °C until RNA extraction. Total RNA was purified by using a QIAGEN RNeasy Mini Kit (Qiagen, USA) following QIAshredder (Qiagen, USA) homogenization according to the manufacturer´s instructions. RNA concentration and purity were measured spectrophotometrically using a NanoPhotometer Classic (Implen, USA). In addition, RNA integrity was evaluated by 1% agarose gel electrophoresis with GelRed™ staining (Biotium, USA). Afterwards, reverse transcription was performed using the master mix SuperScript® VILO™ cDNA Synthesis Kit (Invitrogen, USA) in a 20 μL reaction using up to 2.5 μg of total RNA. cDNA was sequentially diluted to 1:20, 1:80, 1:320 and 1:1,280 and all dilutions were analysed by qPCR. Quantitative real-time PCRs were performed in 25 μL volumes using 12.5 μL of Power SYBR®PCR Master Mix (Applied Biosystems, USA), 10 pmol of each primer and 5 μL of the diluted cDNA samples. Primers are shown in **Table 8**. Reactions were performed in an ABI 7500 FAST Real Time PCR System (Applied Biosystems, USA) (**Figure 12**).

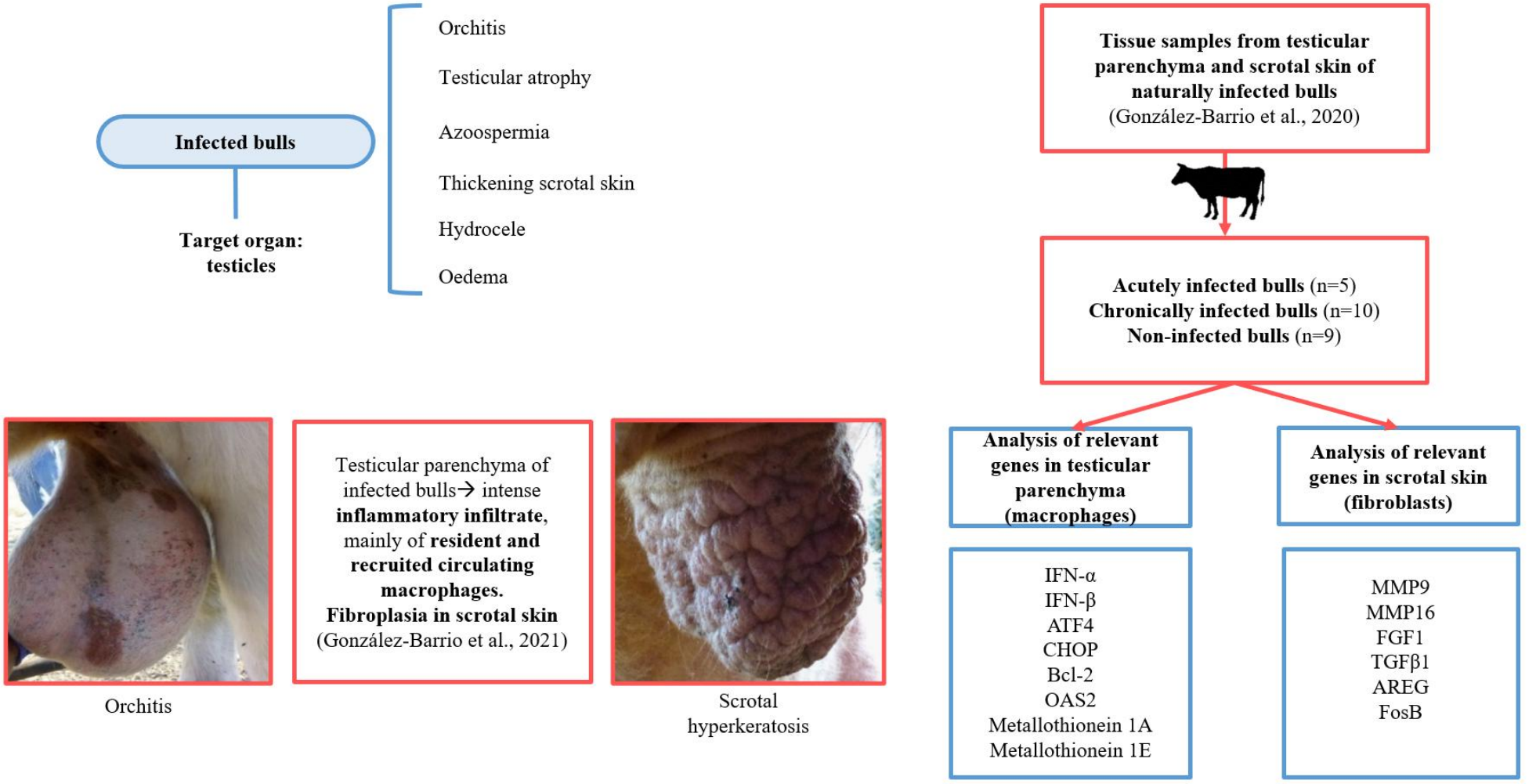


**Figure 12. Overview of gene expression analysis in target tissues of naturally infected bulls.**

**Table 8. Sequences of primers used for quantitative RT–qPCR for *B. taurus* genes.**

| | Target | Primer sequence | Reference |
|---|---|---|---|
| **Primary bovine monocyte-derived macrophages** | IFN-α | F: 5’ ACACACACCTGGTTCAACAC 3’<br>R:5’GATGACAGCAGAAATGAGTCTTCC3’ | Osman et al., 2017 |
| | IFN-β | F: 5’ RTCTGSAGCCAATCCARAAG 3’<br>R: 5’ CAGGCACACCTGTYGTACTC 3’ | Osman et al., 2017 |
| | ATF4 | F: 5’ CCGAGATGAGCTTTCTGAGC 3’<br>R: 5’ AGCATCCTCCTTGCTGTTGT 3’ | Yonekura et al., 2018 |
| | CHOP | F: 5’ CTGAAAGCAGAGCCTGATCC 3’<br>R: 5’ GTCCTCATACCAGGCTTCCA 3’ | Yonekura et al., 2018 |
| | Bcl-2 | F: 5′ ATGTGTGTGGAGAGCGTCAA 3′<br>R: 5′ CTAGGGCCATACAGCTCCAC 3′ | Im et al., 2016 |
| | OAS2 | F: 5’ GATCCCACTGACCCAACCAA 3’<br>R: 5’ GTGATGCAGGCAGAACATTCC 3’ | Rocha et al., 2020 |
| | Metallothionein-1A | F: 5’ CACCTGCAAGGCCTGCAGA 3’<br>R: 5’ CGAGGCCCCTTTGCAGACA 3’ | Fujie et al., 2016 |
| | Metallothionein-1E | F: 5’ CTCTACTTTGCCACTTGCTTTG3’<br>R: 5’ CTTCTTGCAGGAGGGACATC 3’ | Ticianelli et al., 2017 |
| **PBAF** | MMP9 | F:5’TCGACGTGAAGACACAGAAGGT3’<br>R:5’TGATCCTGGCAGAAGTAAGCTTTC3’ | Kizaki et al., 2008 |
| | MMP16 | F: 5’ ACCCCAGGATGTCAGTGC 3’<br>R: 5’ AATAGCTTTACGGGTTTCAGG 3’ | Milner et al., 2006 |
| | PLAUR | F: 5’ ACCACACCTTCCACTTCCTG 3’<br>R: 5’ CTGGGTGGTTACAGCCACTT 3’ | García et al., 2014 |
| | FGF1 | F: 5’ GCTGAAGGAGAAACCACGAC 3’<br>R: 5’ GTTTTCCTCCAACCTTTCCA 3’ | Berisha et al., 2006 |
| | TGFβ1 | F: 5’ TGAGCCAGAGGCGGACTACT 3’<br>R: 5’ TGCCGTATTCCACCATTAGCA 3’ | Sugawara et al., 2010 |

| | | | |
|---|---|---|---|
| | AREG | F: 5’CTATAGCTGCTTTCGTCTCTGC 3’<br>R: 5’CGTTCTTCAGCGACACCTTCA 3’ | Shrestha et al., 2015 |
| | FosB | F: 5’ GAAGTGTAGGAACCGGCGAA 3’<br>R: 5’TTCTCCTTTTGGAGCTCGGC 3’ | Fernández-Álvarez et al., 2023 |
| **House-keeping gene** | β-actin | F: 5’ACACCGCAACCAGTTCGCCAT 3’<br>R: 5’ GTCAGGATGCCTCTCTTGCT 3’ | Horcajo et al., 2017 |

## 4.9. Tachyzoite-bradyzoite conversion

### 4.9.1 Tachyzoite and bradyzoite isolation

As shown in **Figure 13,** for Objective 2, *B. besnoiti* tachyzoites were released from infected MARC-145 host cells by repeated passage through a 25G needle and subsequently purified using disposable PD-10 columns (Sephadex G-25; GE Healthcare, USA). Tachyzoites were counted using a Neubauer chamber. Doses of $10^7$ tachyzoites were prepared, which were kept at -80ºC as stock for the WB extracts. Other doses of the same quantity were were resuspended in 40% formalin-1x PBS, passed through a 25G needle and stored at 4 °C as stock solution for antigen coating on IF slides. In addition, *B. besnoiti* bradyzoites were isolated from skin biopsies obtained from a chronically infected cow in Navarra, Spain. The animal exhibited characteristic clinical signs of chronic besnoitiosis, including alopecia, scleroderma and hyperkeratosis. A skin sample was excised into small pieces and washed multiple times in 1x PBS containing penicillin (500 U/ml), streptomycin (500 µg/ml) and fungizone (0.125 µg/ml). Bradyzoites were released using a Potter Elvehjem tissue homogenizer. The homogenate was passed through an 18G needle. The obtained homogenate volume was filtered first using a 100 µm pore nylon cell strainer (BD Falcon Cell Strainer, Fisher Scientific, USA) and then through a 40 µm pore nylon cell strainer (BD Falcon Cell Strainer, Fisher Scientific, USA). The resulting filtrate was centrifuged at 1,350 x g for 15 minutes at 4ºC. After centrifugation, the supernatant was discarded and the pellet was resuspended in 1x PBS containing penicillin (500 U/ml), streptomycin (500 µg/ml) and fungizone (0.125 µg/ml). The entire volume was passed through a 25G needle. Bradzyoites counts were determined with a Neubauer chamber. Doses of $10^7$ bradyzoites were prepared, which were kept at -80ºC as stock for the WB extracts. Other doses of the same quantity were resuspended in 40% formalin- 1x PBS, passed through a 25G needle and kept at 4ºC as stock for antigen coating on IF slides.

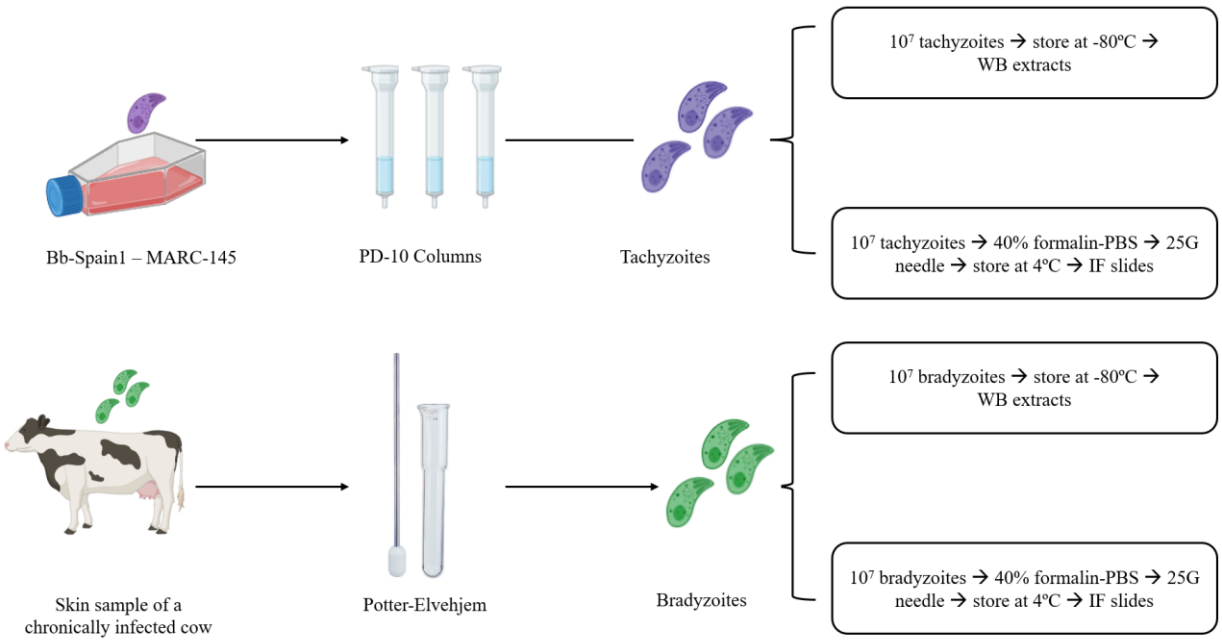


**Figure 13. Graphical abstract of tachyzoite and bradyzoite obtainment procedure.**

### 4.9.2 Screening of stage specific markers for tachyzoite-bradyzoite conversion

As shown in **Figure 14**, as part of Objective 2, several stage-specific markers for tachyzoites and bradyzoites of *N. caninum*, *T. gondii* and *B. besnoiti*—summarized in **Table 9**—were analysed using IF, WB and IHC.

For the IF, 9 µL of formalin-fixed zoites (tachyzoites or bradyzoites) were applied to each well of multiwell IF slides and air-dried at room temperature (RT) for 15 minutes. The slides were then fixed in acetone at −20 °C for 10 minutes, followed by a 10-minute wash in distilled water with gentle agitation. For primary antibody labelling, the slides were incubated for 30 minutes at 37 °C with antibodies specific to tachyzoites or bradyzoites at 1:50 dilution, as listed in **Table 9.** Following three 10-minute washes in 1x PBS, the slides were incubated for 30 minutes at 37 °C with FITC-conjugated secondary antibodies diluted 1:150 in 1x PBS containing 0.2% Evans Blue. In addition, fluorescein isothiocyanate (FITC)-conjugated goat anti-rabbit IgG

(Invitrogen, USA) was used. This step was followed by three additional 1x PBS washes (10 minutes each with agitation). Finally, slides were air-dried in the dark at RT and mounted with Fluoroshield mounting medium (Sigma-Aldrich, USA).

For WB analysis, proteins extracted from *B. besnoiti* tachyzoites or bradyzoites were separated on 15% SDS-polyacrylamide gels under denaturing conditions, following the protocol described by García-Lunar et al. (2013a) with minor modifications. Under reducing conditions, β-mercaptoethanol was added to the fivefold-concentrated sample buffer. Gels were run at 100 V for 90 minutes. Proteins were then electrotransferred onto nitrocellulose membranes using a semi-dry transfer system (Bio-Rad, USA) at 15 V for 60 minutes. Following transfer, membranes were blocked with 5% non-fat dry milk in tris-buffered saline with 0.05% Tween-20 (TBS-T) for 1 hour at RT to prevent non-specific binding. Membranes were then incubated during 1 h at 37 °C with primary antibodies (1:100) diluted in TBS-T containing 1% milk, as detailed in **Table 9**. After three washes of 5 minutes each in TBS-T, membranes were incubated for 1 hour at RT in the dark with HRP-conjugated monoclonal anti-rabbit IgG antibodies, ref. AP132P (Sigma-Aldrich, USA) diluted 1:100 in TBS-T with 1% milk. Membranes were then washed three times in TBS-T and twice in TBS (5 minutes each wash). Bound antibodies were visualized using the 4-chloro-1-naphthol chromogenic substrate (Thermo Scientific, USA), incubated for 5–10 minutes at RT until signal development was observed. The reaction was stopped with ultrapure water, and membranes were dried and scanned using the GS-800 Calibrated Densitometer (Bio-Rad, USA) for densitometric analysis. Negative controls included membranes incubated with pre-immune serum and non-immune milk protein. Polyclonal antibodies against *B. besnoiti* tachyzoites and bradyzoites were used as positive controls.

For IHQ analysis, formalin-fixed, paraffin-embedded (FFPE) skin tissue sections (3–5 μm thick) from animals naturally infected with *B. besnoiti* and containing mature tissue cysts were used. Sections were mounted on poly-L-lysine-coated slides, deparaffinized in xylene (2 × 10 minutes) and rehydrated through a graded ethanol series (100%, 96%, 70%) to distilled water. Antigen retrieval was performed by microwave heating in 10 mM citrate buffer (pH 6.0) at 600 W for 2 × 5 minutes. Endogenous peroxidase activity was blocked by incubating the sections with 3%

hydrogen peroxide in methanol for 15 minutes at RT. To reduce non-specific binding, slides were then blocked with 5% normal goat serum in PBS for 30 minutes. Primary antibodies—including BbSpain-1 polyclonal bradyzoite and tachyzoite antisera, α-NcSAG, α-NcSRS2, α-NcROP2, α-NcSAG4, α-NcBSR4, α-NcSRS9 and α-TgBAG1—were applied at a 1:100 dilution and incubated for 1 hour at 37 °C. Following three 5-minute washes in 1x PBS, the slides were incubated with horseradish peroxidase (HRP)-conjugated goat anti-rabbit IgG secondary antibody (1:200), (Sigma-Aldrich, USA) for 30 minutes at RT. Antigen detection was performed using 3,3′-diaminobenzidine (DAB), (Agilent Technologies, USA), which produced a brown precipitate at the sites of antigen localization. Sections were then counterstained with Harris hematoxylin, dehydrated through an ethanol series, cleared in xylene and mounted with a permanent mounting medium. Negative controls included sections processed without the primary antibody or with non-immune rabbit serum. Positive controls consisted of FFPE tissue sections previously confirmed to contain *B. besnoiti* bradyzoite cysts.

To assess the reliability and reproducibility of stage-specific marker detection across different immunoassays, a combination of blinded evaluations and comparative analysis was applied. For IF, fluorescence signal intensity and distribution were assessed using an epifluorescence microscope by two independent and experienced researchers blinded to sample identity. Inter-observer agreement was monitored to minimize subjective bias and to ensure the consistency of marker detection. For WB analysis, recognition patterns of immunodetection assays (IDAs) were evaluated based on band presence, intensity and molecular weight. Two experienced researchers independently analysed the blots in a blinded manner to confirm the specificity of each antibody and to validate reproducibility across replicates. For IHC analysis, staining intensity (graded as weak, moderate or strong) and antigen distribution (focal *vs* diffuse) were assessed under a light microscope (Leica Microsystems) by two blinded observers. Scoring was performed independently, and discrepancies were resolved through consensus. Results were compared across experimental conditions to evaluate the expression patterns of stage-specific markers in tissue sections containing *B. besnoiti* cysts.

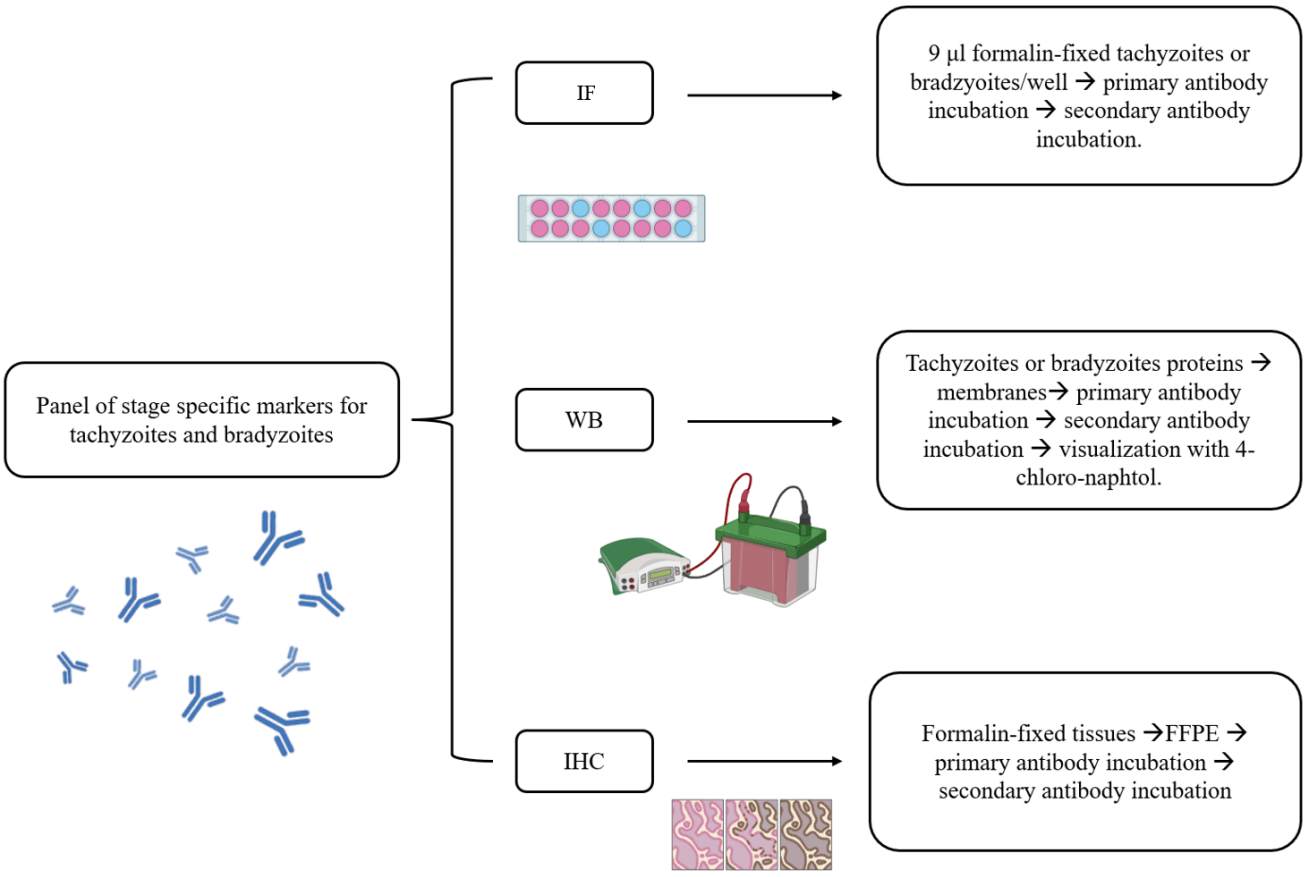


**Figure 14. Graphical abstract of the screening of stage specific markers for tachyzoite-bradyzoite conversion.**

**Table 9. List of specific antibodies directed against *N. caninum, T. gondii* and *B. besnoiti* tachyzoites or bradyzoites stages. Ab: antibody.**

| Denomination | Species | Stage | Localization | Molecular weight (kDa) | Type Ab | Produced in | References |
|---|---|---|---|---|---|---|---|
| α-NcSAG1 | *N. caninum* | Tachyzoite | Surface | 36 | Polyclonal | Rabbit | Sonda et al., 1998 |
| α-NcSRS2 | *N. caninum* | Tachyzoite | Surface | 42 | Polyclonal | Rabbit | Risco-Castillo et al., 2008 |
| α-NcROP2 | *N. caninum* | Tachyzoite | Apical tip of the tachyzoite | 55 | Polyclonal | Rabbit | Risco-Castillo et al., 2008 |
| α-NcSAG4 | *N. caninum* | Bradyzoite | Surface | 19.5 | Polyclonal | Rabbit | Risco-Castillo et al., 2008 |
| α-NcBSR4 | *N. caninum* | Bradyzoite | Surface | 51 | Polyclonal | Rabbit | Risco-Castillo et al., 2008 |
| α-NcSRS9 | *N. caninum* | Bradyzoite | Surface | 37 | Polyclonal | Rabbit | Risco-Castillo et al., 2008 |
| α-TgBAG1 | *T. gondii* | Bradyzoite | Cytoplasm | 28 | Polyclonal | Rabbit | Colos-Arango et al., 2023 |
| BbSpain-1 polyclonal bradyzoite antiserum | *B. besnoiti* | Bradyzoite | Bradyzoite | - | Polyclonal | Rabbit | Gutiérrez-Expósito et al., 2012 |
| BbSpain-1 polyclonal Tachyzoite antiserum | *B. besnoiti* | Tachyzoite | Tachyzoite | - | Polyclonal | Rabbit | Gutiérrez-Expósito et al., 2012 |

## 4.10 Protocols evaluated for inducing *in vitro* tachyzoite-bradyzoite conversion

Bradyzoite stage conversion was induced *in vitro* using a range of experimental protocols adapted from previously established methods for *T. gondii*, as detailed below. Host cell monolayers—including MARC-145, Vero81, HFF and PBAF—were seeded in 24-well plates, each well containing a sterile 10 mm glass coverslip. MARC-145 and Vero81 cells were seeded at a density of $1 \times 10^5$ cells per well, while HFF and PBAF were seeded at a higher density of $4 \times 10^5$ cells per well to ensure optimal confluence and support for stress treatments.

Parasites (BbSpain-1, TgME49 and TgSp3) were maintained under standard culture conditions previously described. Tachyzoites were released from infected host cells by repeated passage through a 25-gauge needle and purified using disposable PD-10 Sephadex G-25 columns (GE Healthcare, USA). Parasite viability was assessed by trypan blue exclusion and concentrations were determined using a Neubauer chamber. All infections were performed within one hour of purification to ensure maximum viability. Infections were carried out as follows: *B. besnoiti* BbSpain-1 tachyzoites were used at a MOI of 2:1, *T. gondii* TgME49 at an MOI of 0.25:1 and TgSp3 at an MOI of 0.5:1. Each cell line was subjected to specific stress protocols designed to induce tachyzoite-to-bradyzoite conversion.

After the treatment period, cultures were fixed in parallel either with 0.05% glutaraldehyde and 3% paraformaldehyde or with cold methanol for 20 minutes at RT. All experiments were performed in three independent biological replicates, each with three technical replicates. A tachyzoite control for each isolate (BbSpain-1, TgME49, and TgSp3), maintained under standard non-stress conditions, was included in every experiment as a reference for comparison.

### 4.10.1 Alkaline culture medium

Following the protocol described by Soête et al. (1994), with the modification that medium alkalinization was performed at 6, 12 and 48 h p.i.—instead of a single change at 6 h p.i.—the standard culture medium was replaced with an alkaline-

modified RPMI 1640 medium supplemented with 5% FBS, 50 mM HEPES, 2 g/L sodium bicarbonate ($NaHCO_3$) and 1% antibiotic-antimycotic solution (penicillin, streptomycin, and amphotericin B), adjusted to pH 8.0 using NaOH. After each medium exchange, infected cultures were incubated in a $CO_2$-free environment to maintain alkaline conditions. This atmosphere was sustained for extended periods of 72, 120 and 168 h, in contrast to the original protocol which maintained the alkaline environment for 48 to 96 h. To ensure a stable pH conducive to bradyzoite induction, the alkaline medium was refreshed every 48 h.

### 4.10.2 Heat-shock

Following the protocol described by Soête et al, 1994, host cells were subjected to a heat shock pre-treatment prior to infection. In contrast to the original protocol, which applied a single temperature of 43 °C, two temperatures—40.5 °C and 43 °C—were evaluated under a 5% $CO_2$ atmosphere for 2 h to induce cellular stress responses. After this thermal conditioning, cells were infected and incubated at 37 °C for 6 h to allow both parasite invasion and host cell recovery. To further enhance bradyzoite differentiation, infected cultures were subsequently transferred to incubators set at either 40.5 °C or 43 °C. Four incubation periods—24, 48, 72 and 120 h—were assessed, expanding upon the original 48 h exposure period used by Soête et al. (1994).

### 4.10.3 Nutrient deprivation

Prior to infection, the standard cell culture medium was replaced with an FBS-free RPMI 1640 medium to eliminate serum-derived nutrients. This serum-free environment was maintained by replacing the medium daily. The nutrient deprivation was sustained until cell fixation, performed 8 days after treatment initiation. This approach was adapted from previously described nutrient deprivation protocols targeting specific nutrients such as arginine, pyrimidines or cholesterol (Fox et al., 2004; Bohne et al., 1997; Ihara et al., 2014). However, in contrast to these studies, the present protocol involved the complete removal of serum and all its associated nutrients, including amino acids, lipids, cholesterol and growth factors.

### 4.10.4 Treatment with sodium nitroprusside (SNP)

To induce oxidative stress, the protocol described by Weiss et al. (1998) was adapted with modifications. At the onset of infection, SNP was added to the culture medium at concentrations of 10, 50, 70 and 100 µM, as part of a dose-response assay. This expands upon the original protocol, which employed a single concentration of 100 µM. To ensure sustained oxidative stress and preserve SNP efficacy, the culture medium was replaced daily with freshly prepared SNP-containing medium. Cell cultures were fixed for analysis at 3 days post-treatment, as in the original study, and additionally at 5 and 7 days post-treatment to assess time-dependent effects on parasite differentiation and host cell response.

### 4.10.5 Treatment with histone deacetylases inhibitors (HDACi)

At 12 h p.i. cell cultures were treated with two HDACi: apicidin and FR235222, following the protocol described by Bougdour et al. (2009). In contrast to the original study, which used a single concentration and a treatment duration of 2–3 days, we evaluated a broader range of concentrations—50, 100, 150 and 200 nM—to assess dose-dependent effects; and the treatment was sustained for an extended period of 15 days when cell cultures were fixed.

### 4.10.6 Treatment with bumped-kinase inhibitor (BKI): BKI1294

During the infection, BKI1294, a selective BKI, was introduced into the culture medium at a 5 µM concentration, following the protocol previously described by Jiménez-Meléndez et al 2017 and based on its use in the closely related apicomplexan parasite *N. caninum* (Winzer et al., 2020). After a period of 3 and 7 days p.i. cell cultures were fixed.

## 4.11 Monitoring of tachyzoite-bradyzoite conversion by IF

The tachyzoite–bradyzoite conversion rate was evaluated using a double IF assay. Coverslips were fixed either with 0.05% glutaraldehyde and 3% paraformaldehyde for 15 minutes or with cold methanol at -20°C for 10 minutes. Cell monolayers were then permeabilized with 0.25% Triton X-100 and blocked for 30 minutes at 37°C using a solution of 3% bovine serum albumin (BSA; Sigma-Aldrich, USA) in 1x PBS. After the blocking step, cell monolayers were incubated for 1 h with a polyclonal rabbit antiserum raised against the bradyzoite-specific antigen α-TgBAG1 (1:500), in combination with fluorescein-conjugated *Dolichos biflorus* agglutinin (DBA), 1:50; Vector Laboratories, USA). After incubation with the primary antibodies, cells were washed three times with PBS and then incubated for 1 hour with the appropriate goat IgG secondary antibody (anti-rabbit), conjugated to Alexa Fluor 594 (1:1000; Invitrogen, USA), diluted in PBS. Following this step, monolayers were again washed three times with PBS. Nuclei were subsequently stained with DAPI (1:2000 in PBS) for 1 min, followed by a final washing step consisting of two 1x PBS rinses and one with distilled water. Coverslips were mounted onto glass slides using ProLong Antifade mountant (Invitrogen, USA), and images were captured using a digital camera (Nikon PCO Tech Microscope Camera Panda, Japan) connected to an inverted fluorescence microscope (Nikon Eclipse TE 200, Japan). Each treatment condition was tested in three independent experiments, each performed with three technical replicates. All fields on each coverslip were carefully examined by two independent observers in a blinded manner. The formation of intermediate tachyzoite–bradyzoite stages was assessed by calculating the percentage of parasitophorous vacuoles that were positive for TgBAG1 staining. For each condition, 10 randomly selected microscopic fields were analysed, and a minimum of 100 parasitophorous vacuoles were counted to ensure precise and representative evaluation of the conversion process.

## 4.12 Data analysis

### 4.12.1 Statistical analysis of parasite invasion assays

As part of Objective 1, Sub-objective 1.1, differences in parasite invasion among groups were assessed using a non-parametric Kruskal–Wallis test, followed by Dunn's post hoc test for multiple comparisons. A p-value $\leq 0.05$ was considered statistically significant.

### 4.12.2 Statistical analysis of parasite proliferation assays

As part of Objective 1, Sub-objective 1.1, differences in parasite proliferation across the various p.i. time points were evaluated using the Kruskal–Wallis test, followed by Dunn's post hoc test for multiple comparisons. A p-value $\leq 0.05$ was considered statistically significant. The doubling time (dT), defined as the time required for a tachyzoite to replicate during the exponential growth phase, was calculated as described by Regidor-Cerrillo et al. (2011), using nonlinear regression analysis and an exponential growth equation in GraphPad Prism (GraphPad Software, USA).

### 4.12.3 Computational analysis of RNA-Seq data

As part of Objective 1, Sub-objective 1.2 and Objective 2, Sub-objective 2:1, raw data quality was first assessed using the FastQC tool. Quality control included evaluation of GC content and detection of duplicated reads, which can indicate sequencing errors, PCR amplification bias, or contamination. Low-quality reads were removed using Picard Tools (version 1.129; http://picard.sourceforge.net). High-quality reads were subsequently assembled and identified using the algorithm implemented in Cufflinks v2.2:1. The raw paired-end reads were mapped against the *B. taurus* genome version UDM3.1 (NCBI:GCA_000003055.3) provided by the ENSEMBL/NCBI database (http://www.ensembl.org/) and the *B. besnoiti* genome deposited in DDBJ/ENA/GenBank under the accession no. NWUJ00000000 using the TopHat2 v2:1.0

algorithm. For the quantification and differential expression of isoforms, the Cufflinks method was employed. The whole transcriptome was normalized by the size of the library using the DESeq2 proposed method to eliminate any statistical deviation that could alter the analysis (Kim et al., 2013).

A differential expression analysis was performed to compare gene transcription levels across the study groups. For primary bovine macrophages, host cell gene expression was analysed between the three target groups (MO-Bb, MO-hkBb and MO) at 4 and 8 h p.i. Similarly, *B. besnoiti* gene expression was compared between 4 h and 8 h p.i. In the case of primary bovine fibroblasts, host cell gene expression was evaluated between the two target groups (FI-Bb and FI) at 12 and 32 h p.i., alongside a comparison of *B. besnoiti* gene expression at the same time points. The differential expression level between sample groups was studied using the Cuffdiff algorithm (Trapnell et al., 2013). Genes and isoforms were considered differentially expressed when they presented a fold-change (FC) $\geq 1.5$ or $\leq -1.5$ and an adjusted p-value (padj) by false discovery rate (FDR) $\leq 0.05$.

To assess the correlation among all replicates from primary bovine macrophages and fibroblasts, a principal component analysis (PCA) was conducted using the prcomp function (with data centering and scaling) from the *Stats* R package (version 4.3.0), based on gene expression levels. The PCA results were visualized using the *ggplot2* R package (version 3.4.2). Sample correlations were further evaluated using the *adegenet* library from the statistical software R (*http://www.r-project.org*, accessed on 1 January 2023) to confirm their suitability as biological replicates. Additionally, heatmaps of a selection of DEGs from primary bovine macrophages and fibroblasts were generated using the heatmap.2 function from the *gplots* R package (version 3.1.3). The RNA-Seq data for primary bovine macrophages have been deposited in the NCBI database under accession number PRJNA785130 and the RNA-Seq data for primary bovine fibroblasts are available under accession number SUB14163821.

For bovine DEGs from both macrophages and fibroblasts, a gene set enrichment analysis was conducted using the g:Profiler web server that can be freely accessed at https://biit.cs.ut.ee/gprofiler/gost. g:Profiler was used to identify the Gene Ontology (GO)

terms (biological process (BP), molecular function (MF) and cellular components (CC)) and the Kyoto Encyclopaedia of Genes and Genomes (KEGG) pathways (https://www.genome.jp/kegg/pathway.html) for DEGs. The statistical domain scope was used for annotated genes. The significance threshold was the g:SCS threshold. Gene set enrichment results were graphically mapped to the enrichment plot produced in SRplot (http://www.bioinformatics.com.cn/srplot).

For functional studies of *B. besnoiti* genes, given the incomplete annotation of the reference genome, the ToxoDB database (*http://toxodb.org/toxo/*, ToxoDB release 56) was utilized to perform orthology and synteny analyses on unannotated genes, leveraging the more comprehensive annotation available for the *T. gondii* genome.

### 4.12.4 Statistical analysis of TUNEL-positive cells

As part of Objective 1, Sub-Objective 1.2, TUNEL-positive cells were quantified by randomly counting 60 different microscopic fields per well. Assays were carried out in triplicate, each with 3 different replicates. The ratio of apoptotic cells was calculated as the number of TUNEL-positive nuclei divided by the total number of nuclei. A nonparametric Kruskal-Wallis test followed by Dunn's post hoc test was used for statistical analysis. A $p$ value $\leq 0.05$ was considered statistically significant.

### 4.12.5 Statistical analysis of gene expression in target tissues of naturally infected bulls

As part of Objective 1, Sub-Objective 1.2, relative gene expression was calculated using the comparative method $2^{-\Delta\Delta Ct}$ (Livak and Schmittgen, 2001) after normalization with the housekeeping gene β-actin (B-actin) (Puech et al., 2015; Horcajo et al., 2017). For statistical analysis of gene expression in target tissues of naturally infected bulls, the Kruskal-Wallis test was used, followed by Dunn's test and $p \leq 0.1$ was considered statistically significant.

# Chapter V: Results

# Chapter V: Results

## 5.1. *Besnoitia besnoiti* efficiently invades and proliferates in primary bovine monocyte-derived macrophages

As part of Objective 1, Subobjective 1.1, our findings revealed that *B. besnoiti* tachyzoites can invade and replicate in primary bovine monocyte-derived macrophages. At 4 h p.i., intracellular tachyzoites were already observed in approximately 15% of macrophages infected with live tachyzoites. Furthermore, the number of intracellular events in macrophages infected with live tachyzoites determined by IF showed a gradual increase with the progression of the infection time (**Figure 15A**), showing exponential growth from 24 h p.i. until the egression that was observed by microscopic visualization at 72 h p.i. (**Figure 15B, C**). At 36 h p.i., all intracellular events visualized in macrophages infected with live tachyzoites consisted of parasitophorous vacuoles composed of more than one tachyzoite (medium to large-sized vacuoles) that are associated with active invasion. The average dT value was 15.13 h. According to the number of intracellular events, phagocytosis of heat-killed tachyzoites was finalized at 12 h p.i. because differences between 12 and 24 h p.i. were not found ($p = 0.17$) (**Figure 15A**). As expected, there was no increase in parasite load in macrophages infected with heat-killed tachyzoites as the infection progressed, indicating a lack of parasite multiplication (**Figure 15B, C**) At 36 h p.i., invasion events were not counted in macrophages infected with heat-killed tachyzoites (**Figure 15A**) since only tachyzoite debris that disappeared at 72 h p.i. was observed (**Figure 15C and D**). Furthermore, when macrophage morphology was assessed microscopically, the results showed that at 36 h p.i., macrophages infected with live tachyzoites were smaller, rounded, lacked filopodial structures and contained several large parasitophorous vacuoles compared to macrophages infected with heat-killed tachyzoites, which were larger and more irregular in shape (**Figure 15C and D**).

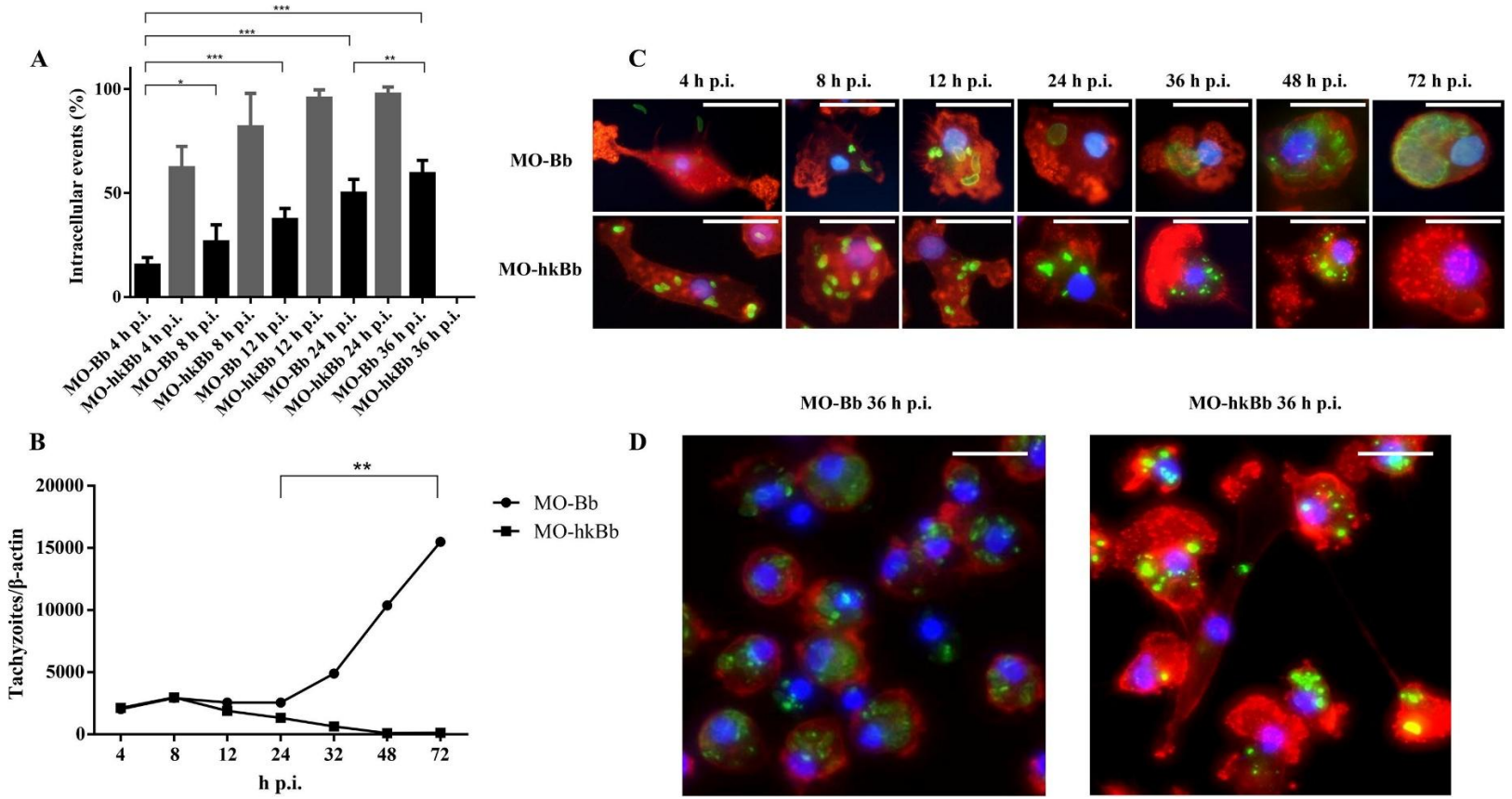


**Figure 15**. ***Besnoitia besnoiti*** **lytic cycle in primary bovine monocyte-derived macrophages. (A) Percentage of intracellular events at different time points p.i. (B)** ***In vitro*** **proliferation kinetics of** ***B. besnoiti*** **tachyzoites determined by qPCR. (C) Lytic cycle of live** ***B. besnoiti*** **tachyzoites (MO-Bb) and heat-killed tachyzoites (MO-hkBb) monitored by IF from 4 to 72 h p.i.** ***Besnoitia besnoiti*** **tachyzoites are stained with a hyperimmune rabbit antiserum directed against** ***B. besnoiti*** **tachyzoites and labelled with Alexa Fluor® 488 (green), phalloidin-labelled F-actin (red) and the nuclei of host cells are stained with DAPI (blue). Scale bars: 20 µm. (D) morphology of MO-Bb and MO-hkBb at 36 h p.i.** ***Besnoitia besnoiti*** **tachyzoites are stained with a rabbit polyclonal antibody against** ***B. besnoiti*** **labelled with Alexa Fluor® 488 (green), phalloidin-labelled F-actin (red) and the nuclei of host cells are stained with DAPI (blue). Scale bars: 100 µm. *Adjusted** ***P*** **values between 0.01 and 0.05; **adjusted** ***P*** **values between 0.01 and 0.001; as determined by Kruskal-Wallis test followed by Dunn's test.**

## 5.2. RNA-Seq analysis in primary bovine cells

### 5.2.1 Sequence mapping and principal component analyses validated the good quality of RNA-Seq data

The quality and quantity of the total RNA was determined in a Bioanalyzer 2100 (Agilent Biotek, USA) and a Qubit 2.0. B (Invitrogen, USA), all samples had an RNA integrity number (RIN) between 9.6 and 10. The sequencing process accounted for approximately 1 billion reads between all samples. After alignment, an average of 70% of the high-quality reads mapped to the reference *B. taurus* genome (**Tables 10 and 11**). Furthermore, PCA revealed that all replicates from the same condition clustered together, as shown in **Figure 16 and 17.**

**Table 10. Library sizes and statistics for transcriptome sequencing from all samples (macrophages infected with *B. besnoiti* live tachyzoites (MO-Bb), macrophages infected with heat-killed tachyzoites (MO-hkBb) and non-infected macrophages (MO) at 4 and 8 h p.i.**

| | Samples | Nº initial reads | Nº mapped reads | % mapped reads | Nº *B. besnoiti* mapped reads | Nº *B. taurus* mapped reads | *% B. besnoiti* mapped reads | % *B. taurus* mapped reads |
|---|---|---|---|---|---|---|---|---|
| 4 h p.i. | MO R1 | 51,300,764 | 38,976,506 | 75.98 | 16 | 38,976,490 | 0.00 | 75.98 |
| | MO R2 | 46,001,179 | 35,612,846 | 77.42 | 10 | 35,612,836 | 0.00 | 77.42 |
| | MO R3 | 52,723,448 | 40,006,340 | 75.88 | 42 | 40,006,298 | 0.00 | 75.88 |
| | MO-hkBb R1 | 68,010,765 | 49,982,350 | 73.49 | 1,232 | 49,981,118 | 0.00 | 73.49 |
| | MO-hkBb R2 | 52,029,327 | 39,668,396 | 76.24 | 1,130 | 39,667,266 | 0.00 | 76.24 |
| | MO-hkBb R3 | 54,819,387 | 41,978,942 | 76.58 | 936 | 41,978,006 | 0.00 | 76.58 |
| | MO-Bb R1 | 62,085,882 | 47,060,256 | 75.80 | 17,286,650 | 29,773,606 | 27.84 | 47.96 |
| | MO-Bb R2 | 59,062,489 | 43,531,104 | 73.70 | 11,621,315 | 31,914,438 | 19.67 | 54.04 |
| | MO-Bb R3 | 56,022,984 | 39,962,630 | 71.33 | 5,927,824 | 34,034,806 | 10.58 | 60.75 |
| 8 h p.i. | MO R1 | 64,665,046 | 47,215,636 | 73.02 | 2,472 | 47,213,164 | 0.00 | 73.01 |
| | MO R2 | 62,397,159 | 44,774,242 | 71.76 | 14 | 44,774,228 | 0.00 | 71.76 |
| | MO R3 | 64,194,147 | 47,281,306 | 73.65 | 534 | 47,280,772 | 0.00 | 73.65 |
| | MO-hkBb R1 | 68,607,657 | 49,059,816 | 71.51 | 654 | 49,059,162 | 0.00 | 71.51 |
| | MO-hkBb R2 | 72,355,667 | 52,874,108 | 73.08 | 67,318 | 52,806,790 | 0.09 | 72.98 |
| | MO-hkBb R3 | 69,901,807 | 53,409,806 | 76.41 | 28,982 | 53,380,824 | 0.04 | 76.37 |
| | MO-Bb R1 | 60,733,174 | 51,053,016 | 84.06 | 9,412,516 | 41,640,500 | 15.49 | 68.56 |
| | MO-Bb R2 | 60,306,213 | 42,799,620 | 70.97 | 29,819,900 | 12,979,720 | 49.44 | 21.52 |
| | MO-Bb R3 | 68,948,912 | 46,388,346 | 67.28 | 32,626,940 | 13,761,406 | 47.32 | 19.96 |

**Table 11. Library sizes and statistics for transcriptome sequencing from all samples (fibroblasts infected with *B. besnoiti* live tachyzoites (FI-Bb) and non-infected fibroblasts (FI) at 12 and 32 h p.i.**

| | Samples | Nº initial reads | Nº mapped reads | % mapped reads | Nº *B. besnoiti* mapped reads | Nº *B. taurus* mapped reads | *% B. besnoiti* mapped reads | % *B. taurus* mapped reads |
|---|---|---|---|---|---|---|---|---|
| 12 h p.i. | FI-Bb R1 | 65,874,627 | 43,255,868 | 65.66 | 348,366 | 42,907,502 | 0.529 | 65.14 |
| | FI-Bb R2 | 47,529,525 | 36,334,128 | 76.45 | 847,518 | 35,486,610 | 1.783 | 74.66 |
| | FI-Bb R3 | 56,335,028 | 43,934,064 | 77.99 | 517,34 | 43,416,724 | 0.918 | 77.07 |
| 32.h p.i. | FI-Bb R1 | 81,012,164 | 55,562,260 | 68.59 | 1,622,324 | 53,939,936 | 2.003 | 66.58 |
| | FI-Bb R2 | 45,851,628 | 33,969,166 | 74.08 | 3,499,710 | 30,469,456 | 7.633 | 66.45 |
| | FI-Bb R3 | 47,688,895 | 34,535,722 | 72.42 | 1,970,114 | 32,565,608 | 4.131 | 68.29 |
| Non-infected | Fi R1 | 51,300,764 | 38,976,506 | 75.98 | 16 | 38,976,490 | 0.000 | 75.98 |
| | Fi R2 | 46,001,179 | 35,612,846 | 77.42 | 10 | 35,612,836 | 0.000 | 77.42 |
| | Fi R3 | 52,723,448 | 40,006,340 | 75.88 | 42 | 40,006,298 | 0.000 | 75.88 |

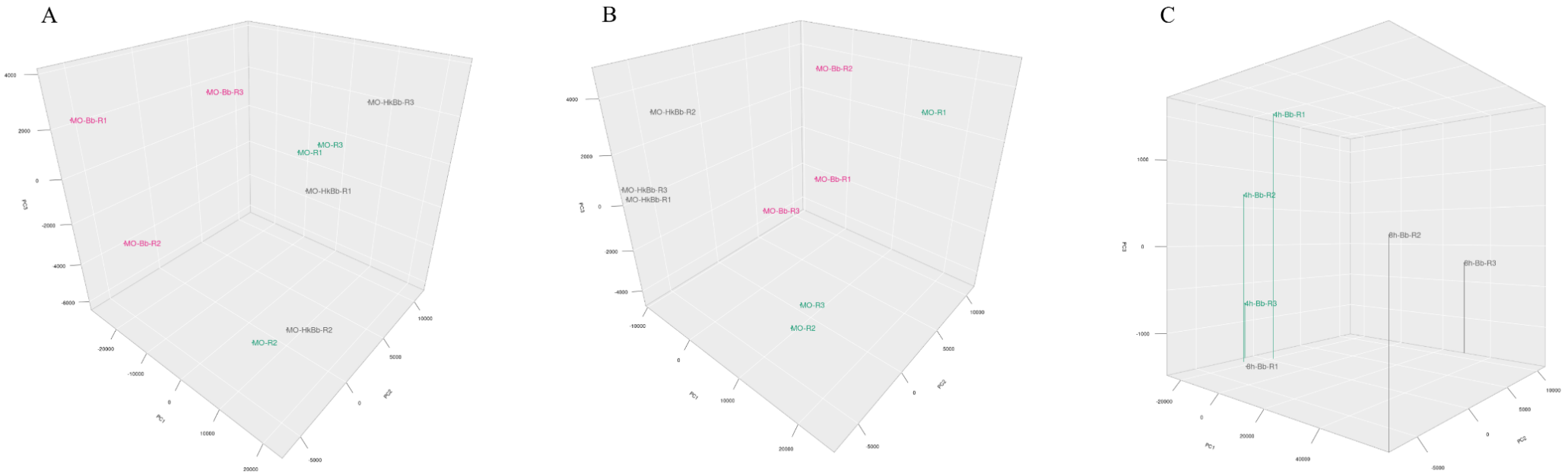


**Figure 16. Principal component analysis (PCA) plots representing the clustering of biological replicates based on gene expression levels of monocyte-derived macrophages at 4 h (A) and 8 h p.i. (B) and *B. besnoiti* at 4 *vs* 8 h p.i. (C).**

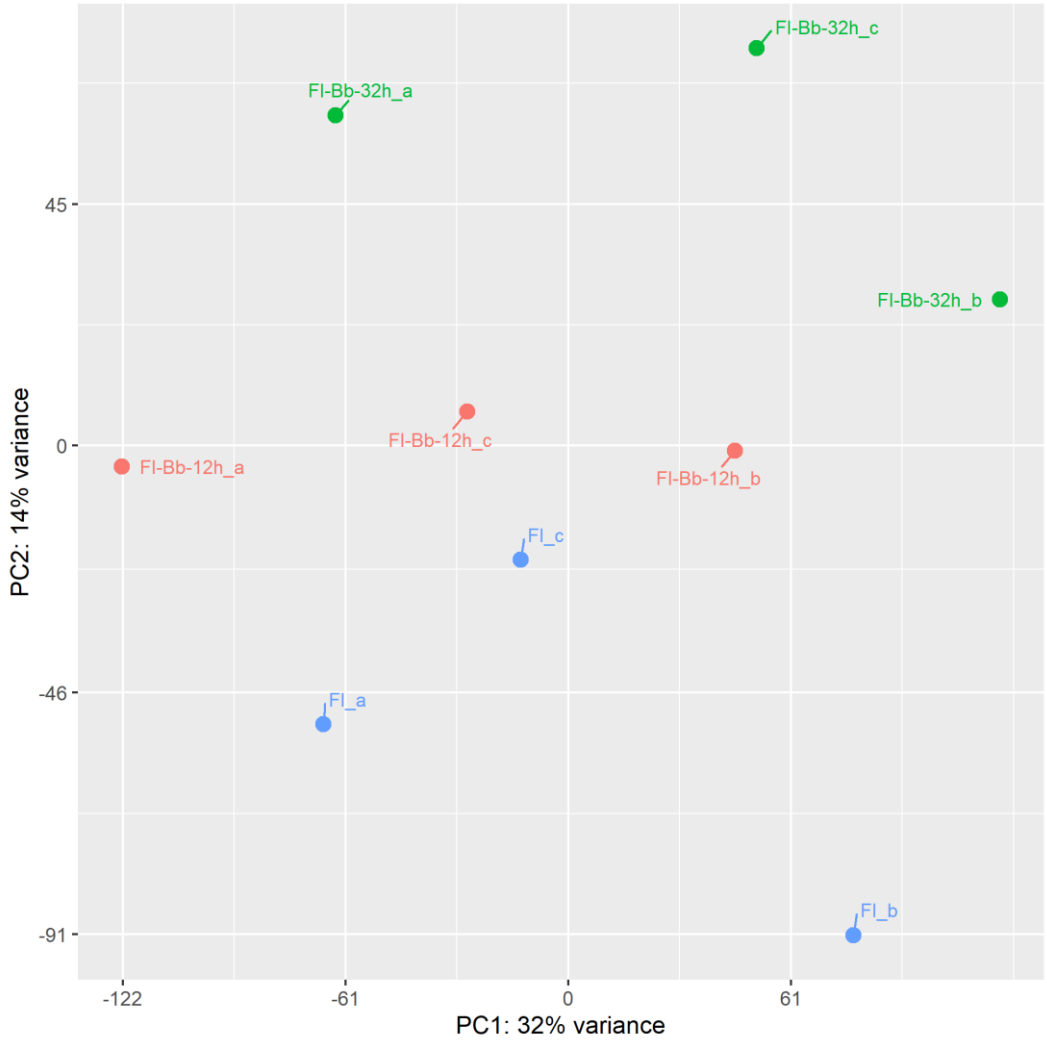


**Figure 17. Principal component analysis (PCA) plots representing the clustering of biological replicates based on gene expression levels of fibroblasts at 12 and 32 h p.i.**

### 5.2.2 Primary bovine monocyte-derived macrophages are activated early upon infection and apoptosis, mitogen-activated protein kinases (MAPKs) and *Herpes simplex* virus 1 infection are the most relevant modulated pathways

*Besnoitia besnoiti* infection initiated a wide alteration of the host transcriptional profile (**Table 12 and 13; Figure 18**). Differential expression analysis revealed that the number of DEGs in the macrophages infected with live tachyzoites *vs* non-infected macrophages comparison increased with the progression of the infection (545 at 4 h p.i. *vs* 1,739 at 8 h p.i.) (**Table 12**). To highlight the host cell modulation by the live tachyzoites, we used heat-killed *B. besnoiti* tachyzoites as a control for the cellular response after phagocytosis. An increase in the number of DEGs over time in macrophages infected with heat-killed tachyzoites *vs* non-infected macrophages comparison was also observed (514 at 4 h p.i. *vs* 2,813 at 8 h p.i.).

The functions of DEGs were predicted using GO and KEGG enrichment analyses (**Table 12**). The macrophages infected with live tachyzoites *vs* non-infected macrophages comparison at 4 h p.i. showed an enrichment in BP involved in host cell defence mechanisms and cellular response to stress. In fact, several DEGs involved in endoplasmic reticulum (ER) stress and the unfolded protein response (UPR) (*IRE1α, IPR3, ITP31, ATF4, CHOP, MMPs, Bcl-2, BH3, GADD45A, GADD45B, HSP40, HSP70*) were upregulated. In terms of MF, DEGs were enriched in categories involved in transmembrane transport and metabolic processes. Furthermore, GO terms for cellular components (CC) indicated that a majority of DEGs were associated with the autophagy machinery and apoptotic complexes, such as Atg1/ULK1 and CHOP-ATF4 complexes. Moreover, the KEGG pathway analysis revealed that DEGs were mainly involved in apoptosis, MAPKs and lysosome modulation. Apoptosis was the top ranked pathway by statistical significance, with 18 genes significantly regulated (17 out of 18 DEGs appeared upregulated) (**Table 13, Figure 19**). In addition, the MAPK pathway was the second-ranked pathway by statistical significance, with 22 genes from the p38 and JNK subfamilies being significantly regulated (**Table 13; Figure 20**). The lysosome pathway was the third-ranked pathway by statistical significance, with 12 genes significantly regulated (**Figure 21**). On the other hand, the transcriptome of cells inoculated with heat-killed tachyzoites was clearly different. The only commonly modulated pathway was the lysosome. Other pathways differentially regulated in macrophages infected with heat-

killed tachyzoites *vs* non-infected macrophages were mineral absorption and carbon folate pathways. In addition, when gene expression between macrophages infected with live tachyzoites *vs* macrophages infected with heat-killed tachyzoites was compared, apoptosis and MAPK pathways again appeared to be differentially regulated, similarly to the MO-Bb *vs* MO comparison described above (**Table 12**).

At 8 h p.i., most of the enriched BP terms in the macrophages infected with live tachyzoites *vs* non-infected macrophages comparison were associated with nutrient deprivation and metabolic processes. Regarding MF terms, enriched categories were related to molecular binding and transport and for CC terms, intracellular membrane-bound organelles and Atg1/ULK1 and CHOP-ATF4 complexes were identified. KEGG pathway analysis only showed that the *Herpes simplex* virus 1 infection signalling pathway was enriched, with 41 genes being significantly regulated. Several type I interferon-stimulated genes (ISGs) were upregulated: *cGAS*, *IFIH1*, zinc-finger (ZNF) protein-encoding genes, *OAS* (oligo adenylate synthetase), *CCL2*, *caspase-3* and *TAB1*, among others (**Table 13; Figure 22**). In addition, heat-killed parasite internalization (MO-hkBb *vs* MO) did not lead to the regulation of the *Herpes simplex* virus 1 infection pathway, but it did regulate other pathways, such as ribosome biogenesis and RNA polymerase. Furthermore, the Atg1/ULK1 and CHOP-ATF4 complexes were also shown to be upregulated when gene expression between macrophages infected with live tachyzoites *vs* macrophages infected with heat-killed tachyzoites was compared (**Table 12**).

**Table 12. Number of DEGs among conditions: macrophages infected with live tachyzoites (MO-Bb), macrophages infected with heat-killed tachyzoites (MO-hkBb) and non-infected macrophages (MO). The table also summarizes the results of functional enrichment analyses, listing the top five most significantly enriched terms in each category: BP, MF and CC; and KEGG pathways.**

| | | Nº DEGs | Upregulated DEGs | Downregulated DEGs | Biological processes | | Molecular function | | Cellular components | | Pathway enrichment | |
|---|---|---|---|---|---|---|---|---|---|---|---|---|
| | | | | | GO term | Adjusted p-value | GO term | Adjusted p-value | GO term | Adjusted p-value | KEGG term | Adjusted p-value |
| 4 h p.i. | MO-Bb *vs* MO | 545 | 347 | 198 | Phosphorylation (GO:0016310) | $1.01x10^{-6}$ | Binding (GO:0005488) | $9.86x10^{-3}$ | Lysosome (GO:0005764) | $3.75x10^{-8}$ | Apoptosis (KEGG:04210) | $2.08x10^{-5}$ |
| | | | | | Regulation of signal transduction (GO:0009966) | $2.05x10^{-5}$ | Enzyme binding (GO:0019899) | $1.08\ x10^{-2}$ | Lytic vacuole (GO:0000323) | $4.07x10^{-8}$ | MAPK signalling pathway (KEGG:04010) | $6.52\ x10^{-3}$ |
| | | | | | Intracellular signal transduction (GO:0035556) | $3.05x10^{-5}$ | - | - | Cytoplasm (GO:0005737) | $1.50x10^{-7}$ | Lysosome (KEGG:04142) | $2.94x10^{-2}$ |
| | | | | | Regulation of response to stimulus (GO:0048583) | $5.26x10^{-5}$ | - | - | Vacuole (GO:0005773) | $3.71x10^{-7}$ | - | - |
| | | | | | Protein phosphorylation (GO:0006468) | $5.71x10^{-5}$ | - | - | Intracellular (GO:0005622) | $2.23x10^{-5}$ | - | - |
| | MO-Bb *vs* MO-hkBb | 148 | 20 | 128 | Response to starvation (GO:0042594) | $1.87x10^{-6}$ | Aminoacyl-tRNA ligase activity (GO: GO:0004812) | $3.39x10^{-3}$ | Cytoplasm (GO:0005737) | $3.22x10^{-4}$ | Aminoacyl-tRNA biosynthesis (KEGG:00970) | $1.27x10^{-3}$ |
| | | | | | Cellular response to stress (GO:0033554) | $8.63x10^{-6}$ | Ligase activity. forming carbon-oxygen bonds (GO:0016875) | $3.39x10^{-3}$ | Atg1/ULK1 kinase complex (GO:1990316) | $3.75x10^{-3}$ | Central carbon metabolism in cancer (KEGG:05230) | $7.37x10^{-3}$ |
| | | | | | Carboxylic acid metabolic process (GO:0019752) | $1.64x10^{-5}$ | L-amino acid transmembrane transporter activity (GO:0015179) | $9.83x10^{-3}$ | Intracellular (GO:0005622) | $9.83x10^{-3}$ | Biosynthesis of amino acids (KEGG:01230) | $1.30x10^{-2}$ |
| | | | | | Oxoacid metabolic process (GO:0043436) | $3.81x10^{-5}$ | Neutral amino acid transmembrane transporter activity (GO:0015175) | $1.18x10^{-2}$ | CHOP-ATF4 complex (GO:1990617) | $1.08x10^{-2}$ | MAPK signalling pathway (KEGG:04010) | $1.84x10^{-2}$ |
| | | | | | Organic acid metabolic process (GO:0006082) | $5.89x10^{-5}$ | Organic anion transmembrane transporter activity (GO:0008514) | $1.45x10^{-2}$ | Cytosol (GO:0005829) | $1.97x10^{-2}$ | Apoptosis (KEGG:04210) | $4.1610^{-2}$ |

| | | | | | | | | | | | | |
|---|---|---|---|---|---|---|---|---|---|---|---|---|
| **8 h p.i.** | **MO-hkBb *vs* MO** | 514 | 301 | 213 | Cellular transition metal ion homeostasis (GO:0046916) | $6.16x10^{-6}$ | - | - | Vacuole (GO:0005773) | $6.11x10^{-13}$ | Mineral absorption (KEGG:04978) | $1.62x10^{-3}$ |
| | | | | | Transition metal ion homeostasis (GO:0055076) | $8.45x10^{-6}$ | - | - | Lysosome (GO:0005764) | $3.01x10^{-12}$ | One carbon pool by folate (KEGG:00670) | $1.15x10^{-2}$ |
| | | | | | Homeostatic process (GO:0042592) | $3.58x10^{-3}$ | - | - | Lytic vacuole (GO:0000323) | $3.33x10^{-12}$ | Lysosome (KEGG:04142) | $1.56x10^{-2}$ |
| | | | | | Cellular response to chemical stimulus (GO:0070887) | $1.66x10^{-2}$ | - | - | Cytoplasm (GO:0005737) | $1.20x10^{-7}$ | - | - |
| | | | | | Iron ion homeostasis (GO:0055072) | $3.8x10^{-2}$ | - | - | Intracellular membrane-bounded organelle (GO:0043231) | $1.47x10^{-6}$ | - | - |
| | **MO-Bb *vs* MO** | 1739 | 998 | 741 | DNA metabolic process (GO:0006259) | $2.91x10^{-5}$ | Binding (GO:0005488)) | $1.47x10^{-6}$ | Intracellular (GO:0005622) | $3.14x10^{-28}$ | *Herpes simplex* virus 1 infection (KEGG:05168) | $9.50x10^{-3}$ |
| | | | | | Cellular metabolic process (GO:0044237) | $3.44x10^{-5}$ | Catalytic activity (GO:0003824) | $1.93x10^{-5}$ | Intracellular membrane-bounded organelle (GO:0043231) | $2.69x10^{-27}$ | - | - |
| | | | | | Nucleic acid metabolic process (GO:0090304) | $5.71x10^{-5}$ | Organic cyclic compound binding (GO:0097159) | $1.20x10^{-3}$ | Membrane-bounded organelle (GO:0043227) | $7.35x10^{-25}$ | - | - |
| | | | | | Heterocycle metabolic process (GO:0046483) | $8.16x10^{-5}$ | Heterocyclic compound binding (GO:1901363) | $1.49x10^{-3}$ | Organelle (GO:0043226) | $9.40x10^{-21}$ | - | - |
| | | | | | Cellular aromatic compound metabolic process (GO:0006725) | $2.79x10^{-4}$ | Nucleic acid binding (GO:0003676) | $4.04x10^{-3}$ | Intracellular organelle (GO:0043229) | $5.26x10^{-19}$ | - | - |
| | **MO-Bb *vs* MO-hkBb** | 231 | 151 | 80 | Response to starvation (GO:0042594) | $1.07x10^{-4}$ | - | - | Autophagosome membrane (GO:0000421) | $1.46x10^{-3}$ | - | - |
| | | | | | Response to nutrient levels (GO:0031667) | $2.48x10^{-3}$ | - | - | Atg1/ULK1 kinase complex (GO:1990316) | 1.73x10-$^{2}$ | - | - |
| | | | | | Cellular response to starvation (GO:0009267) | $3.09x10^{-3}$ | - | - | CHOP-ATF4 complex (GO:1990617) | $3.1x10^{-2}$ | - | - |
| | | | | | Carboxylic acid metabolic process (GO:0019752) | $3.25x10^{-3}$ | - | - | - | - | - | - |
| | | | | | Cellular response to nutrient levels (GO:0031669) | $3.27x10^{-3}$ | - | - | - | - | - | - |

| | | | | | | | | | | | |
|---|---|---|---|---|---|---|---|---|---|---|---|
| **MO-hkBb *vs* MO** | 2813 | 1609 | 1204 | ncRNA processing (GO:0034470) | $1.17x10^{-18}$ | Binding (GO:0005488) | $1.09x10^{-15}$ | Membrane-bounded organelle (GO:0043227) | $5.02x10^{-59}$ | Ribosome biogenesis in eukaryotes (KEGG:03008) | $4.26x10^{-5}$ |
| | | | | ncRNA metabolic process (GO:0034660) | $2.05x10^{-18}$ | Catalytic activity. acting on RNA (GO:0140098) | $4.44x10^{-10}$ | Intracellular membrane-bounded organelle (GO:0043231) | $1.01x10^{-57}$ | Fanconi anemia pathway (KEGG:03460) | $2:15x10^{-4}$ |
| | | | | Cellular metabolic process (GO:0044237) | $7.53x10^{16}$ | Nucleic acid binding (GO:0003676) | $2.63x10^{-8}$ | Intracellular (GO:0005622) | $3.31x10^{-57}$ | RNA polymerase (KEGG:03020) | $1.39x10^{-2}$ |
| | | | | Cellular component organization or biogenesis (GO:0071840) | $1.03x10^{14}$ | Heterocyclic compound binding (GO:1901363) | $1.26x10^{-6}$ | Organelle (GO:0043226) | $4.05x10^{-49}$ | - | - |
| | | | | rRNA processing (GO:0006364) | $3.56x10^{-14}$ | Catalytic activity (GO:0003824) | $1.45x10^{-6}$ | Intracellular organelle (GO:0043229) | $2.45x10^{-48}$ | - | - |

**Table 13. Gene description and FC values of a selection of *B. taurus* DEGs under the different conditions studied.**

| Pathway | Gene ID | Description | FC MO-Bb *vs* MO at 4 h p.i. | FC MO-Bb *vs* MO-hkBb at 4 h p.i. | FC MO-hkBb *vs* MO at 4 h p.i. | FC MO-Bb *vs* MO at 8 h p.i. | FC MO-Bb *vs* MO-hkBb at 8 h p.i. | FC MO-hkBb *vs* MO at 8 h p.i. |
|---|---|---|---|---|---|---|---|---|
| Apoptosis | *TUBA1A* | Microtubules are highly dynamic structures, which consist of α- and β-tubulin heterodimers and are involved in cell apoptosis (Parker et al., 2014) | 2.31 | - | - | 1.92 | 1.76 | - |
| | *TUBA1B* | | 1.59 | - | - | 1.55 | - | - |
| | *LMNB1* | Lamin B1 is a regulator of cell apoptosis (Lv et al., 2024) | 1.6 | - | - | - | - | - |
| | *TRAF1* | TNF receptor associated factor 1 is a specific target of caspases activated during TNF- and Fas-induced apoptosis (Leo et al., 2001) | 1.72 | - | - | - | - | - |
| | *AIFM1* | Apoptosis inducing factor mitochondria associated 1 resides within the intermembrane space of mitochondria and upon programmed cell death induces chromatin condensation and DNA fragmentation (Hevler et al., 2021) | -1.63 | - | - | - | - | - |
| | *CTSB* | Cathepsins have been implicated in directing cells toward apoptosis (de Castro et al., 2016) | 2.08 | - | - | 1.59 | - | - |
| | *CTSZ* | | 1.77 | - | - | 2.03 | - | - |
| | *CASP6* | Caspase 6 promotes the activation of cell apoptosis (Zheng et al., 2020) | 1.67 | 1.61 | - | 1.65 | - | - |
| | *ERN1* | Endoplasmic reticulum to nucleus signalling 1 regulates cell survival or apoptosis in response to ER stress signals (Chen et al., 2013) | 1.52 | - | - | - | - | - |
| | *Bcl-2* | B-cell lymphoma 2 determines whether a cell commits to apoptosis and hence has crucial roles in development, homeostasis and immunity (Czabotar et al., 2014) | 1.9 | - | - | - | - | - |
| | *ITPR1* | Inositol 1,4,5-trisphosphate receptor type 1 is an intracellular $Ca^{2+}$-release channel during apoptosis (Parys et al., 2012) | 1.99 | - | - | -2:11 | - | - |
| | *PMAIP1* | Phorbol-12-myristate-13-acetate-induced protein promotes activation of caspases and therefore apoptosis (Holzerland et al., 2020) | 2.77 | 1.69 | - | 1.55 | 1.9 | - |
| Apoptosis and MAPKs | *FAS* | Fas cell surface death receptor induces apoptosis of cells expressing Fas on the membrane by triggering a cascade of caspases (Timmer et al., 2002) | 1.89 | - | - | - | - | - |
| | *GADD45A* | Growth arrest and DNA damage inducible α and β are genes that are rapidly induced by cell stress and have been implicated in apoptosis (Gupta et al., 2006) | 3.25 | - | - | - | - | - |
| | *GADD45B* | | 2.09 | - | - | - | - | - |
| | *ATF4* | Activating transcription factor 4 is a stress-induced transcription factor that controls the expression of a wide range of adaptive genes that allow cells to endure periods of stress. However, under persistent stress conditions, ATF4 promotes the induction of apoptosis (Wortel et al., 2017) | 2.53 | 2:11 | - | 1.89 | 1.81 | - |
| | *CHOP* | DNA damage inducible transcript 3 plays an important role in ER stress-induced apoptosis (Hu et al., 2019) | 2.35 | 1.78 | - | - | 1.75 | - |
| | *NRAS* | NRAS proto-oncogene, GTPase is important is important for avoidance of apoptosis (Eskandarpour et al., 2005) | 1.56 | - | - | - | - | - |
| MAPKs | *DUSP1* | Dual specificity phosphatases are a family of protein which can dephosphorylate both threonine and tyrosine residues in the Thr-X-Tyr activation motif of MAPKs (Cho et al., 2017) | 1.52 | - | - | - | - | - |
| | *DUSP2* | | 2.53 | 2:13 | - | - | 2.08 | - |
| | *DUSP3* | | 1.8 | - | - | 1.79 | - | - |
| | *DUSP7* | | -1.65 | - | - | - | - | - |
| | *VEGFA* | Secretion of vascular endothelial growth factor A by monocyte-derived macrophages appears to be critical for inducing angiogenesis in tissue repair (Corliss et al., 2016). Moreover, VEGFA is known to recruit macrophages to the site of infection (Harding et al., 2019) | 2.29 | 1.87 | - | - | - | - |

| | | | | | | | | |
|---|---|---|---|---|---|---|---|---|
| | *PLA2G4B* | Phospholipase A2, group IVB. Phospholipases mediated phospholipid hydrolysis and lead to the production of lipid mediators or second messengers that affect signal transduction, thus regulating a variety of physiologic and pathophysiologic processes in macrophages (Spadaro et al., 2017) | -1.87 | - | - | - | - | - |
| | *MAP3K6* | | -1.68 | - | - | - | - | - |
| | *MAPK13* | Stimulation of macrophages by a variety of agents causes activation of signalling cascades of MAPKs (Rao, 2001). The immune response is one of several key functions regulated by MAPKs, with the production of immunomodulatory cytokines and interleukins induced by the activation of p38 MAPK, JNK and ERK pathways (Soares-Silva et al., 2016) | -1.9 | - | - | - | 1.73 | - |
| | *MAPK14* | | -1.79 | - | - | - | - | - |
| | *MKNK2* | | 2.88 | 2.33 | - | 1.6 | 1.98 | - |
| | *CSF1R* | Colony stimulating factor 1 receptor regulates the proliferation, differentiation and functional activation of monocytes (Jones et al., 2013) | -1.67 | - | - | - | - | - |
| | *AREG* | Macrophages express amphiregulin upon tissue damage (Minutti et al., 2019). AREG participates in tissue repair and is an important effector of inflammation regulation (Meng et al., 2015) | 4.94 | 3.25 | - | -3.19 | 3.11 | - |
| **MAPKs and *Herpes simplex* virus 1 infection** | *IRAK1* | Interleukin 1 receptor associated kinase 1 is central for lipid metabolism in macrophages (Rana et al., 2016) | 1.82 | - | - | 1.67 | - | - |
| ***Herpes simplex* virus 1 infection** | *BST2* | Bone marrow stromal cell antigen 2 plays a role in virus retention or release in macrophages (Chu et al., 2012) | - | - | - | -1.76 | - | - |
| | *BST2-like* | | - | - | - | -2:18 | - | - |
| | *CASP3* | Caspase 3 promotes an anti-inflammatory clearance by macrophages (Turner et al., 2003) | - | - | - | -1.52 | - | - |
| | *CCL2* | C–C motif chemokine ligand 2 is a member of the chemokine family that mediates monocyte recruitment into inflamed tissues (Sierra-Filardi et al., 2014). It also plays an important role in scleroderma and fibrosis (Masuda et al., 2013) | 2.25 | - | - | -2.03 | -2.03 | - |
| | *CGAS* | Cyclic GMP–AMP synthase is a cytosolic sensor of foreign DNA. When CGAS is activated, it induces the gene expression of ISGs, several inflammatory mediators, pro-apoptotic genes and chemokines (Decout et al., 2021) | - | - | - | -2.22 | - | - |
| | *EIF2AK2* | EIF2AK2 and EIF2B3 are RNA binding proteins. Translation of mRNAs encoding EIF2AK2 was activated during *Leishmania donovani* macrophage infection (Chaparro et al., 2020) | - | - | - | -2.08 | - | - |
| | *EIF2B3* | | - | - | - | 2.33 | -2.05 | - |
| | *HCFC2* | Host cell factor C2 is necessary for defence against diverse infections (Sun et al., 2017) | - | - | - | 1.74 | - | - |
| | *IFIH1* | Interferon induced with helicase C domain 1is a recognition receptor for RNA that induces a type I interferon response (Dias-Junior et al., 2018) | - | - | - | -1.73 | - | - |
| | *MHC-I* | Macrophages can process and present exogenous antigens on major histocompatibility complex class I molecules through an alternative mechanism involving the internalization of antigens and the secretion of peptides loading MHC class I molecules at the cell surface (Martín-Orozco et al., 2001) | - | - | - | 1.79 | - | - |
| | *OAS1X* | Oligoadenylate synthetases are crucial to limit virus replication and trigger the apoptosis of infected cells (Drappier and Michiels, 2015) | - | - | - | -1.98 | - | - |
| | *OAS1Y* | | - | - | - | -1.96 | - | - |
| | *OAS1Z* | | - | - | - | -2.02 | - | - |
| | *OAS2* | | - | - | - | -2.74 | - | - |
| | *TAB1* | TGF-beta activated kinase 1 (MAP3K7) binding protein 1 regulates macrophage glycolisis (Zeng et al., 2020) | - | - | - | 1.54 | - | - |
| | *ZNF1* | | - | - | - | 2.43 | - | - |

| | | | | | | | |
|---|---|---|---|---|---|---|---|
| *ZNF205* | | - | - | - | 3.6 | - | - |
| *ZNF212* | | - | - | - | 3.21 | - | - |
| *ZNF25* | | - | - | - | -2.76 | - | - |
| *ZNF250* | | - | - | - | 2.35 | - | - |
| *ZNF28* | | - | - | - | 1.66 | - | - |
| *ZNF286A* | | - | - | - | 1.69 | - | - |
| *ZNF30* | | - | - | - | 1.69 | - | - |
| *ZNF34* | | - | - | - | 1.52 | - | - |
| *ZNF354A* | The zinc finger proteins are expressed by the cells in response to different viral attacks. They mark the viral mRNA for degradation contributing to inhibit the translation of proteins from this mRNA (Badshah et al., 2020). Zinc finger proteins promote the resolution of inflammation by helping to eliminate the mRNAs of certain pro-inflammatory cytokines (Fu et al., 2017). Zinc finger proteins are involved in the resolution of infections (Wessels et al., 2017) | - | - | - | 1.75 | - | - |
| *ZNF382* | | - | - | - | 1.79 | - | - |
| *ZNF383* | | - | - | - | 2.46 | - | - |
| *ZNF416* | | - | - | - | -1.81 | - | - |
| *ZNF45* | | - | - | - | -1.58 | - | - |
| *ZNF473* | | - | - | - | 1.86 | - | - |
| *ZNF501* | | - | - | - | 1.74 | - | - |
| *ZNF527* | | - | - | - | 2.05 | - | - |
| *ZNF548* | | - | - | - | -1.53 | - | - |
| *ZNF596* | | - | - | - | -1.64 | - | - |
| *ZNF624* | | - | - | - | 2.25 | - | - |
| *ZNF746* | | - | - | - | 1.75 | - | - |

FC, fold change; MO-Bb, macrophages infected with live *Besnoitia besnoiti* tachyzoites; MO-hkBb, macrophages inoculated with heat-killed *B. besnoiti* tachyzoites; MO, non-infected macrophages; MAPKs, mitogen-activated protein kinases.

-, the gene is not differentially regulated.

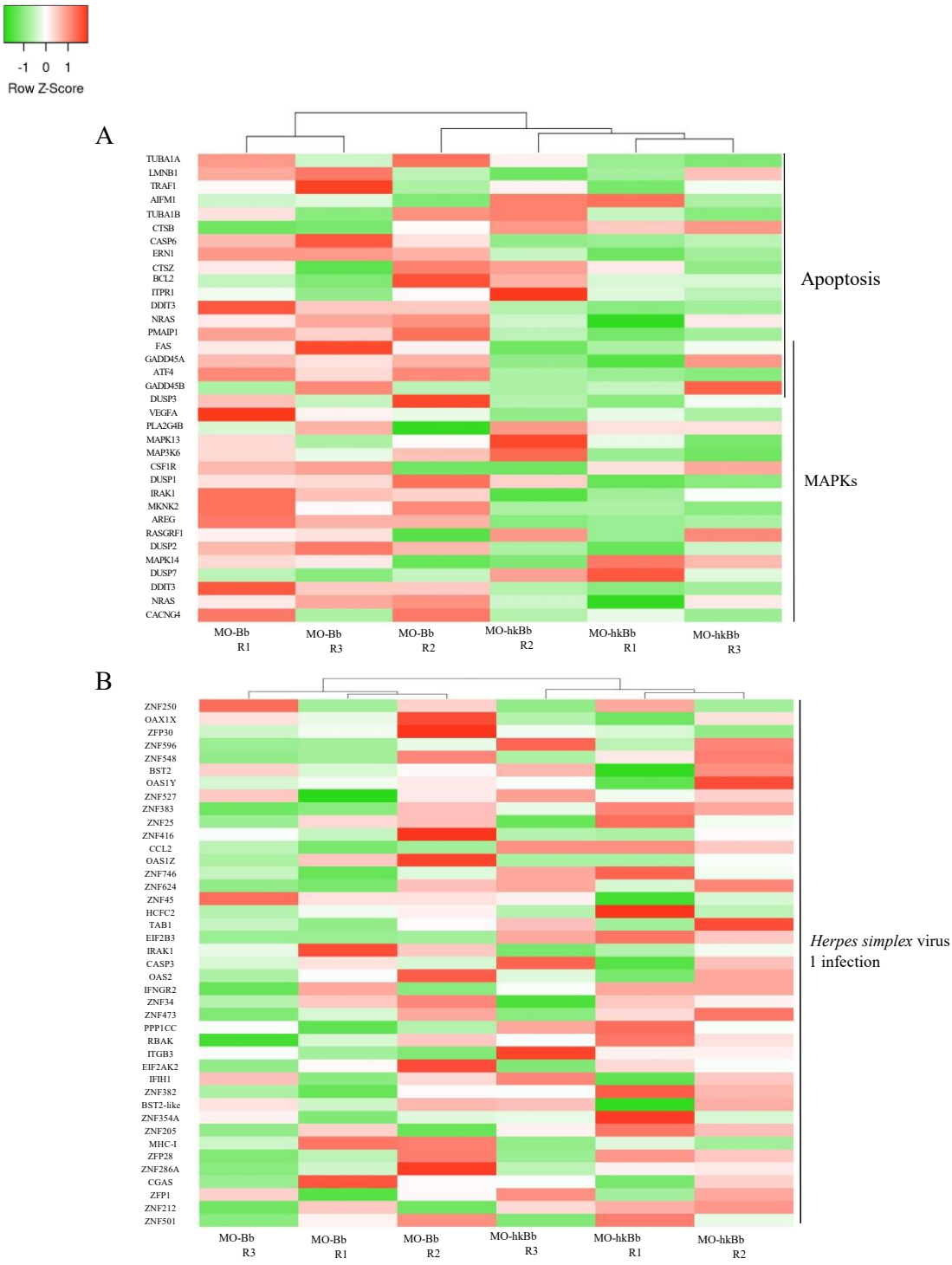


**Figure 18. Heatmaps of a selection of *B. taurus* DEGs in bovine macrophages. (A) A heatmap showing patterns of expression in a selection of *B. taurus* DEGs in macrophages infected with live tachyzoites (MO-Bb) and macrophages infected with heat-killed tachyzoites (MO-hkBb) at 4 h p.i. (B) A heatmap showing patterns of expression in a selection of *B. taurus* DEGs in macrophages infected with live tachyzoites (MO-Bb) and macrophages infected with heat-killed tachyzoites (MO-hkBb) at 8 h p.i.**

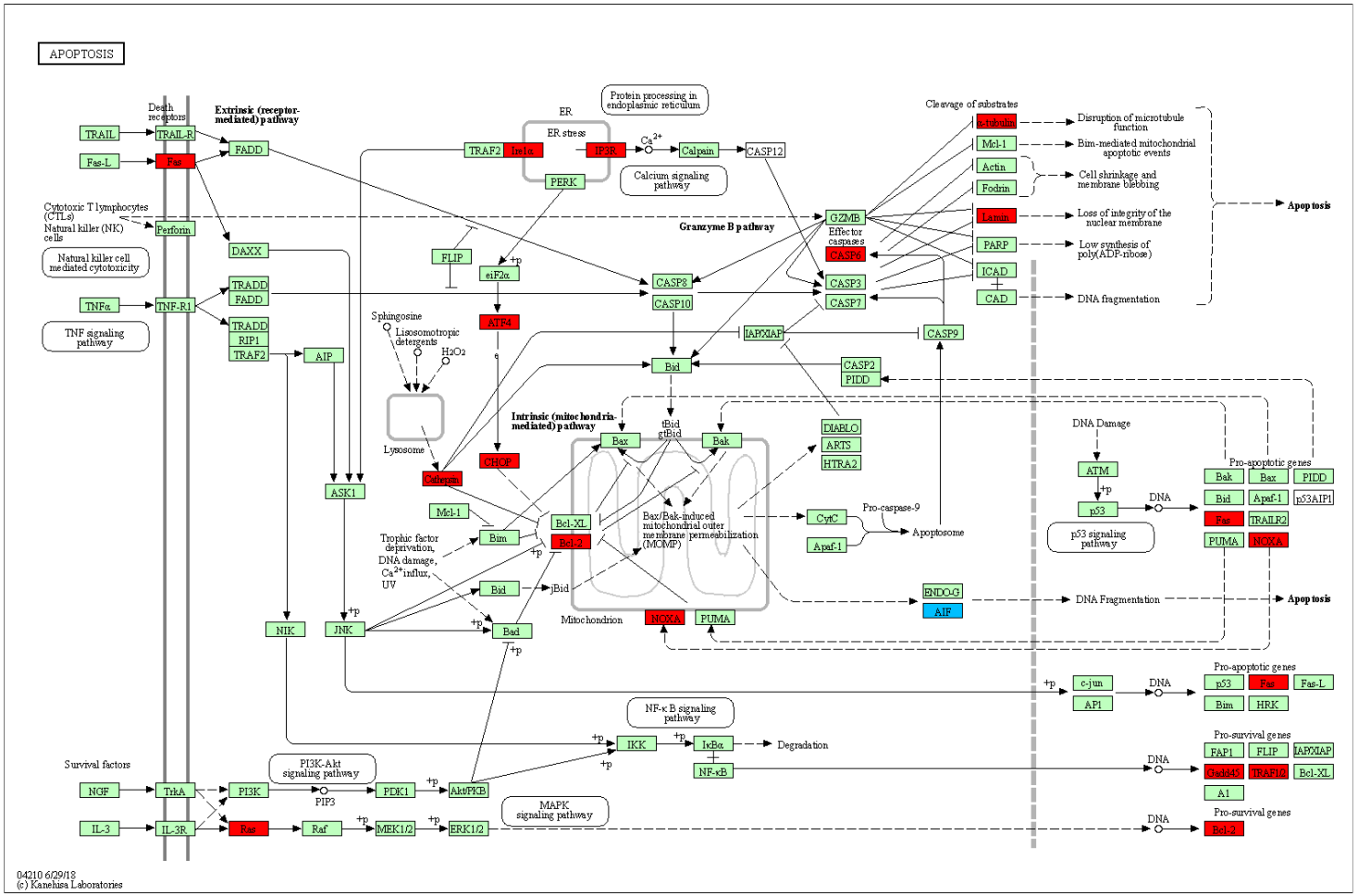


**Figure 19. Kyoto Encyclopaedia of Genes and Genomes (KEGG) pathway map of Apoptosis (bta04210) in primary bovine macrophages infected with *B. besnoiti* tachyzoites (MO-Bb). Differential expressed genes (DEGs) identified in in macrophages infected with live *B. besnoiti* tachyzoites (MO-Bb) compared to non-infected control (MO) at 4 h p.i. are highlighted on the KEGG apoptosis pathway map. Genes upregulated in MO-Bb are shown in red, while downregulated genes are shown in blue. Data represent results from three independent biological replicates per condition.**

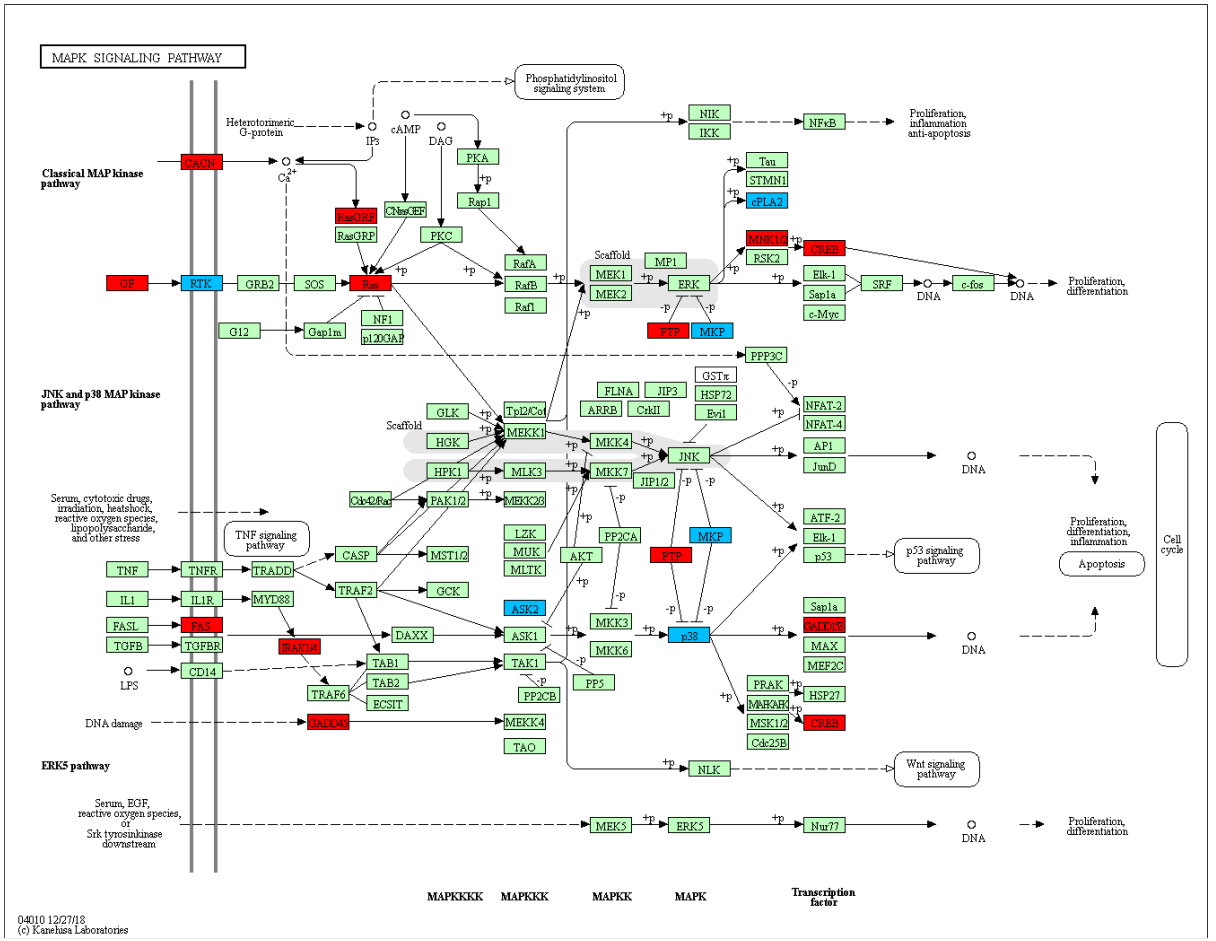


**Figure 20. Kyoto Encyclopaedia of Genes and Genomes (KEGG) pathway map of MAPK (bta04010) in primary bovine macrophages infected with *B. besnoiti* tachyzoites. DEGs identified in in macrophages infected with live *B. besnoiti* tachyzoites (MO-Bb) compared to non-infected control (MO) at 4 h p.i. are highlighted on the KEGG MAPK pathway map. Genes upregulated in MO-Bb are shown in red, while downregulated genes are shown in blue. Data represent results from three independent biological replicates per condition.**

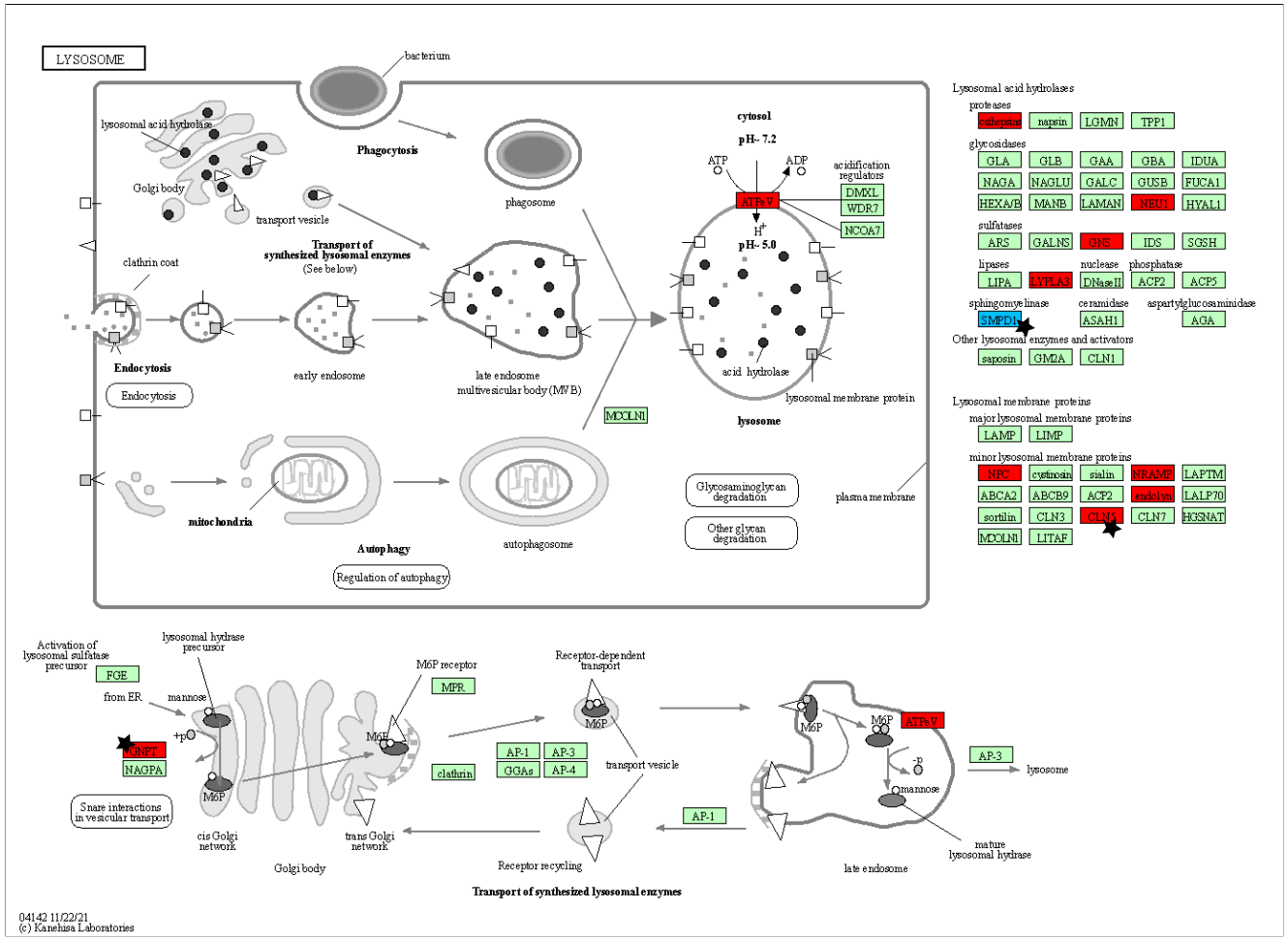


**Figure 21. Kyoto Encyclopaedia of Genes and Genomes (KEGG) pathway map of Lysosome (bta04142) in primary bovine macrophages infected with *B. besnoiti* tachyzoites. DEGs in macrophages infected with live *B. besnoiti* tachyzoites (MO-Bb) or heat-killed parasites (MO-hkBb), compared to non-infected control (MO), at 4 h p.i. Upregulated genes are shown in red and downregulated genes in blue. DEGs marked with a star were exclusively regulated in response to live parasite infection (MO-Bb). Data represent the mean results from three independent biological replicates per condition.**

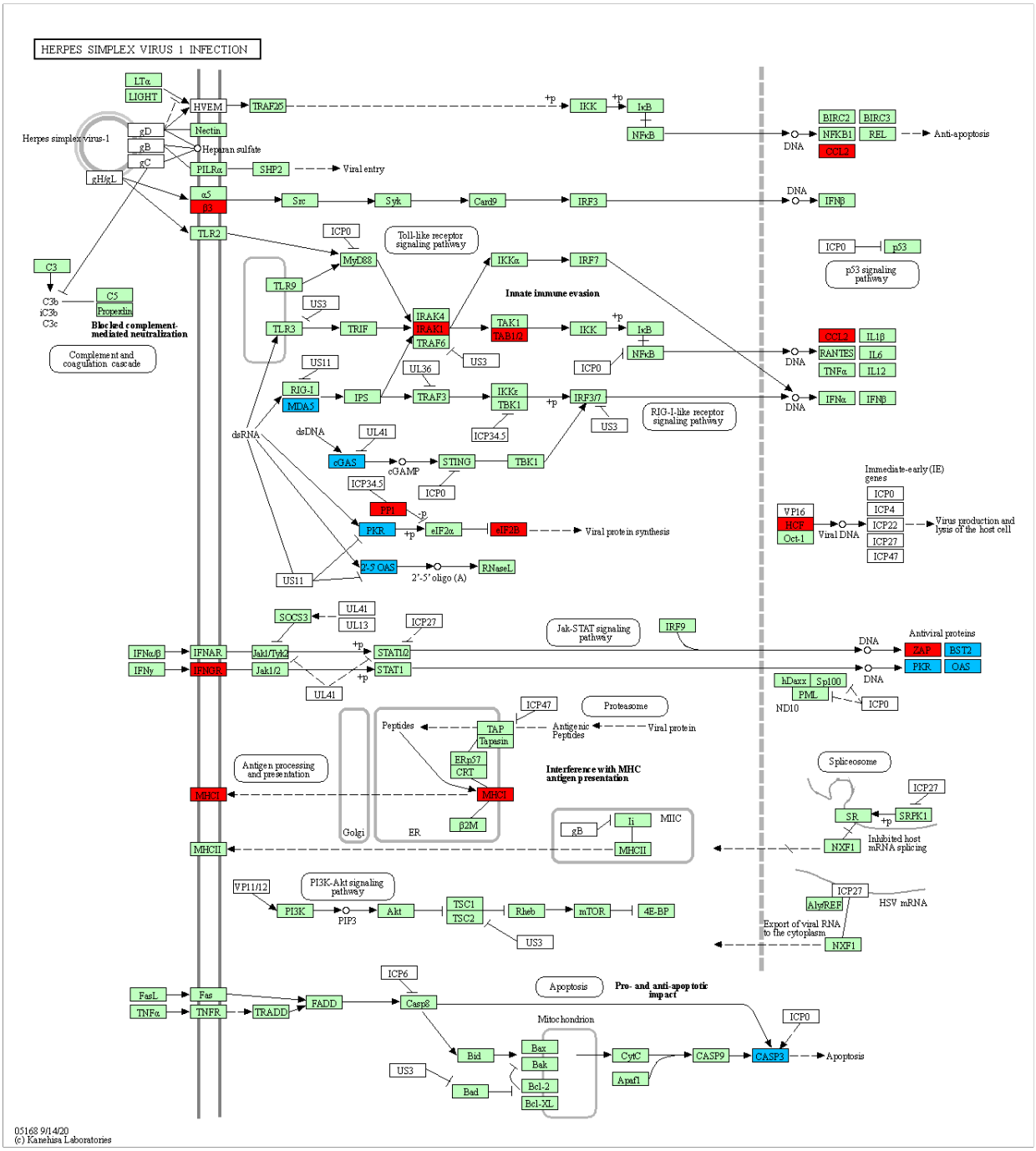


**Figure 22. Kyoto Encyclopaedia of Genes and Genomes (KEGG) pathway map of *Herpes simplex* virus 1 infection (bta05168) in primary bovine macrophages infected with *B. besnoiti* tachyzoites. DEGs in bovine macrophages infected with *B. besnoiti* (MO-Bb) *vs* non-infected macrophages (MO) at 8 h p.i. are highlighted. Upregulated genes are represented in red and downregulated genes are represented in blue. Viral genes involved in viral interference are presented in white. The results were obtained from three biological replicates for each condition.**

### 5.2.3 Validation of apoptosis by TUNEL assay in primary bovine monocyte-derived macrophages

To confirm the transcriptional regulation of apoptosis identified in the transcriptomic analysis, TUNEL assays were performed on primary bovine monocyte-derived macrophages. The results of the TUNEL assay showed an increase in apoptosis in MO-Bb cells at 8 h p.i. At 4 h p.i., there were no differences in the numbers of apoptotic cells among the groups (MO-Bb, MO-hkBb and MO). However, at 8 h p.i., a significant increase ($p < 0.05$) in TUNEL-positive cells was observed in the MO-Bb group (approximately 5-6%) compared to the MO-hkBb and MO groups (<1%). Furthermore, almost 100% of TUNEL-positive cells were uninfected cells at all time points in the study and under all conditions (**Figure 23**).

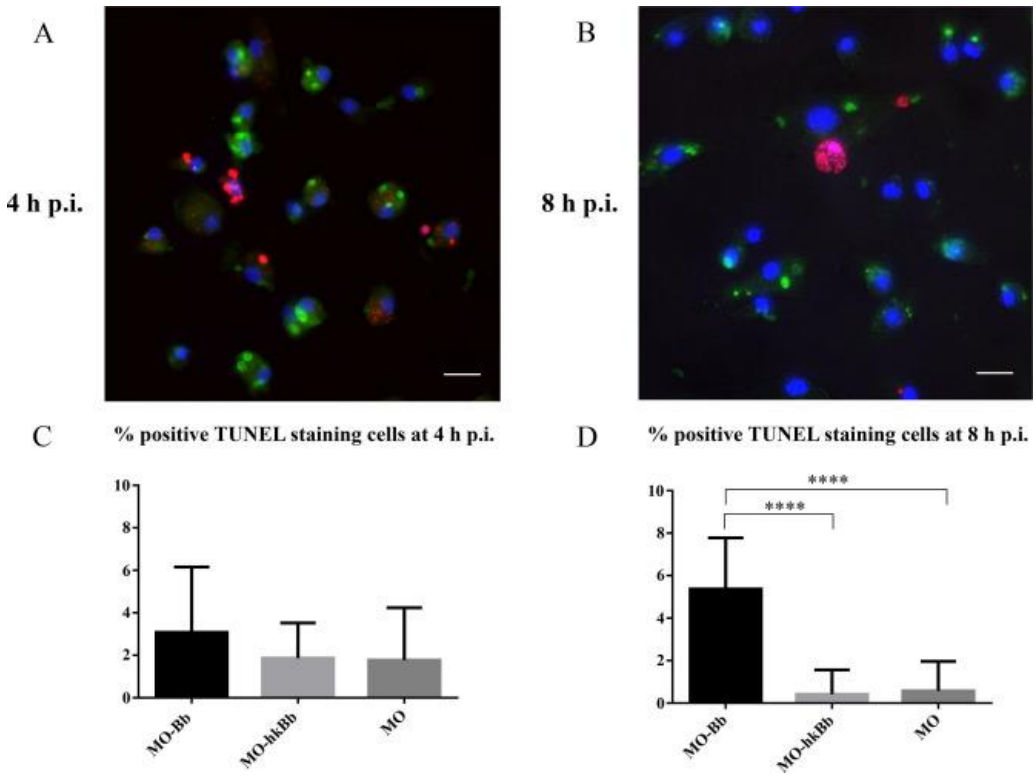


**Figure 23. TUNEL assay in macrophages infected with live *B. besnoiti* tachyzoites at 4 h p.i. (A) and at 8 h p.i. (B) Percentage of macrophages undergoing apoptosis at 4 h (C) and 8 h p.i. (D). Apoptotic macrophages showed TUNEL-positive red-stained nuclei. Scale bars: 100 µm. MO-Bb, macrophages infected with live tachyzoites; MO-hkBb, macrophages infected with heat-killed tachyzoites; MO, non-infected macrophages. ****Adjusted *P* value less than 0.0001; as determined by Kruskal-Wallis test followed by Dunn's test.**

### 5.2.4 Relevant genes modulated in the RNA-Seq analysis of primary bovine monocyte-derived macrophages infected with *B. besnoiti* were also regulated in target tissues during natural infections

Key genes identified as significantly modulated in the transcriptomic analysis of primary bovine monocyte-derived macrophages during *B. besnoiti* infection were further validated in target tissues, specifically the testicular parenchyma from naturally infected bulls. Genes showing the most significant changes in the differential expression analysis and those highlighted in the KEGG enrichment analysis were prioritized for further investigation.

A selected panel of DEGs from the macrophage RNA-Seq data was analysed in testicular parenchyma tissues, chosen for their relevance due to the predominant macrophage activity observed in this region (González-Barrio et al., 2020; 2021b). The expression analysis focused on genes primarily associated with apoptosis and *Herpes simplex* virus 1 infection signalling pathways. Remarkably, four out of the eight analysed genes were found to be significantly modulated in the testicular parenchyma of naturally infected bulls, confirming their involvement in the host-pathogen interaction. The *ATF4* and *CHOP* genes were significantly upregulated *in vitro* in MO-Bb cells compared with MO cells at 4 h p.i. However, they were found to be downregulated in the testicular parenchyma of acutely and chronically infected bulls. Moreover, we found that several ISGs were downregulated *in vitro*, including several *OAS* (oligoadenylate synthetase) and cytosolic sensors *MDA5* and *cGAS*. Interestingly, the type I IFN-α gene was significantly downregulated in acutely infected bulls. *Metallothioneins 1A* and *1E* showed very high FCs *in vitro*, but only *metallothionein-1A* was significantly upregulated *in vivo* in both acutely and chronically infected bulls. The remaining analysed genes (*Bcl-2*, *metallothionein-1E* and *OAS2*) did not show expression changes *in vivo* (**Figure 24**).

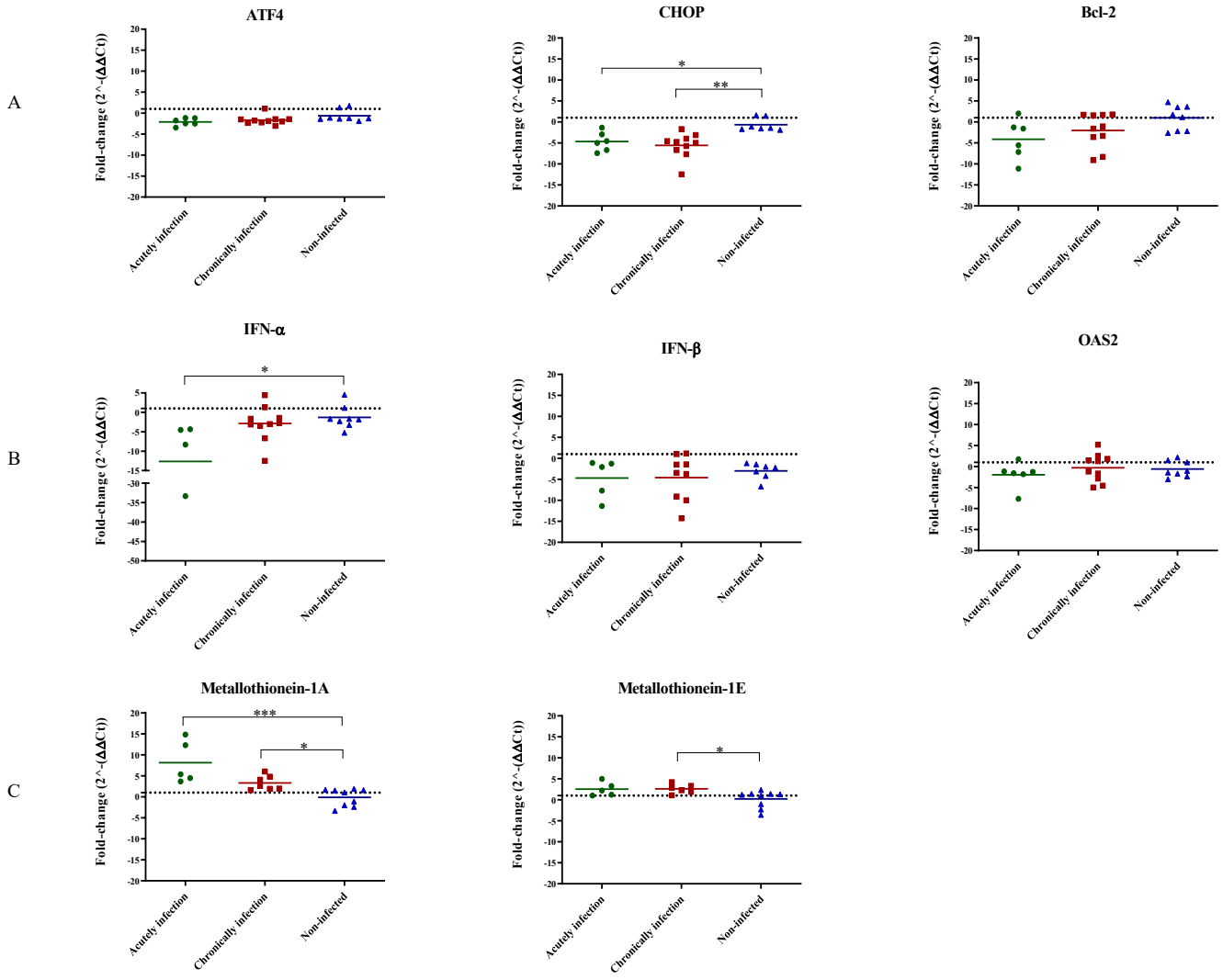


**Figure 24. Scatter plot graphs of relative mRNA expression levels derived from real-time RT-qPCR analysis across testicular parenchyma samples of bulls naturally infected with *B. besnoiti*. Each dot represents data obtained from one bull (acutely infected, chronically infected, non-infected) and the bar represents the average FC for each gene and condition. The genes analysed were those associated with the (A) apoptosis pathway (*ATF4, CHOP, Bcl-2*), (B) *Herpes simplex* virus 1 pathway (*IFNα, IFNβ, OAS2*) and (C) *metallothionein 1A* and *metallothionein 1E*, which showed the highest FC in macrophages infected with live tachyzoites at 8 h p.i. The horizontal discontinuous line set at 1 indicates uninfected, the baseline for animals. *Adjusted P values between 0.01 and 0.05; **adjusted P values between 0.01 and 0.001; *** adjusted P values less than 0.001; as determined by Kruskal-Wallis test followed by Dunn's test.**

### 5.2.5 Key cancer and fibrosis pathways dominate in early transcriptional responses in *B. besnoiti*-infected PBAF

Differential expression analysis revealed a higher number of DEGs in fibroblasts infected with tachyzoites (FI-Bb) compared to non-infected fibroblasts (FI) at 12 h p.i. *vs* 32 h p.i., with a total of 479 DEGs (287 upregulated in infected cells and 192 downregulated) and 280 DEGs (172 upregulated and 108 downregulated DEGs), respectively. Among these DEGs, 91 were DEGs at both time points. To investigate the underlying mechanisms during *B. besnoiti* infection in bovine fibroblasts, we performed functional enrichment analysis for GO and KEGG annotations (**Table 14**). When fibroblasts infected with tachyzoites and non-infected fibroblasts were compared at both 12 and 32 h p.i., an enrichment in BP and MF related to cell proliferation and communication was revealed. Notably, the examination of KEGG pathways highlighted shared regulation at 12 and 32 h p.i. in several cancer-related pathways, namely "Proteoglycans in cancer", "Pathways in cancer", "Gastric cancer" and "MAPK signalling pathway".

Specifically, at 12 h p.i., the comparison between fibroblasts infected with tachyzoites and non-infected fibroblasts demonstrated an enrichment of BP and MF associated with cytokines and growth factor activity. The KEGG pathway analysis identified several pathways, including "Cytokine–cytokine receptor interaction", the "AGE–RAGE signalling pathway" and "TNF signalling pathway". Notably, in infected cells, there was a significant upregulation of the cytokines and cytokine receptor (transforming growth factor β (TGFβ) family, TNF family, IFN family, chemokines family), vascular endothelial growth factors (*VEGFA*, *VEGFC*), the *fibroblast growth factor 1* (*FGF1*) and relevant genes associated to fibrosis such as *fibronectin type III domain-containing protein 3A* (*FNDC3A*), *collagen type VII A1* (*COL7A1)*, *matrix metalloproteinase 9* (*MMP9*) transforming growth factor-beta factors (*TGFβ1*, *TGFβ3*) and *urokinase plasminogen activator surface receptor* (*PLAUR*). Other genes associated with cell proliferation and differentiation were also upregulated (e.g., *NOTCH1*, *FOFB*, a member of the Fos family of AP-1 transcription factors and *phosphatidylinositol-specific phospholipase C, X domain containing 1* (*PLCXD1*) (**Figure 25**).

At 32 h p.i., the comparison between fibroblasts infected with tachyzoites and non-infected fibroblasts demonstrated an enrichment of processes related to cell adhesion. KEGG pathway analysis unveiled several pathways, including “Focal adhesion”, “Cell adhesion molecules, “PI3K–AKT signalling pathway” and the “Malaria” (HGF–MET signalling pathway). Some upregulated genes were also upregulated at 12 h p.i. (*FOSB*, *PLCXD1*, *TGFβ1*). Particularly at 32 h p.i., there was a significant upregulation of several adhesion molecules (*CDH2*, *CLDN15*, *ITGA2*, *ITGA5*, *ITGA6*, *LRRC4*, *SDC4*, *PECAM1*), genes associated with fibrosis (*TGFβ1*, *TGFβ3*, *TGFβR2*, *PLAUR*, *COL13A1*, *MMP16*) and cell proliferation *(FOSB, AREG*) (**Figure 26**).

**Table 14. Number of DEGs among conditions: fibroblasts infected with live *B. besnoiti* tachyzoites (FI-Bb), macrophages infected with heat-killed *B. besnoiti* tachyzoites (MO-hkBb) and non-infected macrophages (MO) at 12 and 32 h p.i. The table also summarizes the results of functional enrichment analyses, listing the top five most significantly enriched terms in each category: BP, MF, CC; and KEGG pathways.**

| | | Nº DEGs | Upregulated DEGs | Downregulated DEGs | Biological processes | | Molecular function | | Cellular components | | Pathway enrichment | |
|---|---|---|---|---|---|---|---|---|---|---|---|---|
| | | | | | GO term | Adjusted *P*-value | GO term | Adjusted *P*-value | GO term | Adjusted *P*-value | KEGG term | Adjusted *P*-value |
| **12 h p.i** | **FI-Bb *vs* FI** | 479 | 287 | 192 | Anatomical structure development (GO:0048856) | $6.48x10^{-20}$ | Molecular function activator activity (GO:0140677) | $6.15x10^{-9}$ | Extracellular space (GO:0005615) | $1.24x10^{-7}$ | Cytokine-cytokine receptor interaction (KEGG:04060) | $3.92x10^{-4}$ |
| | | | | | Developmental process (GO:0032502) | $1.44x10^{-19}$ | Molecular function regulator activity (GO:0098772) | $1.22x10^{-8}$ | Extracellular region (GO:0005576) | $1.97x10^{-7}$ | Pathways in cancer (KEGG:05200) | $3.94x10^{-4}$ |
| | | | | | Anatomical structure Morphogenesis (GO:0009653) | $3.85x10^{-18}$ | Signalling receptor regulator activity (GO:0030545) | $3.09x10^{-8}$ | Cell periphery (GO:0071944) | $3.48x10^{-7}$ | MAPK signalling pathway (KEGG:04010) | $1.32x10^{-3}$ |
| | | | | | Positive regulation of biological process (GO:0048518) | $1.17x10^{-17}$ | Receptor ligand activity (GO:0048018) | $4.22x10^{-8}$ | Plasma membrane (GO:0005886) | $2.54x10^{-4}$ | Proteoglycans in cancer (KEGG:05205) | $5.32x10^{-3}$ |
| | | | | | Multicellular organism development (GO:0007275) | $3.67x10^{-17}$ | Signalling receptor activator activity (GO:0030546) | $6.09x10^{-8}$ | Membrane (GO:0016020) | $3.17x10^{-3}$ | Axon guidance (KEGG:04360) | $3.13x10^{-2}$ |
| **32 h p.i** | **FI-Bb *vs* FI** | 280 | 172 | 108 | Multicellular organism development (GO:0007275) | $7.99x10^{-16}$ | Signalling receptor regulator activity (GO:0030545) | $2.80x10^{-4}$ | Extracellular region (GO:0005576) | $4.90x10^{-7}$ | Proteoglycans in cancer (KEGG:05205) | $4.18x10^{-5}$ |
| | | | | | Anatomical structure Morphogenesis (GO:0009653) | $1.47x10^{-14}$ | Signalling receptor binding (GO:0005102) | $6.41x10^{-4}$ | Extracellular space (GO:0005615) | $6.35x10^{-7}$ | Malaria (KEGG:05144) | $3.59x10^{-3}$ |
| | | | | | Anatomical structure development (GO:0048856) | $5.59x10^{-14}$ | Receptor ligand activity (GO:0048018) | $6.82x10^{-4}$ | Apical plasma membrane (GO:0016324) | $2.48x10^{-5}$ | Focal adhesion (KEGG:04510) | $7.48x10^{-3}$ |

| | | | | | | | | | | | | |
|---|---|---|---|---|---|---|---|---|---|---|---|---|
| | | | | | Developmental process (GO:0032502) | $9.77x10^{-14}$ | Signalling receptor activator activity (GO:0030546) | $8.42x10^{-4}$ | Cell periphery (GO:0071944) | $2.87x10^{-5}$ | Pathways in cancer (KEGG:05200) | $7.51x10^{-3}$ |
| | | | | | System development (GO:0048731) | $7.17x10^{-13}$ | Growth factor activity (GO:0008083) | $3.04x10^{-3}$ | Apical part of cell (GO:0045177) | $5.21x10^{-5}$ | MAPK signalling pathway (KEGG:04010) | $1.08x10^{-2}$ |
| **12 *vs* 32 h p.i** | **FI-Bb 12 h p.i. *vs* FI-Bb 32 h p.i.** | 592 | 547 | 45 | Regulation of cellular process (GO:0050794) | $8.75x10^{-13}$ | Protein binding (GO:0005515) | $7.37x10^{-10}$ | Cytoplasm (GO:0005737) | $3.30x10^{-6}$ | MAPK signalling pathway (KEGG:04010) | $7.43x10^{-5}$ |
| | | | | | Positive regulation of biological process (GO:0048518) | $2.03x10^{-12}$ | Enzyme binding (GO:0019899) | $1.67x10^{-8}$ | Nucleoplasm (GO:0005654) | $2.77x10^{-3}$ | *Salmonella* infection (KEGG:05132) | $4.13x10^{-2}$ |
| | | | | | Intracellular signal transduction (GO:0035556) | $3.86x10^{-12}$ | Kinase binding (GO:0019900) | $1.54x10^{-6}$ | Cytosol (GO:0005829) | $1.23x10^{-2}$ | - | - |
| | | | | | Negative regulation of cellular process (GO:0048523) | $5.43x10^{-12}$ | Protein kinase binding (GO:0019901) | $3.09x10^{-5}$ | Cytoplasmic side of plasma membrane (GO:0009898) | $3.31x10^{-2}$ | - | - |
| | | | | | Positive regulation of cellular process (GO:0048522) | $1.30x10^{-11}$ | Molecular function regulator activity (GO:009877) | $8.26x10^{-4}$ | - | - | - | - |

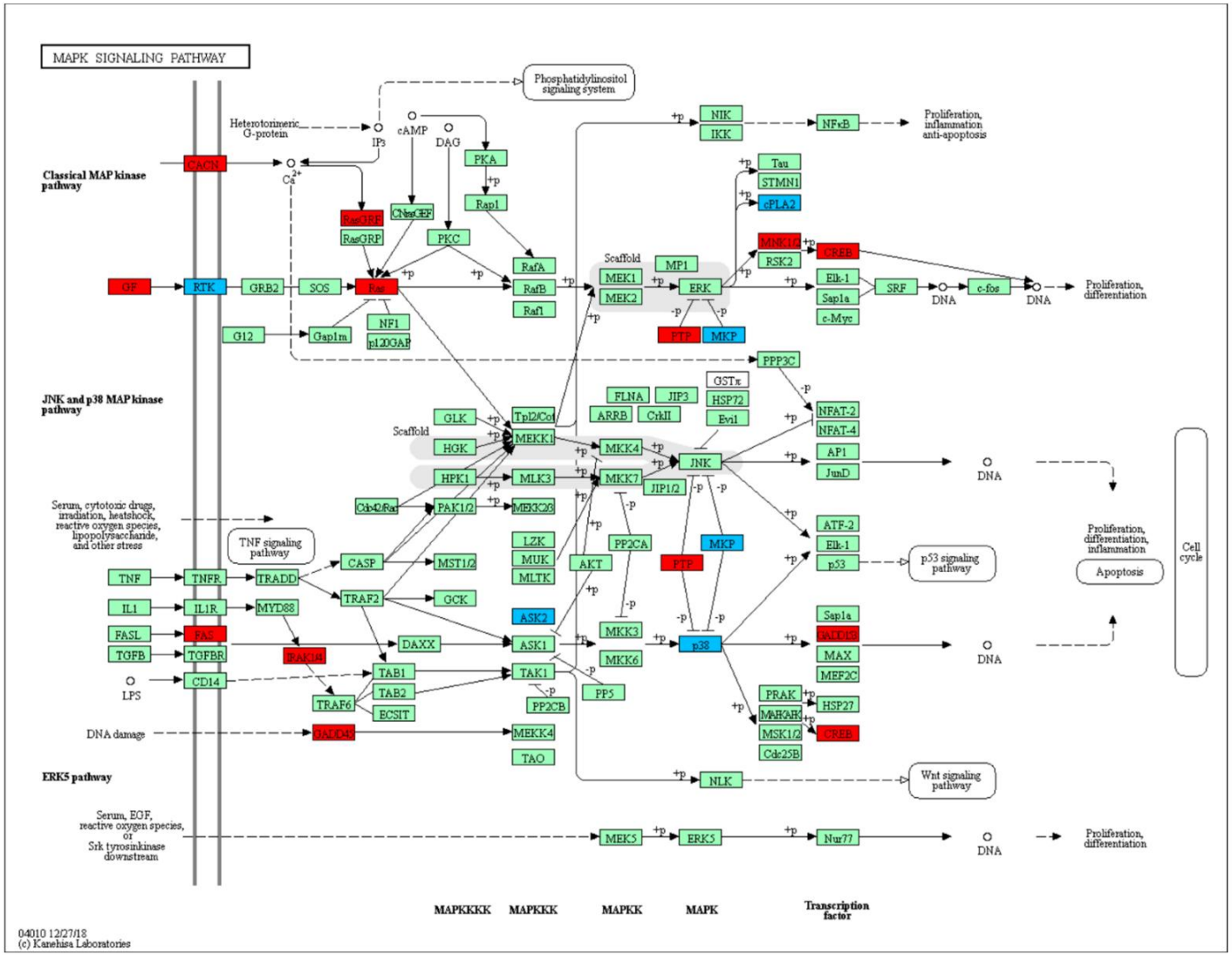


**Figure 25. Kyoto Encyclopaedia of Genes and Genomes (KEGG) pathway map of MAPK (bta04010) in PBAF infected with *B. besnoiti* tachyzoites (FI-Bb). DEGs at 12 h p.i. are shown in blue, while those at 32 h p.i. are displayed in red. Data are based on transcriptomic analysis of infected cells (FI-Bb) compared to non-infected controls (FI).**

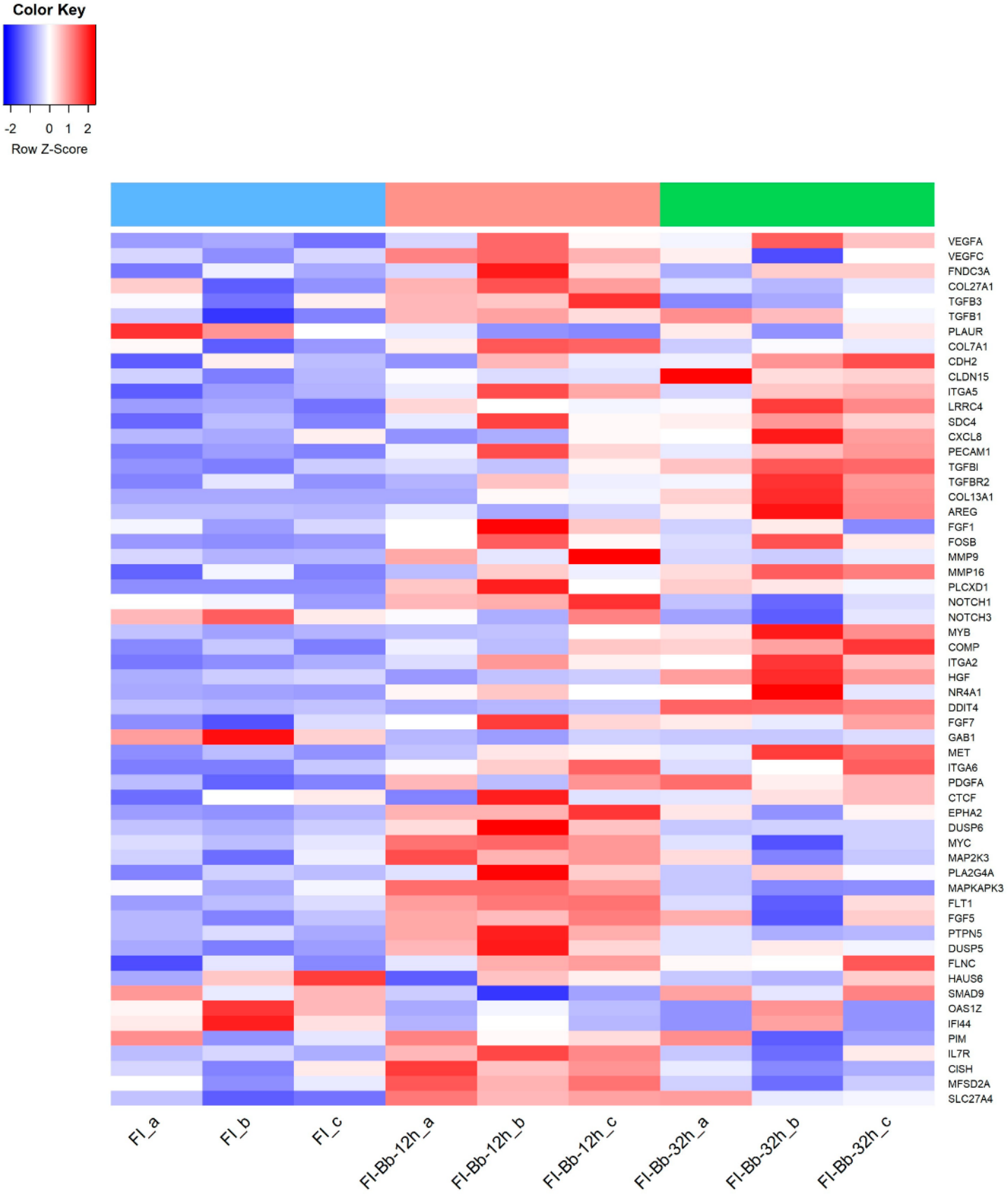


**Figure 26. Heatmap of a selection of *B. taurus* DEGs in fibroblasts infected with *B. besnoiti* tachyzoites (FI-Bb) at 12 (pink colour) and 32 h p.i. (green colour) and non-infected fibroblasts (FI) (blue colour).**

### 5.2.6 Relevant genes modulated in the RNA-Seq analysis of PBAF infected with *B. besnoiti* were also regulated in target tissues during natural infections

Key genes identified as significantly modulated in the transcriptomic analysis of PBAF during *B. besnoiti* infection were further validated in target tissues, specifically the scrotal skin from naturally infected bulls. Scrotal skin tissues were chosen for the analysis of a selected panel of DEGs derived from the fibroblast RNA-Seq data due to their significance in fibrosis, a hallmark of both acute and chronic *B. besnoiti* infections (González-Barrio et al., 2020; 2021b). The expression of key DEGs, including *AREG, FGF1, FOSB, MMP9, MMP16, PLAUR, PLCXD1* and *TGFβ1*, was assessed in scrotal skin samples from naturally infected bulls. Among the eight genes examined, four showed distinct regulatory patterns in the scrotal skin of naturally infected bulls. Specifically, *PLAUR* was upregulated in both acutely and chronically infected animals when compared to non-infected controls; *TGFβ1* expression was significantly elevated in chronically infected bulls compared to both acute and control groups; *FGF1* showed a moderate but significant increase in expression in chronically infected animals relative to acutely infected bulls. In contrast, *FOSB* was the only gene that exhibited significant downregulation in chronic infection. Notably, the remaining assessed genes (*MMP9*, *MMP16*, *AREG*, *PLCXD1*) did not display significant expression changes when infected and non-infected animals were compared (**Figure 27**).

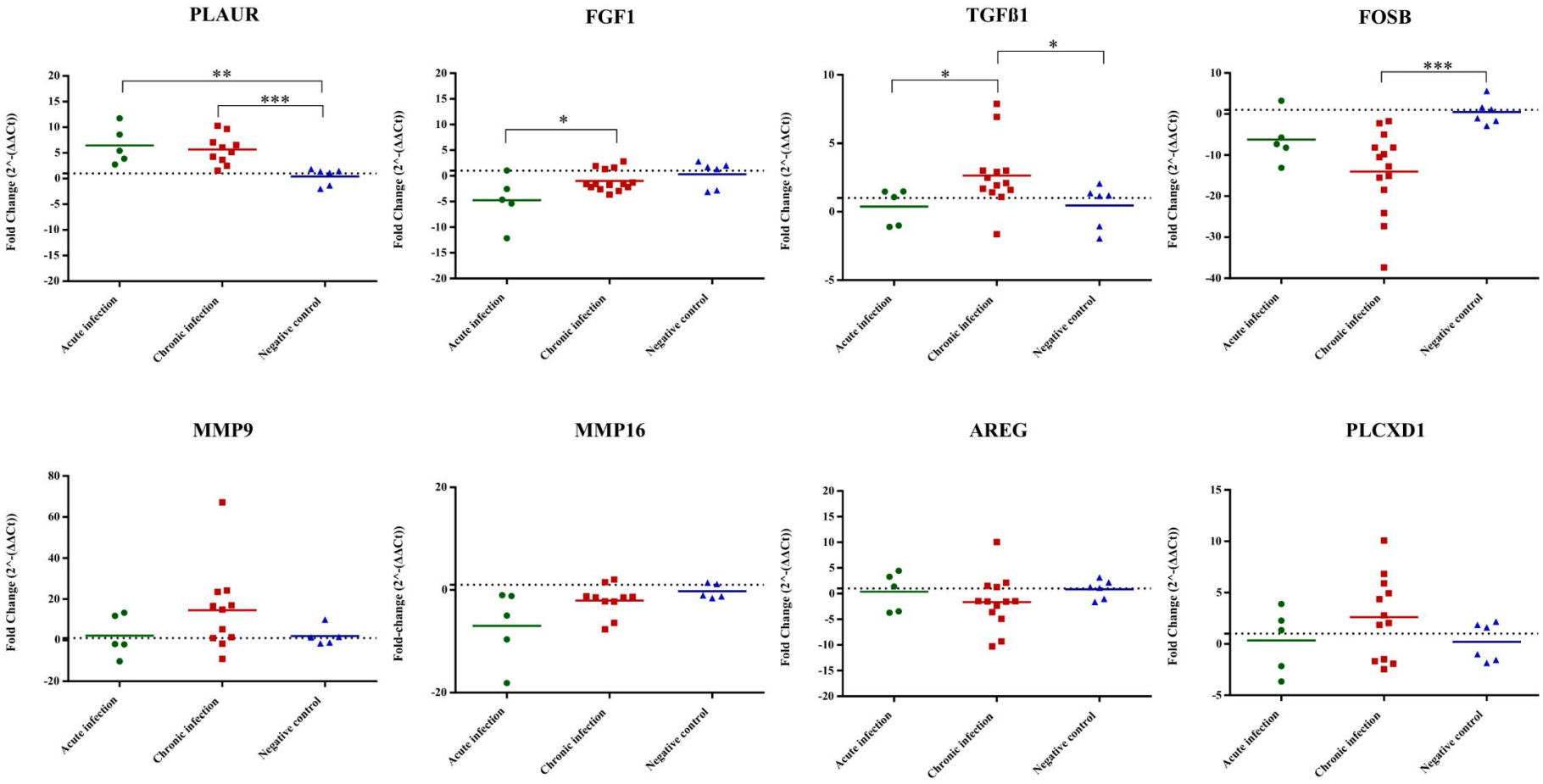


**Figure 27. Scatter plot graphs of relative mRNA expression levels derived from real-time RT-qPCR analysis across scrotal skin samples of bulls naturally infected with *B. besnoiti*. In the scatterplot graphs, each dot represents data obtained from one single bull and the bar represents the average fold change (FC) for each gene and condition. The baseline for uninfected animals is set at 1 (horizontal line). One asterisk (*) corresponds to adjusted *p* values between 0.01 and 0.05; two asterisks (**) to adjusted *p* values between 0.01 and 0.001; and three asterisks (***) to adjusted *p* values less than 0.001 (determined by Kruskal–Wallis test followed by Dunn's test).**

## 5.3 *Besnoitia besnoiti* transcriptome profiling highlights strong regulation of invasion- and metabolism-related genes in primary bovine cells

Transcriptomic analyses of *B. besnoiti*-infected primary bovine monocyte-derived macrophages and PBAF revealed converging host-pathogen interactions, predominantly centred around invasion. In primary bovine monocyte-derived macrophages a total of 538 *B. besnoiti* genes were differentially expressed between 4 and 8 h p.i. It was noted that 537 DEGs were upregulated *vs* only 1 downregulated gene at 8 h p.i. Unfortunately, 199 out of 538 DEGs corresponded to hypothetical proteins. Annotated DEGs for *B. besnoiti* or its syntenic orthologous gene in *T. gondii* belonged mainly to two categories: invasion and metabolism. Within the invasion category (n=29), genes coding for rhoptry proteins (ROP6, ROP11, ROP23, ROP26, ROP31, ROP40, rhoptry metalloprotease toxolysin (TLN1), RON1, RON2, RON3, RON4, RON5, RON6, RON8M, RON9, RON10, RON12, RON14, RON15, RON17, RON18, rhoptry protein and putative (BESB_055810)) were most numerous, followed by the components of the gliding machinery (myosin light chain 1, myosin light chain 4, myosin light chain kinase). However, only one surface antigen (SRS49D) and one microneme-like protein (BESB_067360) were upregulated in bovine macrophages at 8 h p.i. The next category with the highest number of upregulated genes was metabolism with genes (n=18) related to valine, leucine, isoleucine and arginine metabolism; pantothenic acid and coenzyme A (CoA) synthesis and nitrogen metabolism. The only gene downregulated at 8 h p.i. when compared to 4 h p.i. was BESB_064630, which encodes a PAN/Apple domain-containing protein (**Table 15**).

**Table 15. Category, gene ID, gene description, *T. gondii* orthology synteny analysis results and FC of a selection of *B. besnoiti* DEGs of the comparison macrophages infected with live tachyzoites (MO-Bb) at 4 *vs* MO-Bb at 8 h p.i.**

| | Category | Gene ID | Description | *T. gondii* ortholog | FC MO-Bb at 8 h *vs* MO-Bb at 4 h p.i. |
|---|---|---|---|---|---|
| Invasion | Rhoptries | BESB_055810 | Rhoptry protein, putative | TGME49_315210 | 10.41 |
| | | BESB_079420 | Rhoptry neck protein RON3 | TGME49_223920 | 6.98 |
| | | BESB_072910 | Rhoptry neck protein RON5 | TGME49_311470 | 6.97 |
| | | BESB_071010 | Rhoptry neck protein RON9 | TGME49_308810 | 6.56 |
| | | BESB_002170 | Rhoptry neck protein RON10 | TGME49_261750 | 6.41 |
| | | BESB_040860 | Rhoptry neck protein RON2 | TGME49_300100 | 6.40 |
| | | BESB_052840 | Rhoptry metalloprotease toxolysin 1 | TGME49_269885 | 6.28 |
| | | BESB_063670 | Rhoptry neck protein RON6 | TGME49_297960 | 6.26 |
| | | BESB_071470 | Rhoptry neck protein RON1 | TGME49_310010 | 5.70 |
| | | BESB_018150 | Rhoptry neck protein RON8 | TGME49_306060 | 5.68 |
| | | BESB_083570 | Rhoptry neck protein RON4 | TGME49_229010 | 5.07 |
| | | BESB_010080 | Rhoptry kinase family protein ROP37 | . | 17.15 |
| | | BESB_059140 | Rhoptry kinase family protein ROP11 | TGME49_227810 | 11.85 |
| | | BESB_016430 | Rhoptry kinase family protein ROP15 | TGME49_211290 | 11.30 |
| | | BESB_048880 | Rhoptry kinase family protein ROP32 | . | 11.18 |
| | | BESB_019040 | Rhoptry kinase family protein ROP40 | TGME49_291960 | 10.33 |
| | | BESB_055800 | Rhoptry kinase family protein ROP14 | TGME49_315220 | 9.96 |
| | | BESB_016400 | Rhoptry kinase family protein ROP26 | TGME49_211260 | 7.28 |
| | | BESB_082430 | Rhoptry kinase family protein ROP23 | TGME49_239600 | 7.11 |
| | | BESB_002440 | Rhoptry kinase family protein ROP31 | TGME49_258800 | 7.06 |
| | | BESB_084550 | Rhoptry kinase family protein ROP6 | TGME49_258660 | 6.12 |
| | | BESB_065210 | Rhoptry kinase family protein ROP12 | TGME49_203990 | 5.88 |
| | | BESB_084470 | Rhoptry kinase family protein ROP17 | TGME49_258580 | 5.85 |
| | | BESB_013500 | Rhoptry kinase family protein ROP18 | . | 5.31 |
| | | BESB_052840 | Rhoptry metalloprotease toxolysin 1 | TGME49_269885 | 6.28 |

| | | | | | |
|---|---|---|---|---|---|
| | **Micronemes** | BESB_067360 | Microneme-like protein | TGME49_286740 | 3.18 |
| | **Surface antigens** | BESB_033430 | SAG-related sequence SRS49D | TGME49_207160 | 5.65 |
| | **Gliding motility** | BESB_072760 | Myosin light chain 1 | TGME49_311260 | 5.19 |
| | | BESB_052960 | Myosin-light-chain kinase | TGME49_269730 | 4.70 |
| | | BESB_025840 | Myosin light chain 4 | TGME49_294390 | 3.76 |
| **Metabolism** | **Valine, leucine and isoleucine degradation** | BESB_072840 | putative methylmalonate-semialdehyde dehydrogenase [acylating] | TGME49_311370 | 10.81 |
| | | BESB_051790 | putative hydroxymethylglutaryl-CoA lyase | TGME49_204460 | 10.65 |
| | | BESB_007470 | putative acetyl-CoA acyltransferase B | TGME49_273740 | 8.33 |
| | | BESB_079590 | enoyl-CoA hydratase/isomerase family protein | TGME49_224090 | 6.59 |
| | | BESB_076350 | pyruvate carboxylase | TGME49_284190 | 6.02 |
| | | BESB_039920 | AMP-binding enzyme domain-containing protein | TGME49_219230 | 5.29 |
| | | BESB_000260 | aldehyde dehydrogenase | TGME49_264000 | 3.43 |
| | **Pantothenate and CoA biosynthesis** | BESB_069580 | putative Acetyl-coenzyme A transporter | TGME49_215940 | 5.51 |
| | | BESB_044550 | deoxyribose-phosphate aldolase | TGME49_318750 | 5.15 |
| | | BESB_046420 | flavoprotein | TGME49_242880 | 5.13 |
| | | BESB_052960 | myosin-light-chain kinase | TGME49_269730 | 4.70 |
| | | BESB_045210 | Maf family protein | TGME49_240450 | 4.52 |
| | | BESB_078080 | uridine kinase | TGME49_316700 | 4.10 |
| | | BESB_000260 | aldehyde dehydrogenase | TGME49_264000 | 3.43 |
| | **Nitrogen metabolism** | BESB_062910 | hypothetical protein | TGME49_297070 | 7.67 |
| | | BESB_003210 | carbonate dehydratase, eukaryotic-type domain-containing protein | TGME49_259950 | 5.87 |
| | | BESB_071380 | dynein heavy chain family protein | TGME49_309980 | 4.48 |
| | | BESB_025910 | dynein heavy chain | TGME49_294550 | 3.05 |
| | **Arginine biosynthesis** | BESB_085430 | ATP-binding cassette transporter ABC.B1 | TGME49_260310 | 6.18 |
| | | BESB_014390 | peptidase M20D, amidohydrolase | TGME49_213520 | 5.91 |
| | | BESB_071380 | dynein heavy chain family protein | TGME49_309980 | 4.48 |
| | | BESB_003190 | Nitric-oxide synthase | TGME49_259920 | 4.20 |
| | | BESB_025910 | dynein heavy chain | TGME49_294550 | 3.05 |

In contrast to the macrophage, no transcriptional differences were observed in the fibroblast between 12 and 32 h p.i. However, the analysis of the *B. besnoiti* transcriptome within fibroblasts identified a broad set of genes associated with parasite invasion and intracellular adaptation. In addition, a substantial number of genes encoding proteins from secretory organelles were detected, including 114 SAGs, 47 ROPs, 12 MICs and 6 GRAs, among others. All rhoptry neck proteins (RON1 to RON10) previously identified in infected macrophages were also detected in fibroblasts. Several rhoptry proteins (ROP11, ROP12, ROP14, ROP15, ROP17, ROP18, ROP23, ROP26, ROP31, ROP32, ROP37, ROP40 and the metalloprotease TLN1) were found in both cell types. In addition, ROP4, ROP5, ROP6, ROP9, ROP10, ROP14, ROP32, ROP35, ROP39 and ROP41 were also identified. The microneme-like protein *SRS49D* and *myosin light chain 1* were also present in both macrophages and fibroblasts. Notably, a wide repertoire of SRS proteins was identified in fibroblasts (eg. SRS17B, SRS28, SRS42, SRS48K, SRS49B, SRS49D, SRS53B and SRS53F) that may have a redundant role. These findings confirm the presence of a large set of invasion-related genes in both macrophages and fibroblasts (**Table 16.**).

**Table 16. Category, gene ID, gene description and *T. gondii* orthology synteny analysis results, of a selection of *B. besnoiti* genes identified in infected PBAF at 12 and 32 h p.i.**

| Category | Gene ID | Description | *T. gondii* ortholog |
|---|---|---|---|
| Rhoptries | BESB_048870 | Rhoptry kinase family protein ROP32 | NA |
| | BESB_025920 | Rhoptry kinase family protein ROP37 (incomplete catalytic triad) | TGME49_294560 |
| | BESB_078690 | Rhoptry protein ROP14 | TGME49_315940 |
| | BESB_016430 | Rhoptry protein ROP15 | TGME49_211290 |
| | BESB_051150 | Rhoptry protein ROP18 | NA |
| | BESB_013500 | Rhoptry protein ROP18 | NA |
| | BESB_075590 | Rhoptry protein ROP18 | NA |
| | BESB_072910 | Rhoptry neck protein RON5 | TGME49_311470 |
| | BESB_065210 | Rhoptry protein ROP12 | TGME49_203990 |
| | BESB_002170 | Rhoptry neck protein RON10 | TGME49_261750 |
| | BESB_051430 | Rhoptry protein ROP18 | NA |
| | BESB_071690 | Rhoptry protein ROP18 | NA |
| | BESB_063670 | Rhoptry neck protein RON6 | TGME49_297960 |
| | BESB_084550 | Rhoptry protein ROP6 | TGME49_258660 |
| | BESB_016400 | Rhoptry kinase family protein ROP26 (incomplete catalytic triad) | TGME49_211260 |
| | BESB_019040 | Rhoptry kinase family protein ROP40 (incomplete catalytic triad) | TGME49_291960 |
| | BESB_082430 | Rhoptry kinase family protein ROP23 (incomplete catalytic triad) | TGME49_239600 |
| | BESB_057600 | Rhoptry kinase family protein ROP20 | NA |
| | BESB_077460 | Rhoptry protein ROP5 | NA |
| | BESB_071470 | Rhoptry neck protein RON1 | TGME49_310010 |
| | BESB_065400 | Rhoptry protein ROP4 | NA |
| | BESB_055800 | Rhoptry protein ROP14 | TGME49_315220 |
| | BESB_062380 | Rhoptry protein ROP4 | NA |
| | BESB_033100 | Rhoptry protein ROP18 | NA |
| | BESB_040860 | Rhoptry neck protein RON2 | TGME49_300100 |
| | BESB_002440 | Rhoptry kinase family protein ROP31 | TGME49_258800 |
| | BESB_071010 | Rhoptry neck protein RON9 | TGME49_308810 |
| | BESB_048880 | Rhoptry kinase family protein ROP32 | NA |
| | BESB_059140 | Rhoptry kinase family protein ROP11 (incomplete catalytic triad) | TGME49_227810 |
| | BESB_038220 | Rhoptry protein ROP18 | NA |
| | BESB_083570 | Rhoptry neck protein RON4 | TGME49_229010 |
| | BESB_040440 | Rhoptry kinase family protein (incomplete catalytic triad) | NA |
| | BESB_018150 | Rhoptry neck protein RON8 | TGME49_306060 |
| | BESB_001990 | Rhoptry kinase family protein ROP39 | NA |
| | BESB_079140 | Rhoptry protein ROP10 | NA |
| | BESB_004160 | Rhoptry kinase family protein (incomplete catalytic triad) | TGME49_249470 |
| | BESB_013530 | Rhoptry protein ROP4 | NA |
| | BESB_084470 | Rhoptry protein ROP17 | TGME49_258580 |
| | BESB_010080 | Rhoptry kinase family protein ROP37 (incomplete catalytic triad) | NA |
| | BESB_079420 | Rhoptry neck protein RON3 | TGME49_223920 |
| | BESB_014460 | Rhoptry protein ROP9 | TGME49_243730 |
| | BESB_053910 | Rhoptry kinase family protein ROP32 | TGME49_270920 |
| | BESB_077900 | Rhoptry protein ROP18 | NA |

| | | | |
|---|---|---|---|
| **Micronemes** | BESB_064600 | Microneme protein MIC17A | NA |
| | BESB_067250 | Microneme protein MIC12 | NA |
| | BESB_064590 | Microneme protein MIC17A | TGME49_200250 |
| | BESB_064620 | Microneme protein MIC17A | NA |
| | BESB_064610 | Microneme protein MIC17B | NA |
| | BESB_029460 | Microneme protein MIC12 | TGME49_267680 |
| | BESB_006980 | Microneme protein MIC9 | TGME49_245485 |
| | BESB_006970 | Microneme protein MIC8 | TGME49_245490 |
| **Surface proteins** | BESB_050060 | SAG related sequence | NA |
| | BESB_035010 | SAG related sequence | NA |
| | BESB_043720 | SAG related sequence | NA |
| | BESB_050230 | SAG related sequence | NA |
| | BESB_034970 | SAG related sequence | NA |
| | BESB_049990 | SAG related sequence | NA |
| | BESB_057360 | SAG related sequence | NA |
| | BESB_050290 | SAG related sequence | TGME49_267150 |
| | BESB_061530 | SAG related sequence | NA |
| | BESB_050210 | SAG related sequence | NA |
| | BESB_043670 | SAG related sequence | NA |
| | BESB_034130 | SAG related sequence | NA |
| | BESB_061490 | SAG related sequence | NA |
| | BESB_034940 | SAG related sequence | NA |
| | BESB_079240 | SAG related sequence SRS53B | NA |
| | BESB_079220 | SAG related sequence | TGME49_315400 |
| | BESB_057300 | SAG related sequence | NA |
| | BESB_050310 | SAG related sequence | TGME49_267160 |
| | BESB_047440 | SAG related sequence | NA |
| | BESB_034200 | SAG related sequence | NA |
| | BESB_049950 | SAG related sequence | NA |
| | BESB_049940 | SAG related sequence | NA |
| | BESB_057380 | SAG related sequence | NA |
| | BESB_057390 | SAG related sequence | NA |
| | BESB_043600 | SAG related sequence | TGME49_320200 |
| | BESB_049960 | SAG related sequence | NA |
| | BESB_061470 | SAG related sequence | NA |
| | BESB_034140 | SAG related sequence | NA |
| | BESB_057330 | SAG related sequence | NA |
| | BESB_057420 | SAG related sequence | NA |
| | BESB_034950 | SAG related sequence | NA |
| | BESB_050010 | SAG related sequence | NA |
| | BESB_057370 | SAG related sequence | NA |
| | BESB_033880 | SAG related sequence | NA |
| | BESB_057480 | SAG related sequence | NA |
| | BESB_033540 | SAG related sequence SRS48K | NA |
| | BESB_050000 | SAG related sequence | NA |
| | BESB_050260 | SAG related sequence | NA |
| | BESB_057260 | SAG related sequence | NA |
| | BESB_050150 | SAG related sequence | NA |
| | BESB_061480 | SAG related sequence | NA |

| | | |
|---|---|---|
| BESB_057460 | SAG related sequence | NA |
| BESB_057550 | SAG related sequence | NA |
| BESB_057450 | SAG related sequence | NA |
| BESB_033710 | SAG related sequence | NA |
| BESB_038370 | SAG related sequence | NA |
| BESB_061450 | SAG related sequence | NA |
| BESB_057430 | SAG related sequence | NA |
| BESB_034900 | SAG related sequence | NA |
| BESB_001020 | SAG related sequence | NA |
| BESB_057250 | SAG related sequence | NA |
| BESB_057310 | SAG related sequence | NA |
| BESB_061590 | SAG related sequence | NA |
| BESB_061460 | SAG related sequence | NA |
| BESB_035040 | SAG related sequence | NA |
| BESB_077710 | SAG related sequence | NA |
| BESB_057340 | SAG related sequence | NA |
| BESB_062290 | SAG related sequence | NA |
| BESB_062270 | SAG related sequence | NA |
| BESB_017920 | SAG related sequence | NA |
| BESB_001100 | SAG related sequence | NA |
| BESB_037030 | SAG related sequence | NA |
| BESB_057440 | SAG related sequence | NA |
| BESB_065020 | SAG related sequence | NA |
| BESB_061510 | SAG related sequence | NA |
| BESB_049970 | SAG related sequence | NA |
| BESB_062280 | SAG related sequence | NA |
| BESB_001090 | SAG related sequence | NA |
| BESB_034920 | SAG related sequence | NA |
| BESB_057290 | SAG related sequence | NA |
| BESB_072350 | SAG related sequence | NA |
| BESB_061520 | SAG related sequence | NA |
| BESB_050120 | SAG related sequence | NA |
| BESB_033730 | SAG related sequence | NA |
| BESB_001050 | SAG related sequence | NA |
| BESB_057280 | SAG related sequence | NA |
| BESB_052760 | SAG related sequence | NA |
| BESB_034280 | SAG related sequence | NA |
| BESB_057270 | SAG related sequence | NA |
| BESB_040490 | SAG related sequence | NA |
| BESB_071420 | SAG related sequence | NA |
| BESB_057520 | SAG related sequence | NA |
| BESB_061580 | SAG related sequence | NA |
| BESB_079210 | SAG related sequence SRS53F | TGME49_315410 |
| BESB_033560 | SAG related sequence | NA |
| BESB_034190 | SAG related sequence | NA |
| BESB_050270 | SAG related sequence | NA |
| BESB_057470 | SAG related sequence | NA |
| BESB_061540 | SAG related sequence | NA |
| BESB_057510 | SAG related sequence | NA |
| BESB_061570 | SAG related sequence | NA |

| | | | |
|---|---|---|---|
| | BESB_033760 | SAG related sequence | NA |
| | BESB_033550 | SAG related sequence | NA |
| | BESB_057490 | SAG related sequence | NA |
| | BESB_038390 | SAG related sequence | NA |
| | BESB_053070 | SAG related sequence | NA |
| | BESB_034320 | SAG related sequence | NA |
| | BESB_053060 | SAG related sequence | NA |
| | BESB_033850 | SAG related sequence | NA |
| | BESB_038410 | SAG related sequence | NA |
| | BESB_052750 | SAG related sequence | NA |
| | BESB_057500 | SAG related sequence | NA |
| | BESB_062240 | SAG related sequence | NA |
| | BESB_038400 | SAG related sequence | NA |
| | BESB_037020 | SAG related sequence | NA |
| **Dense granules** | BESB_049290 | Dense granule protein GRA7 | NA |
| | BESB_063600 | Dense granule protein DG32 | TGME49_297880 |
| | BESB_029990 | Dense granule protein GRA12 | TGME49_275850 |

## 5.4 Development of a protocol for induction tachyzoite into bradyzoite conversion

### 5.4.1 α-TgBAG1 was the only specific bradyzoite marker with a positive labelling by IHC, WB and IF

To validate the tachyzoite-to-bradyzoite conversion model in *B. besnoiti,* a panel of antibodies against *N. caninum, T. gondii* and *B. besnoiti* antigens was tested by IHC, WB and IF. The results are summarized below.

In IHC, the α-TgBAG1 antibody showed intense labelling of both individual bradyzoites and the cyst wall, with no signal in tachyzoites. α-NcSRS9 also yielded intense labelling of bradyzoites and their cyst wall, though its performance in other techniques diminished its stage specific marker value. α-NcROP2 and α-NcSAG4 both showed positive labelling of bradyzoites, with α-NcROP2 also detecting the cyst wall. α-NcBSR4 displayed patchy labelling with focal areas of increased intensity, and weak cyst wall staining. α-NcSRS2 and α-NcSAG1 produced positive but faint bradyzoite labelling, without cyst wall detection. Finally, both BbSpain-1 polyclonal antisera (bradyzoite and tachyzoite) labelled bradyzoites and cyst walls (**Figure 28**).

Western blot analysis under reducing (R) and non-reducing (NR) conditions supported the findings from IHC. α-TgBAG1 recognized a strong, distinct band at approximately 28–30 kDa exclusively in bradyzoite lysates under both conditions, with no reactivity against tachyzoites, confirming its stage specificity. α-NcSRS9 recognised bands around 37–50 kDa in bradyzoite extracts in both R and NR conditions and α-NcSAG4 detected bands between 25–37 kDa only in bradyzoites, while α-NcROP2 detected a strong single band near 60 kDa under reducing conditions, and a weak recognition of a band under NR. α-NcSRS2 detected bands in the 30–40 kDa range, under both R and NR, and α-NcSAG1 and α-NcBSR4 failed to detect any bands. Both polyclonal antisera revealed multiple bands ranging from 10–250 kDa.

α-TgBAG1 was the only antibody that labelled bradyzoites by IF apart from both polyclonal antisera that labelled bradyzoites and tachyzoites. Full datasets are presented in **Table 17** and **Figures 28 to 30**.

**Table 17: Results obtained with *Neospora caninum, Toxoplasma gondii* and *Besnoitia besnoiti* antibodies tested against *B. besnoiti* tachyzoites and bradyzoites by IHC, WB and IF. (*R: reducing conditions, NR: non-reducing conditions, +: positive, -: negative*)**

| Antibodies | IHC | | WB | | | | IF | |
|---|---|---|---|---|---|---|---|---|
| | Bradyzoite labelling | Cyst wall labelling | Bradyzoite | | Tachyzoite | | Bradyzoite | Tachyzoite |
| | | | R | NR | R | NR | | |
| **α-NcSAG1** | + | - | - | - | - | - | - | + (Weak fluorescence) |
| **α-NcSRS2** | + | - | - (Low intensity of recognition around 30–40 kDa) | - (Low intensity of recognition around 30–40 kDa) | - | - | - | - |
| **α-NcROP2** | + | + | + (60 kDa) | + (60 kDa) | - | - | - | - |
| **α-NcSAG4** | + | - | + (25–37 kDa) | + (25–37 kDa) | - | - | + (Weak fluorescence) | + (Weak fluorescence) |
| **α-NcBSR4** | + (focal areas of increased intensity) | + (Weak labelling) | - | - | - | - | - | - |
| **α-NcSRS9** | + | + (Intense labelling) | + (~37–50 kDa) | + (~37–50 kDa) | - | - | + (Weak fluorescence) | + (Weak fluorescence) |
| **α-TgBAG1** | + | + (Intense labelling) | + (~28–30 kDa) | + (~28–30 kDa) | - | - | + | - |
| **BbSpain-1 polyclonal bradyzoite antiserum (α-Bz)** | + | + | + (multiple bands between ~10–250 kDa) | + (multiple bands between ~10–250 kDa) | + (~20–250 kDa) | + (~20–250 kDa) | + (Intense fluorescence) | + (Intense fluorescence) |
| **BbSpain-1 polyclonal tachyzoite antiserum (α-Bz)** | + | + | + (multiple bands between ~10–250 kDa, but fewer and weaker than the polyclonal bradyzoite antiserum) | + (multiple bands between ~10–250 kDa, but fewer and weaker, than the polyclonal bradyzoite antiserum) | + (multiple bands between ~10–250 kDa) | + (multiple bands between ~10–250 kDa) | + (Intense fluorescence) | + (Intense fluorescence) |

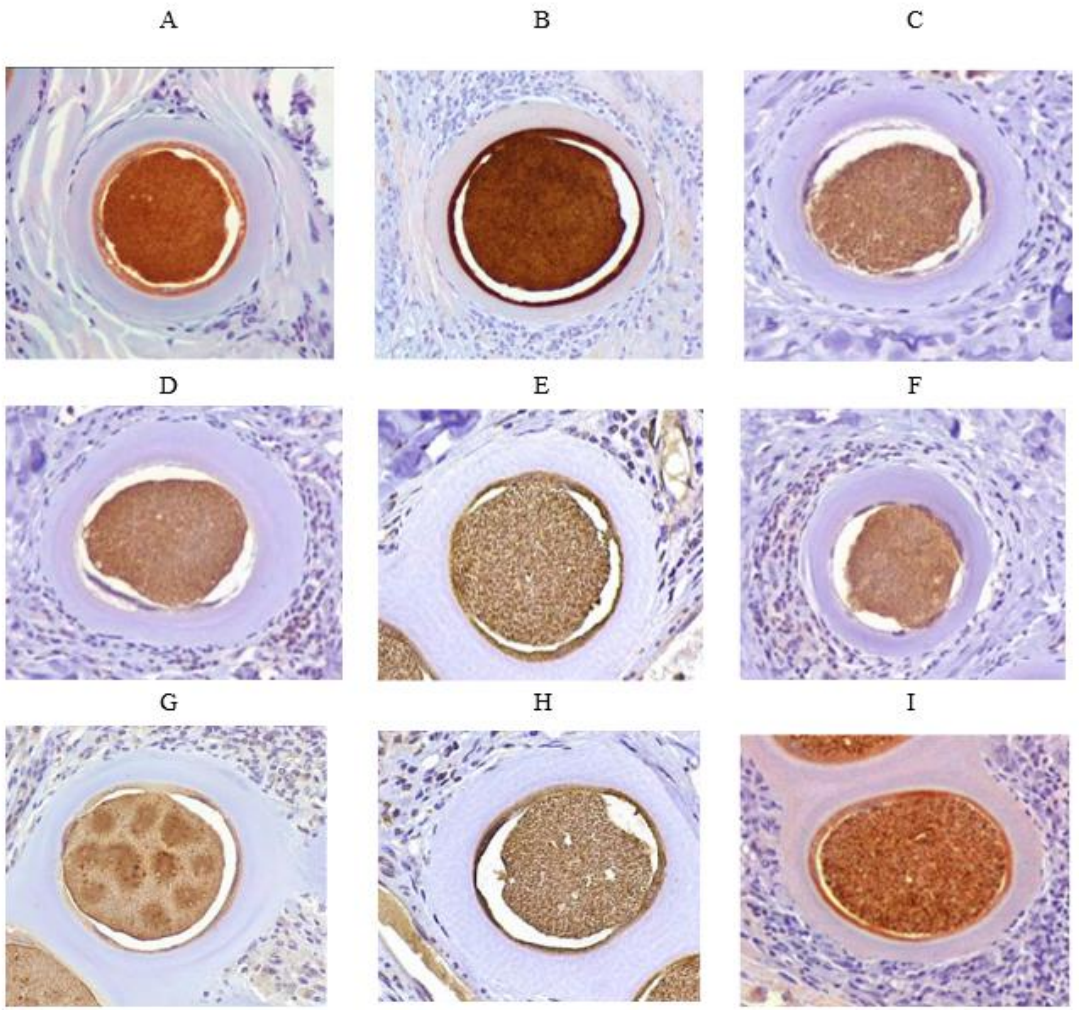


**Figure 28. Representative IHC images showing *B. besnoiti* bradyzoite tissue cysts stained with various antibodies. Sections were incubated with: (A) Polyclonal anti-*B. besnoiti*-tachyzoite (α-Tz), (B) Polyclonal anti-*B. besnoiti*-bradyzoite (α-Bz), (C) α-NcSAG1, (D) α-NcSRS2, (E) α-NcROP2, (F)- α-NcSAG4, (G) α-NcBSR4, (H) α-NcSRS9 and (I) α-TgBAG1 antibodies.**

C

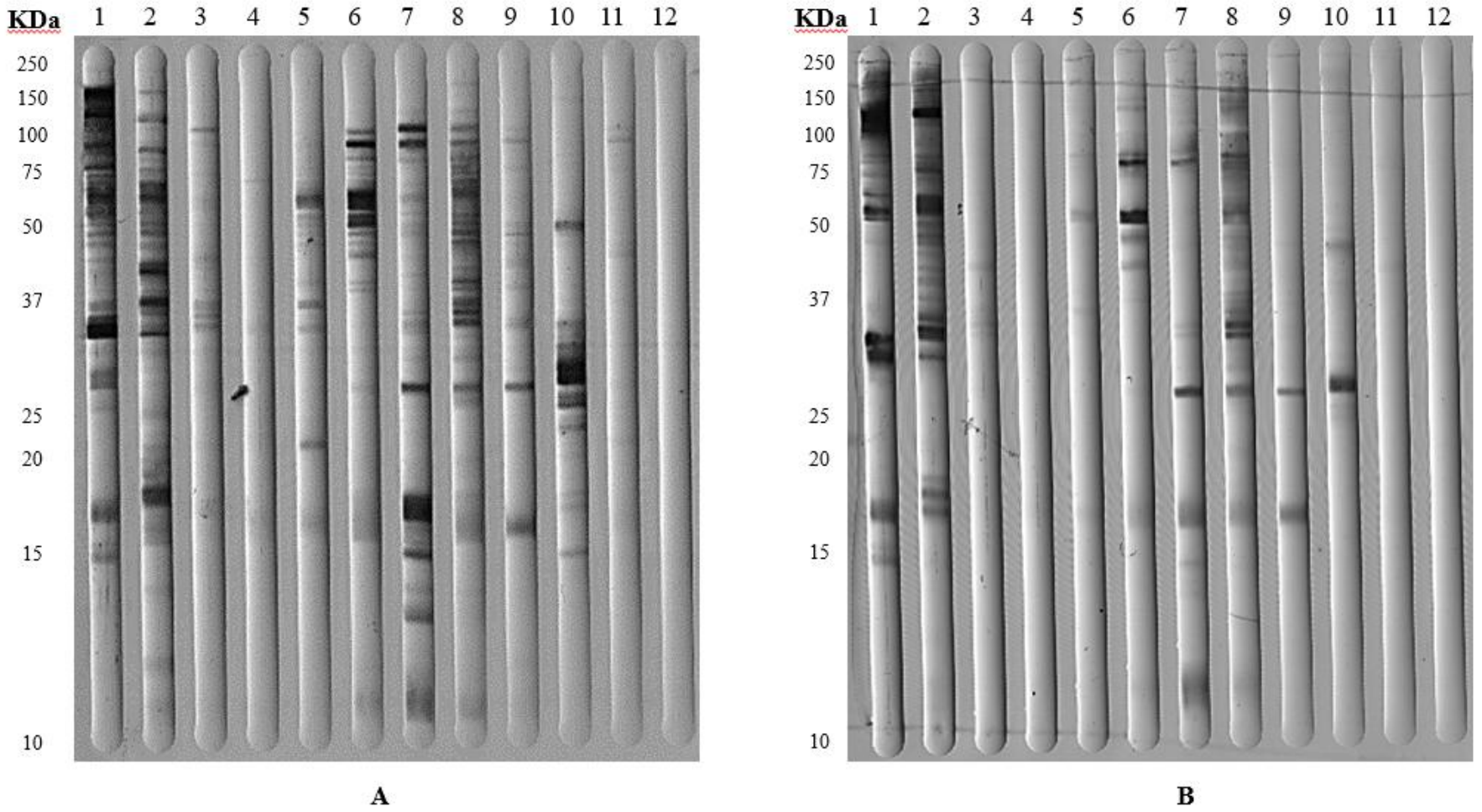


**Figure 29. Western blot (WB) membranes containing *B. besnoiti* bradyzoites, analyzed under R (A) and NR (B) conditions. The membranes were probed with various antibodies: (1) polyclonal anti-*B. besnoiti*-bradyzoite (α-Bz), (2) polyclonal anti-*B. besnoiti*- tachyzoite (α-Tz), (3) pre-immune serum (PIS), (4) α-NcSAG1, (5) α-NcSRSD2, (6) α-NcROP2, (7) α-NcSAG4, (8) α-NcSRS9-a, (9) α-NcSRS9-b, (10) α-TgBAG1, (11) α-NcBSR4 and (12) blocking agent (milk).**

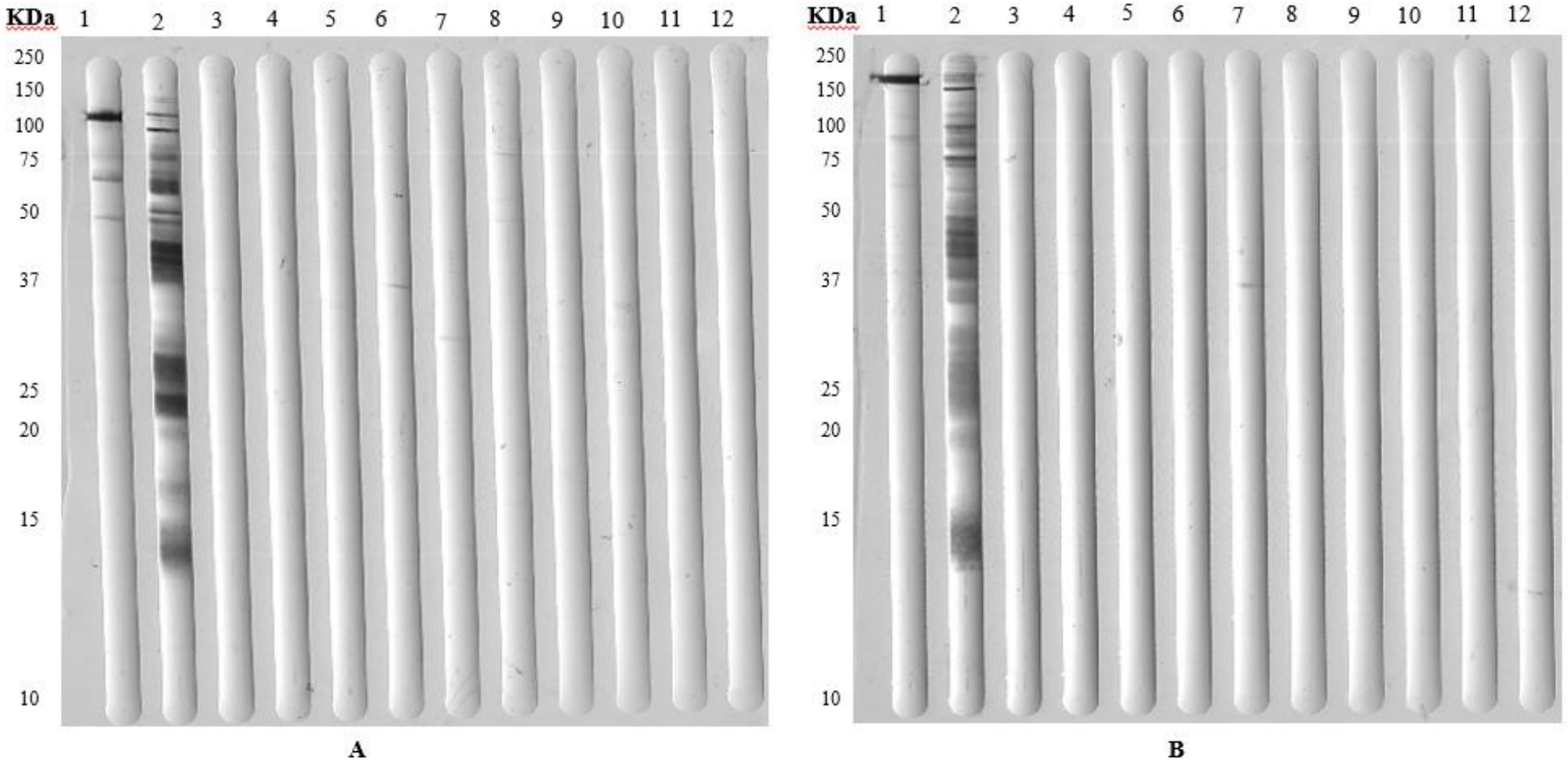


**Figure 30. Western blot (WB) membranes containing *B. besnoiti* tachyzoites, analyzed under R (A) and NR (B) conditions. The membranes were probed with various antibodies: (1) polyclonal anti-*B. besnoiti*-bradyzoite (α-Bz), (2) polyclonal anti-*B. besnoiti*- tachyzoite (α-Tz), (3) pre-immune serum (PIS), (4) α-NcSAG1, (5) α-NcSRSD2, (6) α-NcROP2, (7) α-NcSAG4, (8) α-NcSRS9-a, (9) α-NcSRS9-b, (10) α-TgBAG1, (11) α-NcBSR4 and (12) blocking agent (milk).**

### 5.4.2 *In vitro* induction of BAG1-positive vacuoles in *B. besnoiti* cell cultures under SNP and HDACi treatments

Among the panel of stress conditions evaluated, only three protocols proved partially effective in inducing bradyzoite differentiation in *B. besnoiti* (BbSpain-1): treatment with SNP at 70 µM for 7 days, treatment with 50 µM apicidin for 15 days and treatment with 50 µM FR235222 for 15 days. These treatments showed positive results in HFF cells, while MARC-145 and Vero81 exhibited excessive overgrowth under the same conditions. In contrast, PBAF displayed poor tolerance to prolonged stress, resulting in significant monolayer detachment and cell death.

Importantly, no discernible differences were observed between cold methanol and GA-PFA fixation protocols in terms of immunofluorescence signal quality. Under the most effective conditions in HFFs, only a small proportion of PVs expressed the bradyzoite-specific marker BAG1, with conversion rates estimated at 2% following SNP treatment, and slightly higher values after apicidin (3.5%) and FR235222 (3%) exposure (**Figure 31)**. In contrast, other stress protocols—including alkaline pH, heat shock, nutrient deprivation and exposure to the bumped kinase inhibitor BKI1294—failed to induce BAG1 expression under any tested condition. A complete summary of the experimental conditions tested and their outcomes in both *B. besnoiti* and *T. gondii* is provided in **Table 18**.

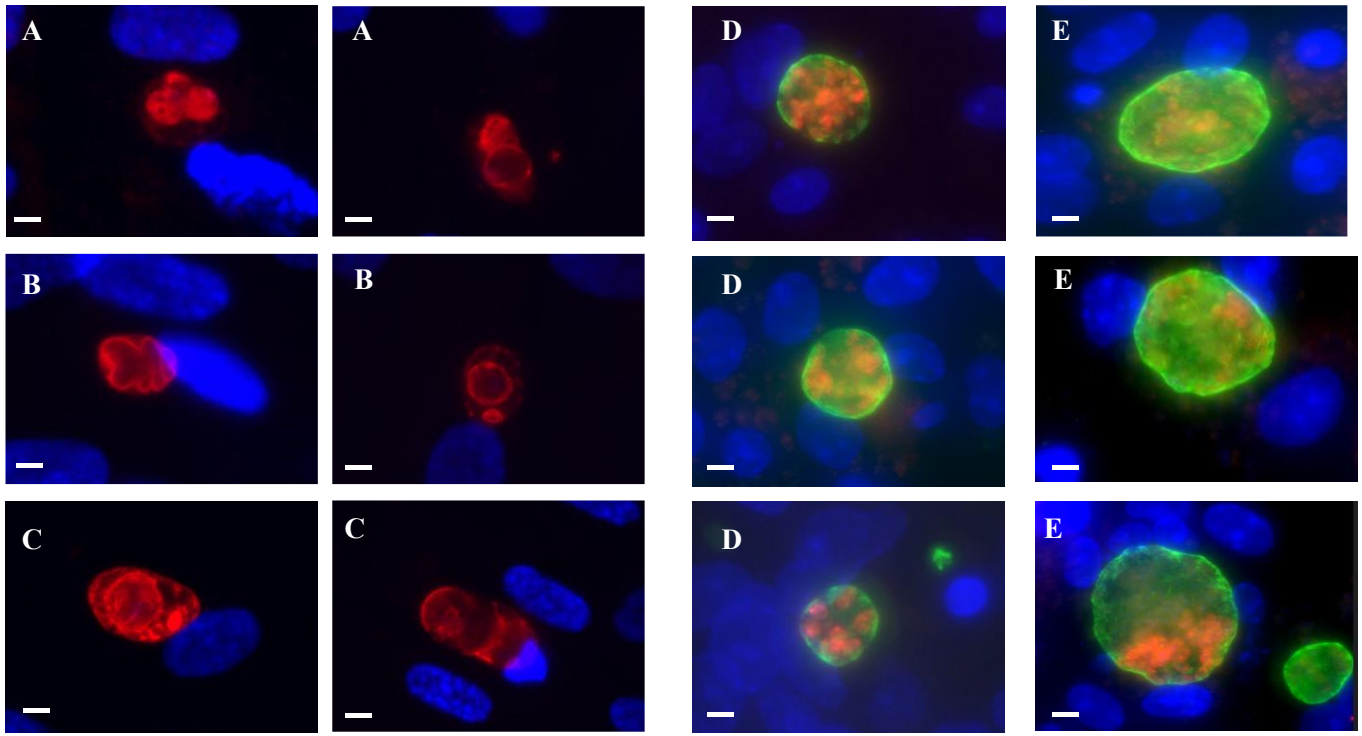


**Figure 31. Representative IF images of *B. besnoiti* and *T. gondii* under bradyzoite induction conditions. Scale bar = 10 µm. (A–C) BAG1-positive vacuoles of *B. besnoiti* (BbSpain-1) in HFF cells following different stress protocols: (A) SNP 70 µM for 7 days, (B) apicidin 50 µM for 15 days, and (C) FR235222 50 µM for 15 days. (D–E) Positive controls showing bradyzoite cysts of *T. gondii* isolates (D) TgSp3 and (E) TgME49 under standard induction protocols. Green: DBA lectin (cyst wall); red: α-TgBAG1 produced in rabbit (bradyzoite marker); blue: DAPI (nuclei). Notably, vacuoles of *B. besnoiti* appeared smaller and less structured than the well-defined cysts observed in *T. gondii* under the same magnification conditions.**

**Table 18. Summary of *in vitro* stress protocols evaluated for tachyzoite-to-bradyzoite conversion of *B. besnoiti* (BbSpain-1) and *T. gondii* (TgME49, TgSp3) in MARC-145, Vero81, HFF and PBAF. Assays showing partial conversion in *B. besnoiti* are shaded in grey.**

| Stress protocol | Time of application | Duration | Cell lines | Parasite isolate | MOI | Bradyzoite conversion |
|---|---|---|---|---|---|---|
| Alkaline medium (pH 8.0) | 6 h p.i. (medium was refreshed bi-daily) | 3 days | MARC-145 | BbSpain-1 | 2:1 | No conversion observed |
| | | | | TgME49 | 0,25:1 | Conversion observed (+DBA + α-TgBAG1) |
| | | | | TgSp3 | 0,5:1 | Conversion observed (+DBA + α-TgBAG1) |
| | | | Vero81 | BbSpain-1 | 2:1 | No conversion observed |
| | | | | TgME49 | 0,25:1 | Conversion observed (+DBA + α-TgBAG1) |
| | | | | TgSp3 | 0,5:1 | Conversion observed (+DBA + α-TgBAG1) |
| | | | HFF | BbSpain-1 | 2:1 | No conversion observed |
| | | | | TgME49 | 0,25:1 | Conversion observed (+DBA + α-TgBAG1) |
| | | | | TgSp3 | 0,5:1 | Conversion observed (+DBA + α-TgBAG1) |
| | | | PBAF | BbSpain-1 | 2:1 | Cells do not withstand stressful treatment |
| | | | | TgME49 | 0,25:1 | Cells do not withstand stressful treatment |
| | | | | TgSp3 | 0,5:1 | Cells do not withstand stressful treatment |

| Stress protocol | Time of application | Duration | Cell lines | Parasite isolate | MOI | Bradyzoite conversion |
|---|---|---|---|---|---|---|
| Alkaline medium (pH 8.0) | 6 h p.i. (medium was refreshed bi-daily) | 5 days | MARC-145 | BbSpain-1 | 2:1 | No conversion observed |
| | | | | TgME49 | 0,25:1 | Conversion observed (+DBA + α-TgBAG1) |
| | | | | TgSp3 | 0,5:1 | Conversion observed (+DBA + α-TgBAG1) |
| | | | Vero81 | BbSpain-1 | 2:1 | No conversion observed |
| | | | | TgME49 | 0,25:1 | Conversion observed (+DBA + α-TgBAG1) |
| | | | | TgSp3 | 0,5:1 | Conversion observed (+DBA + α-TgBAG1) |
| | | | HFF | BbSpain-1 | 2:1 | No conversion observed |
| | | | | TgME49 | 0,25:1 | Conversion observed (+DBA + α-TgBAG1) |
| | | | | TgSp3 | 0,5:1 | Conversion observed (+DBA + α-TgBAG1) |
| | | | PBAF | BbSpain-1 | 2:1 | Cells do not withstand stressful treatment |
| | | | | TgME49 | 0,25:1 | Cells do not withstand stressful treatment |
| | | | | TgSp3 | 0,5:1 | Cells do not withstand stressful treatment |

| Stress protocol | Time of application | Duration | Cell lines | Parasite isolate | MOI | Bradyzoite conversion |
|---|---|---|---|---|---|---|
| Alkaline medium (pH 8.0) | 6 h p.i. (medium was refreshed bi-daily) | 7 days | MARC-145 | BbSpain-1 | 2:1 | Cells do not withstand stressful treatment |
| | | | | TgME49 | 0,25:1 | Cells do not withstand stressful treatment |
| | | | | TgSp3 | 0,5:1 | Cells do not withstand stressful treatment |
| | | | Vero81 | BbSpain-1 | 2:1 | Cells do not withstand stressful treatment |
| | | | | TgME49 | 0,25:1 | Cells do not withstand stressful treatment |
| | | | | TgSp3 | 0,5:1 | Cells do not withstand stressful treatment |
| | | | HFF | BbSpain-1 | 2:1 | Cells do not withstand stressful treatment |
| | | | | TgME49 | 0,25:1 | Cells do not withstand stressful treatment |
| | | | | TgSp3 | 0,5:1 | Cells do not withstand stressful treatment |
| | | | PBAF | BbSpain-1 | 2:1 | Cells do not withstand stressful treatment |
| | | | | TgME49 | 0,25:1 | Cells do not withstand stressful treatment |
| | | | | TgSp3 | 0,5:1 | Cells do not withstand stressful treatment |

| Stress protocol | Time of application | Duration | Cell lines | Parasite isolate | MOI | Bradyzoite conversion |
|---|---|---|---|---|---|---|
| Alkaline medium (pH 8.0) | 12 h p.i. (medium was refreshed bi-daily) | 3 days | MARC-145 | BbSpain-1 | 2:1 | No conversion observed |
| | | | | TgME49 | 0,25:1 | Conversion observed (+DBA + α-TgBAG1) |
| | | | | TgSp3 | 0,5:1 | Conversion observed (+DBA + α-TgBAG1) |
| | | | Vero81 | BbSpain-1 | 2:1 | No conversion observed |
| | | | | TgME49 | 0,25:1 | Conversion observed (+DBA + α-TgBAG1) |
| | | | | TgSp3 | 0,5:1 | Conversion observed (+DBA + α-TgBAG1) |
| | | | HFF | BbSpain-1 | 2:1 | No conversion observed |
| | | | | TgME49 | 0,25:1 | Conversion observed (+DBA + α-TgBAG1) |
| | | | | TgSp3 | 0,5:1 | Conversion observed (+DBA + α-TgBAG1) |
| | | | PBAF | BbSpain-1 | 2:1 | Cells do not withstand stressful treatment |
| | | | | TgME49 | 0,25:1 | Cells do not withstand stressful treatment |
| | | | | TgSp3 | 0,5:1 | Cells do not withstand stressful treatment |

| Stress protocol | Time of application | Duration | Cell lines | Parasite isolate | MOI | Bradyzoite conversion |
|---|---|---|---|---|---|---|
| Alkaline medium (pH 8.0) | 12 h p.i. (medium was refreshed bi-daily) | 5 days | MARC-145 | BbSpain-1 | 2:1 | No conversion observed |
| | | | | TgME49 | 0,25:1 | Conversion observed (+DBA + α-TgBAG1) |
| | | | | TgSp3 | 0,5:1 | Conversion observed (+DBA + α-TgBAG1) |
| | | | Vero81 | BbSpain-1 | 2:1 | No conversion observed |
| | | | | TgME49 | 0,25:1 | Conversion observed (+DBA + α-TgBAG1) |
| | | | | TgSp3 | 0,5:1 | Conversion observed (+DBA + α-TgBAG1) |
| | | | HFF | BbSpain-1 | 2:1 | No conversion observed |
| | | | | TgME49 | 0,25:1 | Conversion observed (+DBA + α-TgBAG1) |
| | | | | TgSp3 | 0,5:1 | Conversion observed (+DBA + α-TgBAG1) |
| | | | PBAF | BbSpain-1 | 2:1 | Cells do not withstand stressful treatment |
| | | | | TgME49 | 0,25:1 | Cells do not withstand stressful treatment |
| | | | | TgSp3 | 0,5:1 | Cells do not withstand stressful treatment |

| Stress protocol | Time of application | Duration | Cell lines | Parasite isolate | MOI | Bradyzoite conversion |
|---|---|---|---|---|---|---|
| Alkaline medium (pH 8.0) | 12 h p.i. (medium was refreshed bi-daily) | 7 days | MARC-145 | BbSpain-1 | 2:1 | Cells do not withstand stressful treatment |
| | | | | TgME49 | 0,25:1 | Cells do not withstand stressful treatment |
| | | | | TgSp3 | 0,5:1 | Cells do not withstand stressful treatment |
| | | | Vero81 | BbSpain-1 | 2:1 | Cells do not withstand stressful treatment |
| | | | | TgME49 | 0,25:1 | Cells do not withstand stressful treatment |
| | | | | TgSp3 | 0,5:1 | Cells do not withstand stressful treatment |
| | | | HFF | BbSpain-1 | 2:1 | Cells do not withstand stressful treatment |
| | | | | TgME49 | 0,25:1 | Cells do not withstand stressful treatment |
| | | | | TgSp3 | 0,5:1 | Cells do not withstand stressful treatment |
| | | | PBAF | BbSpain-1 | 2:1 | Cells do not withstand stressful treatment |
| | | | | TgME49 | 0,25:1 | Cells do not withstand stressful treatment |
| | | | | TgSp3 | 0,5:1 | Cells do not withstand stressful treatment |

| Stress protocol | Time of application | Duration | Cell lines | Parasite isolate | MOI | Bradyzoite conversion |
|---|---|---|---|---|---|---|
| Alkaline medium (pH 8.0) | 48 h p.i. (medium was refreshed bi-daily) | 3 days | MARC-145 | BbSpain-1 | 2:1 | No conversion observed |
| | | | | TgME49 | 0,25:1 | Conversion observed (+DBA + α-TgBAG1) |
| | | | | TgSp3 | 0,5:1 | Conversion observed (+DBA + α-TgBAG1) |
| | | | Vero81 | BbSpain-1 | 2:1 | No conversion observed |
| | | | | TgME49 | 0,25:1 | Conversion observed (+DBA + α-TgBAG1) |
| | | | | TgSp3 | 0,5:1 | Conversion observed (+DBA + α-TgBAG1) |
| | | | HFF | BbSpain-1 | 2:1 | No conversion observed |
| | | | | TgME49 | 0,25:1 | Conversion observed (+DBA + α-TgBAG1) |
| | | | | TgSp3 | 0,5:1 | Conversion observed (+DBA + α-TgBAG1) |
| | | | PBAF | BbSpain-1 | 2:1 | Cells do not withstand stressful treatment |
| | | | | TgME49 | 0,25:1 | Cells do not withstand stressful treatment |
| | | | | TgSp3 | 0,5:1 | Cells do not withstand stressful treatment |

| Stress protocol | Time of application | Duration | Cell lines | Parasite isolate | MOI | Bradyzoite conversion |
|---|---|---|---|---|---|---|
| Alkaline medium (pH 8.0) | 48 h p.i. (medium was refreshed bi-daily) | 5 days | MARC-145 | BbSpain-1 | 2:1 | No conversion observed |
| | | | | TgME49 | 0,25:1 | Conversion observed (+DBA + α-TgBAG1) |
| | | | | TgSp3 | 0,5:1 | Conversion observed (+DBA + α-TgBAG1) |
| | | | Vero81 | BbSpain-1 | 2:1 | No conversion observed |
| | | | | TgME49 | 0,25:1 | Conversion observed (+DBA + α-TgBAG1) |
| | | | | TgSp3 | 0,5:1 | Conversion observed (+DBA + α-TgBAG1) |
| | | | HFF | BbSpain-1 | 2:1 | No conversion observed |
| | | | | TgME49 | 0,25:1 | Conversion observed (+DBA + α-TgBAG1) |
| | | | | TgSp3 | 0,5:1 | Conversion observed (+DBA + α-TgBAG1) |
| | | | PBAF | BbSpain-1 | 2:1 | Cells do not withstand stressful treatment |
| | | | | TgME49 | 0,25:1 | Cells do not withstand stressful treatment |
| | | | | TgSp3 | 0,5:1 | Cells do not withstand stressful treatment |

| Stress protocol | Time of application | Duration | Cell lines | Parasite isolate | MOI | Bradyzoite conversion |
|---|---|---|---|---|---|---|
| Alkaline medium (pH 8.0) | 48 h p.i. (medium was refreshed bi-daily) | 7 days | MARC-145 | BbSpain-1 | 2:1 | Cells do not withstand stressful treatment |
| | | | | TgME49 | 0,25:1 | Cells do not withstand stressful treatment |
| | | | | TgSp3 | 0,5:1 | Cells do not withstand stressful treatment |
| | | | Vero81 | BbSpain-1 | 2:1 | Cells do not withstand stressful treatment |
| | | | | TgME49 | 0,25:1 | Cells do not withstand stressful treatment |
| | | | | TgSp3 | 0,5:1 | Cells do not withstand stressful treatment |
| | | | HFF | BbSpain-1 | 2:1 | Cells do not withstand stressful treatment |
| | | | | TgME49 | 0,25:1 | Cells do not withstand stressful treatment |
| | | | | TgSp3 | 0,5:1 | Cells do not withstand stressful treatment |
| | | | PBAF | BbSpain-1 | 2:1 | Cells do not withstand stressful treatment |
| | | | | TgME49 | 0,25:1 | Cells do not withstand stressful treatment |
| | | | | TgSp3 | 0,5:1 | Cells do not withstand stressful treatment |

| Stress protocol | Time of application | Duration | Cell lines | Parasite isolate | MOI | Bradyzoite conversion |
|---|---|---|---|---|---|---|
| Heat shock 40,5ºC | Heat shock pre-treatment (40,5ºC) of 2 h prior to infection, followed by a recovery period (37ºC) of 6 h p.i. and then the heat-treatment (40,5ºC) of 24 h | 24 h | MARC-145 | BbSpain-1 | 2:1 | No conversion observed |
| | | | | TgME49 | 0,25:1 | Conversion observed (+DBA + α-TgBAG1) |
| | | | | TgSp3 | 0,5:1 | Conversion observed (+DBA + α-TgBAG1) |
| | | | Vero81 | BbSpain-1 | 2:1 | No conversion observed |
| | | | | TgME49 | 0,25:1 | Conversion observed (+DBA + α-TgBAG1) |
| | | | | TgSp3 | 0,5:1 | Conversion observed (+DBA + α-TgBAG1) |
| | | | HFF | BbSpain-1 | 2:1 | No conversion observed |
| | | | | TgME49 | 0,25:1 | Conversion observed (+DBA + α-TgBAG1) |
| | | | | TgSp3 | 0,5:1 | Conversion observed (+DBA + A-TgBAG1) |
| | | | PBAF | BbSpain-1 | 2:1 | Cells do not withstand stressful treatment |
| | | | | TgME49 | 0,25:1 | Cells do not withstand stressful treatment |
| | | | | TgSp3 | 0,5:1 | Cells do not withstand stressful treatment |

| Stress protocol | Time of application | Duration | Cell lines | Parasite isolate | MOI | Bradyzoite conversion |
|---|---|---|---|---|---|---|
| Heat shock 40,5ºC | Heat shock pre-treatment (40,5ºC) of 2 h prior to infection, followed by a recovery period (37ºC) of 6 h p.i. and then the heat-treatment (40,5ºC) of 48 h | 48 h | MARC-145 | BbSpain-1 | 2:1 | No conversion observed |
| | | | | TgME49 | 0,25:1 | Conversion observed (+DBA + α-TgBAG1) |
| | | | | TgSp3 | 0,5:1 | Conversion observed (+DBA + α-TgBAG1) |
| | | | Vero81 | BbSpain-1 | 2:1 | No conversion observed |
| | | | | TgME49 | 0,25:1 | Conversion observed (+DBA + α-TgBAG1) |
| | | | | TgSp3 | 0,5:1 | Conversion observed (+DBA + α-TgBAG1) |
| | | | HFF | BbSpain-1 | 2:1 | No conversion observed |
| | | | | TgME49 | 0,25:1 | Conversion observed (+DBA + α-TgBAG1) |
| | | | | TgSp3 | 0,5:1 | Conversion observed (+DBA + A-TgBAG1) |
| | | | PBAF | BbSpain-1 | 2:1 | Cells do not withstand stressful treatment |
| | | | | TgME49 | 0,25:1 | Cells do not withstand stressful treatment |
| | | | | TgSp3 | 0,5:1 | Cells do not withstand stressful treatment |

| Stress protocol | Time of application | Duration | Cell lines | Parasite isolate | MOI | Bradyzoite conversion |
|---|---|---|---|---|---|---|
| Heat shock 40,5ºC | Heat shock pre-treatment (40,5ºC) of 2 h prior to infection, followed by a recovery period (37ºC) of 6 h p.i. and then the heat-treatment (40,5ºC) of 72 h | 72 h | MARC-145 | BbSpain-1 | 2:1 | No conversion observed |
| | | | | TgME49 | 0,25:1 | Conversion observed (+DBA + α-TgBAG1) |
| | | | | TgSp3 | 0,5:1 | Conversion observed (+DBA + α-TgBAG1) |
| | | | Vero81 | BbSpain-1 | 2:1 | No conversion observed |
| | | | | TgME49 | 0,25:1 | Conversion observed (+DBA + α-TgBAG1) |
| | | | | TgSp3 | 0,5:1 | Conversion observed (+DBA + α-TgBAG1) |
| | | | HFF | BbSpain-1 | 2:1 | No conversion observed |
| | | | | TgME49 | 0,25:1 | Conversion observed (+DBA + α-TgBAG1) |
| | | | | TgSp3 | 0,5:1 | Conversion observed (+DBA + A-TgBAG1) |
| | | | PBAF | BbSpain-1 | 2:1 | Cells do not withstand stressful treatment |
| | | | | TgME49 | 0,25:1 | Cells do not withstand stressful treatment |
| | | | | TgSp3 | 0,5:1 | Cells do not withstand stressful treatment |

| Stress protocol | Time of application | Duration | Cell lines | Parasite isolate | MOI | Bradyzoite conversion |
|---|---|---|---|---|---|---|
| Heat shock 40,5ºC | Heat shock pre-treatment (40,5ºC) of 2 h prior to infection, followed by a recovery period (37ºC) of 6 h p.i. and then the heat-treatment (40,5ºC) of 120 h | 120 h | MARC-145 | BbSpain-1 | 2:1 | No conversion observed |
| | | | | TgME49 | 0,25:1 | Conversion observed (+DBA + α-TgBAG1) |
| | | | | TgSp3 | 0,5:1 | Conversion observed (+DBA + α-TgBAG1) |
| | | | Vero81 | BbSpain-1 | 2:1 | No conversion observed |
| | | | | TgME49 | 0,25:1 | Conversion observed (+DBA + α-TgBAG1) |
| | | | | TgSp3 | 0,5:1 | Conversion observed (+DBA + α-TgBAG1) |
| | | | HFF | BbSpain-1 | 2:1 | No conversion observed |
| | | | | TgME49 | 0,25:1 | Conversion observed (+DBA + α-TgBAG1) |
| | | | | TgSp3 | 0,5:1 | Conversion observed (+DBA + A-TgBAG1) |
| | | | PBAF | BbSpain-1 | 2:1 | Cells do not withstand stressful treatment |
| | | | | TgME49 | 0,25:1 | Cells do not withstand stressful treatment |
| | | | | TgSp3 | 0,5:1 | Cells do not withstand stressful treatment |

| Stress protocol | Time of application | Duration | Cell lines | Parasite isolate | MOI | Bradyzoite conversion |
|---|---|---|---|---|---|---|
| Heat shock 43ºC | Heat shock pre-treatment (43ºC) of 2 h prior to infection, followed by a recovery period (37ºC) of 6 h p.i. and then the heat-treatment (43ºC) of 24 h | 24 h | MARC-145 | BbSpain-1 | 2:1 | Cells do not withstand stressful treatment |
| | | | | TgME49 | 0,25:1 | Cells do not withstand stressful treatment |
| | | | | TgSp3 | 0,5:1 | Cells do not withstand stressful treatment |
| | | | Vero81 | BbSpain-1 | 2:1 | Cells do not withstand stressful treatment |
| | | | | TgME49 | 0,25:1 | Cells do not withstand stressful treatment |
| | | | | TgSp3 | 0,5:1 | Cells do not withstand stressful treatment |
| | | | HFF | BbSpain-1 | 2:1 | Cells do not withstand stressful treatment |
| | | | | TgME49 | 0,25:1 | Cells do not withstand stressful treatment |
| | | | | TgSp3 | 0,5:1 | Cells do not withstand stressful treatment |
| | | | PBAF | BbSpain-1 | 2:1 | Cells do not withstand stressful treatment |
| | | | | TgME49 | 0,25:1 | Cells do not withstand stressful treatment |
| | | | | TgSp3 | 0,5:1 | Cells do not withstand stressful treatment |

| Stress protocol | Time of application | Duration | Cell lines | Parasite isolate | MOI | Bradyzoite conversion |
|---|---|---|---|---|---|---|
| Heat shock 43ºC | Heat shock pre-treatment (43ºC) of 2 h prior to infection, followed by a recovery period (37ºC) of 6 h p.i. and then the heat-treatment (43ºC) of 48 h | 48 h | MARC-145 | BbSpain-1 | 2:1 | Cells do not withstand stressful treatment |
| | | | | TgME49 | 0,25:1 | Cells do not withstand stressful treatment |
| | | | | TgSp3 | 0,5:1 | Cells do not withstand stressful treatment |
| | | | Vero81 | BbSpain-1 | 2:1 | Cells do not withstand stressful treatment |
| | | | | TgME49 | 0,25:1 | Cells do not withstand stressful treatment |
| | | | | TgSp3 | 0,5:1 | Cells do not withstand stressful treatment |
| | | | HFF | BbSpain-1 | 2:1 | Cells do not withstand stressful treatment |
| | | | | TgME49 | 0,25:1 | Cells do not withstand stressful treatment |
| | | | | TgSp3 | 0,5:1 | Cells do not withstand stressful treatment |
| | | | PBAF | BbSpain-1 | 2:1 | Cells do not withstand stressful treatment |
| | | | | TgME49 | 0,25:1 | Cells do not withstand stressful treatment |
| | | | | TgSp3 | 0,5:1 | Cells do not withstand stressful treatment |

| Stress protocol | Time of application | Duration | Cell lines | Parasite isolate | MOI | Bradyzoite conversion |
|---|---|---|---|---|---|---|
| Heat shock 43ºC | Heat shock pre-treatment (43ºC) of 2 h prior to infection, followed by a recovery period (37ºC) of 6 h p.i. and then the heat-treatment (43ºC) of 72 h | 72 h | MARC-145 | BbSpain-1 | 2:1 | Cells do not withstand stressful treatment |
| | | | | TgME49 | 0,25:1 | Cells do not withstand stressful treatment |
| | | | | TgSp3 | 0,5:1 | Cells do not withstand stressful treatment |
| | | | Vero81 | BbSpain-1 | 2:1 | Cells do not withstand stressful treatment |
| | | | | TgME49 | 0,25:1 | Cells do not withstand stressful treatment |
| | | | | TgSp3 | 0,5:1 | Cells do not withstand stressful treatment |
| | | | HFF | BbSpain-1 | 2:1 | Cells do not withstand stressful treatment |
| | | | | TgME49 | 0,25:1 | Cells do not withstand stressful treatment |
| | | | | TgSp3 | 0,5:1 | Cells do not withstand stressful treatment |
| | | | PBAF | BbSpain-1 | 2:1 | Cells do not withstand stressful treatment |
| | | | | TgME49 | 0,25:1 | Cells do not withstand stressful treatment |
| | | | | TgSp3 | 0,5:1 | Cells do not withstand stressful treatment |

| Stress protocol | Time of application | Duration | Cell lines | Parasite isolate | MOI | Bradyzoite conversion |
|---|---|---|---|---|---|---|
| Heat shock 43ºC | Heat shock pre-treatment (43ºC) of 2 h prior to infection, followed by a recovery period (37ºC) of 6 h p.i. and then the heat-treatment (43ºC) of 72 h | 120 h | MARC-145 | BbSpain-1 | 2:1 | Cells do not withstand stressful treatment |
| | | | | TgME49 | 0,25:1 | Cells do not withstand stressful treatment |
| | | | | TgSp3 | 0,5:1 | Cells do not withstand stressful treatment |
| | | | Vero81 | BbSpain-1 | 2:1 | Cells do not withstand stressful treatment |
| | | | | TgME49 | 0,25:1 | Cells do not withstand stressful treatment |
| | | | | TgSp3 | 0,5:1 | Cells do not withstand stressful treatment |
| | | | HFF | BbSpain-1 | 2:1 | Cells do not withstand stressful treatment |
| | | | | TgME49 | 0,25:1 | Cells do not withstand stressful treatment |
| | | | | TgSp3 | 0,5:1 | Cells do not withstand stressful treatment |
| | | | PBAF | BbSpain-1 | 2:1 | Cells do not withstand stressful treatment |
| | | | | TgME49 | 0,25:1 | Cells do not withstand stressful treatment |
| | | | | TgSp3 | 0,5:1 | Cells do not withstand stressful treatment |

| Stress protocol | Time of application | Duration | Cell lines | Parasite isolate | MOI | Bradyzoite conversion |
|---|---|---|---|---|---|---|
| FBS deprivation | Prior to infection (medium was refreshed daily) | 8 days | MARC-145 | BbSpain-1 | 2:1 | No conversion observed |
| | | | | TgME49 | 0,25:1 | No conversion observed |
| | | | | TgSp3 | 0,5:1 | No conversion observed |
| | | | Vero81 | BbSpain-1 | 2:1 | No conversion observed |
| | | | | TgME49 | 0,25:1 | No conversion observed |
| | | | | TgSp3 | 0,5:1 | No conversion observed |
| | | | HFF | BbSpain-1 | 2:1 | No conversion observed |
| | | | | TgME49 | 0,25:1 | No conversion observed |
| | | | | TgSp3 | 0,5:1 | No conversion observed |
| | | | PBAF | BbSpain-1 | 2:1 | Cells do not withstand stressful treatment |
| | | | | TgME49 | 0,25:1 | Cells do not withstand stressful treatment |
| | | | | TgSp3 | 0,5:1 | Cells do not withstand stressful treatment |

| Stress protocol | Time of application | Duration | Concentration | Cell lines | Parasite isolate | MOI | Bradyzoite conversion |
|---|---|---|---|---|---|---|---|
| Sodium nitroprusside (SNP) | At infection time | 3 days | 10 µM | MARC-145 | BbSpain-1 | 2:1 | No conversion observed |
| | | | | | TgME49 | 0,25:1 | Conversion observed (+DBA + α-TgBAG1) |
| | | | | | TgSp3 | 0,5:1 | Conversion observed (+DBA + α-TgBAG1) |
| | | | | Vero81 | BbSpain-1 | 2:1 | No conversion observed |
| | | | | | TgME49 | 0,25:1 | Conversion observed (+DBA + α-TgBAG1) |
| | | | | | TgSp3 | 0,5:1 | Conversion observed (+DBA + α-TgBAG1) |
| | | | | HFF | BbSpain-1 | 2:1 | No conversion observed |
| | | | | | TgME49 | 0,25:1 | Conversion observed (+DBA + α-TgBAG1) |
| | | | | | TgSp3 | 0,5:1 | Conversion observed (+DBA + α-TgBAG1) |
| | | | | PBAF | BbSpain-1 | 2:1 | Cells do not withstand stressful treatment |
| | | | | | TgME49 | 0,25:1 | Cells do not withstand stressful treatment |
| | | | | | TgSp3 | 0,5:1 | Cells do not withstand stressful treatment |

| Stress protocol | Time of application | Duration | Concentration | Cell lines | Parasite isolate | MOI | Bradyzoite conversion |
|---|---|---|---|---|---|---|---|
| Sodium nitroprusside (SNP) | At infection time | 3 days | 50 µM | MARC-145 | BbSpain-1 | 2:1 | No conversion observed |
| | | | | | TgME49 | 0,25:1 | Conversion observed (+DBA + α-TgBAG1) |
| | | | | | TgSp3 | 0,5:1 | Conversion observed (+DBA + α-TgBAG1) |
| | | | | Vero81 | BbSpain-1 | 2:1 | No conversion observed |
| | | | | | TgME49 | 0,25:1 | Conversion observed (+DBA + α-TgBAG1) |
| | | | | | TgSp3 | 0,5:1 | Conversion observed (+DBA + α-TgBAG1) |
| | | | | HFF | BbSpain-1 | 2:1 | No conversion observed |
| | | | | | TgME49 | 0,25:1 | Conversion observed (+DBA + α-TgBAG1) |
| | | | | | TgSp3 | 0,5:1 | Conversion observed (+DBA + α-TgBAG1) |
| | | | | PBAF | BbSpain-1 | 2:1 | Cells do not withstand stressful treatment |
| | | | | | TgME49 | 0,25:1 | Cells do not withstand stressful treatment |
| | | | | | TgSp3 | 0,5:1 | Cells do not withstand stressful treatment |

| Stress protocol | Time of application | Duration | Concentration | Cell lines | Parasite isolate | MOI | Bradyzoite conversion |
|---|---|---|---|---|---|---|---|
| Sodium nitroprusside (SNP) | At infection time | 3 days | 70 µM | MARC-145 | BbSpain-1 | 2:1 | No conversion observed |
| | | | | | TgME49 | 0,25:1 | Conversion observed (+DBA + α-TgBAG1) |
| | | | | | TgSp3 | 0,5:1 | Conversion observed (+DBA + α-TgBAG1) |
| | | | | Vero81 | BbSpain-1 | 2:1 | No conversion observed |
| | | | | | TgME49 | 0,25:1 | Conversion observed (+DBA + α-TgBAG1) |
| | | | | | TgSp3 | 0,5:1 | Conversion observed (+DBA + α-TgBAG1) |
| | | | | HFF | BbSpain-1 | 2:1 | No conversion observed |
| | | | | | TgME49 | 0,25:1 | Conversion observed (+DBA + α-TgBAG1) |
| | | | | | TgSp3 | 0,5:1 | Conversion observed (+DBA + α-TgBAG1) |
| | | | | PBAF | BbSpain-1 | 2:1 | Cells do not withstand stressful treatment |
| | | | | | TgME49 | 0,25:1 | Cells do not withstand stressful treatment |
| | | | | | TgSp3 | 0,5:1 | Cells do not withstand stressful treatment |

| Stress protocol | Time of application | Duration | Concentration | Cell lines | Parasite isolate | MOI | Bradyzoite conversion |
|---|---|---|---|---|---|---|---|
| Sodium nitroprusside (SNP) | At infection time | 3 days | 100 µM | MARC-145 | BbSpain-1 | 2:1 | Cells do not withstand stressful treatment |
| | | | | | TgME49 | 0,25:1 | Cells do not withstand stressful treatment |
| | | | | | TgSp3 | 0,5:1 | Cells do not withstand stressful treatment |
| | | | | Vero81 | BbSpain-1 | 2:1 | Cells do not withstand stressful treatment |
| | | | | | TgME49 | 0,25:1 | Cells do not withstand stressful treatment |
| | | | | | TgSp3 | 0,5:1 | Cells do not withstand stressful treatment |
| | | | | HFF | BbSpain-1 | 2:1 | Cells do not withstand stressful treatment |
| | | | | | TgME49 | 0,25:1 | Cells do not withstand stressful treatment |
| | | | | | TgSp3 | 0,5:1 | Cells do not withstand stressful treatment |
| | | | | PBAF | BbSpain-1 | 2:1 | Cells do not withstand stressful treatment |
| | | | | | TgME49 | 0,25:1 | Cells do not withstand stressful treatment |
| | | | | | TgSp3 | 0,5:1 | Cells do not withstand stressful treatment |

| Stress protocol | Time of application | Duration | Concentration | Cell lines | Parasite isolate | MOI | Bradyzoite conversion |
|---|---|---|---|---|---|---|---|
| Sodium nitroprusside (SNP) | At infection time | 5 days | 10 µM | MARC-145 | BbSpain-1 | 2:1 | No conversion observed |
| | | | | | TgME49 | 0,25:1 | Conversion observed (+DBA + α-TgBAG1) |
| | | | | | TgSp3 | 0,5:1 | Conversion observed (+DBA + α-TgBAG1) |
| | | | | Vero81 | BbSpain-1 | 2:1 | No conversion observed |
| | | | | | TgME49 | 0,25:1 | Conversion observed (+DBA + α-TgBAG1) |
| | | | | | TgSp3 | 0,5:1 | Conversion observed (+DBA + α-TgBAG1) |
| | | | | HFF | BbSpain-1 | 2:1 | No conversion observed |
| | | | | | TgME49 | 0,25:1 | Conversion observed (+DBA + α-TgBAG1) |
| | | | | | TgSp3 | 0,5:1 | Conversion observed (+DBA + α-TgBAG1) |
| | | | | PBAF | BbSpain-1 | 2:1 | Cells do not withstand stressful treatment |
| | | | | | TgME49 | 0,25:1 | Cells do not withstand stressful treatment |
| | | | | | TgSp3 | 0,5:1 | Cells do not withstand stressful treatment |

| Stress protocol | Time of application | Duration | Concentration | Cell lines | Parasite isolate | MOI | Bradyzoite conversion |
|---|---|---|---|---|---|---|---|
| Sodium nitroprusside (SNP) | At infection time | 5 days | 50 µM | MARC-145 | BbSpain-1 | 2:1 | No conversion observed |
| | | | | | TgME49 | 0,25:1 | Conversion observed (+DBA + α-TgBAG1) |
| | | | | | TgSp3 | 0,5:1 | Conversion observed (+DBA + α-TgBAG1) |
| | | | | Vero81 | BbSpain-1 | 2:1 | No conversion observed |
| | | | | | TgME49 | 0,25:1 | Conversion observed (+DBA + α-TgBAG1) |
| | | | | | TgSp3 | 0,5:1 | Conversion observed (+DBA + α-TgBAG1) |
| | | | | HFF | BbSpain-1 | 2:1 | No conversion observed |
| | | | | | TgME49 | 0,25:1 | Conversion observed (+DBA + α-TgBAG1) |
| | | | | | TgSp3 | 0,5:1 | Conversion observed (+DBA + α-TgBAG1) |
| | | | | PBAF | BbSpain-1 | 2:1 | Cells do not withstand stressful treatment |
| | | | | | TgME49 | 0,25:1 | Cells do not withstand stressful treatment |
| | | | | | TgSp3 | 0,5:1 | Cells do not withstand stressful treatment |

| Stress protocol | Time of application | Duration | Concentration | Cell lines | Parasite isolate | MOI | Bradyzoite conversion |
|---|---|---|---|---|---|---|---|
| Sodium nitroprusside (SNP) | At infection time | 5 days | 70 µM | MARC-145 | BbSpain-1 | 2:1 | No conversion observed |
| | | | | | TgME49 | 0,25:1 | Conversion observed (+DBA + α-TgBAG1) |
| | | | | | TgSp3 | 0,5:1 | Conversion observed (+DBA + α-TgBAG1) |
| | | | | Vero81 | BbSpain-1 | 2:1 | No conversion observed |
| | | | | | TgME49 | 0,25:1 | Conversion observed (+DBA + α-TgBAG1) |
| | | | | | TgSp3 | 0,5:1 | Conversion observed (+DBA + α-TgBAG1) |
| | | | | HFF | BbSpain-1 | 2:1 | No conversion observed |
| | | | | | TgME49 | 0,25:1 | Conversion observed (+DBA + α-TgBAG1) |
| | | | | | TgSp3 | 0,5:1 | Conversion observed (+DBA + α-TgBAG1) |
| | | | | PBAF | BbSpain-1 | 2:1 | Cells do not withstand stressful treatment |
| | | | | | TgME49 | 0,25:1 | Cells do not withstand stressful treatment |
| | | | | | TgSp3 | 0,5:1 | Cells do not withstand stressful treatment |

| Stress protocol | Time of application | Duration | Concentration | Cell lines | Parasite isolate | MOI | Bradyzoite conversion |
|---|---|---|---|---|---|---|---|
| Sodium nitroprusside (SNP) | At infection time | 5 days | 100 µM | MARC-145 | BbSpain-1 | 2:1 | Cells do not withstand stressful treatment |
| | | | | | TgME49 | 0,25:1 | Cells do not withstand stressful treatment |
| | | | | | TgSp3 | 0,5:1 | Cells do not withstand stressful treatment |
| | | | | Vero81 | BbSpain-1 | 2:1 | Cells do not withstand stressful treatment |
| | | | | | TgME49 | 0,25:1 | Cells do not withstand stressful treatment |
| | | | | | TgSp3 | 0,5:1 | Cells do not withstand stressful treatment |
| | | | | HFF | BbSpain-1 | 2:1 | Cells do not withstand stressful treatment |
| | | | | | TgME49 | 0,25:1 | Cells do not withstand stressful treatment |
| | | | | | TgSp3 | 0,5:1 | Cells do not withstand stressful treatment |
| | | | | PBAF | BbSpain-1 | 2:1 | Cells do not withstand stressful treatment |
| | | | | | TgME49 | 0,25:1 | Cells do not withstand stressful treatment |
| | | | | | TgSp3 | 0,5:1 | Cells do not withstand stressful treatment |

| Stress protocol | Time of application | Duration | Concentration | Cell lines | Parasite isolate | MOI | Bradyzoite conversion |
|---|---|---|---|---|---|---|---|
| Sodium nitroprusside (SNP) | At infection time | 7 days | 10 µM | MARC-145 | BbSpain-1 | 2:1 | No conversion observed |
| | | | | | TgME49 | 0,25:1 | Conversion observed (+DBA + α-TgBAG1) |
| | | | | | TgSp3 | 0,5:1 | Conversion observed (+DBA + α-TgBAG1) |
| | | | | Vero81 | BbSpain-1 | 2:1 | No conversion observed |
| | | | | | TgME49 | 0,25:1 | Conversion observed (+DBA + α-TgBAG1) |
| | | | | | TgSp3 | 0,5:1 | Conversion observed (+DBA + α-TgBAG1) |
| | | | | HFF | BbSpain-1 | 2:1 | No conversion observed |
| | | | | | TgME49 | 0,25:1 | Conversion observed (+DBA + α-TgBAG1) |
| | | | | | TgSp3 | 0,5:1 | Conversion observed (+DBA + α-TgBAG1) |
| | | | | PBAF | BbSpain-1 | 2:1 | Cells do not withstand stressful treatment |
| | | | | | TgME49 | 0,25:1 | Cells do not withstand stressful treatment |
| | | | | | TgSp3 | 0,5:1 | Cells do not withstand stressful treatment |

| Stress protocol | Time of application | Duration | Concentration | Cell lines | Parasite isolate | MOI | Bradyzoite conversion |
|---|---|---|---|---|---|---|---|
| Sodium nitroprusside (SNP) | At infection time | 7 days | 50 µM | MARC-145 | BbSpain-1 | 2:1 | No conversion observed |
| | | | | | TgME49 | 0,25:1 | Conversion observed (+DBA + α-TgBAG1) |
| | | | | | TgSp3 | 0,5:1 | Conversion observed (+DBA + α-TgBAG1) |
| | | | | Vero81 | BbSpain-1 | 2:1 | No conversion observed |
| | | | | | TgME49 | 0,25:1 | Conversion observed (+DBA + α-TgBAG1) |
| | | | | | TgSp3 | 0,5:1 | Conversion observed (+DBA + α-TgBAG1) |
| | | | | HFF | BbSpain-1 | 2:1 | No conversion observed |
| | | | | | TgME49 | 0,25:1 | Conversion observed (+DBA + α-TgBAG1) |
| | | | | | TgSp3 | 0,5:1 | Conversion observed (+DBA + α-TgBAG1) |
| | | | | PBAF | BbSpain-1 | 2:1 | Cells do not withstand stressful treatment |
| | | | | | TgME49 | 0,25:1 | Cells do not withstand stressful treatment |
| | | | | | TgSp3 | 0,5:1 | Cells do not withstand stressful treatment |

| Stress protocol | Time of application | Duration | Concentration | Cell lines | Parasite isolate | MOI | Bradyzoite conversion |
|---|---|---|---|---|---|---|---|
| Sodium nitroprusside (SNP) | At infection time | 7 days | 70 µM | MARC-145 | BbSpain-1 | 2:1 | No conversion observed |
| | | | | | TgME49 | 0,25:1 | Conversion observed (+DBA + α-TgBAG1) |
| | | | | | TgSp3 | 0,5:1 | Conversion observed (+DBA + α-TgBAG1) |
| | | | | Vero81 | BbSpain-1 | 2:1 | No conversion observed |
| | | | | | TgME49 | 0,25:1 | Conversion observed (+DBA + α-TgBAG1) |
| | | | | | TgSp3 | 0,5:1 | Conversion observed (+DBA + α-TgBAG1) |
| | | | | HFF | BbSpain-1 | 2:1 | Partial conversion observed (-DBA + α-TgBAG1) |
| | | | | | TgME49 | 0,25:1 | Conversion observed (+DBA + α-TgBAG1) |
| | | | | | TgSp3 | 0,5:1 | Conversion observed (+DBA + α-TgBAG1) |
| | | | | PBAF | BbSpain-1 | 2:1 | Cells do not withstand stressful treatment |
| | | | | | TgME49 | 0,25:1 | Cells do not withstand stressful treatment |
| | | | | | TgSp3 | 0,5:1 | Cells do not withstand stressful treatment |

| Stress protocol | Time of application | Duration | Concentration | Cell lines | Parasite isolate | MOI | Bradyzoite conversion |
|---|---|---|---|---|---|---|---|
| Sodium nitroprusside (SNP) | At infection time | 7 days | 100 µM | MARC-145 | BbSpain-1 | 2:1 | Cells do not withstand stressful treatment |
| | | | | | TgME49 | 0,25:1 | Cells do not withstand stressful treatment |
| | | | | | TgSp3 | 0,5:1 | Cells do not withstand stressful treatment |
| | | | | Vero81 | BbSpain-1 | 2:1 | Cells do not withstand stressful treatment |
| | | | | | TgME49 | 0,25:1 | Cells do not withstand stressful treatment |
| | | | | | TgSp3 | 0,5:1 | Cells do not withstand stressful treatment |
| | | | | HFF | BbSpain-1 | 2:1 | Cells do not withstand stressful treatment |
| | | | | | TgME49 | 0,25:1 | Cells do not withstand stressful treatment |
| | | | | | TgSp3 | 0,5:1 | Cells do not withstand stressful treatment |
| | | | | PBAF | BbSpain-1 | 2:1 | Cells do not withstand stressful treatment |
| | | | | | TgME49 | 0,25:1 | Cells do not withstand stressful treatment |
| | | | | | TgSp3 | 0,5:1 | Cells do not withstand stressful treatment |

| Stress protocol | Time of application | Duration | Concentration | Cell lines | Parasite isolate | MOI | Bradyzoite conversion |
|---|---|---|---|---|---|---|---|
| Apicidin | 12 h p.i. | 15 days | 50 µM | MARC-145 | BbSpain-1 | 2:1 | No conversion observed |
| | | | | | TgME49 | 0,25:1 | Conversion observed (+DBA + α-TgBAG1) |
| | | | | | TgSp3 | 0,5:1 | Conversion observed (+DBA + α-TgBAG1) |
| | | | | Vero81 | BbSpain-1 | 2:1 | No conversion observed |
| | | | | | TgME49 | 0,25:1 | Conversion observed (+DBA + α-TgBAG1) |
| | | | | | TgSp3 | 0,5:1 | Conversion observed (+DBA + α-TgBAG1) |
| | | | | HFF | BbSpain-1 | 2:1 | Partial conversion observed (-DBA +α-TgBAG1) |
| | | | | | TgME49 | 0,25:1 | Conversion observed (+DBA + α-TgBAG1) |
| | | | | | TgSp3 | 0,5:1 | Conversion observed (+DBA + α-TgBAG1) |
| | | | | PBAF | BbSpain-1 | 2:1 | Cells do not withstand stressful treatment |
| | | | | | TgME49 | 0,25:1 | Cells do not withstand stressful treatment |
| | | | | | TgSp3 | 0,5:1 | Cells do not withstand stressful treatment |

| Stress protocol | Time of application | Duration | Concentration | Cell lines | Parasite isolate | MOI | Bradyzoite conversion |
|---|---|---|---|---|---|---|---|
| Apicidin | 12 h p.i. | 15 days | 100 µM | MARC-145 | BbSpain-1 | 2:1 | No conversion observed |
| | | | | | TgME49 | 0,25:1 | Conversion observed (+DBA + α-TgBAG1) |
| | | | | | TgSp3 | 0,5:1 | Conversion observed (+DBA + α-TgBAG1) |
| | | | | Vero81 | BbSpain-1 | 2:1 | No conversion observed |
| | | | | | TgME49 | 0,25:1 | Conversion observed (+DBA + α-TgBAG1) |
| | | | | | TgSp3 | 0,5:1 | Conversion observed (+DBA + α-TgBAG1) |
| | | | | HFF | BbSpain-1 | 2:1 | No conversion observed |
| | | | | | TgME49 | 0,25:1 | Conversion observed (+DBA + α-TgBAG1) |
| | | | | | TgSp3 | 0,5:1 | Conversion observed (+DBA + α-TgBAG1) |
| | | | | PBAF | BbSpain-1 | 2:1 | Cells do not withstand stressful treatment |
| | | | | | TgME49 | 0,25:1 | Cells do not withstand stressful treatment |
| | | | | | TgSp3 | 0,5:1 | Cells do not withstand stressful treatment |

| Stress protocol | Time of application | Duration | Concentration | Cell lines | Parasite isolate | MOI | Bradyzoite conversion |
|---|---|---|---|---|---|---|---|
| Apicidin | 12 h p.i. | 15 days | 150 µM | MARC-145 | BbSpain-1 | 2:1 | Cells do not withstand stressful treatment |
| | | | | | TgME49 | 0,25:1 | Cells do not withstand stressful treatment |
| | | | | | TgSp3 | 0,5:1 | Cells do not withstand stressful treatment |
| | | | | Vero81 | BbSpain-1 | 2:1 | Cells do not withstand stressful treatment |
| | | | | | TgME49 | 0,25:1 | Cells do not withstand stressful treatment |
| | | | | | TgSp3 | 0,5:1 | Cells do not withstand stressful treatment |
| | | | | HFF | BbSpain-1 | 2:1 | Cells do not withstand stressful treatment |
| | | | | | TgME49 | 0,25:1 | Cells do not withstand stressful treatment |
| | | | | | TgSp3 | 0,5:1 | Cells do not withstand stressful treatment |
| | | | | PBAF | BbSpain-1 | 2:1 | Cells do not withstand stressful treatment |
| | | | | | TgME49 | 0,25:1 | Cells do not withstand stressful treatment |
| | | | | | TgSp3 | 0,5:1 | Cells do not withstand stressful treatment |

| Stress protocol | Time of application | Duration | Concentration | Cell lines | Parasite isolate | MOI | Bradyzoite conversion |
|---|---|---|---|---|---|---|---|
| Apicidin | 12 h p.i. | 15 days | 200 µM | MARC-145 | BbSpain-1 | 2:1 | Cells do not withstand stressful treatment |
| | | | | | TgME49 | 0,25:1 | Cells do not withstand stressful treatment |
| | | | | | TgSp3 | 0,5:1 | Cells do not withstand stressful treatment |
| | | | | Vero81 | BbSpain-1 | 2:1 | Cells do not withstand stressful treatment |
| | | | | | TgME49 | 0,25:1 | Cells do not withstand stressful treatment |
| | | | | | TgSp3 | 0,5:1 | Cells do not withstand stressful treatment |
| | | | | HFF | BbSpain-1 | 2:1 | Cells do not withstand stressful treatment |
| | | | | | TgME49 | 0,25:1 | Cells do not withstand stressful treatment |
| | | | | | TgSp3 | 0,5:1 | Cells do not withstand stressful treatment |
| | | | | PBAF | BbSpain-1 | 2:1 | Cells do not withstand stressful treatment |
| | | | | | TgME49 | 0,25:1 | Cells do not withstand stressful treatment |
| | | | | | TgSp3 | 0,5:1 | Cells do not withstand stressful treatment |

| Stress protocol | Time of application | Duration | Concentration | Cell lines | Parasite isolate | MOI | Bradyzoite conversion |
|---|---|---|---|---|---|---|---|
| FR235222 | 12 h p.i. | 15 days | 50 µM | MARC-145 | BbSpain-1 | 2:1 | No conversion observed |
| | | | | | TgME49 | 0,25:1 | Conversion observed (+DBA + α-TgBAG1) |
| | | | | | TgSp3 | 0,5:1 | Conversion observed (+DBA + α-TgBAG1) |
| | | | | Vero81 | BbSpain-1 | 2:1 | No conversion observed |
| | | | | | TgME49 | 0,25:1 | Conversion observed (+DBA + α-TgBAG1) |
| | | | | | TgSp3 | 0,5:1 | Conversion observed (+DBA + α-TgBAG1) |
| | | | | HFF | BbSpain-1 | 2:1 | Partial conversion observed (-DBA +α-TgBAG1) |
| | | | | | TgME49 | 0,25:1 | Conversion observed (+DBA + α-TgBAG1) |
| | | | | | TgSp3 | 0,5:1 | Conversion observed (+DBA + α-TgBAG1) |
| | | | | PBAF | BbSpain-1 | 2:1 | Cells do not withstand stressful treatment |
| | | | | | TgME49 | 0,25:1 | Cells do not withstand stressful treatment |
| | | | | | TgSp3 | 0,5:1 | Cells do not withstand stressful treatment |

| Stress protocol | Time of application | Duration | Concentration | Cell lines | Parasite isolate | MOI | Bradyzoite conversion |
|---|---|---|---|---|---|---|---|
| FR235222 | 12 h p.i. | 15 days | 100 µM | MARC-145 | BbSpain-1 | 2:1 | No conversion observed |
| | | | | | TgME49 | 0,25:1 | Conversion observed (+DBA + α-TgBAG1) |
| | | | | | TgSp3 | 0,5:1 | Conversion observed (+DBA + α-TgBAG1) |
| | | | | Vero81 | BbSpain-1 | 2:1 | No conversion observed |
| | | | | | TgME49 | 0,25:1 | Conversion observed (+DBA + α-TgBAG1) |
| | | | | | TgSp3 | 0,5:1 | Conversion observed (+DBA + α-TgBAG1) |
| | | | | HFF | BbSpain-1 | 2:1 | No conversion observed |
| | | | | | TgME49 | 0,25:1 | Conversion observed (+DBA + α-TgBAG1) |
| | | | | | TgSp3 | 0,5:1 | Conversion observed (+DBA + α-TgBAG1) |
| | | | | PBAF | BbSpain-1 | 2:1 | Cells do not withstand stressful treatment |
| | | | | | TgME49 | 0,25:1 | Cells do not withstand stressful treatment |
| | | | | | TgSp3 | 0,5:1 | Cells do not withstand stressful treatment |

| Stress protocol | Time of application | Duration | Concentration | Cell lines | Parasite isolate | MOI | Bradyzoite conversion |
|---|---|---|---|---|---|---|---|
| FR235222 | 12 h p.i. | 15 days | 150 µM | MARC-145 | BbSpain-1 | 2:1 | Cells do not withstand stressful treatment |
| | | | | | TgME49 | 0,25:1 | Cells do not withstand stressful treatment |
| | | | | | TgSp3 | 0,5:1 | Cells do not withstand stressful treatment |
| | | | | Vero81 | BbSpain-1 | 2:1 | Cells do not withstand stressful treatment |
| | | | | | TgME49 | 0,25:1 | Cells do not withstand stressful treatment |
| | | | | | TgSp3 | 0,5:1 | Cells do not withstand stressful treatment |
| | | | | HFF | BbSpain-1 | 2:1 | Cells do not withstand stressful treatment |
| | | | | | TgME49 | 0,25:1 | Cells do not withstand stressful treatment |
| | | | | | TgSp3 | 0,5:1 | Cells do not withstand stressful treatment |
| | | | | PBAF | BbSpain-1 | 2:1 | Cells do not withstand stressful treatment |
| | | | | | TgME49 | 0,25:1 | Cells do not withstand stressful treatment |
| | | | | | TgSp3 | 0,5:1 | Cells do not withstand stressful treatment |

| Stress protocol | Time of application | Duration | Concentration | Cell lines | Parasite isolate | MOI | Bradyzoite conversion |
|---|---|---|---|---|---|---|---|
| FR235222 | 12 h p.i. | 15 days | 200 µM | MARC-145 | BbSpain-1 | 2:1 | Cells do not withstand stressful treatment |
| | | | | | TgME49 | 0,25:1 | Cells do not withstand stressful treatment |
| | | | | | TgSp3 | 0,5:1 | Cells do not withstand stressful treatment |
| | | | | Vero81 | BbSpain-1 | 2:1 | Cells do not withstand stressful treatment |
| | | | | | TgME49 | 0,25:1 | Cells do not withstand stressful treatment |
| | | | | | TgSp3 | 0,5:1 | Cells do not withstand stressful treatment |
| | | | | HFF | BbSpain-1 | 2:1 | Cells do not withstand stressful treatment |
| | | | | | TgME49 | 0,25:1 | Cells do not withstand stressful treatment |
| | | | | | TgSp3 | 0,5:1 | Cells do not withstand stressful treatment |
| | | | | PBAF | BbSpain-1 | 2:1 | Cells do not withstand stressful treatment |
| | | | | | TgME49 | 0,25:1 | Cells do not withstand stressful treatment |
| | | | | | TgSp3 | 0,5:1 | Cells do not withstand stressful treatment |

| Stress protocol | Time of application | Duration | Concentration | Cell lines | Parasite isolate | MOI | Bradyzoite conversion |
|---|---|---|---|---|---|---|---|
| BKI1294 | At infection time | 3 days | 5 µM | MARC-145 | BbSpain-1 | 2:1 | No conversion observed |
| | | | | | TgME49 | 0,25:1 | Conversion observed (+DBA + α-TgBAG1) |
| | | | | | TgSp3 | 0,5:1 | Conversion observed (+DBA + α-TgBAG1) |
| | | | | Vero81 | BbSpain-1 | 2:1 | No conversion observed |
| | | | | | TgME49 | 0,25:1 | Conversion observed (+DBA + α-TgBAG1) |
| | | | | | TgSp3 | 0,5:1 | Conversion observed (+DBA + α-TgBAG1) |
| | | | | HFF | BbSpain-1 | 2:1 | No conversion observed |
| | | | | | TgME49 | 0,25:1 | Conversion observed (+DBA + α-TgBAG1) |
| | | | | | TgSp3 | 0,5:1 | Conversion observed (+DBA + α-TgBAG1) |
| | | | | PBAF | BbSpain-1 | 2:1 | Cells do not withstand stressful treatment |
| | | | | | TgME49 | 0,25:1 | Cells do not withstand stressful treatment |
| | | | | | TgSp3 | 0,5:1 | Cells do not withstand stressful treatment |
| | | 7 days | 5 µM | MARC-145 | BbSpain-1 | 2:1 | No conversion observed |
| | | | | | TgME49 | 0,25:1 | Conversion observed (+DBA + α-TgBAG1) |
| | | | | | TgSp3 | 0,5:1 | Conversion observed (+DBA + α-TgBAG1) |
| | | | | Vero81 | BbSpain-1 | 2:1 | No conversion observed |
| | | | | | TgME49 | 0,25:1 | Conversion observed (+DBA + α-TgBAG1) |
| | | | | | TgSp3 | 0,5:1 | Conversion observed (+DBA + α-TgBAG1) |
| | | | | HFF | BbSpain-1 | 2:1 | No conversion observed |
| | | | | | TgME49 | 0,25:1 | Conversion observed (+DBA + α-TgBAG1) |
| | | | | | TgSp3 | 0,5:1 | Conversion observed (+DBA + α-TgBAG1) |
| | | | | PBAF | BbSpain-1 | 2:1 | Cells do not withstand stressful treatment |
| | | | | | TgME49 | 0,25:1 | Cells do not withstand stressful treatment |
| | | | | | TgsP3 | 0,5:1 | Cells do not withstand stressful treatment |

# Chapter VI: Discussion

# Chapter VI: Discussion

In this Thesis, we have broadened our knowledge of host-pathogen interactions of *B. besnoiti* with target cells: macrophages, which are among the first cells to encounter the parasite during the acute phase; and fibroblasts, which are involved in the establishment of chronic infection in target tissues. To this end, we explored *B. besnoiti* modulation of both cell lines and identified relevant host and parasite enriched pathways and genes. We have also attempted to develop an *in vitro* protocol to induce the transformation of tachyzoites into bradyzoites, which is a parasite evasion mechanism that leads to parasite persistence and chronification of the infection that remains poorly understood in *B. besnoiti* compared to other apicomplexan parasites like *T. gondii*.

*Besnoitia besnoiti* can survive and proliferate in a specialized phagocytic immune cell, the primary bovine monocyte-derived macrophage. Moreover, live parasites can modulate macrophages in a specific manner. Several host-cell enriched pathways and parasite effectors were identified upon infection. *Besnoitia* parasites displayed a lytic cycle characterized by a high host cell invasion rate and morphological changes in invaded macrophages that differed from those induced by dead parasites (control of phagocytosis). An invasion rate higher than 50% was demonstrated at 36 h p.i., when only degraded dead tachyzoites were present in the control phagocytosis wells. Moreover, phagocytosis of *B. besnoiti* tachyzoites was completed at 12 h p.i., whereas active invasion progressively increased up to 36 h p.i. *Neospora caninum* showed a lower invasion rate at 36 h p.i. (García-Sanchez et al., 2019). Additional features showed that the *B. besnoiti* tachyzoite lytic cycle is slower than in the case of a virulent *Neospora* isolate: a higher dT is observed (15.13 h *vs* 13.15 h in *N. caninum*-infected macrophages), and egression continues at 72 h p.i. when it is already finished in macrophages infected with *N. caninum*. The asynchronous life cycle of *B. besnoiti* and delayed egression at 72 h p.i. were also observed in other primary bovine cells (BAEC and PBAF) (Jiménez-Meléndez et al., 2019) as well as in established cell lines (e.g. MARC-145 cells) (Frey et al., 2016). It has been hypothesized that this *in vitro* behaviour could be related to prolonged survival of extracellular *Besnoitia* tachyzoites to retain their

infectivity for extended periods of time, which might favour mechanical vector-borne transmission. Moreover, at 36 h p.i. onwards, macrophages infected with live parasites showed a round cell shape and lacked cytoplasmic extensions compared with macrophages that phagocytosed dead parasites. The latter were elongated and presented several cytoplasmic extensions that are directly related to their phagocytic activity (McWhorter et al., 2013). These findings were already described in dendritic and microglial cells infected with *T. gondii* tachyzoites (Bhandage and Barragan, 2019) and monocyte-derived macrophages infected with *T. gondii* and *N. caninum* tachyzoites *in vitro*. In fact, macrophages infected with *T. gondii* and *N. caninum* tachyzoites exhibited a hypermigratory phenotype characterized by a hypermotility state accompanied by these morphological changes in the host cell (rounded shape, absence of podosomes and loss of filopodia) that contributed to parasite dissemination (Weidner et al., 2013, García-Sánchez et al., 2019). A similar cell morphology score (rounded cells, absence of podosomes and presence of cell extensions, veils and ruffles) was observed in *B. besnoiti*-infected dendritic cells when compared with *N. caninum* and *T. gondii* infections (Pastor-Fernández et al., unpublished data) that could be compatible with a migratory phenotype. In this regard, further studies should attempt to obtain conclusive results in *B. besnoiti*-infected bovine macrophages.

The macrophage activation by live parasites shown by the morphological changes was also reflected at the transcriptomic level. The number of DEGs increased at 8 h p.i. and could reflect an intracellular environment more prone to favour parasite immune evasion and survival. This hypothesis is supported by a higher number of intracellular events present at 8 h p.i. The GO and KEGG terms showed that *B. besnoiti* infection predominantly modulates the apoptosis and MAPK pathways at 4 h p.i. *vs* the *Herpes simplex* virus 1 infection pathway at 8 h p.i., since these pathways were not enriched in macrophages that phagocytosed dead parasites when compared with non-infected cells. The transcriptional response induced by live parasites revealed features of programmed cell death at 4 h p.i. A wide variety of DEGs, including death receptors and apoptosis regulators from both intrinsic (*FAS*, *ERN1*, *ITPR1*, *Caspase 6*, *Tubulin-α*, Laminin *b1*) and extrinsic pathways (*ATF4*, *CHOP*, *Bcl-2*, Cathepsin Z, *NRAS*, *GADD45*) were upregulated. Moreover, prolonged ER stress activates the apoptotic pathway (Galluzi et al., 2016), and significant

upregulation of ER stress- and UPR-related genes was also observed (e.g. *IRE1α* and *ITPR1*). These results correlate with a significantly higher number of apoptotic cells visualized by IF at 8 h p.i. *vs* 4 h p.i. in macrophage cultures infected with live parasites. This asynchrony between transcriptomic and proteomic changes could be attributed to the fact that the regulation of transcription and translation contains a time-delayed component in eukaryote species (Maier et al., 2009, de Sousa Abreu et al., 2009, Wang et al., 2010). Remarkably, apoptotic cells were not infected by *B. besnoiti*, although apoptosis was likely induced by live parasites since these apoptotic cells were not present in non-infected macrophage control wells. Similar observations were reported in *T. gondii* infection, and it was hypothesized that the parasite might still protect the infected cell from apoptosis, while cell death is efficiently induced in non-infected cells (Mordue et al., 2001). Several studies have provided feasible explanations for how programmed cell death that is thought to promote efficient pathogen clearance can also contribute to parasite immune evasion (reviewed by Bosurgi and Rothlin, 2021). Indeed, apoptosis induction or inhibition by *Toxoplasma* is quite complex, and the mode of action is thought to be dependent on both parasite strain and host cell type. In this sense, a highly virulent type I *Toxoplasma* strain may induce apoptosis in lymphocytes and other immune cells, facilitating parasite immune evasion and virulence during the acute phase of infection (Gavrilescu et al., 2001), whereas type II strains can interfere with the host cell apoptosis machinery at different levels (Besteiro, 2015, Lima and Lodoen, 2019). The ability of *B. besnoiti* to prevent host cell apoptosis should also be considered, as it might facilitate parasite survival during the chronic phase of infection, similar to how other relevant tissue cyst-forming parasites act (Mammari et al., 2019, Rosenberg and Sibley, 2021). In this regard, transcriptional changes such as the downregulation of *Caspase-3*, an apoptosis executioner caspase, and the modulation of *Herpes simplex* virus 1 infection at 8 h p.i., together with the results obtained in the testicular parenchyma of naturally infected bulls, might serve as indicators.

*Herpes simplex* virus 1 infection was the only pathway regulated by live parasites at 8 h p.i., which agrees with previous reports in *T. gondii* infection (Bougdour et al., 2013, Wang et al., 2019). It is known that during *Herpes simplex* virus 1 infection, the main immune evasion mechanism consists of dampening of type-I interferon production and its downstream signalling pathway (Su et al., 2016, Danastas et al., 2020).

Several type-I ISG genes that participate in the immune response raised against *Herpes simplex* virus and are involved in apoptosis, were downregulated (*OAS2*, *IFIH1* and *cGAS*) (Melchjorsen et al., 2010, Pierog et al., 2017, Zheng et al., 2022).

The modulation of these relevant pathways by the parasite *in vivo* was supported by the downregulation of *CHOP* and *IFNα* in the testicular parenchyma of infected bulls that could favour parasite persistence and tissue cyst formation. Upon infection by pathogens, effector proteins in ER are activated and further involved in regulation of apoptosis, whereas knockdown of the *CHOP* gene has been related with a defect in the cellular stress response pathway which attenuates ER stress-induced apoptosis (Hu et al., 2019). Moreover, it is known that *T. gondii* effector TgIST blocks type-I IFN signalling to promote infection (Matta et al., 2019).

Finally, type-I metallothioneins (*MT1A, MT1E*), that were regulated in infected macrophages, have been demonstrated to be essential stress proteins in maintaining physiological balance and regulating immune homeostasis. In particular, *MT1A* is a relevant marker of chronic inflammation and a leukocyte chemotactic protein that is synthesized in response to acute phase cytokines (Dai et al., 2021). Despite the undoubted value of these tissue samples, the correlation of transcriptomic results obtained *in vitro* and *in vivo* is hampered, as it is influenced by the complexity of the tissue composition and the time points p.i. In fact, gene expression of cells may differ *in vitro* and *in vivo* (Nilsson et al., 2020), and this could be because functional dynamic genetic effects on gene regulation are specific to particular cell types, but also due to environmental conditions (Findley et al., 2021).

Additional parasite survival strategies should be considered and investigated in future studies. Herein, the classical proinflammatory activation characterized by the induction of a predominantly M1 phenotype was not triggered at early infection, which could prevent the macrophage immune response to infection. On the other hand, the lysosome pathway was modulated by both live and dead parasites. However, live parasites exhibited a different regulation pattern, which might be related to the parasite's ability to reside in a parasitophorous vacuole and avoid lysosomal

degradation. In addition, previous studies showed that the low virulence *N. caninum* isolate (NcSpain-1H) was able to regulate the lysosome pathway. However, none of the *N. caninum*-regulated genes, except for cathepsins, were regulated by *B. besnoiti*, which modulated other genes (García-Sánchez et al., 2020).

On the other hand, PBAFs were chosen as the *in vitro* model for this study due to their relevance as target cells for the parasite, as well as their intrinsic roles as immune modulators and pivotal contributors to fibrosis processes. It is noteworthy, however, that transcriptomic profiles may exhibit variability across fibroblasts of different origins. Fibroblasts represent a heterogenous cell population with diverse functional capacities, as exemplified by studies focused on skin-derived fibroblasts (Jelaska et al., 2000; Jiang et al., 2022). Nonetheless, our *in vitro* model holds promise as a valuable tool for studying fibrosis in the context of *B. besnoiti* infection, supported by the upregulation of classic fibrotic markers such as *TGFβ1*, *FNDC3A* and *COL7A1*. Under physiological conditions, myofibroblasts are relatively rare. However, following infection and injury, fibroblasts typically undergo a transformation into myofibroblasts, serving as key drivers in the wound-healing process (Coehlo et al., 2018). In our study, the upregulation of *TGFβ1*, *VEGFs* and *NOTCH1*, all known promoters of this fibroblast-to-myofibroblast transformation, was observed.

However, it is worth noting that the full transition to a myofibroblast phenotype generally involves the expression of alpha-smooth muscle actin (α-SMA) (Sousa et al., 2006), which was not differentially expressed in *B. besnoiti*-infected fibroblasts. Therefore, it is possible that the observed changes represent an early step in myofibroblast transformation. The differential expression analysis revealed a notably higher number of DEGs in FI-Bb *vs* FI at 12 h p.i. compared to 32 h p.i., suggesting an intensive early cellular reaction to the pathogen during invasion. However, the common core set of genes regulated at both time points showed initial steps of fibrosis, also observed at the host–tumor interface, evidenced by several enriched cancer-related pathways such as angiogenesis, apoptosis inhibition, cell proliferation and migration, which in turn related to innate immunity required for control and clearance of invading pathogens (Osherov et al., 2016; Mammari et al., 2019). In addition, the MAPK pathway was upregulated at both times p.i., which is significant in relation to fibrosis, as it governs

well-preserved cascades regulating cell proliferation, immune response and inflammation (Liu et al., 2007).

Three phases are often presented sequentially during the fibrotic process: inflammation, proliferation and maturation (Murtha et al., 2017). Our transcriptomics findings suggest a gradual regulation of the fibrotic process. At 12 h p.i., pathways associated with the inflammatory response were enriched (e.g., "Cytokine–cytokine receptor interaction" "TNF signalling pathway" "AGE–RAGE signalling pathway"). Inflammation might facilitate the recruitment of immune cells, driven by the action of cytokines (Kany et al., 2019). Nevertheless, inflammation could act as a double-edged sword; while it could effectively help to eliminate the invading parasite, prolonged activation could lead to tissue damage and, ultimately, fibrosis. Additionally, the upregulation of the "AGE–RAGE signalling pathway" could be contributing to this process by inducing oxidative stress and inflammation (Corica et al., 2019).

With parasite replication at 32 h p.i., the transcriptomic response evolves towards cell proliferation and ECM remodelling. The "PI3K–AKT signalling pathway" is well-known for its role in promoting cell survival and growth (Zhang et al., 2000; Wang et al., 2022). The process of tissue repair relies on fibroblasts' ability to anchor themselves to ECM, which in turn leads to cell migration and ECM contraction. In fact, upregulation of adhesion signalling pathways is a key phenotypic hallmark of fibrotic cells (Kennedy et al., 2008). While adhesion serves as a central feature of the proliferation phase, its significance perseveres and even amplifies as the fibrotic process advances into the maturation phase, since cell adhesion molecules are involved in binding to the extracellular matrix (Wight et al., 2011; Zhao et al., 2022). Moreover, the upregulation of the "Malaria" pathway, and more specifically, the HGF–MET signalling axis within this pathway, might promote a favourable environment for parasite infection by the inhibition of cell apoptosis (Leirião et al., 2005). Additionally, previous investigations have elucidated the role of the HGF–MET signalling pathway in inducing a hypermigratory phenotype in dendritic cells infected with *T. gondii* (Ólafsson et al., 2020).

All these findings led us to identify potential fibrosis markers that displayed upregulation exclusively at 12 h p.i. (*FNDC3A*, *COL7A1*, *MMP9*) (Piccinini et al., 2014; Walton et al., 2017), at 32 h p.i. (*TGFβR2*, *COL13A1*, *MMP16*) (Biernacka et al., 2011; Zheng et al., 2023) or at both time points (*PLAUR*, *TGFβ1*, *TGFβ3*) (Shmakova et al., 2023; Kim et al., 2018; Guo et al., 2020). Among a set of selected and highly regulated DEGs involved in the different stages of the fibrotic process, *PLAUR*, *TGFβ1* and *FOSB* evidenced their potential as relevant biomarkers of disease progression in the scrotal skin of naturally infected bulls. *PLAUR* is involved in fibroblast-to-myofibroblast differentiation and fibrosis (Bernstein et al., 2007; Schuliga et al., 2017) and was upregulated in both acutely and chronically infected bulls. *TGFβ1* is intricately linked to the pathogenesis of fibrosis (Maroni et al., 2012) and has been correlated with the activation of MAPK activity in fibroblasts during the fibrosis progression (McKenzie et al., 2015). Herein, chronically infected bulls exhibited upregulation of *TGFβ1*, and the MAPK pathway was upregulated at both time points. In contrast, *FOSB* expression did not correlate between the *in vitro* and *in vivo* assays. *FOSB* was downregulated in the scrotal skin of chronically infected bulls but was upregulated *in vitro* at both times p.i. Downregulated expression of *FOSB* has been associated with cell migration (metastasis) and advanced tumorigenic stages (Tan et al., 2016) whereas its upregulation is associated with regulation of ECM production. Consequently, tissue complexity and infection timing likely contributed to differences between the *in vitro* and *in vivo* models and to the variability observed in the mRNA expression levels in the chronically infected group.

It is not surprising that the KEGG pathway "Pathways in cancer" was significantly enriched at both time points analysed, as many of its components are involved in fibrosis-related mechanisms, which are also activated during *B. besnoiti* infection. Cancer-associated fibrosis is a hallmark of the tumour microenvironment and is closely linked to disease progression and prognosis (Piersma et al., 2020). This fibrotic process is characterized by ECM deposition, extensive tissue remodelling, and angiogenesis, features that were also observed in fibroblasts infected by *B. besnoiti*. In this context, it is particularly relevant that the pro-angiogenic gene *VEGFA* was consistently upregulated at both 12 and 32 h p.i., indicating the promotion of angiogenic and fibrotic programs. *VEGFA* is a central regulator of angiogenesis and mediates its

effects primarily through the activation of downstream signalling cascades such as the RAS/MAPK (ERK) pathway, which governs cell proliferation and the PI3K–AKT pathway, which promotes cell survival and metabolic adaptation. Both pathways were significantly enriched in our transcriptomic data, supporting their involvement in the host response to infection. Importantly, previous functional *in vitro* studies have shown that inhibition of ERK signalling at 12 h p.i. using specific inhibitors can reduce endothelial sprouting by suppressing VEGFA expression, highlighting the key role of this axis in modulating the angiogenic response (Bellou et al., 2009). Furthermore, it has been reported that VEGF can autoregulate the MAPK signalling network through feedback mechanisms involving MAPK phosphatases such as *DUSP5* and *DUSP6*, which limit ERK1/2 and p38 activation. Notably, both *DUSP5* and *DUSP6* were found to be significantly upregulated in infected fibroblasts at 12 h p.i., suggesting the activation of a compensatory negative feedback loop aimed at modulating the intensity and duration of MAPK signalling during early infection stages. These findings collectively suggest that *B. besnoiti* actively engages host fibrotic and angiogenic pathways, co-opting signalling networks typically associated with tumour biology and chronic tissue remodelling to establish a microenvironment favourable to its persistence. The parallel with cancer-associated fibrosis reinforces the hypothesis that chronic *B. besnoiti* infection may lead to long-term alterations in fibroblast function and tissue architecture.

Comparable transcriptomic studies conducted on other primary bovine cell types targeted by *B. besnoiti*, specifically BAEC and monocyte-derived macrophages, have revealed overlapping patterns of gene regulation and pathway enrichment, particularly in relation to immune activation and fibrotic responses. Among the shared fibrotic mechanisms, upregulation of the *TGFβ* signalling pathway was consistently observed across all cell types. This pathway is a well-known mediator of fibrosis and tissue remodelling, reinforcing the notion that *B. besnoiti* infection elicits a pro-fibrotic cellular environment regardless of the host cell lineage. The antiviral immune response was also a prominent shared feature, with several DEGs implicated in this defence mechanism, including *OAS1Z, IFI44, PIM, IL7R*, and *CISH*, as well as the JAK–STAT signalling pathway. While *OAS1Z* and *IFI44* are classically associated with viral infections (contributing to interferon-mediated antiviral responses (Pasieka et al., 2006; Sánchez et al., 2007)), their induction has also been documented in response to protozoan

parasites such as *T. gondii*, *N. caninum*, and *Trypanosoma cruzi* (Carneiro et al., 2016; Pierog et al., 2018; Menard et al., 2021). This indicates that ISGs may play a broader role in host defence, extending to apicomplexan infections like *B. besnoiti*.

The JAK–STAT pathway, which mediates the expression of numerous ISGs, is central to innate antiviral immunity and is similarly activated in response to apicomplexans such as *T. gondii* (Schneider et al., 2013) and *N. caninum* (Fereig et al., 2020). In line with this, a recent study demonstrated the activation of ISGs during *B. besnoiti* infection in bovine macrophages, underscoring the parasite's capacity to engage classical interferon responses (Fernández-Álvarez et al., 2023). These findings point to a conserved immune strategy by the host involving IFN-inducible genes and JAK–STAT signalling as a first line of defence, even in non-viral contexts.

Genes associated with programmed cell death were also found to be regulated in all three cell types. This may represent a strategy exploited by the parasite to modulate host cell fate, enhancing its intracellular survival, an effect well-documented in other apicomplexans such as *T. gondii* (Besteiro et al., 2015). Consistent with this, apoptosis was identified as a major regulated pathway during the early stages of *B. besnoiti* infection in primary bovine macrophages (Fereig et al., 2020), suggesting that *B. besnoiti* may similarly manipulate host cell death pathways for its benefit.

Furthermore, a set of commonly regulated adhesion molecules was identified, highlighting their crucial role in host defence. These molecules are involved not only in pathogen recognition and internalization but also in cytoskeletal reorganization and the modulation of intracellular signalling cascades that influence gene expression and cellular phenotype (Hauck et al., 2006; Harjunpää et al., 2019). Their upregulation across different cell types suggests a conserved host response aimed at coordinating immune surveillance and cellular adaptation to infection.

The transcriptome of *B. besnoiti* revealed two distinct host cell-specific gene expression programs during early infection, reflecting the parasite's differential adaptation to primary bovine monocyte-derived macrophages and PBAF. While infection in macrophages led to the identification of 538 DEGs between 4 and 8 h p.i., of which

537 were upregulated, no DEGs were found between 12 and 32 h p.i. in fibroblasts. However, a broad set of invasion-related genes and parasite effectors were detected in fibroblasts, despite the absence of statistically significant transcriptional changes in that timeframe. The discrepancy in DEGs detection between the two host cell types likely reflects fundamental differences in the intracellular environments they offer. Macrophages are professional phagocytes equipped with antimicrobial defences (Stafford et al., 2002). In response, *B. besnoiti* appears to undergo a rapid and robust transcriptional reprogramming upon entry into macrophages, upregulating invasion-related and metabolic genes necessary for intracellular establishment and immune evasion. The high number of DEGs observed at 8 h p.i. in macrophages (vs. 4 h p.i.) likely captures this acute adaptation phase. In contrast, fibroblasts constitute a non-phagocytic and immunologically less reactive environment. The absence of DEGs between 12 and 32 h p.i. may reflect that *B. besnoiti* rapidly establishes a stable intracellular niche in this cell type, maintaining a constitutive expression of core effector genes without the need for major transcriptional reprogramming during this phase. Our results partially agree with a previous study that reported a similar expression profile displayed by *B. besnoiti* tachyzoites in BAEC at the same time points analyzed (Jimenez-Melendez et al., 2020). Indeed, *B. besnoiti* tachyzoites showed a similar lytic cycle in both cell types (BAEC and fibroblasts) characterized by 50% of invasion events between 4 and 8 hpi, and an exponential growth from 12 h p.i. onwards, with a significant increase in the number of tachyzoites per well from 24 h p.i. onwards (Jiménez-Melendez et al., 2019). The main difference between both works was that 105 DEGs were identified in BAEC when the two infection time points were compared, most of them upregulated at 32 h p.i. (Jiménez-Melendez et al., 2020). This difference could be explained by an earlier parasite proliferation in fibroblasts in the present study at 12 h p.i. that should not differ in the transcription machinery of the parasite when compared at 32 h p.i. when at least two rounds of parasite replication have been completed.

Among the most prominent DEGs identified in macrophages were transcripts encoding ROPs and RONs, in line with their pivotal roles in apicomplexan invasion and host cell modulation (Hakimi and Bougdour, 2015). Notably, a conserved subset of rhoptry genes was expressed in both macrophages and fibroblasts, including ROP6, ROP11, ROP12, ROP14, ROP15, ROP17, ROP18, ROP23, ROP26, ROP31,

ROP32, ROP37, ROP40, as well as RON1 through RON10. The presence of these shared transcripts suggests the existence of a core invasion module that facilitates effective host cell entry and early intracellular establishment, irrespective of the host cell type. However, fibroblasts exhibited a broader rhoptry gene repertoire, expressing additional ROPs not detected in macrophages, such as ROP4, ROP5, ROP9, ROP10, ROP20, ROP35 and ROP39. Some of these genes, notably ROP5, encode well-characterized virulence factors in *T. gondii* that contribute to immune evasion by interfering with host defence mechanisms (Reese et al., 2011). Importantly, several of these rhoptry proteins have been implicated in the transcriptional reprogramming of host cells. In particular, ROP18 represents a compelling candidate, as its orthologue in *T. gondii* has been shown to inhibit type I interferon production via direct interaction with the cytosolic DNA sensor cGAS (Melo et al., 2013; Wang et al., 2019; Chen et al., 2022). Given the evidence that *B. besnoiti* also modulates the cGAS-STING pathway (Fernández-Álvarez et al., 2023), the potential role of ROP18 and other rhoptry effectors in shaping the host cell transcriptome needs further investigation.

Another relevant finding is the major role that SAG-related proteins may have in the lytic cycle of the parasite. In macrophages, only one surface antigen (SRS49D) was identified as we only focused on DEGs. However, when we looked for transcripts particularly in *B. besnoiti* tachyzoites infecting PBAF over 80 SAG-related sequences were found, including named isoforms SRS48K, SRS53B and SRS53F. These antigens are expected to contribute to parasite adhesion, vacuole integrity and immune evasion during longer intracellular residency and could have a redundant role. Similar findings have been reported in bradyzoites of *T. gondii*, where surface antigens are upregulated during cyst formation and persistence (Buchholz et al., 2013). The broad SRS expression supports the hypothesis that *B. besnoiti* adopts remodelling strategies, possibly influenced by the immunological permissiveness of the target tissue environment.

Interestingly, metabolic genes were among the most upregulated DEGs in macrophages. Upregulated pathways included valine, leucine, isoleucine and arginine metabolism, as well as pantothenic acid and Coenzyme A biosynthesis and nitrogen metabolism. These essential amino acids and cofactors are known to be acquired from the host in *T. gondii* and *Plasmodium* (Krishnan et al., 2021; Lunghi et al., 2022), reflecting

the auxotrophic nature of apicomplexans. The strong induction of these genes in macrophages likely reflects a metabolic stress response, as the parasite faces a hostile, nutrient-restrictive environment requiring rapid resource acquisition and biosynthesis.

The only gene downregulated in macrophages at 8 h p.i. was BESB_064630, encoding a PAN/Apple domain-containing protein, which may be involved in early parasite adhesion and interspecies molecular interactions (Gong et al., 2012). Its early expression at 4 h p.i. followed by downregulation suggests a role during host cell recognition and entry.

Our findings align with those of Ramakrishnan et al. (2022), who characterized stage-specific expression profiles in *B. besnoiti* tachyzoites and bradyzoites. The consistent detection of multiple ROPs, RONs and SRSs across studies points to highly conserved virulence modules, while the additional cell-type-specific effectors described here further refine our understanding of *B. besnoiti*'s host adaptation strategy. The combined data suggest that *B. besnoiti* utilizes a modular, plastic transcriptional program, rapidly adjusting its effector expression depending on the host cell type to balance invasion, immune evasion and metabolic needs. These insights highlight candidate targets for chemotherapeutic intervention, biomarker discovery and stage-specific diagnostics.

Building upon the transcriptomic parasite insights gained in this study, we next aimed to functionally explore the conditions that may promote stage conversion in *B. besnoiti in vitro*. Understanding the molecular and cellular mechanisms that regulate bradyzoite differentiation and cyst formation in this species remains one of the major challenges in the field. To address this, we attempted to develop a reliable induction protocol, guided by established conversion strategies in *T. gondii* and *N. caninum*.

For the first time, a systematic screening of a broad panel of stage-specific antibodies directed against *T. gondii*, *N. caninum* and *B. besnoiti* has been conducted. Notably, α-TgBAG1 was the only antibody that exhibited both high sensitivity and specificity for bradyzoites across all detection methods (IHC, WB and IF). While other candidates such as α-NcSRS9 and α-NcSAG4 showed acceptable performance in

IHC and WB, their cross-reactivity and limited specificity in IF compromised their utility as reliable stage-specific markers. Additionally, polyclonal antisera, despite demonstrating strong overall reactivity, failed to provide stage-selective discrimination due to their broad epitope recognition profile. This result highlights the deep evolutionary conservation of BAG1 as a molecular signature of stress-induced bradyzoite differentiation in Apicomplexan parasites. This finding aligns with previous research in *T. gondii*, where BAG1 is a well-established bradyzoite marker, upregulated under stress and associated with mitochondrial protection and latency maintenance (Bohne et al., 1995; Cleary et al., 2002). A similar expression pattern has been described in *N. caninum* (Weiss, 1999), although cyst wall formation occurs less readily than in *T. gondii*. In *B. besnoiti*, Dubey et al. (2013) confirmed that all intracystic bradyzoites were BAG1-positive, despite notable morphological heterogeneity and variable PAS staining of mylopectin granules. Altogether, these findings validate BAG1 as a robust and conserved marker of the chronic stage across closely related coccidian parasites.

In contrast, the role of *SAG4* and *SRS9* as bradyzoite markers remains more ambiguous. Although both antigens have been proposed as indicators of the chronic stage in *T. gondii* and *N. caninum*, particularly in relation to cyst wall formation and immune evasion (Risco-Castillo et al., 2004), our data in *B. besnoiti* are inconclusive. Their non-specific reactivity in IF, detected in both tachyzoites and bradyzoites, suggests a potential association with chronic infection, but the lack of consistent stage-specific expression limits their current stage specific marker value. Nevertheless, these antigens should not be ruled out. Their partial performance in WB and IHC points to a possible involvement in bradyzoite biology that should be further investigated.

Importantly, the interpretation of such markers must also be considered in light of the cellular environment in which differentiation occurs. Indeed, the choice of host cell line emerged as a key factor influencing the success of *B. besnoiti* stage conversion *in vitro*. HFFs provided a stable, contact-inhibited monolayer that supported prolonged stress exposure, an essential condition for enabling the full conversion of tachyzoites into bradyzoites and subsequent cyst formation. In contrast, MARC-145 and Vero81 cells exhibited rapid proliferative overgrowth, limiting culture duration and compromising the application of sustained stress protocols. PBAF, although initially

promising, due to their relevance as a primary bovine target cell, proved highly stress-sensitive and consistently detached from the culture surface even under mild treatment conditions, thus precluding their use in extended differentiation protocols. Maintaining the parasite under culture conditions for prolonged periods is particularly relevant, as extended exposure times have been shown to enhance bradyzoite differentiation efficiency. For instance, Risco-Castillo et al. (2008) demonstrated that optimal stage conversion of *N. caninum* in MARC-145 cells occurred at 7 days p.i. following treatment with 70 µM SNP. Similarly, in *Hammondia heydorni*, Gondim et al. (2015) successfully established a long-term *in vitro* protocol using a finite primary cell line derived from embryonic bovine heart (KH-R), which allowed maintenance of the parasite for up to 4.5 months. In this model, bradyzoites were first detected at 7 days p.i. using stage-specific antibodies (α-BAG1 and mAbCC2), and by 18 to 21 days p.i., most parasites were organized into mature tissue cysts that reached up to 135 µm in length. These findings underscore the importance of developing robust and stable host cell systems capable of sustaining long-term infections, as they are instrumental in facilitating full stage conversion and promoting cyst maturation under controlled *in vitro* conditions.

Among the panel of stressors tested, only three protocols showed partial success in inducing bradyzoite-like features in HFF infected with *B. besnoiti* tachyzoites: treatment with 70 µM SNP for 7 days, and treatment with 50 µM apicidin or FR235222 for 15 days. These compounds act through distinct stress pathways. SNP is a nitric oxide (NO) donor that mimics the oxidative and nitrosative stress generated by activated macrophages during infection. In *T. gondii*, exposure to NO donors promotes bradyzoite conversion by triggering redox-sensitive signalling cascades and metabolic reprogramming (Bohne et al., 1994; Tomavo and Boothroyd, 1995). Although the precise sensing mechanism in *B. besnoiti* remains unclear, the modest response to SNP suggests some degree of evolutionary conservation in stress recognition. On the other hand, apicidin and FR235222 are HDACi that interfere with chromatin remodelling by inhibiting class I and II HDACs. In *T. gondii*, HDAC inhibition has a dramatic effect on tachyzoite growth and induces tachyzoite-to-bradyzoite conversion *in vitro* (Maubon et al., 2010; Bougdour et al., 2009). FR235222 selectively inhibits TgHDAC3, which is essential for tachyzoite proliferation and repression of differentiation (Vanagas et al., 2012). In *B. besnoiti*, the phenotypic response to these treatments was modest.

Immunofluorescence-BAG1-positive vacuoles were observed at low frequencies, ~2% following SNP treatment and slightly higher rates with apicidin (~3.5%) and FR235222 (~3%). Notably, none of these vacuoles exhibited positive staining with DBA. This observation raises doubts about the suitability of DBA as a marker for *B. besnoiti* cyst walls. While DBA is widely used to detect *T. gondii* cysts due to its specific affinity for N-acetyl-D-galactosamine residues in the glycoprotein-rich cyst wall matrix (Weiss and Kim, 2000; Ferguson and Hutchison, 1987), its applicability in *B. besnoiti* remains unproven. *Toxoplasma gondii* expresses CST1, a mucin-domain glycoprotein essential for cyst wall integrity and DBA binding. Although *B. besnoiti* encodes an orthologue of CST1 (BESB_048010), which is highly upregulated in tissue cysts (>240-fold), its predicted protein structure lacks a canonical signal peptide and mucin domain, key features required for O-glycosylation and DBA reactivity. To date, there is no experimental confirmation that BESB_048010 binds DBA or participates in cyst wall assembly (Ramakrishnan et al., 2022). The absence of a validated *in vitro* model for mature cyst formation in *B. besnoiti* further limits the functional characterization of this candidate. These findings contrast sharply with those from other apicomplexans. In *N. caninum*, SNP treatment induces up to 96% BAG1-positive vacuoles and 21% containing exclusively bradyzoites, with well-defined cyst walls (Risco-Castillo et al., 2008). Similarly, in *T. gondii*, HDACi such as apicidin or FR235222 can achieve conversion rates of 80–90% under defined *in vitro* conditions (Maubon et al., 2010; Hakimi and Bougdour, 2015). These comparisons highlight the markedly lower developmental plasticity of *B. besnoiti* under conventional stress protocols and suggest that it may depend on distinct or more complex cues to complete the conversion process. In *T. gondii*, BAG1 expression frequently coincides with DBA-positive cyst walls, as observed here in both type II (TgME49) and atypical (TgSp3) strains. These strains exhibited robust and consistent conversion in response to all tested stressors, with BAG1-positive vacuoles ranging from 40% to 75%, aligning with prior studies (Soête et al., 1994; Weiss et al., 1995; Dzierszinski et al., 2004; Sullivan and Jeffers, 2012; Radke et al., 2013). The stark contrast in conversion efficiency between *B. besnoiti* and *T. gondii* underscores fundamental biological differences in their regulation of stage conversion. Several factors may explain this divergence:

- Longer induction times may be necessary: whereas *T. gondii* typically initiates bradyzoite conversion within 3–5 days of stress exposure (Dzierszinski et al., 2004), *B. besnoiti* cystogenesis *in vivo* follows a more protracted timeline. Tissue

cysts become evident in cattle 15 to 26 days post-infection, primarily in dermal and endothelial tissues (Álvarez-García et al., 2014b). Therefore, *in vitro* models may require extended culture durations (beyond 15 days) to allow for full differentiation.

- Conversion may be host- or tissue-specific: *T. gondii* can differentiate in various host cell types including neurons, muscle cells and fibroblasts (Weiss et al., 1995; Ferreira da Silva et al., 2009). In contrast, *B. besnoiti* exhibits a narrower tropism and may require specific host cell environments, such as bovine dermal fibroblasts or endothelial cells, to support full bradyzoite maturation.
- Limited response to canonical stressors: in *T. gondii*, environmental stressors such as alkaline pH and heat shock activate AP2 transcription factors and epigenetic modifiers that drive the bradyzoite gene program (Radke et al., 2013; Waldman et al., 2020). *Besnoitia besnoiti* may lack homologous stress sensors or require alternative cues, such as metabolic or immune-derived signals, to trigger conversion. Cytokines like IFN-γ have been shown to modulate cystogenesis in other apicomplexans (Ferreira da Silva et al., 2009), and emerging transcriptomic data in *B. besnoiti* suggests a role for type I interferon signalling during chronic infection stages (Ramakrishnan et al., 2022).
- Epigenetic regulation may differ although partial responses to apicidin and FR235222 indicate a degree of epigenetic sensitivity, the overall low conversion rates suggest that *B. besnoiti* may possess repressive chromatin landscapes or lack critical transcriptional activators needed to fully enact the bradyzoite gene expression program (Bougdour et al., 2009; Sullivan and Jeffers., 2012).

Collectively, these findings underscore the limitations of extrapolating *T. gondii* differentiation protocols to *B. besnoiti* and emphasize the need for tailored approaches based on its unique biology and host interactions. Future studies should prioritize: testing longer induction periods, especially in dermal or endothelial cell lines; evaluating combinatorial stress protocols, such as HDAC inhibition combined with oxidative or immune stress; incorporating cytokine treatments, including IFN-α or IFN-β, to mimic host immune environments; advancing model systems through dual RNA-Seq, 3D co-culture models, or organ-on-chip platforms to better recapitulate *in vivo* conditions.

However, this approach has led to the identification of HDACi as novel therapeutic tools since these compounds suppressed the tachyzoite growth *in vitro* as in *T. gondii* (Boissavy et al., 2023), where these enzymes are key for the tachyzoite survival. Accordingly, the enzymes regulating histone acetylation could be potent therapeutic targets for the treatment of besnoitiosis that deserves further research.

# Chapter VII: Conclusions

# Chapter VII: Conclusions

## Objective 1: Study of host cell-dependent factors involved in the parasite-host cell interaction

1st. Primary bovine monocyte-derived macrophages and aorta-derived fibroblasts represent robust and biologically relevant *in vitro* models for studying early host–parasite interactions during *B. besnoiti* infection. The parasite efficiently invades and replicates within both cell types, triggering distinct host cell responses. Infection with live tachyzoites induced clear transcriptomic reprogramming, underscoring the utility of these primary models for dissecting the molecular pathways involved in parasite entry, immune activation and early intracellular adaptation.

2nd. During early invasion of primary bovine macrophages, *B. besnoiti* induces a transcriptional response characterized by activation of MAPK signalling and apoptotic pathways, indicating active modulation of host cell stress and survival mechanisms. At later time points, the enrichment of the *Herpes simplex* virus 1 infection pathway—associated with inhibition of type I interferon responses—suggests that the parasite mimics viral immune evasion strategies to subvert host defences. These findings underscore *B. besnoiti*'s capacity to reprogram macrophage responses, enhancing its ability to evade immune detection and persist intracellularly.

3rd. In *B. besnoiti*-infected fibroblasts, transcriptomic analysis revealed a temporal shift from early inflammatory signalling to pathways associated with fibrosis and cell survival. The initial regulation of cytokine–cytokine receptor interaction, TNF signalling and AGE–RAGE pathways indicates an early innate immune response to infection. Over time, the upregulation of PI3K–AKT and the HGF–MET axis—components of the Malaria pathway—suggests that the parasite promotes host cell survival and inhibits apoptosis. This pattern contrasts sharply with the pro-apoptotic response observed in infected macrophages and supports the notion that *B. besnoiti* manipulates fibroblasts to establish a permissive, fibrotic microenvironment conducive to long-term persistence.

4th. MAPK signalling emerged as a key regulatory axis in *B. besnoiti* infection, activated in both primary bovine macrophages and fibroblasts. Its role as a central mediator of cellular stress, inflammation and survival allows the parasite to fine-tune host responses according to cell type. In macrophages, MAPK activation might contribute to pro-apoptotic outcomes. In contrast, in fibroblasts, the same pathway might support cell survival and tissue remodelling, facilitating fibrosis and long-term parasite

persistence. This capacity to modulate a shared pathway toward distinct cellular outcomes highlights a sophisticated mechanism of host adaptation.

5th. The transcriptomic analysis identified a subset of differentially expressed genes—*CHOP, IFNα, MT1A, MT1E, PLAUR, FGF1, TGFβ1* and *FOSB*—that were also modulated in the testicular parenchyma and scrotal skin of naturally infected bulls. Their consistent regulation across both *in vitro* and *in vivo* settings highlights their potential role as biomarkers. These genes may serve as valuable indicators for monitoring disease progression, guiding diagnostic development and assessing therapeutic strategies in bovine besnoitiosis.

**Objective 2: Study of parasite-dependent factors involved in the parasite-host cell interaction.**

6th. The transcriptomic profile of *B. besnoiti* tachyzoites in primary bovine macrophages between 4 and 8 h p.i. is characterized by the upregulation of genes involved in host cell invasion (e.g., ROP and RON families) and metabolic adaptation (including pathways for amino acid biosynthesis and energy metabolism) coinciding with the first steps of the parasite lytic cycle. In contrast, in aorta-derived fibroblasts, the absence of significant differential gene expression between 12 and 32 h p.i. may reflect that *B. besnoiti* establishes a stable intracellular niche without the need for a rapid transcriptional reprogramming at this stage of the lytic cycle.

7th. To date, anti-TgBAG1 remains the most specific and reliable marker currently available for identifying *B. besnoiti* bradyzoites, consistently detected by means of IHC, WB and IF assays. Further characterization of anti-NcBSR9 and anti-NcSAG4 should be done under optimized bradyzoite differentiation conditions to clarify their potential value as *B. besnoiti* bradyzoite markers.

8th. Sodium nitroprusside (SNP) and HDAC inhibitors partially triggered the switch of *B. besnoiti* tachyzoites into bradyzoites, as shown by the low number of BAG1 positive vacuoles. These results represent a meaningful step toward establishing an *in vitro* model for stage conversion and the results suggest a regulatory role for histone acetylation in stage differentiation. However, *B. besnoiti* may require alternative or more complex stimuli to achieve full bradyzoite development compared to *T. gondii*. Future studies should explore induction strategies targeting type I interferon signalling and MAPK-related pathways and should prioritize the use of primary bovine cells with enhanced stress tolerance to better mimic *in vivo* conditions.

9th. The suppression of *B. besnoiti* tachyzoite growth by HDAC inhibitors underscores their potential as therapeutic tools against bovine besnoitiosis. This finding warrants further investigation into their safety and efficacy in both *in vitro* and *in vivo* models.

# Capítulo IV: Conclusiones

## Objetivo 1: Estudio de los factores dependientes del hospedador implicados en la interacción parásito-célula hospedadora

1ª. Los macrófagos derivados de monocitos y los fibroblastos derivados de aorta primarios bovinos representan modelos *in vitro* robustos y biológicamente relevantes para el estudio de las interacciones tempranas entre el hospedador y *B. besnoiti*. El parásito invade y se replica de manera eficiente en ambos tipos celulares, desencadenando respuestas celulares diferenciadas. La infección con taquizoítos viables indujo una clara reprogramación transcriptómica, resaltando el valor de estos modelos primarios para elucidar las vías moleculares implicadas en la entrada del parásito, la activación inmunitaria y la adaptación intracelular en las fases iniciales de la infección.

2ª. Durante la fase inicial de invasión en macrófagos bovinos primarios, *B. besnoiti* induce una respuesta transcriptómica caracterizada por la activación de las vías de señalización MAPK y de apoptosis, lo que indica una modulación activa de los mecanismos celulares de estrés y supervivencia del hospedador. En fases posteriores, el enriquecimiento de la ruta de infección por el virus *Herpes simplex* tipo 1—relacionada con la inhibición de la respuesta de interferón tipo I—sugiere que el parásito imita estrategias virales de evasión inmunitaria para subvertir las defensas del hospedador. Estos hallazgos ponen de relieve la capacidad de *B. besnoiti* para reprogramar las respuestas de los macrófagos, favoreciendo su evasión del sistema inmunitario y su persistencia intracelular.

3ª. En fibroblastos infectados por *B. besnoiti*, el análisis transcriptómico reveló un cambio temporal desde una señalización inflamatoria temprana hacia rutas asociadas con la fibrosis y la supervivencia celular. La regulación inicial de las vías de interacción citoquina–receptor de citoquina, señalización por TNF y AGE–RAGE indica una respuesta inmunitaria innata temprana frente a la infección. Con el tiempo, la sobreexpresión de las rutas PI3K–AKT y del eje HGF–MET—componentes de la vía de señalización relacionada con la malaria—sugiere que el parásito favorece la supervivencia de la célula hospedadora e inhibe la apoptosis. Este patrón contrasta marcadamente con la respuesta proapoptótica observada en macrófagos infectados y respalda la hipótesis de que *B. besnoiti* manipula a los fibroblastos para establecer un microambiente permisivo y fibrótico que favorece su persistencia a largo plazo.

4ª. La ruta de señalización MAPK emergió como un eje regulador clave durante la infección por *B. besnoiti*, activado tanto en macrófagos como en fibroblastos

bovinos primarios. Su función como mediador central del estrés celular, la inflamación y la supervivencia permite al parásito ajustar las respuestas del hospedador en función del tipo celular. En macrófagos, la activación de MAPK podría favorecer la apoptosis, mientras que en los fibroblastos la misma vía podría favorecer la supervivencia celular y la remodelación tisular, facilitando la fibrosis y la persistencia del parásito a largo plazo. Esta capacidad para modular una vía común hacia respuestas celulares divergentes refleja un sofisticado mecanismo de adaptación al hospedador.

5ª. El análisis transcriptómico identificó un conjunto de genes diferencialmente expresados—*CHOP, IFNα, MT1A, MT1E, PLAUR, FGF1, TGFβ1* y *FOSB*—que también se encontraron modulados en el parénquima testicular y la piel escrotal de toros infectados de forma natural. Su regulación consistente tanto *in vitro* como *in vivo* resalta su potencial como biomarcadores. Estos genes podrían constituir indicadores valiosos para el seguimiento de la progresión de la enfermedad, el desarrollo de herramientas diagnósticas y la evaluación de estrategias terapéuticas en la besnoitiosis bovina.

**Objetivo 2: Estudio de los factores dependientes del parásito implicados en la interacción parásito-célula hospedadora**

6ª. El perfil transcriptómico de los taquizoítos de *B. besnoiti* en macrófagos bovinos primarios entre las 4 y las 8 h p.i. se caracteriza por la sobreexpresión de genes implicados en la invasión de la célula hospedadora (por ejemplo, las familias ROP y RON) y en la adaptación metabólica (incluyendo rutas de biosíntesis de aminoácidos y metabolismo energético), coincidiendo con las primeras etapas del ciclo lítico del parásito. En cambio, en fibroblastos derivados de aorta, la ausencia de una expresión génica diferencial significativa entre las 12 y las 32 h p.i. podría reflejar que *B. besnoiti* establece un nicho intracelular estable sin necesidad de una rápida reprogramación transcripcional en esta fase del ciclo lítico.

7ª. Hasta la fecha, el anticuerpo anti-TgBAG1 sigue siendo el marcador más específico y fiable disponible para la identificación de los bradizoítos de *B. besnoiti*, siendo detectado de forma constante mediante técnicas de IHQ, WB e IFI. La caracterización adicional de los anticuerpos anti-NcBSR9 y anti-NcSAG4 debería llevarse a cabo en condiciones optimizadas de diferenciación a bradizoíto, con el fin de esclarecer su posible utilidad como marcadores de bradizoítos de *B. besnoiti*.

8ª. El nitroprusiato sódico (SNP) y los inhibidores de las HDAC indujeron parcialmente la conversión de los taquizoítos de *B. besnoiti* en bradizoítos, como se evidenció por el escaso número de vacuolas positivas para BAG1. Estos resultados suponen un avance significativo hacia el establecimiento de un modelo *in vitro*

de conversión de estadio y sugieren un papel regulador de la acetilación de histonas en la diferenciación. Sin embargo, *B. besnoiti* podría requerir estímulos alternativos o más complejos para alcanzar un desarrollo completo de bradizoítos en comparación con *T. gondii*. Futuros estudios deberían explorar estrategias de inducción dirigidas a la señalización del interferón tipo I y a rutas relacionadas con MAPK, y priorizar el uso de células primarias bovinas con mayor tolerancia al estrés, con el fin de reproducir mejor las condiciones *in vivo*.

9ª. La inhibición del crecimiento de los taquizoítos de *B. besnoiti* mediante inhibidores de HDAC pone de relieve su potencial como herramientas terapéuticas frente a la besnoitiosis bovina. Este hallazgo justifica la necesidad de seguir investigando su seguridad y eficacia tanto en modelos *in vitro* como *in vivo*.

# Chapter VIII: References

# Chapter VIII: References


Adl, S.M., Bass, D., Lane, C.E., Lukeš, J., Schoch, C.L., Smirnov, A., Agatha, S., et al., 2019. Revisions to the Classification, Nomenclature, and Diversity of Eukaryotes. J. Eukaryot. Microbiol., 66: 4-119. https://doi.org/10.1111/jeu.12691.

Agosti, M., Belloni, A., Morini, A., Vacirca, G., 1994. Segnalazione di un focolaio di Besnoitiosi in bovini da carne importati. In: Anonymous Praxis, 15, 5-6 pp.

Álvarez-García, G., Frey, C.F., Mora, L.M., Schares, G., 2013. A century of bovine besnoitiosis: An unknown disease re-emerging in Europe. Trends Parasitol. 29 (8), 407-415, 10.1016/j.pt.2013.06.002.

Álvarez-García, G., Fernández-García, A., Gutiérrez-Expósito, D., Quiteria, J.A., Aguado-Martínez, A., Ortega- Mora, L.M., 2014a. Seroprevalence of *Besnoitia besnoiti* infection and associated risk factors in cattle from an endemic region in Europe. Vet. J. 200 (2), 328-331, 10.1016/j.tvjl.2014.02.013.

Álvarez-García, G., García-Lunar, P., Gutiérrez-Expósito, D., Shkap, V., Ortega-Mora, L.M., 2014b. Dynamics of *Besnoitia besnoiti* infection in cattle. Parasitology. 141 (11), 1419-1435, 10.1017/S0031182014000729.

Álvarez-García, G., 2016. From the mainland to Ireland -bovine besnoitiosis and its spread in Europe. Vet. Rec. 178 (24), 605-607, 10.1136/vr.i3175.

Alzieu, J.P., 2007. Re-emerging cattle besnoitiosis (*Besnoitia besnoiti*) in France: Update on clinical and epidemiological aspects. In: Proceedings of 21st International Conference WAAVP, Gante, Belgium, 222 pp.

Anastácio C., Bexiga R., Nolasco S., Zúquete S., Delgado ILS., Nunes T., Leitão A. Impact of Endemic Besnoitiosis on the Performance of a Dairy Cattle Herd. Animals (Basel). 2022 May 18;12(10):1291. doi: 10.3390/ani12101291. PMID: 35625138; PMCID: PMC9137998.

Arrabal JP., Moré G, Orozco MM., Helman E., Notarnicola J., Basso W., Hartmann BB., Schapira A., Minatel L. A putative new *Besnoitia* species in the southern black-eared opossum *Didelphis aurita*. Int J Parasitol Parasites Wildl. 2024 Sep 21;25:100998. doi: 10.1016/j.ijppaw.2024.100998. PMID: 39376793; PMCID: PMC11456783.

Ashmawy, K.I., Abu-Akkada, S.S., 2014. Evidence for bovine besnoitiosis in Egypt-first serosurvey of *Besnoitia besnoiti* in cattle and water buffalo (*Bubalus bubalis*) in Egypt. Trop. Anim. Health Prod. 46 (3), 519-522, 10.1007/s11250-013-0522-0.

Badshah SL., Ullah A. and Syed, S. The role of zinc-finger antiviral proteins in immunity against viruses. Mol. Genet. Microbiol. 2020. Virol. 35, 78. https://doi.org/10.3103/S0891416820020020.

Basso, W., Schares, G., Gollnick, N.S., Rutten, M., Deplazes, P., 2011. Exploring the life cycle of *Besnoitia besnoiti* -experimental infection of putative definitive and intermediate host species. Vet. Parasitol. 178 (3-4), 223- 234, 10.1016/j.vetpar.2011.01.027.

Basso, W., Lesser, M., Grimm, F., Hilbe, M., Sydler, T., Trosch, L., Ochs, H., Braun, U., Deplazes, P., 2013. Bovine besnoitiosis in Switzerland: Imported cases and local transmission. Vet. Parasitol. 198 (3-4), 265-273, 10.1016/j.vetpar.2013.09.013.

Basson, P.A., Van Niekerk, J., McCully, R.M., Bigalke, R.D., 1965. Besnoitiosis in South African antelopes: A preliminary note on the occurrence of *Besnoitia* cysts in the cardio-vascular system.

Jl S. Afr. Vet. Med. Ass. 36, 578.

Basson, P.A., McCully, R.M., Bigalke, R.D., 1970. Observations on the pathogenesis of bovine and antelope strains of *Besnoitia besnoiti* (Marotel, 1912) infection in cattle and rabbits. Onderstepoort J. Vet. Res. 37 (2), 105- 126.

Beck, R., Stokovic, I., Pleadin, J. and Beck, A., 2013. Bovine besnoitiosis in Croatia. In: Proceedings of the 2nd. International Meeting on Apicowplexan Parasite in Farm Animals, Kusadasi, Turkey.

Bellou S., Hink M.A., Bagli E., Panopoulou E., Bastiaens P.I., Murphy C., Fotsis T. VEGF autoregulates its proliferative and migratory ERK1/2 and p38 cascades by enhancing the expression of DUSP1 and DUSP5 phosphatases in endothelial cells. Am J Physiol Cell Physiol. 2009 Dec;297(6):C1477-89. doi: 10.1152/ajpcell.00058.2009. Epub 2009 Sep 9. PMID: 19741200.

Bennett, S.C.J. A Peculiar Equine Sarcosporidium in the Anglo-Egyptian Sudan, The Veterinary Journal (1900), Volume 83, Issue 6, 1927, Pages 297-304, ISSN 0372-5545, https://doi.org/10.1016/S0372-5545(17)42817-3.

Berisha B., Welter H.; Shimizu T., Miyamoto A., Meyer H.H., Schams D. Expression of fibroblast growth factor 1 (FGF1) and FGF7 in mature follicles during the periovulatory period after GnRH in the cow. J Reprod Dev 2006, 52(2), 307–313. https://doi.org/10.1262/jrd.17077.

Bernstein A.M., Twining S.S., Warejcka D.J., Tall E., Masur S.K. Urokinase receptor cleavage: a crucial step in fibroblast-to-myofibroblast differentiation. Mol Biol Cell. 2007 Jul;18(7):2716-27. doi: 10.1091/mbc.e06-10-0912. Epub 2007 May 16. PMID: 17507651; PMCID: PMC1924808.

Berthelot, X., Ronsin, P., Alzieu, J.P., Marois, M., Corboz, N., Peglion, M., Vilardell, C., Liénard, E., Bouhsira, E., Castillo, J.A., Franc, M., Jacquiet, P., 2014. No detection of *Besnoitia besnoiti*-DNA in the semen of chronically infected bulls. Parasitol. Res. 113 (6), 2355-2362, 10.1007/s00436-014-3894-9.

Besnoit, C., Robin, V., 1912. Sarcosporidiose cutanée chez un vache. Rev. Vet, 649-663.

Besteiro S. *Toxoplasma* control of host apoptosis: the art of not biting too hard the hand that feeds you. Microb Cell. 2015 May 30;2(6):178-181. doi: 10.15698/mic2015.06.209. PMID: 28362004; PMCID: PMC5349139.

Bhandage A.K., Barragan A. Calling in the Caνalry-*Toxoplasma gondii* Hijacks GABAergic Signaling and Voltage-Dependent Calcium Channel Signaling for *Trojan horse*-Mediated Dissemination. Front Cell Infect Microbiol. 2019 Mar 20;9:61. doi: 10.3389/fcimb.2019.00061. PMID: 30949456; PMCID: PMC6436472.

Biernacka A., Dobaczewski M., Frangogiannis N.G. TGF-β signaling in fibrosis. Growth Factors. 2011 Oct;29(5):196-202. doi: 10.3109/08977194.2011.595714. Epub 2011 Jul 11. PMID: 21740331; PMCID: PMC4408550.

Bigalke, R., Naude, T., 1962. The diagnostic value of cysts in the scleral conjunctiva in bovine besnoitiosis. JS Afr Vet Med Assoc 33 (1), 21- 27.

Bigalke, R.D., 1967. The artificial transmission of *Besnoitia besnoiti* (Marotel, 1912) from chronically infected to susceptible cattle and rabbits. Onderstepoort J. Vet. Res. 34 (2), 303-316.

Bigalke, R.D., 1968. New concepts on the epidemiological features of bovine besnoitiosis as determined by laboratory and field investigations. Onderstepoort J. Vet. Res. 35 (1), 3-137.

Bigalke, R.D., Schoeman, J.H., McCully, R.M., 1974. Immunization against bovine besnoitiosis with a live vaccine prepared from a blue wildebeest strain of *Besnoitia besnoiti* grown in cell

cultures. 1. Studies on rabbits. Onderstepoort J. Vet. Res. 41 (1), 1-5.

Black M.W., Boothroyd J.C. Lytic cycle of *Toxoplasma gondii*. Microbiol Mol Biol Rev. 2000 Sep;64(3):607-23. doi: 10.1128/MMBR.64.3.607-623.2000. PMID: 10974128; PMCID: PMC99006.

Bohne W., Heesemann J., Gross U. Reduced replication of *Toxoplasma gondii* is necessary for induction of bradyzoite-specific antigens: a possible role for nitric oxide in triggering stage conversion. Infect Immun. 1994 May;62(5):1761-7. doi: 10.1128/iai.62.5.1761-1767.1994. PMID: 8168938; PMCID: PMC186404.

Bohne W., Gross U., Ferguson D.J., Heesemann J. Cloning and characterization of a bradyzoite-specifically expressed gene (hsp30/bag1) of *Toxoplasma gondii*, related to genes encoding small heat-shock proteins of plants. Mol Microbiol. 1995 Jun;16(6):1221-30. doi: 10.1111/j.1365-2958.1995.tb02344.x. PMID: 8577255.

Bohne W., Roos D.S. Stage-specific expression of a selectable marker in *Toxoplasma gondii* permits selective inhibition of either tachyzoites or bradyzoites. Mol Biochem Parasitol. 1997 Sep;88(1-2):115-26. doi: 10.1016/s0166-6851(97)00087-x. PMID: 9274873.

Boissavy T., Rotili D., Mouveaux T., Roger E., Aliouat E.M., Pierrot C., Valente S., Mai A., Gissot M. Hydroxamate-based compounds are potent inhibitors of *Toxoplasma gondii* HDAC biological activity. Antimicrob Agents Chemother. 2023 Nov 15;67(11):e0066123. doi: 10.1128/aac.00661-23. Epub 2023 Oct 18. PMID: 37850734; PMCID: PMC10648960.

Bosurgi, L., Rothlin, C.V. Management of cell death in parasitic infections. *Semin Immunopathol* **43**, 481–492 (2021). https://doi.org/10.1007/s00281-021-00875-8.

Bougdour A., Maubon D., Baldacci P., Ortet P., Bastien O., Bouillon A., Barale J.C., Pelloux H., Ménard R., Hakimi M.A. Drug inhibition of HDAC3 and epigenetic control of differentiation in Apicomplexa parasites. J Exp Med. 2009 Apr 13;206(4):953-66. doi: 10.1084/jem.20082826. Epub 2009 Apr 6. PMID: 19349466; PMCID: PMC2715132.

Bougdour, A., Durandau, E., Brenier-Pinchart, M.P., Ortet, P., Barakat, M., Kieffer, S., Curt-Varesano, A., Curt-Bertini, R.L., Bastien, O., Coute, Y., Pelloux, H., Hakimi, M.A., 2013. Host cell subversion by *Toxoplasma* GRA16, an exported dense granule protein that targets the host cell nucleus and alters gene expression. Cell Host Microbe 13 (4), 489–500. https://doi.org/10.1016/j.chom.2013.03.002.

Cadéac, 1884. Identité de l'élèphantiasis et de l'anasarque du boeuf. Description de cette maladie. Rev. Vét., 521.

Carboni, D., Tully, T.N., 2009. Marsupials. In: Manual of Exotic Pet Practice, pp. 299–325. https://doi.org/10.1016/B978-141600119-5.50014-7.

Carneiro, M.W., Fukutani, K.F., Andrade, B.B., Curvelo, R.P., Cristal, J.R., Carvalho, A.M., Barral, A., Van Weyenbergh, J., Barral-Netto, M., de Oliveira, C.I., 2016. Gene expression profile of high IFN-γ producers stimulated with *Leishmania braziliensis* identifies genes associated with cutaneous leishmaniasis. PLoS Negl. Trop. Dis. 10 (11), e0005116. https://doi.org/10.1371/journal.pntd.0005116.

Cerutti, A., Blanchard, N., Besteiro, S., 2020. The bradyzoite: a key developmental stage for the persistence and pathogenesis of toxoplasmosis. Pathogens 9 (3), 234. https://doi.org/10.3390/pathogens9030234.

Cervantes-Valencia, M.E., Hermosilla, C., Alcala-Canto, Y., Tapia, G., Taubert, A., Silva, L.M., 2018. Antiparasitic efficacy of curcumin against *Besnoitia besnoiti* tachyzoites *in vitro*. Front. Vet.

Sci. 5, 333. https://doi.org/10.3389/fvets.2018.00333.

Chaparro, V., Leroux, L.P., Masvidal, L., Lorent, J., Graber, T.E., Zimmermann, A., Arango Duque, G., Descoteaux, A., Alain, T., Larsson, O., Jaramillo, M., 2020. Translational profiling of macrophages infected with *Leishmania donovani* identifies mTOR- and eIF4A-sensitive immune-related transcripts. PLoS Pathog. 16 (6), e1008291. https://doi.org/10.1371/journal.ppat.1008291.

Cheema, A.H., Toofanian, F., 1979. Besnoitiosis in wild and domestic goats in Iran. Cornell Vet. 69 (3), 159–168.

Chen, Y., Brandizzi, F., 2013. IRE1: ER stress sensor and cell fate executor. Trends Cell Biol. 23 (11), 547–555. https://doi.org/10.1016/j.tcb.2013.06.005.

Chen, M., Yao, L., Zhou, L., Yang, P., Zou, W., Xu, L., Li, S., Peng, H., 2022. *Toxoplasma gondii* ROP18I inhibits host innate immunity through cGAS–STING signaling. FASEB J. 36 (2), e22171. https://doi.org/10.1096/fj.202101347R.

Christiansen, C., Maus, D., Hoppenz, E., Murillo-León, M., Hoffmann, T., Scholz, J., Melerowicz, F., Steinfeldt, T., Seeber, F., Blume, M., 2022. *In vitro* maturation of *Toxoplasma gondii* bradyzoites in human myotubes and their metabolomic characterization. Nat. Commun. 13, 1168. https://doi.org/10.1038/s41467-022-28730-w.

Cho, S.S.L., Han, J., James, S.J., Png, C.W., Weerasooriya, M., Alonso, S., Zhang, Y., 2017. Dual-specificity phosphatase 12 targets p38 MAP kinase to regulate macrophage response to intracellular bacterial infection. Front. Immunol. 8, 1259. https://doi.org/10.3389/fimmu.2017.01259.

Chu, H., Wang, J.J., Qi, M., Yoon, J.J., Chen, X., Wen, X., Hammonds, J., Ding, L., Spearman, P., 2012. Tetherin/BST-2 is essential for the formation of the intracellular virus-containing compartment in HIV-infected macrophages. Cell Host Microbe 12 (3), 360–372. https://doi.org/10.1016/j.chom.2012.07.011.

Cleary, M.D., Singh, U., Blader, I.J., Brewer, J.L., Boothroyd, J.C., 2002. *Toxoplasma gondii* asexual development: identification of developmentally regulated genes and distinct patterns of gene expression. Eukaryot. Cell 1 (3), 329–340. https://doi.org/10.1128/EC.1.3.329-340.2002.

Coelho, L.L., Pereira, I.R., Pereira, M.C.S., Mesquita, L., Lannes-Vieira, J., Adesse, D., Garzoni, L.R., 2018. *Trypanosoma cruzi* activates mouse cardiac fibroblasts *in vitro* leading to fibroblast–myofibroblast transition and increase in expression of extracellular matrix proteins. Parasit. Vectors 11, 72. https://doi.org/10.1186/s13071-018-2614-1.

Coelho, J., Domingues, J., Waap, H., Stilwell, G., 2023. Epidemiological characteristics of bovine besnoitiosis (*Besnoitia besnoiti*) in a beef cattle farm: a cross-sectional serological assessment. Front. Vet. Sci. 10, 1158235. https://doi.org/10.3389/fvets.2023.1158235.

Colos-Arango, A., Largo-de la Torre, A., Calero-Bernal, R., Ortega-Mora, L.M., Regidor-Cerrillo, J., 2023. Short-term culture adaptation of *Toxoplasma gondii* archetypal II and III field isolates affects cystogenic capabilities and modifies virulence in mice. Int. J. Parasitol. 53 (9), 491–504. https://doi.org/10.1016/j.ijpara.2023.03.004.

Conejeros, I., Velásquez, Z.D., Grob, D., Zhou, E., Salecker, H., Hermosilla, C., Taubert, A., 2019. Histone H2A and bovine neutrophil extracellular traps induce damage of *Besnoitia besnoiti*-infected host endothelial cells but fail to affect total parasite proliferation. Biology (Basel) 8 (4), 78. https://doi.org/10.3390/biology8040078.

Corica, D., Aversa, T., Ruggeri, R.M., Cristani, M., Alibrandi, A., Pepe, G., De Luca, F., Wasniewska, M., 2019. Could AGE/RAGE-related oxidative homeostasis dysregulation enhance susceptibility to pathogenesis of cardio-metabolic complications in childhood obesity? Front.

Endocrinol. (Lausanne) 10, 426. https://doi.org/10.3389/fendo.2019.00426.

Corliss, B.A., Azimi, M.S., Munson, J.M., Peirce, S.M., Murfee, W.L., 2016. Macrophages: an inflammatory link between angiogenesis and lymphangiogenesis. Microcirculation 23 (2), 95–121. https://doi.org/10.1111/micc.12259.

Cortes, H.C., Leitão, A., Vidal, R., Vila-Viçosa, M.J., Ferreira, M.L., Caeiro, V., Hjerpe, C.A., 2005. Besnoitiosis in bulls in Portugal. Vet. Rec. 157 (9), 262–264.

Cortes, H.C., Reis, Y., Waap, H., Marcelino, E., Vaz, Y., Nunes, T., Fanzendeiro, I., Caeiro, V., Leitao, A., 2006. Longitudinal study of *Besnoitia besnoiti* infection prevalence rates in a beef cattle herd in Alentejo, Portugal. In: Proc. COST 854 Final Conference, Liège, Belgium, 20 pp.

Cortes, H.C., Muller, N., Boykin, D., Stephens, C.E., Hemphill, A., 2011. *In vitro* effects of arylimidamides against *Besnoitia besnoiti* infection in Vero cells. Parasitology 138 (5), 583–592. https://doi.org/10.1017/S0031182011000114.

Czabotar, P.E., Lessene, G., Strasser, A., Adams, J.M., 2014. Control of apoptosis by the BCL-2 protein family: implications for physiology and therapy. Nat. Rev. Mol. Cell Biol. 15 (1), 49–63. https://doi.org/10.1038/nrm3722.

Dai, H., Wang, L., Li, L., Huang, Z., Ye, L., 2021. Metallothionein 1: a new spotlight on inflammatory diseases. Front. Immunol. 12, 739918. https://doi.org/10.3389/fimmu.2021.739918.

Danastas, K., Miranda-Saksena, M., Cunningham, A.L., 2020. Herpes simplex virus type 1 interactions with the interferon system. Int. J. Mol. Sci. 21 (14), 5150. https://doi.org/10.3390/ijms21145150.

de Castro, M.A., Bunt, G., Wouters, F.S., 2016. Cathepsin B launches an apoptotic exit effort upon cell death-associated disruption of lysosomes. Cell Death Discov. 2, 16012. https://doi.org/10.1038/cddiscovery.2016.12.

de Sousa Abreu, R., Penalva, L.O., Marcotte, E.M., Vogel, C., 2009. Global signatures of protein and mRNA expression levels. Mol. Biosyst. 5 (12), 1512–1526. https://doi.org/10.1039/b908315d.

Decout, A., Katz, J.D., Venkatraman, S., Ablasser, A., 2021. The cGAS–STING pathway as a therapeutic target in inflammatory diseases. Nat. Rev. Immunol. 21 (9), 548–569. https://doi.org/10.1038/s41577-021-00524-z.

Delooz L, Evrard J, Mpouam SE, Saegerman C. Emergence of *Besnoitia besnoiti* in Belgium. Pathogens. 2021 Nov 23;10(12):1529. doi: 10.3390/pathogens10121529. PMID: 34959484; PMCID: PMC8706464.

Dias-Junior, A.G., Sampaio, N.G., Rehwinkel, J., 2019. A balancing act: MDA5 in antiviral immunity and autoinflammation. Trends Microbiol. 27 (1), 75–85. https://doi.org/10.1016/j.tim.2018.08.007.

Diesing, L., Heydorn, A.O., Matuschka, F.R., Bauer, C., Pipano, E., de Waal, D.T., Potgieter, F.T., 1988. *Besnoitia besnoiti*: studies on the definitive host and experimental infections in cattle. Parasitol. Res. 75 (2), 114–117.

Diezma-Díaz, C., Jiménez-Meléndez, A., Re, M.T., et al., 2018. Effect of parasite dose and host age on the infection with *Besnoitia besnoiti* tachyzoites in cattle. Transbound. Emerg. Dis. 65, 1979–1990. https://doi.org/10.1111/tbed.12980.

Diezma-Díaz, C., Ferre, I., Re, M., Jiménez-Meléndez, A., Tabanera, E., González-Huecas, M., Pizarro-Díaz, M., Yanguas-Pérez, D., Brum, P.L., Blanco-Murcia, J., Ortega-Mora, L.M., Álvarez-García, G., 2019. The route of *Besnoitia besnoiti* tachyzoites inoculation does not

influence the clinical outcome of the infection in calves. Vet. Parasitol. 267, 21–25. https://doi.org/10.1016/j.vetpar.2019.02.001.

Diezma-Díaz, C., Tabanera, E., Ferre, I., Pizarro-Díaz, M., González-Huecas, M., Blanco-Murcia, J., Ortega-Mora, L.M., Álvarez-García, G., 2020. Histological findings in experimentally infected male calves with chronic besnoitiosis. Vet. Parasitol. 281, 109120. https://doi.org/10.1016/j.vetpar.2020.109120.

Drappier, M., Michiels, T., 2015. Inhibition of the OAS/RNase L pathway by viruses. Curr. Opin. Virol. 15, 19–26. https://doi.org/10.1016/j.coviro.2015.07.002.

Dubey, J., 1998. Toxoplasmosis, Sarcocystosis, Isosporosis, and Cyclosporosis. Zoonoses. USDA, 579–597 pp.

Dubey, J.P., Lindsay, D.S., 2003. Development and ultrastructure of *Besnoitia oryctofelisi* tachyzoites, tissue cysts, bradyzoites, schizonts and merozoites. Int. J. Parasitol. 33 (8), 807–819. https://doi.org/10.1016/S0020-7519(03)00087-0.

Dubey, J.P., Sreekumar, C., Donovan, T., Rozmanec, M., Rosenthal, B.M., Vianna, M.C., Davis, W.P., Belden, J.S., 2005. Redescription of *Besnoitia bennetti* (Protozoa: Apicomplexa) from the donkey (*Equus asinus*). Int. J. Parasitol. 35 (6), 659–672. https://doi.org/10.1016/j.ijpara.2005.01.004.

Dubey, J.P., Yabsley, M.J., 2010. *Besnoitia neotomofelis* n. sp. (Protozoa: Apicomplexa) from the southern plains woodrat (*Neotoma micropus*). Parasitology 137 (12), 1731–1747. https://doi.org/10.1017/S0031182010000636.

Dubey, J.P., van Wilpe, E., Blignaut, D.J., Schares, G., Williams, J.H., 2013. Development of early tissue cysts and associated pathology of *Besnoitia besnoiti* in a naturally infected bull (*Bos taurus*) from South Africa. J. Parasitol. 99 (3), 459–466. https://doi.org/10.1645/12-128.1.

Dzierszinski, F., Nishi, M., Ouko, L., Roos, D.S., 2004. Dynamics of *Toxoplasma gondii* differentiation. Eukaryot. Cell 3 (4), 992–1003. https://doi.org/10.1128/EC.3.4.992-1003.2004.

Eberhard, N., Balmer, V., Müller, J., Müller, N., Winter, R., Pou, S., Nilsen, A., Riscoe, M., Francisco, S., Leitao, A., Doggett, J.S., Hemphill, A., 2020. Activities of Endochin-Like Quinolones Against *in vitro* Cultured *Besnoitia besnoiti* Tachyzoites. Front. Vet. Sci. 7, 96. https://doi.org/10.3389/fvets.2020.00096.

EFSA (European Food Safety Authority), 2010. Bovine besnoitiosis: an emerging disease in Europe. Scientific statement on bovine besnoitiosis. EFSA J. 8, 1499.

Ellis, J.T., Holmdahl, O.J., Ryce, C., Njenga, J.M., Harper, P.A., Morrison, D.A., 2000. Molecular phylogeny of *Besnoitia* and the genetic relationships among *Besnoitia* of cattle, wildebeest and goats. Protist 151 (4), 329–336.

Eskandarpour, M., Kiaii, S., Zhu, C., Castro, J., Sakko, A.J., Hansson, J., 2005. Suppression of oncogenic NRAS by RNA interference induces apoptosis of human melanoma cells. Int. J. Cancer 115 (1), 65–73. https://doi.org/10.1002/ijc.20873.

Espinosa, G., Conejeros, I., Rojas-Barón, L., Hermosilla, C.R., Taubert, A., 2023. *Besnoitia besnoiti*-induced neutrophil clustering and neutrophil extracellular trap formation depend on P2X1 purinergic receptor signaling. Front. Immunol. 14, 1244068. https://doi.org/10.3389/fimmu.2023.1244068.

Esteban-Gil, A., Grisez, C., Prevot, F., Florentin, S., Decaudin, A., Picard-Hagen, N., 2023. Fereig, R.M., Nishikawa, Y., 2020. From signaling pathways to distinct immune responses: key factors for establishing or combating *Neospora caninum* infection in different susceptible hosts.

Pathogens 9 (5), 384. https://doi.org/10.3390/pathogens9050384.

Ferguson, D.J., Hutchison, W.M., 1987. An ultrastructural study of the early development and tissue cyst formation of *Toxoplasma gondii* in the brains of mice. Parasitol. Res. 73 (6), 483–491. https://doi.org/10.1007/BF00535321.

Fernández-Álvarez, M., Horcajo, P., Jiménez-Meléndez, A., Diezma-Díaz, C., Ferre, I., Pastor-Fernández, I., Ortega-Mora, L.M., Álvarez-García, G., 2023. Transcriptional changes associated with apoptosis and type I IFN underlie the early interaction between *Besnoitia besnoiti* tachyzoites and monocyte-derived macrophages. Int. J. Parasitol. 53 (9), 505–521. https://doi.org/10.1016/j.ijpara.2023.05.002.

Fernández-García, A., Risco-Castillo, V., Pedraza-Díaz, S., Aguado-Martínez, A., Álvarez-García, G., Gómez-Bautista, M., Collantes-Fernández, E., Ortega-Mora, L.M., 2009a. First isolation of *Besnoitia besnoiti* from a chronically infected cow in Spain. J. Parasitol. 95 (2), 474–476. https://doi.org/10.1645/GE-1772.1.

Fernández-García, A., Álvarez-García, G., Risco-Castillo, V., Aguado-Martínez, A., Marugán-Hernández, V., Ortega-Mora, L.M., 2009b. Pattern of recognition of *Besnoitia besnoiti* tachyzoite and bradyzoite antigens by naturally infected cattle. Vet. Parasitol. 164 (2–4), 104–110. https://doi.org/10.1016/j.vetpar.2009.06.020.

Fernández-García, A., Álvarez-García, G., Risco-Castillo, V., Aguado-Martínez, A., Marcen, J.M., Rojo-Montejo, S., Castillo, J.A., Ortega-Mora, L.M., 2010. Development and use of an indirect ELISA in an outbreak of bovine besnoitiosis in Spain. Vet. Rec. 166 (26), 818–822. https://doi.org/10.1136/vr.b4874.

Fernández-García, A., Álvarez-García, G., Marugán-Hernández, V., García-Lunar, P., Aguado-Martínez, A., Risco-Castillo, V., Ortega-Mora, L.M., 2013. Identification of *Besnoitia besnoiti* proteins that showed differences in abundance between tachyzoite and bradyzoite stages by difference gel electrophoresis. Parasitology 140 (8), 999–1008. https://doi.org/10.1017/S003118201300036X.

Ferreira-da-Silva, Mda F., Takács, A.C., Barbosa, H.S., Gross, U., Lüder, C.G., 2009. Primary skeletal muscle cells trigger spontaneous *Toxoplasma gondii* tachyzoite-to-bradyzoite conversion at higher rates than fibroblasts. Int. J. Med. Microbiol. 299 (5), 381–388. https://doi.org/10.1016/j.ijmm.2008.10.002.

Findley, A.S., Monziani, A., Richards, A.L., Rhodes, K., Ward, M.C., Kalita, C.A., Alazizi, A., Pazokitoroudi, A., Sankararaman, S., Wen, X., Lanfear, D.E., Pique-Regi, R., Gilad, Y., Luca, F., 2021. Functional dynamic genetic effects on gene regulation are specific to particular cell types and environmental conditions. eLife 10, e67077. https://doi.org/10.7554/eLife.67077.

Florin-Christensen, M., Schnittger, L. (Eds.), 2018. *Parasitic protozoa of farm animals and pets*. Springer.

Franc, M., Cardiegues, M., 1999. La besnoitiose bovine: attitude diagnostique et thérapeutique. Bull. GTV Bovins Parasitol., 119–124.

Franco, C., Borges, L., 1915. Nota Sobre a Sarcosporidiose Bovina. Rev. Med. Vet., 255–299 pp.

Frank, M., Pipano, E., Rosenberg, A., 1977. Prevalence of antibodies against *Besnoitia besnoiti* in beef and dairy cattle in Israel. Refuah Veterinarith 34 (3), 83–86.

Frenkel, J., Wilson, H., 1972. Effects of radiation on specific cellular immunities: Besnoitiosis and a herpesvirus infection of hamsters. J. Infect. Dis. 125 (3), 216–230.

Frenkel, J., Dubey, J., Hoff, R., 1976. Loss of stages after continuous passage of *Toxoplasma*

*gondii* and *Besnoitia jellisoni*. J. Eukaryot. Microbiol. 23 (3), 421–424.

Frey, C.F., Gutiérrez-Expósito, D., Ortega-Mora, L.M., Benavides, J., Marcen, J.M., Castillo, J.A., Casasus, I., Sanz, A., García-Lunar, P., Esteban-Gil, A., Álvarez-García, G., 2013. Chronic bovine besnoitiosis: intra-organ parasite distribution, parasite loads and parasite-associated lesions in subclinical cases. Vet. Parasitol. 197 (1–2), 95–103. https://doi.org/10.1016/j.vetpar.2013.04.023.

Frey, C.F., Regidor-Cerrillo, J., Marreros, N., García-Lunar, P., Gutiérrez-Expósito, D., Schares, G., Dubey, J.P., Gentile, A., Jacquiet, P., Shkap, V., 2016. *Besnoitia besnoiti* lytic cycle *in vitro* and differences in invasion and intracellular proliferation among isolates. Parasites Vectors 9 (1), 1. https://doi.org/10.1186/s13071-016-1405-9.

Fox, B.A., Gigley, J.P., Bzik, D.J., 2004. *Toxoplasma gondii* lacks the enzymes required for *de novo* arginine biosynthesis and arginine starvation triggers cyst formation. Int. J. Parasitol. 34 (3), 323–331. https://doi.org/10.1016/j.ijpara.2003.12.001.

Fu, M., Blackshear, P.J., 2017. RNA-binding proteins in immune regulation: a focus on CCCH zinc finger proteins. Nat. Rev. Immunol. 17 (2), 130–143. https://doi.org/10.1038/nri.2016.129.

Fujie, T., Murakami, M., Yoshida, E., Yasuike, S., Kimura, T., Fujiwara, Y., Yamamoto, C., Kaji, T., 2016. Transcriptional induction of Metallothionein by tris(pentafluorophenyl)stibane in cultured bovine aortic endothelial cells. Int. J. Mol. Sci. 17 (9), 1381. https://doi.org/10.3390/ijms17091381.

Galluzzi, L., Diotallevi, A., De Santi, M., Ceccarelli, M., Vitale, F., Brandi, G., Magnani, M., 2016. *Leishmania infantum* induces mild unfolded protein response in infected macrophages. PLoS One 11 (12), e0168339. https://doi.org/10.1371/journal.pone.0168339.

García-Lunar, P., Regidor-Cerrillo, J., Gutiérrez-Expósito, D., Ortega-Mora, L.M., Álvarez-García, G., 2013a. First 2-DE approach towards characterising the proteome and immunome of *Besnoitia besnoiti* in the tachyzoite stage. Vet. Parasitol. 195 (1–2), 24–34. https://doi.org/10.1016/j.vetpar.2012.12.040.

García-Lunar, P., Ortega-Mora, L.M., Schares, G., Gollnick, N.S., Jacquiet, P., Grisez, C., Prevot, F., Frey, C.F., Gottstein, B., Álvarez-García, G., 2013b. An inter-laboratory comparative study of serological tools employed in the diagnosis of *Besnoitia besnoiti* infection in bovines. Transbound. Emerg. Dis. 60 (1), 59–68. https://doi.org/10.1111/j.1865-1682.2012.01318.x.

García-Lunar, P., Schares, G., Sanz-Fernández, A., Jiménez-Meléndez, A., García-Soto, I., Regidor-Cerrillo, J., Pastor-Fernández, I., Hemphill, A., Fernández-Álvarez, M., Ortega-Mora, L.M., Álvarez-García, G., 2019. Development and characterization of monoclonal antibodies against *Besnoitia besnoiti* tachyzoites. *Parasitology* 146(2), 187–196. https://doi.org/10.1017/S0031182018001336

García-Sánchez, M., Jiménez-Pelayo, L., Horcajo, P., Regidor-Cerrillo, J., Collantes-Fernández, E., Ortega-Mora, L.M., 2019. Gene expression profiling of *Neospora caninum* in bovine macrophages reveals differences between isolates associated with key parasite functions. *Front. Cell Infect. Microbiol.* 9, 354. https://doi.org/10.3389/fcimb.2019.00354

García-Sánchez, M., Jiménez-Pelayo, L., Horcajo, P., Collantes-Fernández, E., Ortega-Mora, L.M., Regidor-Cerrillo, J., 2020. *Neospora caninum* infection induces an isolate virulence-dependent pro-inflammatory gene expression profile in bovine monocyte-derived macrophages. *Parasit. Vectors* 13(1), 374. https://doi.org/10.1186/s13071-020-04239-3

García, D.C., Miceli, D.C., Valdecantos, P.A., García, E.V., Roldán-Olarte, M., 2014. Expression of urokinase type plasminogen activator receptor (uPAR) in the bovine oviduct: Relationship with uPA effect on oviductal epithelial cells. *Res. Vet. Sci.* 97(1), 118–123.

https://doi.org/10.1016/j.rvsc.2014.05.012

Garrido-Castañé, I., Romero, A.O., Espuny, J.C., Hentrich, B., Basso, W., 2019. *Besnoitia besnoiti* seroprevalence in beef, dairy and bullfighting cattle in Catalonia (northeastern Spain): A cross-sectional study. *Parasitol. Int.* 69, 71–74. https://doi.org/10.1016/j.parint.2018.12.001

Gazzonis, A.L., García, G., Zanzani, S.A., Garippa, G., Rossi, L., Maggiora, M., Dini, V., Invernizzi, A., Luini, M., Tranquillo, V.M., Mora, L., Manfredi, M., 2014. *Besnoitia besnoiti* among cattle in insular and northwestern Italy: Endemic infection or isolated outbreaks? *Parasit. Vectors* 7(1), 585. https://doi.org/10.1186/s13071-014-0585-4

Gazzonis, A.L., Álvarez-García, G., Maggioni, A., Zanzani, S.A., Olivieri, E., Compiani, R., Sironi, G., Ortega-Mora, L.M., Manfredi, M.T., 2017. Serological dynamics and risk factors of *Besnoitia besnoiti* infection in breeding bulls from an endemically infected purebred beef herd. *Parasitol. Res.* 116(4), 1383–1393. https://doi.org/10.1007/s00436-017-5418-x

Genest, M., 2008. *La besnoitiose bovine à Besnoitia besnoiti: Enquête sérologique et écologique dans un foyer d'émergence du Maine-et-Loire*. Doctoral Thesis, University of Nantes, France.

Gentile, A., Militerno, G., Schares, G., Nanni, A., Testoni, S., Bassi, P., Gollnick, N.S., 2012. Evidence for bovine besnoitiosis being endemic in Italy – First *in vitro* isolation of *Besnoitia besnoiti* from cattle born in Italy. *Vet. Parasitol.* 184(2–4), 10.1016/j.vetpar.2011.09.014

Gobel, E., Widauer, R., Reimann, M., Munz, E., 1985. Ultrastructure of the asexual multiplication of *Besnoitia besnoiti* (Marotel, 1912) in Vero- and CRFK-cell cultures. *Zentralbl. Veterinarmed. B* 32(3), 202–212.

Gollnick, N.S., Scharr, J.C., Schares, G., Langenmayer, M.C., 2015. Natural *Besnoitia besnoiti* infections in cattle: Chronology of disease progression. *BMC Vet. Res.* 11, 10.1186/s12917-015-0344-6

Gollnick, N., Scharr, J., Schares, S., Bärwald, A., Schares, G., Langenmayer, M., 2018. Naturally acquired bovine besnoitiosis: Disease frequency, risk and outcome in an endemically infected beef herd. *Transbound. Emerg. Dis.* 65(3), 833–843. https://doi.org/10.1111/tbed.12810

González-Barrio, D., Diezma-Díaz, C., Tabanera, E., Aguado-Criado, E., Pizarro, M., González-Huecas, M., Ferre, I., Jiménez-Meléndez, A., Gutiérrez-Expósito, D., Ortega-Mora, L.M., Álvarez-García, G., 2020. Vascular wall injury and inflammation are key pathogenic mechanisms responsible for early testicular degeneration during acute besnoitiosis in bulls. *Parasit. Vectors* 13(1), 113. https://doi.org/10.1186/s13071-020-3959-9

González-Barrio, D., Köster, P.C., Habela, M.A., Martín-Pérez, M., Fernández-García, J.L., Balseiro, A., Barral, M., Nájera, F., Figueiredo, A.M., Palacios, M., Mateo, M., Carmena, D., Álvarez-García, G., Calero-Bernal, R., 2021a. Molecular survey of *Besnoitia* spp. (Apicomplexa) in faeces from European wild mesocarnivores in Spain. *Transbound. Emerg. Dis.* 68, 3156–3166.

González-Barrio, D., Diezma-Díaz, C., Gutiérrez-Expósito, D., Tabanera, E., Jiménez-Meléndez, A., Pizarro, M., González-Huecas, M., Ferre, I., Ortega-Mora, L.M., Álvarez-García, G., 2021b. Identification of molecular biomarkers associated with disease progression in the testis of bulls infected with *Besnoitia besnoiti*. *Vet. Res.* 52(1), 106. https://doi.org/10.1186/s13567-021-00974-2

Gavrilescu, L.C., Denkers, E.Y., 2001. IFN-gamma overproduction and high level apoptosis are associated with high but not low virulence *Toxoplasma gondii* infection. *J. Immunol.* 167(2), 902–909. https://doi.org/10.4049/jimmunol.167.2.902

Gondim, L.F., Meyer, J., Peters, M., Rezende-Gondim, M.M., Vrhovec, M.G., Pantchev, N., Bauer, C., Conraths, F.J., Schares, G., 2015. *In vitro* cultivation of *Hammondia heydorni*:

Generation of tachyzoites, stage conversion into bradyzoites, and evaluation of serologic cross-reaction with *Neospora caninum*. *Vet. Parasitol.* 210(3–4), 131–140. https://doi.org/10.1016/j.vetpar.2015.03.028

Gong, H., Kobayashi, K., Sugi, T., Takemae, H., Kurokawa, H., Horimoto, T., Akashi, H., Kato, K., 2012. A novel PAN/apple domain-containing protein from *Toxoplasma gondii*: Characterization and receptor identification. *PLoS One* 7(1), e30169. https://doi.org/10.1371/journal.pone.0030169

Guo, J., Liu, W., Zeng, Z., Lin, J., Zhang, X., Chen, L., 2020. TGFβ3 and MMP13 regulated the initiation of liver fibrosis progression as dynamic network biomarkers. *J. Cell. Mol. Med.* 25(2), 867–879. https://doi.org/10.1111/jcmm.16140

Gupta, M., Gupta, S.K., Hoffman, B., Liebermann, D.A., 2006. Gadd45a and Gadd45b protect hematopoietic cells from UV-induced apoptosis via distinct signaling pathways, including p38 activation and JNK inhibition. *J. Biol. Chem.* 281(26), 17552–17558. https://doi.org/10.1074/jbc.M600950200

Gutiérrez-Expósito, D., Ortega-Mora, L.M., Gajadhar, A.A., García-Lunar, P., Dubey, J.P., Álvarez-García, G., 2012. Serological evidence of *Besnoitia* spp. infection in Canadian wild ruminants and strong cross-reaction between *Besnoitia besnoiti* and *Besnoitia tarandi*. *Vet. Parasitol.* 190(1–2), 19–28. https://doi.org/10.1016/j.vetpar.2012.06.017

Gutiérrez-Expósito, D., Arnal, M.C., Martínez-Durán, D., Regidor-Cerrillo, J., Revilla, M., de Luco, D.L.F., Jiménez-Meléndez, A., Calero-Bernal, R., Habela, M.A., García-Bocanegra, I., 2016. The role of wild ruminants as reservoirs of *Besnoitia besnoiti* infection in cattle. *Vet. Parasitol.* 223, 7–13.

Gutiérrez-Expósito, D., Ortega-Mora, L.M., García-Lunar, P., Rojo-Montejo, S., Zabala, J., Serrano, M., Álvarez-García, G., 2017. Clinical and serological dynamics of *Besnoitia besnoiti* infection in three endemically infected beef cattle herds. *Transbound. Emerg. Dis.* 64(2), 538–546. https://doi.org/10.1111/tbed.12402

Hadwen, S., 1922. Cyst-forming protozoa in reindeer and caribou, and a sarcosporidian parasite of the seal (*Phoca richardi*). *Can. Dep. Agric. Bull.* 61, 282–374.

Hakimi, M.A., Bougdour, A., 2015. *Toxoplasma*'s ways of manipulating the host transcriptome via secreted effectors. *Curr. Opin. Microbiol.* 26, 24–31. https://doi.org/10.1016/j.mib.2015.04.003

Harding, J.S., Herbath, M., Chen, Y., Rayasam, A., Ritter, A., Csoka, B., Hasko, G., Michael, I.P., Fabry, Z., Nagy, A., Sandor, M., 2019. VEGF-A from granuloma macrophages regulates granulomatous inflammation by a non-angiogenic pathway during mycobacterial infection. *Cell Rep.* 27(7), 2119–2131.e6. https://doi.org/10.1016/j.celrep.2019.04.072

Harjunpää, H., Llort Asens, M., Guenther, C., Fagerholm, S.C., 2019. Cell adhesion molecules and their roles and regulation in the immune and tumor microenvironment. *Front. Immunol.* 10, 1078. https://doi.org/10.3389/fimmu.2019.01078

Hauck, C.R., Agerer, F., Muenzner, P., Schmitter, T., 2006. Cellular adhesion molecules as targets for bacterial infection. *Eur. J. Cell Biol.* 85(3–4), 235–242. https://doi.org/10.1016/j.ejcb.2005.08.002

Hevler, J.F., Zenezeni Chiozzi, R., Cabrera-Orefice, A., Brandt, U., Arnold, S., Heck, A.J.R., 2021. Molecular characterization of a complex of apoptosis-inducing factor 1 with cytochrome c oxidase of the mitochondrial respiratory chain. *Proc. Natl. Acad. Sci. U. S. A.* 118(39), e2106950118. https://doi.org/10.1073/pnas.2106950118

Hofmeyr, C.F.B., 1945. Globidiosis in cattle. *J. S. Afr. Vet. Med. Assoc.* 16, 102–109.

Hoarau-Véchot, J., Rafii, A., Touboul, C., Pasquier, J., 2018. Halfway between 2D and animal models: Are 3D cultures the ideal tool to study cancer–microenvironment interactions? *Int. J. Mol. Sci.* 19(1), 181. https://doi.org/10.3390/ijms19010181

Holzerland, J., Fénéant, L., Banadyga, L., Hölper, J.E., Knittler, M.R., Groseth, A., 2020. BH3-only sensors Bad, Noxa and Puma are key regulators of Tacaribe virus-induced apoptosis. *PLoS Pathog.* 16(10), e1008948. https://doi.org/10.1371/journal.ppat.1008948

Horcajo, P., Jiménez-Pelayo, L., García-Sánchez, M., Regidor-Cerrillo, J., Collantes-Fernández, E., Rozas, D., Hambruch, N., Pfarrer, C., Ortega-Mora, L.M., 2017. Transcriptome modulation of bovine trophoblast cells in vitro by *Neospora caninum*. *Int. J. Parasitol.* 47(12), 791–799. https://doi.org/10.1016/j.ijpara.2017.08.007

Hornok, S., Fedak, A., Baska, F., Hofmann-Lehmann, R., Basso, W., 2014. Bovine besnoitiosis emerging in Central-Eastern Europe, Hungary. *Parasit. Vectors* 7(1), 20. https://doi.org/10.1186/1756-3305-7-20

Hornok, S., Fedak, A., Baska, F., Basso, W., Dencso, L., Toth, G., Szeredi, L., Abonyi, T., Denes, B., 2015. Vector-borne transmission of *Besnoitia besnoiti* by blood-sucking and secretophagous flies: Epidemiological and clinicopathological implications. *Parasit. Vectors* 8(1), 450. https://doi.org/10.1186/s13071-015-1058-0

Hu, H., Tian, M., Ding, C., Yu, S., 2019. The C/EBP homologous protein (CHOP) transcription factor functions in endoplasmic reticulum stress-induced apoptosis and microbial infection. *Front. Immunol.* 9, 3083. https://doi.org/10.3389/fimmu.2018.03083

Ihara, F., Nishikawa, Y., 2014. Starvation of low-density lipoprotein-derived cholesterol induces bradyzoite conversion in *Toxoplasma gondii*. *Parasit. Vectors* 7, 248. https://doi.org/10.1186/1756-3305-7-248

Im, Y.B., Jung, M., Shin, M.-K., Kim, S., Yoo, H.S., 2016. Expression of cytokine and apoptosis-related genes in bovine peripheral blood mononuclear cells stimulated with *Brucella abortus* recombinant proteins. *Vet. Res.* 47, 30. https://doi.org/10.1186/s13567-016-0311-7

Jacquiet, P., Liénard, E., Franc, M., 2010. Bovine besnoitiosis: Epidemiological and clinical aspects. *Vet. Parasitol.* 174(1–2), 30–36. https://doi.org/10.1016/j.vetpar.2010.08.013

Janitschke, K., De Vos, A.J., Bigalke, R.D., 1984. Serodiagnosis of bovine besnoitiosis by ELISA and immunofluorescence tests. *Onderstepoort J. Vet. Res.* 51(4), 239–243.

Jelaska, A., Strehlow, D., Korn, J.H., 1999. Fibroblast heterogeneity in physiological conditions and fibrotic disease. *Springer Semin. Immunopathol.* 21(4), 385–395.

Jiang, D., Guo, R., Machens, H.G., Rinkevich, Y., 2023. Diversity of fibroblasts and their roles in wound healing. *Cold Spring Harb. Perspect. Biol.* 15(3), a041222. https://doi.org/10.1101/cshperspect.a041222

Jiménez-Meléndez, A., Ojo, K.K., Wallace, A.M., Smith, T.R., Hemphill, A., Balmer, V., Regidor-Cerrillo, J., Ortega-Mora, L.M., Hehl, A.B., Fan, E., Maly, D.J., Van Voorhis, W.C., Álvarez-García, G., 2017. In vitro efficacy of bumped kinase inhibitors against *Besnoitia besnoiti* tachyzoites. *Int. J. Parasitol.* 47(12), 811–821. https://doi.org/10.1016/j.ijpara.2017.08.005

Jiménez-Meléndez, A., Rico-San Román, L., Hemphill, A., Balmer, V., Ortega-Mora, L.M., Álvarez-García, G., 2018. Repurposing of commercially available anti-coccidials identifies diclazuril and decoquinate as potential therapeutic candidates against *Besnoitia besnoiti* infection. *Vet. Parasitol.* 261, 77–85. https://doi.org/10.1016/j.vetpar.2018.08.015

Jiménez-Meléndez, A., Fernández-Álvarez, M., Calle, A., Ramírez, M.Á., Diezma-Díaz, C., Vázquez-Arbaizar, P., Ortega-Mora, L.M., Álvarez-García, G., 2019. Lytic cycle of *Besnoitia besnoiti* tachyzoites displays similar features in primary bovine endothelial cells and fibroblasts. *Parasit. Vectors* 12(1), 517. https://doi.org/10.1186/s13071-019-3777-0

Jiménez-Meléndez, A., Ramakrishnan, C., Hehl, A.B., Russo, G., Álvarez-García, G., 2020. RNA-Seq analyses reveal that endothelial activation and fibrosis are induced early and progressively by *Besnoitia besnoiti* host cell invasion and proliferation. *Front. Cell Infect. Microbiol.* 10, 218. https://doi.org/10.3389/fcimb.2020.00218

Jiménez-Pelayo, L., García-Sánchez, M., Regidor-Cerrillo, J., Horcajo, P., Collantes-Fernández, E., Gómez-Bautista, M., Hambruch, N., Pfarrer, C., Ortega-Mora, L.M., 2017. Differential susceptibility of bovine caruncular and trophoblast cell lines to infection with high and low virulence isolates of *Neospora caninum*. *Parasit. Vectors* 10(1), 463. https://doi.org/10.1186/s13071-017-2409-9

Jiménez-Pelayo, L., García-Sánchez, M., Collantes-Fernández, E., Regidor-Cerrillo, J., Horcajo, P., Gutiérrez-Expósito, D., Espinosa, J., Benavides, J., Osoro, K., Pfarrer, C., Ortega-Mora, L.M., 2020. Crosstalk between *Neospora caninum* and the bovine host at the maternal-foetal interface determines the outcome of infection. *Vet. Res.* 51(1), 83. https://doi.org/10.1186/s13567-020-00803-y

Jones, C.V., Ricardo, S.D., 2013. Macrophages and CSF-1: implications for development and beyond. *Organogenesis* 9(4), 249–260. https://doi.org/10.4161/org.25676

Kadesch, P., Hollubarsch, T., Gerbig, S., Schneider, L., Silva, L.M.R., Hermosilla, C., Taubert, A., Spengler, B., 2020. Intracellular parasites *Toxoplasma gondii* and *Besnoitia besnoiti*, unveiled in single host cells using AP-SMALDI MS imaging. *J. Am. Soc. Mass Spectrom.* 31(9), 1815–1824. https://doi.org/10.1021/jasms.0c00043

Kany S., Vollrath J.T., Relja B. Cytokines in inflammatory disease. *Int J Mol Sci.* 2019 Nov 28;20(23):6008. doi: 10.3390/ijms20236008. PMID: 31795299; PMCID: PMC6929211.

Kennedy L., Shi-Wen X., Carter D.E., Abraham D.J., Leask A. Fibroblast adhesion results in the induction of a matrix remodeling gene expression program. *Matrix Biol.* 2008 May;27(4):274–81. doi: 10.1016/j.matbio.2008.01.004. PMID: 18291634.

Kim D., Pertea G., Trapnell C., Pimentel H., Kelley R., Salzberg S.L. TopHat2: accurate alignment of transcriptomes in the presence of insertions, deletions and gene fusions. *Genome Biol.* 2013 Apr 25;14(4):R36. doi: 10.1186/gb-2013-14-4-r36. PMID: 23618408; PMCID: PMC4053844.

Kim K., Weiss L.M. *Toxoplasma gondii*: the model apicomplexan. *Int J Parasitol.* 2004;34(3):423–32.

Kim K.K., Sheppard D., Chapman H.A. TGF-β1 signaling and tissue fibrosis. *Cold Spring Harb Perspect Biol.* 2018 Apr 2;10(4):a022293. doi: 10.1101/cshperspect.a022293. PMID: 28432134; PMCID: PMC5880172.

Kizaki K., Ushizawa K., Takahashi T., Yamada O., Todoroki J., Sato T., Ito A., Hashizume K. Gelatinase (MMP-2 and -9) expression profiles during gestation in the bovine endometrium. *Reprod Biol Endocrinol.* 2008;6:66. doi: 10.1186/1477-7827-6-66.

Krishnan A., Soldati-Favre D. Amino acid metabolism in Apicomplexan parasites. *Metabolites.* 2021 Jan 20;11(2):61. doi: 10.3390/metabo11020061. PMID: 33498308; PMCID: PMC7909243.

Kumi-Diaka J., Wilson S., Sanusi A., Njoku C.E., Osori D.I. Bovine besnoitiosis and its effect on the male reproductive system. *Theriogenology.* 1981;16(5):523–30.

Langenmayer M.C., Scharr J.C., Sauter-Louis C., Schares G., Gollnick N.S. Natural *Besnoitia besnoiti* infections in cattle: Hematological alterations and changes in serum chemistry and enzyme activities. *BMC Vet Res.* 2015;11(1):32. doi: 10.1186/s12917-015-0326-8.

Leirião P., Albuquerque S.S., Corso S., van Gemert G.J., Sauerwein R.W., Rodriguez A., Giordano S., Mota M.M. HGF/MET signalling protects *Plasmodium*-infected host cells from apoptosis. *Cell Microbiol.* 2005 Apr;7(4):603–9. doi: 10.1111/j.1462-5822.2004.00490.x. PMID: 15760460.

Leitao J.L.D.S. Globidiose bovina por *Globidium besnoiti*. *Rev Med Vet (Portugal).* 1949;44(330):152–6.

Leo E., Deveraux Q.L., Buchholtz C., Welsh K., Matsuzawa S., Stennicke H.R., Salvesen G.S., Reed J.C. TRAF1 is a substrate of caspases activated during tumor necrosis factor receptor-alpha-induced apoptosis. *J Biol Chem.* 2001 Mar 16;276(11):8087–93. doi: 10.1074/jbc.M009450200. PMID: 11098060.

Lesser M., Braun U., Deplazes P., Gottstein B., Hilbe M., Basso W. First cases of besnoitiosis in cattle in Switzerland. *Schweiz Arch Tierheilkd.* 2012;154(11):469–74. doi: 10.1024/0036-7281/a000389.

Liénard E., Salem A., Jacquiet P., Grisez C., Prévot F., Blanchard B., Bouhsira E., Franc M. Development of a protocol testing the ability of *Stomoxys calcitrans* to transmit *Besnoitia besnoiti*. *Parasitol Res.* 2013 Feb;112(2):479–86. doi: 10.1007/s00436-012-3157-6. PMID: 23064799; PMCID: PMC3556472.

Liénard E., Pop L., Prevot F., Grisez C., Mallet V., Raymond-Letron I., Bouhsira É., Franc M., Jacquiet P. Experimental infections of rabbits with proliferative and latent stages of *Besnoitia besnoiti*. *Parasitol Res.* 2015 Oct;114(10):3815–3826. doi: 10.1007/s00436-015-4612-y. Epub 2015 Jul 7. PMID: 26143866; PMCID: PMC4562009.

Lima T.S., Lodoen M.B. Mechanisms of human innate immune evasion by *Toxoplasma gondii*. *Front Cell Infect Microbiol.* 2019 Apr 16;9:103. doi: 10.3389/fcimb.2019.00103. PMID: 31041194; PMCID: PMC6476913.

Liu Y., Shepherd E.G., Nelin L.D. MAPK phosphatases – regulating the immune response. *Nat Rev Immunol.* 2007 Mar;7(3):202–212. doi: 10.1038/nri2035. PMID: 17318231.

Livak K.J., Schmittgen T.D. Analysis of relative gene expression data using real-time quantitative PCR and the 2(−ΔΔC(T)) Method. *Methods.* 2001 Dec;25(4):402–408. doi: 10.1006/meth.2001.1262. PMID: 11846609.

Lunghi M., Kloehn J., Krishnan A., Varesio E., Vadas O., Soldati-Favre D. Pantothenate biosynthesis is critical for chronic infection by the neurotropic parasite *Toxoplasma gondii*. *Nat Commun.* 2022 Jan 17;13(1):345. doi: 10.1038/s41467-022-27996-4. PMID: 35039477; PMCID: PMC8764084.

Lv T., Wang C., Zhou J., Feng X., Zhang L., Fan Z. Mechanism and role of nuclear laminin B1 in cell senescence and malignant tumors. *Cell Death Discov.* 2024 Jun 1;10(1):269. doi: 10.1038/s41420-024-02045-9. PMID: 38824174; PMCID: PMC11144256.

Madubata C., Dunams-Morel D.B., Elkin B., Oksanen A., Rosenthal B.M. Evidence for a recent population bottleneck in an apicomplexan parasite of caribou and reindeer, *Besnoitia tarandi*. *Infect Genet Evol.* 2012;12(8):1605–1613. doi: 10.1016/j.meegid.2012.06.007.

Maier T., Güell M., Serrano L. Correlation of mRNA and protein in complex biological samples. *FEBS Lett.* 2009 Dec 17;583(24):3966–3973. doi: 10.1016/j.febslet.2009.10.036. PMID: 19850042.

Majzoub M., Breuer W., Gollnick N.S., Rostaher A., Schares G., Hermanns W. Ein Ausbruch von Besnoitiose bei Rindern in Deutschland: Pathomorphologische, ultrastrukturelle und molekularbiologische Untersuchungen. *Wien Tierarztl Monatssch.* 2010;97:9–15.

Maksimov P., Hermosilla C., Kleinertz S., Hirzmann J., Taubert A. *Besnoitia besnoiti* infections activate primary bovine endothelial cells and promote PMN adhesion and NET formation under physiological flow condition. *Parasitol Res.* 2016 May;115(5):1991–2001. doi: 10.1007/s00436-016-4941-5.

Mammari N., Halabi M.A., Yaacoub S., Chlala H., Dardé M.L., Courtioux B. *Toxoplasma gondii* modulates the host cell responses: an overview of apoptosis pathways. *Biomed Res Int.* 2019 Apr 4;2019:6152489. doi: 10.1155/2019/6152489. PMID: 31080827; PMCID: PMC6475534.

Maroni D., Davis J.S. Transforming growth factor beta 1 stimulates profibrotic activities of luteal fibroblasts in cows. *Biol Reprod.* 2012 Nov 29;87(5):127. doi: 10.1095/biolreprod.112.100735. PMID: 22811573; PMCID: PMC5597442.

Martín-Orozco N., Isibasi A., Ortiz-Navarrete V. Macrophages present exogenous antigens by class I major histocompatibility complex molecules via a secretory pathway as a consequence of interferon-gamma activation. *Immunology.* 2001 May;103(1):41–48. doi: 10.1046/j.0019-2805.2001.01226.x. PMID: 11380691; PMCID: PMC1783223.

Masuda A., Yasuoka H., Satoh T., Okazaki Y., Yamaguchi Y., Kuwana M. Versican is upregulated in circulating monocytes in patients with systemic sclerosis and amplifies a CCL2-mediated pathogenic loop. *Arthritis Res Ther.* 2013 Jul 11;15(4):R74. doi: 10.1186/ar4251. PMID: 23845159; PMCID: PMC3979134.

Matta S.K., Olias P., Huang Z., Wang Q., Park E., Yokoyama W.M., Sibley L.D. *Toxoplasma gondii* effector TgIST blocks type I interferon signaling to promote infection. *Proc Natl Acad Sci U S A.* 2019 Aug 27;116(35):17480–17491. doi: 10.1073/pnas.1904637116. Epub 2019 Aug 14. PMID: 31413201; PMCID: PMC6717281.

Maubon D., Bougdour A., Wong Y.S., Brenier-Pinchart M.P., Curt A., Hakimi M.A., Pelloux H. Activity of the histone deacetylase inhibitor FR235222 on *Toxoplasma gondii*: inhibition of stage conversion of the parasite cyst form and study of new derivative compounds. *Antimicrob Agents Chemother.* 2010 Nov;54(11):4843–4850. doi: 10.1128/AAC.00462-10. Epub 2010 Aug 16. PMID: 20713670; PMCID: PMC2976123.

Mayoral J., Di Cristina M., Carruthers V.B., Weiss L.M. *Toxoplasma gondii*: bradyzoite differentiation in vitro and in vivo. *Methods Mol Biol.* 2020;2071:269–282. doi: 10.1007/978-1-4939-9857-9_15. PMID: 31758458; PMCID: PMC7059825.

McAnulty R.J. Fibroblasts and myofibroblasts: their source, function and role in disease. *Int J Biochem Cell Biol.* 2007;39:666–671. doi: 10.1016/j.biocel.2006.11.005.

McCully R.M., Basson P.A., Van Niekerk J.W., Bigalkie R.D. Observations on *Besnoitia* cysts in the cardiovascular system of some wild antelopes and domestic cattle. *Onderstepoort J Vet Res.* 1966;33(2):245–276.

McKenzie B., Korfei M., Henneke I., Sibinska Z., Tian X., Hezel S., Dilai S., Wasnick R., Schneider B., Wilhelm J., El Agha E., Klepetko W., Seeger W., Schermuly R., Günther A., Bellusci S. Increased FGF1–FGFRc expression in idiopathic pulmonary fibrosis. *Respir Res.* 2015 Jul 3;16(1):83. doi: 10.1186/s12931-015-0242-2. PMID: 26138239; PMCID: PMC4495640.

McWhorter F.Y., Wang T., Nguyen P., Chung T., Liu W.F. Modulation of macrophage phenotype by cell shape. *Proc Natl Acad Sci U S A.* 2013 Oct 22;110(43):17253–17258. doi: 10.1073/pnas.1308887110. Epub 2013 Oct 7. PMID: 24101477; PMCID: PMC3808615.

Melchjorsen J., Rintahaka J., Søby S., Horan K.A., Poltajainen A., Østergaard L., Paludan S.R., Matikainen S. Early innate recognition of Herpes simplex virus in human primary macrophages is mediated via the MDA5/MAVS-dependent and MDA5/MAVS/RNA polymerase III-independent pathways. *J Virol.* 2010 Nov;84(21):11350–11358. doi: 10.1128/JVI.01106-10. Epub 2010 Aug 25. PMID: 20739519; PMCID: PMC2953193.

Melo M.B., Nguyen Q.P., Cordeiro C., Hassan M.A., Yang N., McKell R., Rosowski E.E., Julien L., Butty V., Dardé M.L., Ajzenberg D., Fitzgerald K., Young L.H., Saeij J.P. Transcriptional analysis of murine macrophages infected with different *Toxoplasma* strains identifies novel regulation of host signaling pathways. *PLoS Pathog.* 2013;9(12):e1003779. doi: 10.1371/journal.ppat.1003779. Epub 2013 Dec 19. PMID: 24367253; PMCID: PMC3868521.

Menard K.L., Bu L., Denkers E.Y. Transcriptomics analysis of *Toxoplasma gondii*-infected mouse macrophages reveals coding and noncoding signatures in the presence and absence of MyD88. *BMC Genomics.* 2021 Feb 23;22(1):130. doi: 10.1186/s12864-021-07437-0. PMID: 33622246; PMCID: PMC7903719.

Meng C., Liu G., Mu H., Zhou M., Zhang S., Xu Y. Amphiregulin may be a new biomarker of classically activated macrophages. *Biochem Biophys Res Commun.* 2015 Oct 23;466(3):393–399. doi: 10.1016/j.bbrc.2015.09.037. Epub 2015 Sep 10. PMID: 26365345.

Millán J., Sobrino R., Rodríguez A., Oleaga A., Gortazar C., Schares G. Large-scale serosurvey of *Besnoitia besnoiti* in free-living carnivores in Spain. *Vet Parasitol.* 2012 Nov 23;190(1–2):241–245. doi: 10.1016/j.vetpar.2012.06.014. Epub 2012 Jun 21. PMID: 22770702.

Milner J.M., Rowan A.D., Cawston T.E., Young D.A. Metalloproteinase and inhibitor expression profiling of resorbing cartilage reveals pro-collagenase activation as a critical step for collagenolysis. *Arthritis Res Ther.* 2006;8(5):R142. https://doi.org/10.1186/ar2034.

Minutti C.M., Modak R.V., Macdonald F., Li F., Smyth D.J., Dorward D.A., Blair N., Husovsky C., Muir A., Giampazolias E., Dobie R., Maizels R.M., Kendall T.J., Griggs D.W., Kopf M., Henderson N.C., Zaiss D.M. A macrophage-pericyte axis directs tissue restoration via amphiregulin-induced transforming growth factor beta activation. *Immunity.* 2019 Mar 19;50(3):645–654.e6. doi: 10.1016/j.immuni.2019.01.008. Epub 2019 Feb 12. PMID: 30770250; PMCID: PMC6436929.

Moine E., Denevault-Sabourin C., Debierre-Grockiego F., Silpa L., Gorgette O., Barale J., Jacquiet P., Brossier F., Gueiffier A., Dimier-Poisson I. A small-molecule cell-based screen led to the identification of biphenylimidazoazines with highly potent and broad-spectrum anti-apicomplexan activity. *Eur J Med Chem.* 2015;89:386–400.

Mordue D.G., Monroy F., La Regina M., Dinarello C.A., Sibley L.D. Acute toxoplasmosis leads to lethal overproduction of Th1 cytokines. *J Immunol.* 2001 Oct 15;167(8):4574–4584. doi: 10.4049/jimmunol.167.8.4574. PMID: 11591786.

Müller J., Manser V., Hemphill A. In vitro treatment of *Besnoitia besnoiti* with the naphtoquinone buparvaquone results in marked inhibition of tachyzoite proliferation, mitochondrial alterations and rapid adaptation of tachyzoites to increased drug concentrations. *Parasitology.* 2018;146:112–120.

Muñoz-Caro T., Silva L.M., Ritter C., Taubert A., Hermosilla C. *Besnoitia besnoiti* tachyzoites induce monocyte extracellular trap formation. *Parasitol Res.* 2014;113(11):4189–4197.

Murtha L.A., Schuliga M.J., Mabotuwana N.S., Hardy S.A., Waters D.W., Burgess J.K., Knight D.A., Boyle A.J. The processes and mechanisms of cardiac and pulmonary fibrosis. *Front Physiol.* 2017 Oct 12;8:777. doi: 10.3389/fphys.2017.00777. PMID: 29075197; PMCID: PMC5643461.

Neuman M. Serological survey of *Besnoitia besnoiti* (Marotel 1912) infection in Israel by immunofluorescence. *Zentralbl Veterinarmed B.* 1972;19(5):391–396.

Neuman M. Cultivation of *Besnoitia besnoiti* (Marotel, 1912), in cell culture. *Tropenmed Parasitol.* 1974;25(2):243–249.

Ness S.L., Peters-Kennedy J., Schares G., Dubey J.P., Mittel L.D., Mohammed H.O., Bowman D.D., Felippe M.J., Wade S.E., Shultz N., Divers T.J. Investigation of an outbreak of besnoitiosis in donkeys in northeastern Pennsylvania. *J Am Vet Med Assoc.* 2012;240(11):1329–1337. doi: 10.2460/javma.240.11.1329.

Njenga J., Bwangamoi O., Mutiga E., Kangethe E., Mugera G. Preliminary findings from an experimental study of caprine besnoitiosis in Kenya. *Vet Res Commun.* 1993;17(3):203–208.

Nieto-Rodríguez J.M., Calero-Bernal R., Álvarez-García G., Gutiérrez-Expósito D., Redondo-García E., Fernández-García J.L., Martínez-Estéllez M.Á. Characterization of an outbreak of emerging bovine besnoitiosis in southwestern Spain. *Parasitol Res.* 2016;115(7):2887–2892. doi: 10.1007/s00436-016-5050-1.

Nilsson L.M., Castresana-Aguirre M., Scott L., Brismar H. RNA-seq reveals altered gene expression levels in proximal tubular cell cultures compared to renal cortex but not during early glucotoxicity. *Sci Rep.* 2020 Jun 25;10(1):10390. doi: 10.1038/s41598-020-67361-3. PMID: 32587318; PMCID: PMC7316724.

Nobel T.A., Neumann M., Klopper U., Perl S. Cysts of *Besnoitia besnoiti* in genital organs of the cow. *Bull Acad Med Vet France.* 1981;50:569–574.

Ólafsson E.B., Barragan A. The unicellular eukaryotic parasite *Toxoplasma gondii* hijacks the migration machinery of mononuclear phagocytes to promote its dissemination. *Biol Cell.* 2020 Sep;112(9):239–250. doi: 10.1111/boc.202000005. Epub 2020 May 19. PMID: 32359185.

Olias P., Schade B., Mehlhorn H. Molecular pathology, taxonomy and epidemiology of *Besnoitia* species (Protozoa: Sarcocystidae). *Infect Genet Evol.* 2011;11(7):1564–1576. doi: 10.1016/j.meegid.2011.08.006.

Osherov N., Ben-Ami R. Correction: Modulation of host angiogenesis as a microbial survival strategy and therapeutic target. *PLoS Pathog.* 2016 Aug 17;12(8):e1005838. doi: 10.1371/journal.ppat.1005838. Erratum for: *PLoS Pathog.* 2016 Apr 14;12(4):e1005479. PMID: 27533051; PMCID: PMC4988771.

Osman R., Gonzalez-Cano P., Brownlie R., Griebel P.J. Induction of interferon and interferon-induced antiviral effector genes following a primary bovine herpesvirus-1 (BHV-1) respiratory infection. *J Gen Virol.* 2017;98(7):1831–1842. https://doi.org/10.1099/jgv.0.000825.

Pakshir P., Alizadehgiashi M., Wong B., Coelho N.M., Chen X., Gong Z., Shenoy V.B., McCulloch C.A., Hinz B. Dynamic fibroblast contractions attract remote macrophages in fibrillar collagen matrix. *Nat Commun.* 2019;10:1850. doi: 10.1038/s41467-019-09709-6.

Parker A.L., Kavallaris M., McCarroll J.A. Microtubules and their role in cellular stress in cancer. *Front Oncol.* 2014 Jun 18;4:153. doi: 10.3389/fonc.2014.00153. PMID: 24995158; PMCID: PMC4061531.

Peteshev V.M., Galuzo I.G., Polomoshnov A.P. Koshki – definitivnye khoziaeva besnoitii (*Besnoitia besnoiti*) [Cats – definitive hosts of *Besnoitia besnoiti*]. *Izvest Akad Nauk Kazakh Ser Biol.* 1974;1:33–38.

Papadopoulos E., Arsenos G., Ptochos S., Katsoulos P., Oikonomou G., Karatzia M., Karatzias H. First report of *Besnoitia besnoiti* seropositive cattle in Greece. *J Hellenic Vet Med Soc.*

2014;65(2):115-120.

Parys J.B., Bultynck G., Vervliet T. IP3 receptor biology and endoplasmic reticulum calcium dynamics in cancer. *Prog Mol Subcell Biol.* 2021;59:215–237. doi: 10.1007/978-3-030-67696-4_11. PMID: 34050869.

Pasieka T.J., Baas T., Carter V.S., Proll S.C., Katze M.G., Leib D.A. Functional genomic analysis of Herpes simplex virus type 1 counteraction of the host innate response. *J Virol.* 2006 Aug;80(15):7600–7612. doi: 10.1128/JVI.00333-06. PMID: 16840339; PMCID: PMC1563739.

Piccinini A.M., Midwood K.S. Illustrating the interplay between the extracellular matrix and microRNAs. *Int J Exp Pathol.* 2014 Jun;95(3):158–180. doi: 10.1111/iep.12079. Epub 2014 Apr 25. PMID: 24761792; PMCID: PMC4351853.

Pierog P.L., Zhao Y., Singh S., Dai J., Yap G.S., Fitzgerald-Bocarsly P. *Toxoplasma gondii* inactivates human plasmacytoid dendritic cells by functional mimicry of IL-10. *J Immunol.* 2018 Jan 1;200(1):186–195. doi: 10.4049/jimmunol.1701045. Epub 2017 Nov 27. PMID: 29180487; PMCID: PMC7441501.

Piersma B., Hayward M.K., Weaver V.M. Fibrosis and cancer: a strained relationship. *Biochim Biophys Acta Rev Cancer.* 2020 Apr;1873(2):188356. doi: 10.1016/j.bbcan.2020.188356. Epub 2020 Mar 5. PMID: 32147542; PMCID: PMC7733542.

Pols J.W. Studies on bovine besnoitiosis with special reference to the aetiology. *Onderstepoort J Vet Res.* 1960;28(3):265–356.

Puech C., Dedieu L., Chantal I., Rodrigues V. Design and evaluation of a unique SYBR Green real-time RT-PCR assay for quantification of five major cytokines in cattle, sheep and goats. *BMC Vet Res.* 2015 Mar 17;11:65. doi: 10.1186/s12917-015-0382-0. PMID: 25889787; PMCID: PMC4369058.

Radke J.B., Lucas O., De Silva E.K., Ma Y., Sullivan W.J. Jr., Weiss L.M., Llinas M., White M.W. ApiAP2 transcription factor restricts development of the *Toxoplasma* tissue cyst. *Proc Natl Acad Sci U S A.* 2013 Apr 23;110(17):6871–6876. doi: 10.1073/pnas.1300059110. Epub 2013 Apr 9. PMID: 23572590; PMCID: PMC3637731.

Rana M., Kumar A., Tiwari R.L., Singh V., Chandra T., Dikshit M., Barthwal M.K. IRAK regulates macrophage foam cell formation by modulating genes involved in cholesterol uptake and efflux. *Bioessays.* 2016 Jul;38(7):591–604. doi: 10.1002/bies.201600085. Epub 2016 Jun 8. PMID: 27270491.

Ramakrishnan C., Krishnan A., Francisco S., Schmid M.W., Russo G., Leitão A., Hemphill A., Soldati-Favre D., Hehl A.B. Dissection of *Besnoitia besnoiti* intermediate host life cycle stages: from morphology to gene expression. *PLoS Pathog.* 2022 Nov 17;18(11):e1010955. doi: 10.1371/journal.ppat.1010955. PMID: 36395346; PMCID: PMC9714946.

Rao K.M. MAP kinase activation in macrophages. *J Leukoc Biol.* 2001 Jan;69(1):3–10. PMID: 11200064.

Reese M.L., Zeiner G.M., Saeij J.P., Boothroyd J.C., Boyle J.P. Polymorphic family of injected pseudokinases is paramount in *Toxoplasma* virulence. *Proc Natl Acad Sci U S A.* 2011 Jun 7;108(23):9625–9630. doi: 10.1073/pnas.1015980108. Epub 2011 Mar 21. PMID: 21436047; PMCID: PMC3111280.

Regidor-Cerrillo J., Gómez-Bautista M., Sodupe I., Aduriz G., Álvarez-García G., Del Pozo I., Ortega-Mora L.M. In vitro invasion efficiency and intracellular proliferation rate comprise virulence-related phenotypic traits of *Neospora caninum*. *Vet Res.* 2011 Feb 23;42(1):41. doi: 10.1186/1297-9716-42-41. PMID: 21345202; PMCID: PMC3052184.

Rinaldi L., Maurelli M.P., Musella V., Bosco A., Cortes H., Cringoli G. First cross-sectional serological survey on *Besnoitia besnoiti* in cattle in Italy. *Parasitol Res.* 2013 Apr;112(4):1805–1807. doi: 10.1007/s00436-012-3241-y. Epub 2012 Dec 30. PMID: 23274487.

Risco-Castillo V., Fernández-García A., Ortega-Mora L.M. Comparative analysis of stress agents in a simplified in vitro system of *Neospora caninum* bradyzoite production. *J Parasitol.* 2004;90(3):466–470.

Risco-Castillo V. *Identificación y caracterización de antígenos específicos del estadio de bradizoíto de Neospora caninum*. Doctoral dissertation. Madrid (Spain): Universidad Complutense de Madrid; 2008.

Rocha C.C., da Silva Andrade S.C., de Melo G.D., Motta I.G., Coutinho L.L., Gonella-Diaza A.M., Binelli M., Pugliesi G. Early pregnancy-induced transcripts in peripheral blood immune cells in *Bos indicus* heifers. *Sci Rep.* 2020;10(1):13733. https://doi.org/10.1038/s41598-020-70616-8.

Rosa R.B., Dantas W.M., do Nascimento J.C.F., da Silva M.V., de Oliveira R.N., Pena L.J. In vitro and in vivo models for studying SARS-CoV-2, the etiological agent responsible for COVID-19 pandemic. *Viruses.* 2021 Feb 27;13(3):379. doi: 10.3390/v13030379. PMID: 33673614; PMCID: PMC7997194.

Rosenberg A., Sibley L.D. *Toxoplasma gondii* secreted effectors co-opt host repressor complexes to inhibit necroptosis. *Cell Host Microbe.* 2021 Jul 14;29(7):1186–1198.e8. doi: 10.1016/j.chom.2021.04.016. Epub 2021 May 26. PMID: 34043960; PMCID: PMC8711274.

Rostaher A., Mueller R.S., Majzoub M., Schares G., Gollnick N.S. Bovine besnoitiosis in Germany. *Vet Dermatol.* 2010;21:329–334. doi: 10.1111/j.1365-3164.2009.00813.x.

Ryan E.G., Lee A., Carty C., O'Shaughnessy J., Kelly P., Cassidy J.P., Sheehan M., Johnson A., de Waal T. Bovine besnoitiosis (*Besnoitia besnoiti*) in an Irish dairy herd. *Vet Rec.* 2016;178(24):608–615. doi: 10.1136/vr.103683.

Saegerman C., Evrard J., Houtain J.Y., Alzieu J.P., Bianchini J., Mpouam S.E., Schares G., Liénard E., Jacquiet P., Villa L., Álvarez-García G., Gazzonis A.L., Gentile A., Delooz L. First expert elicitation of knowledge on drivers of emergence of bovine besnoitiosis in Europe. *Pathogens.* 2022 Jul 1;11(7):753. doi: 10.3390/pathogens11070753. PMID: 35889998; PMCID: PMC9323894.

Sambo S., Ibrahim N.D.G., Esievo K.A.N., Kazeem H.M. Prevalence of *Besnoitia besnoiti* antibodies in bovine sera and milk in Northern Nigeria. *Sokoto J Vet Sci.* 2014;12(1):29. doi: 10.4314/sokjvs.v12i1.5.

Samish M., Shkap V., Bin H., Pipano E.M. Cultivation of *Besnoitia besnoiti* in four tick cell lines. *Int J Parasitol.* 1988;18(3):291–296.

Sánchez R., Mohr I. Inhibition of cellular 2'-5' oligoadenylate synthetase by the Herpes simplex virus type 1 Us11 protein. *J Virol.* 2007 Apr;81(7):3455–3464. doi: 10.1128/JVI.02520-06. Epub 2007 Jan 17. PMID: 17229694; PMCID: PMC1866071.

Schares G., Basso W., Majzoub M., Cortes H.C., Rostaher A., Selmair J., Hermanns W., Conraths F.J., Gollnick N.S. First in vitro isolation of *Besnoitia besnoiti* from chronically infected cattle in Germany. *Vet Parasitol.* 2009;163(4):315–322. doi: 10.1016/j.vetpar.2009.04.033.

Schares G., Venepally P., Lorenzi H.A. Draft genome sequence and annotation of the apicomplexan parasite *Besnoitia besnoiti*. *Genome Announc.* 2017;5(46).

Schares G., Joeres M., Rachel F., Tuschy M., Czirják G.Á., Maksimov P., Conraths F.J., Wachter

B. Molecular analysis suggests that Namibian cheetahs (*Acinonyx jubatus*) are definitive hosts of a so far undescribed *Besnoitia* species. *Parasit Vectors.* 2021 Apr 14;14(1):201. doi: 10.1186/s13071-021-04697-3. PMID: 33853647; PMCID: PMC8048190.

Schneider A.G., Abi Abdallah D.S., Butcher B.A., Denkers E.Y. *Toxoplasma gondii* triggers phosphorylation and nuclear translocation of dendritic cell STAT1 while simultaneously blocking IFNγ-induced STAT1 transcriptional activity. *PLoS One.* 2013;8(3):e60215. doi: 10.1371/journal.pone.0060215. PMID: 23527309; PMCID: PMC3603897.

Schuliga M., Jaffar J., Harris T., Knight D.A., Westall G., Stewart A.G. The fibrogenic actions of lung fibroblast-derived urokinase: a potential drug target in IPF. *Sci Rep.* 2017 Jan 31;7:41770. doi: 10.1038/srep41770. PMID: 28139758; PMCID: PMC5282574.

Schulz K.C.A. A report on naturally acquired besnoitiosis in bovines with special reference to its pathology. *J S Afr Vet Med Assoc.* 1960;31:21–35.

Sharif S, Jacquiet P, Prevot F, Grisez C, Raymond-Letron I, Semin MO, Geffré A, Trumel C, Franc M, Bouhsira É, Liénard E. Stomoxys calcitrans, mechanical vector of virulent *Besnoitia besnoiti* from chronically infected cattle to susceptible rabbit. Med Vet Entomol. 2019 Jun;33(2):247-255. doi: 10.1111/mve.12356. Epub 2019 Jan 21. PMID: 30666684; PMCID: PMC6850491.

Shkap V., De Waal D.T., Potgieter F.T. Chemotherapy of experimental *Besnoitia besnoiti* infection in rabbits. *Onderstepoort J Vet Res.* 1985;52(4):289.

Shkap V. *Antigenicity of Besnoitia besnoiti with special reference to prophylactic immunization*. Doctoral Thesis. Hebrew University, Jerusalem; 1986.

Shkap V., Pipano E., Ungar-Waron H. *Besnoitia besnoiti*: Chemotherapeutic trials in vivo and in vitro. *Rev Elev Med Vet Pays Trop.* 1987;40(3):259–264.

Shkap V., Pipano E., Marcus S., Krigel Y. Bovine besnoitiosis: transfer of colostral antibodies with observations possibly relating to natural transmission of the infection. *Onderstepoort J Vet Res.* 1994;61(3):273–275.

Shkap V., Reske A., Pipano E., Fish L., Baszler T. Immunological relationship between *Neospora caninum* and *Besnoitia besnoiti*. *Vet Parasitol.* 2002 May 30;106(1):35–43. doi: 10.1016/s0304-4017(02)00030-4. PMID: 11992709.

Shmakova A.A., Popov V.S., Romanov I.P., Khabibullin N.R., Sabitova N.R., Karpukhina A.A., Kozhevnikova Y.A., Kurilina E.V., Tsokolaeva Z.I., Klimovich P.S., Rubina K.A., Vassetzky Y.S., Semina E.V. Urokinase system in pathogenesis of pulmonary fibrosis: a hidden threat of COVID-19. *Int J Mol Sci.* 2023 Jan 10;24(2):1382. doi: 10.3390/ijms24021382. PMID: 36674896; PMCID: PMC9867169.

Shrestha K., Lukasik K., Baufeld A., Vanselow J., Moallem U., Meidan R. Regulation of ovulatory genes in bovine granulosa cells: lessons from siRNA silencing of *PTGS2*. *Reproduction.* 2015;149(1):21–29. https://doi.org/10.1530/REP-14-0337.

Sierra-Filardi E., Nieto C., Domínguez-Soto A., Barroso R., Sánchez-Mateos P., Puig-Kröger A., López-Bravo M., Joven J., Ardavín C., Rodríguez-Fernández J.L., Sánchez-Torres C., Mellado M., Corbí A.L. CCL2 shapes macrophage polarization by GM-CSF and M-CSF: identification of CCL2/CCR2-dependent gene expression profile. *J Immunol.* 2014 Apr 15;192(8):3858–3867. doi: 10.4049/jimmunol.1302821. Epub 2014 Mar 17. PMID: 24639350.

Sitali M.C., Schmidt V., Mwenda R., Sikasunge C.S., Mwape K.E., Simuunza M.C., et al. Experimental animal models and their use in understanding cysticercosis: a systematic review. *PLOS ONE.* 2022;17(7):e0271232. doi: 10.1371/journal.pone.0271232.

Skariah S., McIntyre M.K., Mordue D.G. *Toxoplasma gondii*: determinants of tachyzoite to bradyzoite conversion. *Parasitol Res.* 2010 Jul;107(2):253–260. doi: 10.1007/s00436-010-1899-6. Epub 2010 Jun 1. PMID: 20514494; PMCID: PMC3327608.

Soares-Silva M., Diniz F.F., Gomes G.N., Bahia D. The Mitogen-Activated Protein Kinase (MAPK) pathway: role in immune evasion by trypanosomatids. *Front Microbiol.* 2016 Feb 24;7:183. doi: 10.3389/fmicb.2016.00183. PMID: 26941717; PMCID: PMC4764696.

Soête M., Camus D., Dubremetz J.F. Experimental induction of bradyzoite-specific antigen expression and cyst formation by the RH strain of *Toxoplasma gondii* in vitro. *Exp Parasitol.* 1994 Jun;78(4):361–370. doi: 10.1006/expr.1994.1039. PMID: 8206135.

Sokol-Borrelli S.L., Coombs R.S., Boyle J.P. A comparison of stage conversion in the coccidian apicomplexans *Toxoplasma gondii*, *Hammondia hammondi*, and *Neospora caninum*. *Front Cell Infect Microbiol.* 2020 Dec 3;10:608283. doi: 10.3389/fcimb.2020.608283. PMID: 33344268; PMCID: PMC7744739.

Sonda S., Fuchs N., Connolly B., Fernandez P., Gottstein B., Hemphill A. The major 36 kDa *Neospora caninum* tachyzoite surface protein is closely related to the major *Toxoplasma gondii* surface antigen. *Mol Biochem Parasitol.* 1998 Nov 30;97(1–2):97–108. doi: 10.1016/s0166-6851(98)00133-9. PMID: 9879890.

Sousa A.M., Liu T., Guevara O., Stevens J., Fanburg B.L., Gaestel M., Toksoz D., Kayyali U.S. Smooth muscle alpha-actin expression and myofibroblast differentiation by TGF-beta are dependent upon MK2. *J Cell Biochem.* 2006 Apr 15;100(6):1581–1592. doi: 10.1002/jcb.21154. PMID: 17163490; PMCID: PMC2586991.

Spadaro F., Cecchetti S., Fantuzzi L. Macrophages and phospholipases at the intersection between inflammation and the pathogenesis of HIV-1 infection. *Int J Mol Sci.* 2017 Jun 29;18(7):1390. doi: 10.3390/ijms18071390. PMID: 28661459; PMCID: PMC5535883.

Speer C.A., Dubey J.P., McAllister M.M., Blixt J.A. Comparative ultrastructure of tachyzoites, bradyzoites and tissue cysts of *Neospora caninum* and *Toxoplasma gondii*. *Int J Parasitol.* 1999 Oct;29(10):1509–1519.

Shkap V. Antigenicity of *Besnoitia besnoiti* with special reference to prophylactic immunization. Doctoral Thesis. Hebrew University, Jerusalem; 1986.

Stafford J.L., Neumann N.F., Belosevic M. Macrophage-mediated innate host defense against protozoan parasites. *Crit Rev Microbiol.* 2002;28(3):187–248. doi: 10.1080/1040-840291046731. PMID: 12385499.

Su X., Yu Y., Zhong Y., et al. Interferon-γ regulates cellular metabolism and mRNA translation to potentiate macrophage activation. *Nat Immunol.* 2015;16:838–849. https://doi.org/10.1038/ni.3205.

Su C., Zhan G., Zheng C. Evasion of host antiviral innate immunity by HSV-1, an update. *Virol J.* 2016 Mar 8;13:38. doi: 10.1186/s12985-016-0495-5. PMID: 26952111; PMCID: PMC4782282.

Sullivan W.J. Jr., Jeffers V. Mechanisms of *Toxoplasma gondii* persistence and latency. *FEMS Microbiol Rev.* 2012 May;36(3):717–733. doi: 10.1111/j.1574-6976.2011.00305.x. Epub 2011 Oct 4. PMID: 22091606; PMCID: PMC3319474.

Sun L., Jiang Z., Acosta-Rodriguez V.A., Berger M., Du X., Choi J.H., Wang J., Wang K.W., Kilaru G.K., Mohawk J.A., Quan J., Scott L., Hildebrand S., Li X., Tang M., Zhan X., Murray A.R., La Vine D., Moresco E.M.Y., Takahashi J.S., Beutler B. HCFC2 is needed for IRF1- and IRF2-dependent Tlr3 transcription and for survival during viral infections. *J Exp Med.* 2017 Nov 6;214(11):3263–3277. doi: 10.1084/jem.20161630. Epub 2017 Oct 2. PMID: 28970238; PMCID:

PMC5679162.

Sugawara K., Kizaki K., Herath C.B., Hasegawa Y., Hashizume K. Transforming growth factor beta family expression at the bovine feto-maternal interface. *Reprod Biol Endocrinol.* 2010;8:120. https://doi.org/10.1186/1477-7827-8-120.

Talafha A.Q., Al-Majali A.M., Ababneh M.M., Abutarbush S.M. Epidemiologic study on *Besnoitia besnoiti* infection in dairy herds in Jordan. *Parasitol Res.* 2015 Jul;114(7):2491–2497. doi: 10.1007/s00436-015-4448-5.

Tan C., Jiang Y., Shao W., Shi W., Gao X., Qin W., Jiang T., Wang F., Feng S. Abnormal expression of FOSB correlates with tumor progression and poor survival in patients with gastric cancer. *Int J Oncol.* 2016 Oct;49(4):1489–1496. doi: 10.3892/ijo.2016.3661. Epub 2016 Aug 18. PMID: 27633497.

Ticianelli J.S., Emanuelli I.P., Satrapa R.A., Castilho A.C., Loureiro B., Sudano M.J., Fontes P.K., Pinto R.F., Razza E.M., Surjus R.S., Sartori R., Assumpção M.E., Visintin J.A., Barros C.M., Paula-Lopes F.F. Gene expression profile in heat-shocked Holstein and Nelore oocytes and cumulus cells. *Reprod Fertil Dev.* 2017;29(9):1787. https://doi.org/10.1071/rd16154.

Timmer T., de Vries E.G., de Jong S. Fas receptor-mediated apoptosis: a clinical application? *J Pathol.* 2002 Feb;196(2):125–134. doi: 10.1002/path.1028. PMID: 11793363.

Tomavo S., Boothroyd J.C. Interconnection between organellar functions, development and drug resistance in the protozoan parasite, *Toxoplasma gondii*. *Int J Parasitol.* 1995 Nov;25(11):1293–1299. doi: 10.1016/0020-7519(95)00066-b. PMID: 8635881.

Tracy L.E., Minasian R.A., Caterson E.J. Extracellular matrix and dermal fibroblast function in the healing wound. *Adv Wound Care.* 2016;5:119–136. doi: 10.1089/wound.2014.0561.

Turner C., Devitt A., Parker K., MacFarlane M., Giuliano M., Cohen G.M., Gregory C.D. Macrophage-mediated clearance of cells undergoing caspase-3-independent death. *Cell Death Differ.* 2003 Mar;10(3):302–312. doi: 10.1038/sj.cdd.4401170. PMID: 12700630.

Vanagas L., Jeffers V., Bogado S.S., Dalmasso M.C., Sullivan W.J. Jr., Angel S.O. *Toxoplasma* histone acetylation remodelers as novel drug targets. *Expert Rev Anti Infect Ther.* 2012 Oct;10(10):1189–1201. doi: 10.1586/eri.12.100. PMID: 23199404; PMCID: PMC3581047.

Velásquez Z.D., Lopez-Osorio S., Pervizaj-Oruqaj L., Herold S., Hermosilla C., Taubert A. *Besnoitia besnoiti*-driven endothelial host cell cycle alteration. *Parasitol Res.* 2020 Aug;119(8):2563–2577. doi: 10.1007/s00436-020-06744-x. Epub 2020 Jun 17. PMID: 32548739; PMCID: PMC7366594.

Waap H., Nunes T., Cortes H., Leitao A., Vaz Y. Prevalence and geographic distribution of *Besnoitia besnoiti* infection in cattle herds in Portugal. *Parasitol Res.* 2014 Oct;113(10):3703–3711. doi: 10.1007/s00436-014-4035-1.

Wallace G.D., Frenkel J.K. *Besnoitia* species (Protozoa, Sporozoa, Toxoplasmatidae): recognition of cyclic transmission by cats. *Science.* 1975;188(4186):369–371.

Waldman B.S., Schwarz D., Wadsworth M.H. 2nd, Saeij J.P., Shalek A.K., Lourido S. Identification of a master regulator of differentiation in *Toxoplasma*. *Cell.* 2020 Jan 23;180(2):359–372.e16. doi: 10.1016/j.cell.2019.12.013. Epub 2020 Jan 16. PMID: 31955846; PMCID: PMC6978799.

Walton K.L., Johnson K.E., Harrison C.A. Targeting TGF-β mediated SMAD signaling for the prevention of fibrosis. *Front Pharmacol.* 2017 Jul 14;8:461. doi: 10.3389/fphar.2017.00461. PMID: 28769795; PMCID: PMC5509761.

Wang H., Wang Q., Pape U.J., Shen B., Huang J., Wu B., Li X. Systematic investigation of global coordination among mRNA and protein in cellular society. *BMC Genomics.* 2010 Jun 9;11:364. doi: 10.1186/1471-2164-11-364. PMID: 20529381; PMCID: PMC2900266.

Wang P., Li S., Zhao Y., Zhang B., Li Y., Liu S., Du H., Cao L., Ou M., Ye X., Li P., Gao X., Wang P., Jing C., Shao F., Yang G., You F. The GRA15 protein from *Toxoplasma gondii* enhances host defense responses by activating the interferon stimulator STING. *J Biol Chem.* 2019 Nov 8;294(45):16494–16508. doi: 10.1074/jbc.RA119.009172. Epub 2019 Aug 15. PMID: 31416833; PMCID: PMC6851339.

Wang J., Hu K., Cai X., Yang B., He Q., Wang J., Weng Q. Targeting PI3K/AKT signaling for treatment of idiopathic pulmonary fibrosis. *Acta Pharm Sin B.* 2022 Jan;12(1):18–32. doi: 10.1016/j.apsb.2021.07.023. Epub 2021 Jul 29. PMID: 35127370; PMCID: PMC8799876.

Weidner J.M., Kanatani S., Hernández-Castañeda M.A., Fuks J.M., Rethi B., Wallin R.P., Barragan A. Rapid cytoskeleton remodelling in dendritic cells following invasion by *Toxoplasma gondii* coincides with the onset of a hypermigratory phenotype. *Cell Microbiol.* 2013 Oct;15(10):1735–1752. doi: 10.1111/cmi.12145. Epub 2013 Apr 17. PMID: 23534541.

Weiss L.M., Laplace D., Takvorian P.M., Tanowitz H.B., Cali A., Wittner M. A cell culture system for study of the development of *Toxoplasma gondii* bradyzoites. *J Eukaryot Microbiol.* 1995 Mar–Apr;42(2):150–157. doi: 10.1111/j.1550-7408.1995.tb01556.x. PMID: 7757057.

Weiss L.M., Ma Y.F., Takvorian P.M., Tanowitz H.B., Wittner M. Bradyzoite development in *Toxoplasma gondii* and the hsp70 stress response. *Infect Immun.* 1998 Jul;66(7):3295–3302. doi: 10.1128/IAI.66.7.3295-3302.1998. PMID: 9632598; PMCID: PMC108345.

Weiss L.M., Ma Y.F., Halonen S., McAllister M.M., Zhang Y.W. The in vitro development of *Neospora caninum* bradyzoites. *Int J Parasitol.* 1999 Oct;29(10):1713–1723. doi: 10.1016/s0020-7519(99)00130-7. PMID: 10608459; PMCID: PMC3086365.

Weiss L.M., Kim K. The development and biology of bradyzoites of *Toxoplasma gondii*. *Front Biosci.* 2000 Apr 1;5:D391–405. doi: 10.2741/weiss. PMID: 10762601; PMCID: PMC3109641.

Wessels I., Maywald M., Rink L. Zinc as a gatekeeper of immune function. *Nutrients.* 2017 Nov 25;9(12):1286. doi: 10.3390/nu9121286. PMID: 29186856; PMCID: PMC5748737.

Wight T.N., Potter-Perigo S. The extracellular matrix: an active or passive player in fibrosis? *Am J Physiol Gastrointest Liver Physiol.* 2011 Dec;301(6):G950–G955. doi: 10.1152/ajpgi.00132.2011. Epub 2011 Apr 21. PMID: 21512158; PMCID: PMC3233785.

Winzer P., Müller J., Imhof D., Ritler D., Uldry A.C., Braga-Lagache S., Heller M., Ojo K.K., Van Voorhis W.C., Ortega-Mora L.M., Hemphill A. *Neospora caninum*: differential proteome of multinucleated complexes induced by the Bumped Kinase Inhibitor BKI-1294. *Microorganisms.* 2020 May 26;8(6):801. doi: 10.3390/microorganisms8060801. PMID: 32466554; PMCID: PMC7355844.

Wortel I.M.N., van der Meer L.T., Kilberg M.S., van Leeuwen F.N. Surviving stress: modulation of ATF4-mediated stress responses in normal and malignant cells. *Trends Endocrinol Metab.* 2017 Nov;28(11):794–806. doi: 10.1016/j.tem.2017.07.003. Epub 2017 Aug 7. PMID: 28797581; PMCID: PMC5951684.

Wu W., Chen Q., Zou W., Chen J., Zhu D., Yang H., Ouyang L., Liu X., Peng H. *Toxoplasma gondii* bradyzoite-specific BAG1 is nonessential for cyst formation due to compensation by other heat-shock proteins. *Parasit Vectors.* 2024 Jul 30;17(1):322. doi: 10.1186/s13071-024-06339-w. PMID: 39080770; PMCID: PMC11290284.

Xuan Y., Chen C., Wen Z., Wang D.W. The roles of cardiac fibroblasts and endothelial cells in

myocarditis. *Front Cardiovasc Med.* 2022;9:882027. doi: 10.3389/fcvm.2022.882027.

Yao L., Rathnakar B.H., Kwon H.R., Sakashita H., Kim J.H., Rackley A., Tomasek J.J., Berry W.L., Olson L.E. Temporal control of pdgfrα regulates the fibroblast-to-myofibroblast transition in wound healing. Cell Rep. 2022;40:111192. doi: 10.1016/j.celrep.2022.111192.

Yonekura, S., Tsuchiya, M., Tokutake, Y., Mizusawa, M., Nakano, M., Miyaji, M., Ishizaki, H., Haga, S., 2018. The unfolded protein response is involved in both differentiation and apoptosis of bovine mammary epithelial cells. J. Dairy Sci. 101(4), 3568–3578. https://doi.org/10.3168/jds.2017-13718.

Zeng H., Qi X., Xu X., Wu Y. TAB1 regulates glycolysis and activation of macrophages in diabetic nephropathy. *Inflamm Res.* 2020 Dec;69(12):1215–1234. doi: 10.1007/s00011-020-01411-4. Epub 2020 Oct 12. PMID: 33044562; PMCID: PMC7658079.

Zhang X.L., Xing R.G., Chen L., Liu C.R., Miao Z.G. PI3K/Akt signaling is involved in the pathogenesis of bleomycin-induced pulmonary fibrosis via regulation of epithelial–mesenchymal transition. *Mol Med Rep.* 2016 Dec;14(6):5699–5706. doi: 10.3892/mmr.2016.5960. Epub 2016 Nov 22. PMID: 27878273.

Zhao X., Chen J., Sun H., Zhang Y., Zou D. New insights into fibrosis from the ECM degradation perspective: the macrophage-MMP-ECM interaction. *Cell Biosci.* 2022 Jul 27;12(1):117. doi: 10.1186/s13578-022-00856-w. Erratum in: *Cell Biosci.* 2022 Aug 26;12(1):138. doi: 10.1186/s13578-022-00881-9. PMID: 35897082; PMCID: PMC9327238.

Zheng M., Karki R., Vogel P., Kanneganti T.D. Caspase-6 Is a Key Regulator of Innate Immunity, Inflammasome Activation, and Host Defense. *Cell.* 2020 Apr 30;181(3):674–687.e13. doi: 10.1016/j.cell.2020.03.040. Epub 2020 Apr 15. PMID: 32298652; PMCID: PMC7425208.

Zheng Z.Q., Fu Y.Z., Wang S.Y., Xu Z.S., Zou H.M., Wang Y.Y. Herpes simplex virus protein UL56 inhibits cGAS-mediated DNA sensing to evade antiviral immunity. *Cell Insight.* 2022 Feb 12;1(2):100014. doi: 10.1016/j.cellin.2022.100014. PMID: 37193132; PMCID: PMC10120305.

Zheng K.X., Yuan S.L., Dong M., Zhang H.L., Jiang X.X., Yan C.L., Ye R.C., Zhou H.Q., Chen L., Jiang R., Cheng Z.Y., Zhang Z., Wang Q., Jin W.Z., Xie W. Dihydroergotamine ameliorates liver fibrosis by targeting transforming growth factor β type II receptor. World J Gastroenterol. 2023 May 28;29(20):3103-3118. doi: 10.3748/wjg.v29.i20.3103. PMID: 37346154; PMCID: PMC10280794.

Zhou E., Conejeros I., Velásquez Z.D., Muñoz-Caro T., Gärtner U., Hermosilla C., Taubert A. Simultaneous and positively correlated NET formation and autophagy in *Besnoitia besnoiti* tachyzoite-exposed bovine polymorphonuclear neutrophils. Front Immunol. 2019 May 22;10:1131. doi: 10.3389/fimmu.2019.01131. PMID: 31191523; PMCID: PMC6540735.

Zhou E., Conejeros I., Gärtner U., Mazurek S., Hermosilla C., Taubert A. Metabolic requirements of *Besnoitia besnoiti* tachyzoite-triggered NETosis. Parasitol Res. 2020 Feb;119(2):545-557. doi: 10.1007/s00436-019-06543-z. Epub 2019 Nov 28. PMID: 31782011.

# Chapter IX: Appendices

# Chapter IX: Appendices

The present Doctoral Thesis includes results that have been published in the following articles:

1. Fernández-Álvarez M, Horcajo P, Jiménez-Meléndez A, Diezma-Díaz C, Ferre I, Pastor-Fernández I, Ortega-Mora LM, Álvarez-García G. Transcriptional changes associated with apoptosis and type I IFN underlie the early interaction between *Besnoitia besnoiti* tachyzoites and monocyte-derived macrophages. Int J Parasitol. 2023 Aug;53(9):505-521. doi: 10.1016/j.ijpara.2023.05.002. Epub 2023 May 18. PMID: 37207972.
2. Fernández-Álvarez M, Horcajo P, Jiménez-Meléndez A, Lara PA, Huertas-López A, Huertas-López F, Ferre I, Ortega-Mora LM, Álvarez-García G. Transcriptomics of *Besnoitia besnoiti*-Infected Fibroblasts Reveals Hallmarks of Early Fibrosis and Cancer Progression. Microorganisms. 2024 Mar 15;12(3):586. doi: 10.3390/microorganisms12030586. PMID: 38543637; PMCID: PMC10975890.

These publications have been integrated into the relevant chapters of the present Doctoral Thesis and are also included in full as appendices at the end of the document.

International Journal for Parasitology 53 (2023) 505–521

Contents lists available at ScienceDirect

International Journal for Parasitology

journal homepage: www.elsevier.com/locate/ijpara

# Transcriptional changes associated with apoptosis and type I IFN underlie the early interaction between *Besnoitia besnoiti* tachyzoites and monocyte-derived macrophages ☆

María Fernández-Álvarez, Pilar Horcajo, Alejandro Jiménez-Meléndez, Carlos Diezma-Díaz, Ignacio Ferre, Iván Pastor-Fernández, Luis Miguel Ortega-Mora, Gema Álvarez-García *

*SALUVET, Animal Health Department, Faculty of Veterinary Sciences, Complutense University of Madrid, Spain*[1]

ARTICLE INFO

*Article history:*
Received 7 November 2022
Received in revised form 3 April 2023
Accepted 3 May 2023
Available online 18 May 2023

*Keywords:*
*Besnoitia besnoiti*
Bovine monocyte-derived macrophages
Lytic cycle
RNA-Seq
Apoptosis
MAPKs
Type I IFN

ABSTRACT

*Besnoitia besnoiti*-infected bulls may develop severe systemic clinical signs and orchitis that may ultimately cause sterility during the acute infection. Macrophages might play a relevant role in pathogenesis of the disease and the immune response raised against *B. besnoiti* infection. This study aimed to dissect the early interaction between *B. besnoiti* tachyzoites and primary bovine monocyte-derived macrophages in vitro. First, the *B. besnoiti* tachyzoite lytic cycle was characterized. Next, dual transcriptomic profiling of *B. besnoiti* tachyzoites and macrophages was conducted at early infection (4 and 8 h p.i.) by high-throughput RNA sequencing. Macrophages inoculated with heat-killed tachyzoites (MO-hkBb) and non-infected macrophages (MO) were used as controls. *Besnoitia besnoiti* was able to invade and proliferate in macrophages. Upon infection, macrophage activation was demonstrated by morphological and transcriptomic changes. Infected macrophages were smaller, round and lacked filopodial structures, which might be associated with a migratory phenotype demonstrated in other apicomplexan parasites. The number of differentially expressed genes (DEGs) increased substantially during infection. In *B. besnoiti*-infected macrophages (MO-Bb), apoptosis and mitogen-activated protein kinase (MAPK) pathways were regulated at 4 h p.i., and apoptosis was confirmed by TUNEL assay. The *Herpes simplex* virus 1 infection pathway was the only significantly enriched pathway in MO-Bb at 8 h p.i. Relevant DEGs of the *Herpes simplex* virus 1 infection (*IFNα*) and the apoptosis pathways (*CHOP-2*) were also significantly regulated in the testicular parenchyma of naturally infected bulls. Furthermore, the parasite transcriptomic analysis revealed DEGs mainly related to host cell invasion and metabolism. These results provide a deep overview of the earliest macrophage modulation by *B. besnoiti* that may favour parasite survival and proliferation in a specialized phagocytic immune cell. Putative parasite effectors were also identified.


## 1. Introduction

Bovine besnoitiosis is a parasitic disease caused by the intracellular pathogen *Besnoitia besnoiti,* a protist cyst-forming apicomplexan parasite closely related to *Toxoplasma gondii* and *Neospora caninum*. The disease relevance relies on the significant financial hardship inflicted through cattle raised under extensive husbandry systems. Bull sterility, loss of body condition and skin lesions impair production and reproduction parameters (Álvarez-García et al., 2013).

The clinical course of bovine besnotiosis develops in two sequential stages. At an early stage, rapidly replicating tachyzoites may infect target cells such as endothelial cells and macrophages, causing fever, depression, anorexia, subcutaneous oedema, nasal and ocular discharge, respiratory disorders and orchitis. At a later stage, tachyzoites switch into slowly dividing bradyzoites that gather inside tissue cysts in myofibroblasts and fibroblasts, mainly in subcutaneous tissues (Álvarez-García et al., 2013, 2014; Gollnick et al., 2015). Clinical manifestations of chronically infected animals are skin lesions (hyperkeratosis, folding, alopecia, nodules and scars in the udder) and pathognomonic visible tissue cysts in the scleral conjunctive and vestibulum vaginae. Orchitis evolves to scrotal skin thickening and results in testicular atrophy and sterility. Clinical signs and lesion severity are variable. Indeed, most animals remain subclinically infected and a small percentage develop visible and severe clinical signs and lesions which

☆ Note: Nucleotide sequence data reported in this paper is available in GenBank under accession number **PRJNA785130**.

* Corresponding author.
*E-mail address:* gemaga@ucm.es (G. Álvarez-García).
[1] @SALUVET_UCM

https://doi.org/10.1016/j.ijpara.2023.05.002
0020-7519/

sometimes lead them to succumb to the infection (Álvarez-García et al., 2013, 2014; Gollnick et al., 2015).

Identifying the underlying molecular mechanisms that determine the establishment and progression of the infection might help to combat parasite persistence and transmission. In this scenario, endothelial cells and macrophages are key innate immune system factors that might be crucial during the initial parasite-host interaction (Pols, 1960; McCully et al., 1966; Schares et al., 2009; Álvarez-García et al., 2013). Previous studies demonstrated that *B. besnoiti* is able to proliferate and modulate bovine endothelial cells from the umbilical cord (BUVECs) and aorta (BAECs) (Muñoz-Caro et al., 2014; Maksimov et al., 2016; Jiménez-Meléndez et al., 2019). *Besnoitia besnoiti* tachyzoite infection affects BUVEC cell cycle progression in a species-specific manner by impairing G1-phase progression (Velásquez et al., 2020) that complements the lipidomic and metabolomic data obtained in the same infected primary cell line (Kadesch et al., 2020). In addition, upon infection of BAECs with *B. besnoiti* tachyzoites, endothelial cells sequentially experienced loss of vascular integrity, expression of leucocyte adhesion molecules and a proinflammatory, prothrombotic and profibrotic phenotype (Jiménez-Meléndez et al., 2020). These in vitro findings were supported by the histopathological findings observed in the testes from naturally acutely and chronically infected breeding bulls. These bulls showed an intense inflammatory infiltrate in the testicular parenchyma, where macrophages constituted a predominant immune cell population (González-Barrio et al., 2020, 2021). Macrophages are suspected to play a relevant role in pathogenesis of the disease, based on the scarce studies performed with in vitro and in vivo experimental models. Muñoz-Caro et al. (2014) described that upon exposure of macrophages to viable tachyzoites, the formation of extracellular traps (ETs) was promoted to entrap the parasite and block cell invasion. Moreover, an experimental infection model for acute bovine besnoitiosis revealed that after infection, an innate IFNγ response developed, followed by an acquired immune response demonstrated by seroconversion at 2–3 weeks p.i. (Diezma-Díaz et al., 2018), and the role of IFNγ in macrophage priming and inflammatory response activation is well known (Su et al., 2015).

Regarding *B. besnoiti*, a recent comparative transcriptomics study between tachyzoite and bradyzoite stages estimated a total genome size of *B. besnoiti* of 58.9 Mb with a high synteny preservation and genomic rearrangement very similar to other genomes of the family Sarcocystidae (eg. *T. gondii* and *N. caninum*) (Ramakrishnan et al., 2022). These authors described stage-specific markers and metabolic pathways in this parasite. However, there is very limited information about the *B. besnoiti* genes implicated in host cell invasion and lytic cycle progression. A previous transcriptomic study carried out in BAECs showed that *B. besnoiti* modulates different functions in bovine endothelial cells through the regulation of several surface genes (*SAG*), microneme genes (*MIC*), AP-2 transcription factors and rhoptry genes, among others (Jiménez-Meléndez et al., 2020).

In this context, knowing whether macrophages offer a niche wherein *B. besnoiti* can invade and replicate becomes necessary. Previous studies showed that the employment of an in vitro system based on primary bovine monocyte-derived macrophages helped to explore the innate macrophage-derived response against *N. caninum* that could be extrapolated to in vivo models (García-Sanchez et al., 2019; Jiménez-Pelayo et al., 2020). Accordingly, the aim of this study was to explore the interaction between *B. besnoiti* tachyzoites and primary bovine monocyte-derived macrophages in vitro. First, the *B. besnoiti* tachyzoite lytic cycle was characterized. Next, dual transcriptomic profiling of *B. besnoiti* tachyzoites and macrophages was carried out by means of RNA sequencing (RNA-Seq) at two representative time points of early host-parasite interaction (4 and 8 h p.i.). RNA-Seq results of the host cell were validated in vitro by a Terminal deoxynucleotidyl transferase dUTP nick end labelling (TUNEL) assay. In addition, samples from the testicular parenchyma of naturally infected bulls were employed to investigate whether a similar parasite-host interaction occurs in vitro and in vivo.

## 2. Materials and methods

### 2.1. Ethics statement

Animal welfare was considered in carrying out these experiments. Protocols were approved by the Animal Welfare Committee of the Community of Madrid, Spain (permit number PROEX 236/17). In addition, all procedures were performed following current Spanish and European legislation, and good practices were in accordance with the European Directive 2010/63/EU, which is transposed into national legislation through the Spanish Royal Decree (RD) 53/2013 for the protection of animals used for research experimentation and other scientific purposes.

### 2.2. Bovine monocyte isolation and in vitro macrophage differentiation

Heparinized peripheral blood was obtained from a healthy adult *Bos taurus* (Holstein-Friesian) which tested negative for infectious bovine rinotracheitis virus (IBRV) by ELISA-IBR-gE Ab (Idexx, Netherlands), bovine viral diarrhoea virus (BVDV) by ELISA-BDV-p80 (Idexx), Pestivirus by real-time quantitative reverse-transcription PCR (RT-qPCR) (Hoffman et al., 2006) and *B. besnoiti* and *N. caninum* by western blotting (Fernández-García et al., 2009; García-Lunar et al., 2012).

Bovine monocyte isolation was carried out by immunomagnetic separation using anti-human CD14–conjugated magnetic microbeads (Miltenyi Biotec, Germany) following the protocol previously described by García-Sánchez et al. (2019). Briefly, immunomagnetic purified monocytes were incubated in 6-well culture plates at a density of $3 \times 10^6$ cells/well at 37 °C and 5% $CO_2$ in RPMI 1640 medium (GE Healthcare, USA) containing 10% heat-inactivated FCS, 50 μM 2-beta-mercaptoethanol, 100 IU $mL^{-1}$ penicillin, 100 μg $mL^{-1}$ streptomycin, and 100 ng $mL^{-1}$ recombinant bovine granulocyte macrophage colony-stimulating factor (GM-CSF) (Kingfisher Biotech, USA). After 3 days of culture, 1 mL of the culture medium from each well was replaced with 1 mL of fresh medium. Two days later, the monocytes which differentiated into macrophages were reseeded in 24-well and 6-well culture plates at the density of viable cells indicated for each assay. The plates were incubated at 37 °C in a 5% $CO_2$ atmosphere for 24 h before parasite infection.

### 2.3. Parasite culture

*Besnoitia besnoiti* BbSp1 isolate tachyzoites were maintained in monolayer cultures of a monkey kidney cell line (MARC-145 cells) at a multiplicity of infection (MOI) of 2:1 (parasite:host cell), according to previously published procedures (Jiménez-Meléndez et al., 2017). To avoid parasite adaptation to cell culture, only low-passage tachyzoites were included in the studies (passage numbers 10 to 21). For bovine macrophage infection, three different MOIs were initially tested (two, five and ten). A MOI of 5:1 was selected, based on the increased number of intracellular events at 4 h p.i. (approximately 15% versus 3–4% in MARC-145 cells with the maintenance MOI of 2:1). Tachyzoites were harvested 3 days p.i., when most tachyzoites were still intracellular, and parasites were liberated from their host cells by passing them repeatedly through a G25 needle, followed by purification through disposable

PD-10 columns (Sephadex G-25; GE Healthcare). Tachyzoite viability was confirmed by trypan blue exclusion, and tachyzoites were counted in a Neubauer chamber. Next, in all experiments, macrophages were infected within 1 h after tachyzoite purification to prevent loss of parasite viability.

### 2.4. Immunofluorescence assays

Macrophages were seeded on sterile coverslips in 24-well plates at a density of $2.5 \times 10^5$ cells/well and inoculated with live BbSp1 tachyzoites (MO-Bb) at an MOI of 5:1, followed by incubation at 37 °C. In addition, macrophages were inoculated with heat-killed BbSp1 tachyzoites (MO-hkBb) at the same MOI as a control for phagocytosis. Tachyzoites were killed by incubation at 56 °C for 30 min as previously described by García-Sánchez et al. (2019). The trypan blue dye exclusion test indicated that 100% of the heat-treated tachyzoites were dead. In addition, heat-treated tachyzoites were inoculated into MARC-145 cell cultures for 7 days and it was confirmed that there was no parasite growth by microscopy and quantitative PCR (qPCR). Inoculated macrophages (MO-Bb and MO-hkBb) were fixed with 0.05% glutaraldehyde and 3% paraformaldehyde at 4, 8, 12, 24 36, 48 and 72 h p.i.. Afterwards, a double immunofluorescence (IF) probe was performed (Jiménez-Pelayo et al., 2017). Briefly, after fixation, hyperimmune rabbit antiserum directed against *B. besnoiti* tachyzoites (1:500) was employed as the primary antibody (Gutiérrez-Expósito et al., 2012), and Alexa Fluor-488-labelled secondary antibody (Thermo Fisher Scientific, USA) was employed. Afterwards, the cells were permeabilized with 0.25% Triton X-100 (Thermo Fisher Scientific). Subsequently, extracellular and intracellular parasites were stained using hyperimmune rabbit antiserum directed against *B. besnoiti* tachyzoites (1:500) as the primary antibody and Alexa Fluor-594-labelled secondary antibody (Thermo Fisher Scientific). The nuclei were stained by washing the cells with a solution of 1:5,000 DAPI (Thermo Fisher Scientific) in 1x PBS, and the coverslips were embedded in Prolong (Thermo Fisher Scientific). Intracellular tachyzoites were stained red, while extracellular tachyzoites were stained green and red. The number of cells containing at least one tachyzoite was determined by counting in 10 arbitrarily selected fields using an inverted fluorescence microscope (Nikon Eclipse TE 200, Japan) at a magnification of 200x. A mean value of 50 cells was counted in each field by a single operator. Three independent assays were performed, each with three different replicates. To assess the differences in parasite invasion among groups, a non-parametric Kruskal-Wallis test followed by Dunn's post hoc test was performed. A $P$ value $\leq 0.05$ was considered statistically significant.

In addition, macrophage morphology was assessed microscopically by staining the cells with fluorescently labelled phalloidin. Macrophages were seeded on sterile coverslips in 24-well plates at a density of $2.5 \times 10^5$ cells/well and inoculated with live BbSp1 tachyzoites (MO-Bb) and heat-killed tachyzoites (MO-hkBb) at an MOI of 5:1, followed by incubation at 37 °C. Cultures were fixed at 4, 8, 12, 24, 36, 48 and 72 h p.i. with 0.05% glutaraldehyde and 3% paraformaldehyde. Afterwards, the cells were permeabilized with 0.25% Triton X-100 (Thermo Fisher Scientific). Parasites were stained using hyperimmune rabbit antiserum directed against *B. besnoiti* tachyzoites (1:500) as the primary antibody and Alexa Fluor-488-labelled secondary antibody (Thermo Fisher Scientific). In addition, Alexa Fluor-594-labelled phalloidin (Thermo Fisher Scientific) was used for the staining of F-actin. The nuclei were stained by washing the cells with a solution of 1:5,000 DAPI (Thermo Fisher Scientific) in 1x PBS, and the coverslips were embedded in Prolong (Thermo Fisher Scientific). Based on microscopic analysis of cells under different experimental conditions, macrophages were classified according to two distinct morphologies: i) small and rounded with short and irregular filopodia and ii) large and elongated with long filopodia.

### 2.5. Proliferation assays

Proliferation assays were performed in 6-well plates. Macrophages were seeded at a density of $3 \times 10^6$ cells/well and infected with live tachyzoites (MO-Bb) at an MOI of 5:1. In parallel, MO-hkBb was used as a control. DNA was extracted according to Jiménez-Meléndez et al. (2019) at different times p.i. (4, 8, 12, 24, 32, 48 and 72 h p.i.). DNA concentration and quality were measured by UV spectrometry using a Biotek Multiplate Reader (Agilent Biotek, USA). Quantification of *B. besnoiti* was performed by qPCR, and the proliferation kinetics were displayed by plotting the parasite loads against their respective time points of collection (4, 8, 12, 24, 32, 48 and 72 h p.i.), following the indications previously described by Jiménez-Meléndez et al. (2019). Proliferation was also monitored by IF staining using hyperimmune rabbit antiserum directed against *B. besnoiti* tachyzoites, as described above. Assays were carried out in triplicate, each with three different replicates.

To assess the differences in parasite proliferation among the different time points p.i. studied, the Kruskal-Wallis test followed by Dunn's post hoc test was performed. A $P$ value $\leq 0.05$ was considered statistically significant. The doubling time (dT), defined as the period required for a tachyzoite to duplicate during the exponential multiplication phase, was calculated as previously described (Regidor-Cerrillo et al., 2011), by applying non-linear regression analysis and an exponential growth equation using GraphPad Prism (GraphPad Software, USA).

### 2.6. Transcriptome analyses

#### 2.6.1. Experimental design and RNA extraction

Macrophages were seeded in 6-well plates at a density of $3 \times 10^6$ cells/well, infected with live tachyzoites (MO-Bb) at an MOI of 5:1 and inoculated with heat-killed tachyzoites (MO-hkBb) at the same MOI. MO was used as a control. Total RNA from three independent biological replicates was purified from the pellet of inoculated macrophages at 4 and 8 h p.i. by using a QIAGEN RNeasy Mini Kit (Qiagen, Germany), following QIAshredder (Qiagen) homogenization according to the manufacturer's instructions. Additionally, RNA integrity was evaluated by 1% agarose gel electrophoresis with GelRed™ staining (Biotium, USA).

#### 2.6.2. Quality control of total RNA, library preparation and sequencing

The quality and quantity of the total RNA was determined with a Bioanalyzer 2100 (Agilent Biotek) and a Qubit 2.0. B (Invitrogen, USA). The poly(A) + mRNA fraction was isolated from the total RNA, and cDNA libraries were obtained following the recommendations of Illumina. Briefly, poly(A) + mRNA was isolated on poly-T oligo-attached magnetic beads and chemically fragmented prior to reverse transcription and cDNA generation. The cDNA fragments were then subjected to a repair process, addition of a single 'A' base to the 3′ end and ligation of the adapters. The products were purified and enriched with PCR to create the indexed final double-stranded cDNA library. The quantity of the libraries was determined by qPCR with a LightCycler 480 (Roche, Switzerland), and quality was analysed with a Bioanalyzer 2100 (Agilent Biotek) high sensitivity assay. Prior to cluster generation in cBot (Illumina, USA), equimolar pooling of the libraries was performed. The pool of the cDNA libraries was sequenced by paired-end sequencing (100 bp × 2) with an Illumina HiSeq 2000 sequencer (Illumina).

#### 2.6.3. Computational analysis of RNA-Seq data

First, raw data quality assessment was undertaken using the FastQC tool. Briefly, the quality checks involved GC content and

the presence of duplicated reads to detect sequencing errors, PCR amplification bias or contamination. Low-quality reads were eliminated using Picard Tools software, version 1.129 (https://picard.sourceforge.net).

The raw paired-end reads were mapped against the *B. taurus* genome version UDM3.1 (NCBI:GCA_000003055.3) provided by the ENSEMBL/NCBI database (https://www.ensembl.org/) and the *B. besnoiti* genome deposited in DDBJ/ENA/GenBank under the accession no. **NWUJ00000000** using the TopHat2 v2.1.0 algorithm (Kim et al., 2013). Gene quantification was carried out using htseq_count 0.6.1p1 (Anders et al., 2015). A differential expression analysis was carried out between the three groups, MO-Bb, MO-hkBb and MO, at 4 and 8 h p.i. for macrophage analyses and for *B. besnoiti,* the expression at 4 and 8 h p.i. was compared. Differential expression between sample groups was studied using the algorithm proposed by DESeq2 (Anders and Huber, 2010), with a binomial negative distribution for determination of the statistical significance (Love et al., 2014). Genes were considered differentially expressed when they presented a Fold Change (FC) $\geq$ 1.5 and a false discovery rate (FDR)–adjusted (Benjamini and Hochberg, 1995) *P*-value (*P* adj) $\leq$ 0.05, following previous studies (Horcajo et al., 2017; Jiménez-Meléndez et al., 2020).

To explore the correlation among all replicates, a principal component analysis (PCA) was performed according to the expression level of differentially expressed genes (DEGs). The correlation among samples was determined by using the adegenet library (Jombart, 2008) of the statistical software package R (https://www.r-project.org) for their acceptance as biological replicates.

Volcano plots showing log2 (FC) against -log10 (adjusted *P*-value) of all expressed genes were generated by using the https://www.bioinformatics.com.cn/en online tool. Heatmaps were generated with a selection of bovine macrophage DEGs by using the https://www.heatmapper.ca/expression/ online tool. The RNA-Seq data reported in this study have been deposited in the NCBI database under accession number **PRJNA785130**.

#### 2.6.4. Functional enrichment analyses

For bovine DEGs, a gene set enrichment analysis was conducted using the g:Profiler web server that can be freely accessed at https://biit.cs.ut.ee/gprofiler/gost. g:Profiler was used to identify the Gene Ontology (GO) terms (biological process (BP), molecular function (MF) and cellular components (CC)) and the Kyoto Encyclopaedia of Genes and Genomes (KEGG) pathways (https://www.genome.jp/kegg/pathway.html) for DEGs. The statistical domain scope was used for annotated genes. The significance threshold was the g:SCS threshold, which is the g:Profiler default method for computing multiple testing correction for *P*-values gained from GO and KEGG pathway enrichment analysis. It corresponds to an experiment-wide threshold of a = 0.05.

For functional studies of *B. besnoiti* genes, considering that the reference genome is not completely annotated, we used the ToxoDB database (https://toxodb.org/toxo/, ToxoDB release 56) to carry out an orthology and synteny analysis of non-annotated genes due to the more complete annotation of the *T. gondii* genome. The orthology and synteny analysis was performed using a ToxoDB tool called OrthoMCL, which clusters genes based on their sequence similarity and then infers orthology relationships based on the clustering patterns. In addition, the synteny analysis was carried out using a ToxoDB tool called MCScanX, which identifies syntenic blocks by comparing the gene order and orientation between different genomes. The mapping criteria was 1:1, meaning that each gene in *B. besnoiti* was typically matched to a single orthologous gene in *T. gondii*.

### 2.7. TUNEL assay

TUNEL assays were performed using the In Situ Cell Detection Kit TMR red (Roche) according to the manufacturer's instructions to verify and quantify apoptosis. Briefly, macrophages were cultured on sterile coverslips in 24-well plates at a density of $2.5 \times 10^5$ cells/well and inoculated with MO-Bb and heat-killed MO-hkBb at an MOI of 5:1, followed by incubation at 37 °C. Cultures were fixed at 4 and 8 h p.i. with 4% paraformaldehyde. Apoptotic cells were visualized by fluorescence microscopy (Nikon Eclipse TE 200). TUNEL-positive cells were quantified by randomly counting 60 different microscopic fields per well. Assays were carried out in triplicate, each with three different replicates. The ratio of apoptotic cells was calculated as the number of TUNEL-positive nuclei divided by the total number of nuclei. A non-parametric Kruskal-Wallis test followed by Dunn's post-hoc test was used for statistical analysis. A *P* value $\leq$ 0.05 was considered statistically significant.

### 2.8. Analysis of gene expression in the testicular parenchyma of naturally infected bulls

Samples from testicular parenchyma of naturally infected bulls were employed to analyse the expression of a panel of DEGs selected from the transcriptomic data. We selected genes that showed the most significant changes in the differential expression analysis and significant genes from the KEGG enrichment analysis. Fifteen naturally infected breeding bulls from extensive beef herds were included in this study (acute infection $n = 5$; chronic infection $n = 10$, negative control $n = 9$). Acutely infected animals showed signs compatible with acute besnoitiosis, mainly fever and orchitis, and only one presented 2–3 tissue cysts per section (González-Barrio et al., 2020). Chronically infected animals were sterile bulls that presented skin lesions and testis atrophy with azoospermia (González-Barrio et al., 2021). Testicular parenchyma tissue samples were collected from each bull, and samples were frozen at − 80 °C until RNA extraction. Total RNA was purified by using a QIAGEN RNeasy Mini Kit (Qiagen) following QIAshredder (Qiagen) homogenization according to the manufactureŕs instructions. RNA concentration and purity were measured spectrophotometrically using a NanoPhotometer Classic (Implen, USA). In addition, RNA integrity was evaluated by 1% agarose gel electrophoresis with GelRed™ staining (Biotium). Afterwards, reverse transcription was performed using the master mix SuperScript® VILO™ cDNA Synthesis Kit (Invitrogen) in a 20 µL reaction using up to 2.5 µg of total RNA. cDNA was sequentially diluted to 1:20, 1:80, 1:320 and 1:1,280, and all dilutions were analysed by qPCR. qPCRs were performed in 25 µL volumes using 12.5 µL of Power SYBR®PCR Master Mix (Applied Biosystems, USA), 10 pmol of each primer and 5 µL of the diluted cDNA samples. Primers are shown in Supplementary Table S1. Reactions were performed in an ABI 7500 FAST Real Time PCR System (Applied Biosystems). Relative expression was calculated using the comparative method $2^{-\Delta\Delta Ct}$ (Livak and Schmittgen, 2001) after normalization with the housekeeping gene β-actin (B-actin) (Puech et al., 2015; Horcajo et al., 2017). For statistical analysis, the Kruskal-Wallis test was used, followed by Dunn's test, and $P \leq 0.05$ was considered statistically significant.

## 3. Results

### 3.1. Besnoitia besnoiti efficiently invades and proliferates in primary bovine monocyte-derived macrophages

*Besnoitia besnoiti* tachyzoites can invade and replicate in primary bovine monocyte-derived macrophages. At 4 h p.i., intracel-

lular tachyzoites were already observed in approximately 15% of MO-Bb. Furthermore, the number of intracellular events in MO-Bb determined by IF showed a gradual increase with progression of the infection time (Fig. 1A), showing exponential growth from 24 h p.i. until the egression that was observed by microscopic visualization at 72 h p.i. (Fig. 1B, C). At 36 h p.i., all intracellular events visualized in MO-Bb consisted of parasitophorous vacuoles composed of more than one tachyzoite (medium to large-sized vacuoles) that are associated with active invasion. The average dT value was 15.13 h. According to the number of intracellular events, phagocytosis of heat-killed tachyzoites was finalized at 12 h p.i. because differences between 12 and 24 h p.i. were not found ($P = 0.17$) (Fig. 1A). As expected, there was no increase in parasite load in MO-hkBb as the infection progressed, indicating a lack of parasite multiplication (Fig. 1B, C). At 36 h p.i., invasion events were not counted in MO-hkBb (Fig. 1A) since only tachyzoite debris that disappeared at 72 h p.i. was observed (Fig. 1C, D). Furthermore, when macrophage morphology was assessed microscopically, the results showed that at 36 h p.i., MO-Bb were smaller, rounded, lacked filopodial structures and contained several large parasitophorous vacuoles compared with MO-hkBb, which were larger and more irregular in shape (Fig. 1C, D).

### 3.2. Transcriptional changes in Besnoitia besnoiti-infected primary bovine monocyte-derived macrophages identify relevant pathways triggered upon infection

#### 3.2.1. Sequence mapping and principal component analyses validated the good quality of RNA-Seq data

All samples had an RNA integrity number (RIN) between 9.6 and 10. The sequencing process accounted for approximately 1 billion reads between all samples. After alignment, an average of 70% of the high-quality reads mapped to the reference *B. taurus* and *B. besnoiti* genomes. Approximately 87% of the total RNA population was attributable to *B. taurus*, and 13% to *B. besnoiti* (Supplementary Table S2). Furthermore, PCA revealed that all replicates from the same condition clustered together, as shown in Supplementary Fig. S1.

#### 3.2.2. Macrophages are activated early in infection and apoptosis; mitogen-activated protein kinases and Herpes simplex virus 1 infection are the most relevant modulated pathways

*Besnoitia besnoiti* infection initiated a wide alteration of the host transcriptional profile (Table 1; Supplementary Table S3; Fig. 2). Differential expression analysis revealed that the number of DEGs in the MO-Bb versus MO comparison increased with progression of the infection (545 at 4 h p.i. versus 1,739 at 8 h p.i.) (Supplementary Fig. S2; Table 1). To highlight host cell modulation by the live tachyzoites, we used heat-killed *B. besnoiti* tachyzoites as a control for the cellular response after phagocytosis. An increase in the number of DEGs over time in MO-hkBb versus MO was also observed (514 at 4 h p.i. versus 2,813 at 8 h p.i.) (Supplementary Fig. S2).

The functions of DEGs were predicted using GO and KEGG enrichment analyses (Table 1). The MO-Bb versus MO comparison at 4 h p.i. showed an enrichment in BP involved in host cell defence mechanisms and cellular response to stress. In fact, several DEGs involved in endoplasmic reticulum (ER) stress and the unfolded protein response (UPR) (*IRE1α, IPR3, ITP31, ATF4, CHOP, MMPs, Bcl-2, BH3, GADD45A, GADD45B, HSP40, HSP70*) were upregulated. In terms of MF, DEGs were enriched in categories involved in transmembrane transport and metabolic processes. Furthermore, GO terms for CC indicated that a majority of DEGs were associated with the autophagy machinery and apoptotic complexes such as Atg1/ULK1 and CHOP-ATF4 complexes. Moreover, the KEGG pathway analysis revealed that DEGs were mainly involved in apoptosis, mitogen-activated protein kinases (MAPKs) and lysosome modulation (Table 1; Fig. 2A). Apoptosis was the top ranked path-

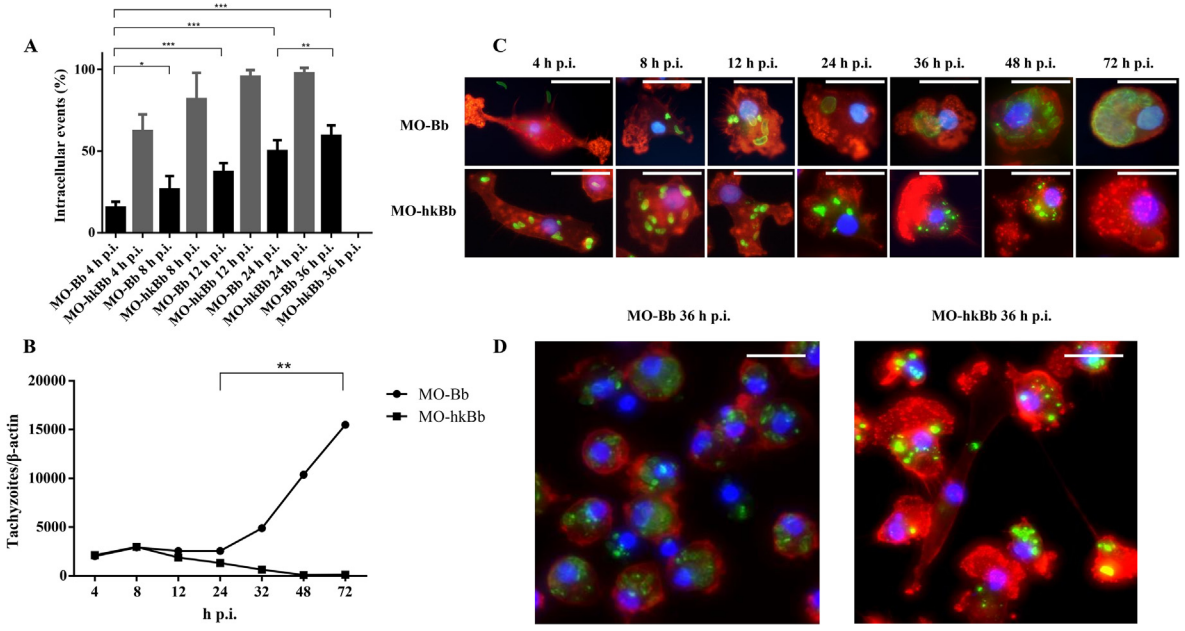


**Fig. 1.** *Besnoitia besnoiti* lytic cycle in primary bovine monocyte-derived macrophages. (A) Percentage of intracellular events at different time points p.i. (B) In vitro proliferation kinetics of *B. besnoiti* tachyzoites determined by quantitative PCR (qPCR). (C) Lytic cycle of live *B. besnoiti* tachyzoites (MO-Bb) and heat-killed tachyzoites (MO-hkBb) monitored by immunofluorescence (IF) from 4 h p.i. to 72 h p.i. *Besnoitia besnoiti* tachyzoites are stained with a hyperimmune rabbit antiserum directed against *B. besnoiti* tachyzoites and labelled with Alexa Fluor® 488 (green), phalloidin-labelled F-actin (red), and the nuclei of host cells are stained with DAPI (blue). Scale bars: 20 μm. (D) Morphology of MO-Bb and MO-hkBb at 36 h p.i. *Besnoitia besnoiti* tachyzoites are stained with a rabbit polyclonal antibody against *B. besnoiti* labelled with Alexa Fluor® 488 (green), phalloidin-labelled F-actin (red), and the nuclei of host cells are stained with DAPI (blue). Scale bars: 100 μm. *Adjusted *P* values between 0.01 and 0.05; **adjusted *P* values between 0.01 and 0.001; as determined by Kruskal-Wallis test followed by Dunn's test.

**Table 1**
Number of differentially expressed genes (DEGs) among conditions (macrophages infected with live tachyzoites (MO-Bb), macrophages infected with heat-killed tachyzoites (MO-hkBb) and non-infected macrophages (MO)), and functional enrichment analysis results (top five most significant Gene Ontology (GO) terms: biological processes (BP), molecular functions (MF), cellular components (CC); and Kyoto Encyclopedia of Genes and Genomes (KEGG) pathways).

| | | N° DEGs | Upregulated DEGs | Downregulated DEGs | Biological processes | | Molecular function | | Cellular components | | Pathway enrichment | |
|---|---|---|---|---|---|---|---|---|---|---|---|---|
| | | | | | GO term | Adjusted *P*-value | GO term | Adjusted *P*-value | GO term | Adjusted *P*-value | KEGG term | Adjusted *P*-value |
| **4 h p.i.** | **MO-Bb vs MO** | 545 | 347 | 198 | Phosphorylation (GO:0016310) | $1.01x10^{-6}$ | Binding (GO:0005488) | $9.86x10^{-3}$ | Lysosome (GO:0005764) | $3.75x10^{-8}$ | Apoptosis (KEGG:04210) | $2.08x10^{-5}$ |
| | | | | | Regulation of signal transduction (GO:0009966) | $2.05x10^{-5}$ | Enzyme binding (GO:0019899) | $1.08\ x10^{-2}$ | Lytic vacuole (GO:0000323) | $4.07x10^{-8}$ | MAPK signalling pathway (KEGG:04010) | $6.52\ x10^{-3}$ |
| | | | | | Intracellular signal transduction (GO:0035556) | $3.05x10^{-5}$ | - | - | Cytoplasm (GO:0005737) | $1.50x10^{-7}$ | Lysosome (KEGG:04142) | $2.94x10^{-2}$ |
| | | | | | Regulation of response to stimulus (GO:0048583) | $5.26x10^{-5}$ | - | - | Vacuole (GO:0005773) | $3.71x10^{-7}$ | - | - |
| | | | | | Protein phosphorylation (GO:0006468) | $5.71x10^{-5}$ | - | - | Intracellular (GO:0005622) | $2.23x10^{-5}$ | - | - |
| | **MO-Bb vs MO-hkBb** | 148 | 20 | 128 | Response to starvation (GO:0042594) | $1.87x10^{-6}$ | Aminoacyl-tRNA ligase activity (GO: GO:0004812) | $3.39x10^{-3}$ | Cytoplasm (GO:0005737) | $3.22x10^{-4}$ | Aminoacyl-tRNA biosynthesis (KEGG:00970) | $1.27x10^{-3}$ |
| | | | | | Cellular response to stress (GO:0033554) | $8.63x10^{-6}$ | Ligase activity. forming carbon–oxygen bonds (GO:0016875) | $3.39x10^{-3}$ | Atg1/ULK1 kinase complex (GO:1990316) | $3.75x10^{-3}$ | Central carbon metabolism in cancer (KEGG:05230) | $7.37x10^{-3}$ |
| | | | | | Carboxylic acid metabolic process (GO:0019752) | $1.64x10^{-5}$ | L-amino acid transmembrane transporter activity (GO:0015179) | $9.83x10^{-3}$ | Intracellular (GO:0005622) | $9.83x10^{-3}$ | Biosynthesis of amino acids (KEGG:01230) | $1.30x10^{-2}$ |
| | | | | | Oxoacid metabolic process (GO:0043436) | $3.81x10^{-5}$ | Neutral amino acid transmembrane transporter activity (GO:0015175) | $1.18x10^{-2}$ | CHOP-ATF4 complex (GO:1990617) | $1.08x10^{-2}$ | MAPK signalling pathway (KEGG:04010) | $1.84x10^{-2}$ |
| | | | | | Organic acid metabolic process (GO:0006082) | $5.89x10^{-5}$ | Organic anion transmembrane transporter activity (GO:0008514) | $1.45x10^{-2}$ | Cytosol (GO:0005829) | $1.97x10^{-2}$ | Apoptosis (KEGG:04210) | $4.1610^{-2}$ |

**Table 1** (*continued*)

| | | N° DEGs | Upregulated DEGs | Downregulated DEGs | Biological processes | | Molecular function | | Cellular components | | Pathway enrichment | |
|---|---|---|---|---|---|---|---|---|---|---|---|---|
| | | | | | **GO term** | **Adjusted *P*-value** | **GO term** | **Adjusted *P*-value** | **GO term** | **Adjusted *P*-value** | **KEGG term** | **Adjusted *P*-value** |
| | **MO-hkBb vs MO** | 514 | 301 | 213 | Cellular transition metal ion homeostasis (GO:0046916) | $6.16x10^{-6}$ | - | - | Vacuole (GO:0005773) | $6.11x10^{-13}$ | Mineral absorption (KEGG:04978) | $1.62x10^{-3}$ |
| | | | | | Transition metal ion homeostasis (GO:0055076) | $8.45x10^{-6}$ | - | - | Lysosome (GO:0005764) | $3.01x10^{-12}$ | One carbon pool by folate (KEGG:00670) | $1.15x10^{-2}$ |
| | | | | | Homeostatic process (GO:0042592) | $3.58x10^{-3}$ | - | - | Lytic vacuole (GO:0000323) | $3.33x10^{-12}$ | Lysosome (KEGG:04142) | $1.56x10^{-2}$ |
| | | | | | Cellular response to chemical stimulus (GO:0070887) | $1.66x10^{-2}$ | - | - | Cytoplasm (GO:0005737) | $1.20x10^{-7}$ | - | - |
| | | | | | Iron ion homeostasis (GO:0055072) | $3.8x10^{-2}$ | - | - | Intracellular membrane-bounded organelle (GO:0043231) | $1.47x10^{-6}$ | - | - |
| **8 h p.i** | **.MO-Bb vs MO** | 1739 | 998 | 741 | DNA metabolic process (GO:0006259) | $2.91x10^{-5}$ | Binding (GO:0005488)) | $1.47x10^{-6}$ | Intracellular (GO:0005622) | $3.14x10^{-28}$ | Herpes simplex virus 1 infection (KEGG:05168) | $9.50x10^{-3}$ |
| | | | | | Cellular metabolic process (GO:0044237) | $3.44x10^{-5}$ | Catalytic activity (GO:0003824) | $1.93x10^{-5}$ | Intracellular membrane-bounded organelle (GO:0043231) | $2.69x10^{-27}$ | - | - |
| | | | | | Nucleic acid metabolic process (GO:0090304) | $5.71x10^{-5}$ | Organic cyclic compound binding (GO:0097159) | $1.20x10^{-3}$ | Membrane-bounded organelle (GO:0043227) | $7.35x10^{-25}$ | - | - |
| | | | | | Heterocycle metabolic process (GO:0046483) | $8.16x10^{-5}$ | Heterocyclic compound binding (GO:1901363) | $1.49x10^{-3}$ | Organelle (GO:0043226) | $9.40x10^{-21}$ | - | - |
| | | | | | Cellular aromatic compound metabolic process (GO:0006725) | $2.79x10^{-4}$ | Nucleic acid binding (GO:0003676) | $4.04x10^{-3}$ | Intracellular organelle (GO:0043229) | $5.26x10^{-19}$ | - | - |
| | **MO-Bb vs MO-hkBb** | 231 | 151 | 80 | Response to starvation (GO:0042594) | $1.07x10^{-4}$ | - | - | Autophagosome membrane (GO:0000421) | $1.46x10^{-3}$ | - | - |
| | | | | | Response to nutrient levels (GO:0031667) | $2.48x10^{-3}$ | - | - | Atg1/ULK1 kinase complex (GO:1990316) | $1.73x10^{-2}$ | - | - |
| | | | | | Cellular response to starvation (GO:0009267) | $3.09x10^{-3}$ | - | - | CHOP-ATF4 complex (GO:1990617) | $3.1x10^{-2}$ | - | - |
| | | | | | Carboxylic acid metabolic process (GO:0019752) | $3.25x10^{-3}$ | - | - | - | - | - | - |
| | | | | | Cellular response to nutrient levels (GO:0031669) | $3.27x10^{-3}$ | - | - | - | - | - | - |

(*continued on next page*)

**Table 1** (*continued*)

| | N° DEGs | Upregulated DEGs | Downregulated DEGs | Biological processes | | Molecular function | | Cellular components | | Pathway enrichment | |
|---|---|---|---|---|---|---|---|---|---|---|---|
| | | | | GO term | Adjusted *P*-value | GO term | Adjusted *P*-value | GO term | Adjusted *P*-value | KEGG term | Adjusted *P*-value |
| **MO-hkBb vs MO** | 2813 | 1609 | 1204 | ncRNA processing (GO:0034470) | $1.17x10^{-18}$ | Binding (GO:0005488) | $1.09x10^{-15}$ | Membrane-bounded organelle (GO:0043227) | $5.02x10^{-59}$ | Ribosome biogenesis in eukaryotes (KEGG:03008) | $4.26x10^{-5}$ |
| | | | | ncRNA metabolic process (GO:0034660) | $2.05x10^{-18}$ | Catalytic activity. acting on RNA (GO:0140098) | $4.44x10^{-10}$ | Intracellular membrane-bounded organelle (GO:0043231) | $1.01x10^{-57}$ | Fanconi anemia pathway (KEGG:03460) | $2.15x10^{-4}$ |
| | | | | Cellular metabolic process (GO:0044237) | $7.53x10^{16}$ | Nucleic acid binding (GO:0003676) | $2.63x10^{-8}$ | Intracellular (GO:0005622) | $3.31x10^{-57}$ | RNA polymerase (KEGG:03020) | $1.39x10^{-2}$ |
| | | | | Cellular component organization or biogenesis (GO:0071840) | $1.03x10^{14}$ | Heterocyclic compound binding (GO:1901363) | $1.26x10^{-6}$ | Organelle (GO:0043226) | $4.05x10^{-49}$ | - | - |
| | | | | rRNA processing (GO:0006364) | $3.56x10^{-14}$ | Catalytic activity (GO:0003824) | $1.45x10^{-6}$ | Intracellular organelle (GO:0043229) | $2.45x10^{-48}$ | - | - |

MO-Bb, macrophages infected with live *Besnoitia besnoiti* tachyzoites; MO-hkBb, macrophages inoculated with heat-killed *B. besnoiti* tachyzoites; MO, non-infected macrophages.

way by statistical significance, with 18 genes significantly regulated (17 out of 18 DEGs appeared upregulated) (Fig. 3; Supplementary Table S3). In addition, the MAPK pathway was the second-ranked pathway by statistical significance, with 22 genes from the p38 and JNK subfamilies being significantly regulated (Fig. 4 and Supplementary Table S3). The lysosome pathway was the third-ranked pathway by statistical significance, with 12 genes significantly regulated (Supplementary Fig. S3). On the other hand, the transcriptome of cells inoculated with heat-killed tachyzoites was clearly different. The only commonly modulated pathway was the lysosome. Other pathways differentially regulated in MO-hkBb versus MO were mineral absorption and carbon folate pathways. In addition, when gene expression between MO-Bb versus MO-hkBb was compared, apoptosis and MAPK pathways again appeared to be differentially regulated, similarly to the MO-Bb versus MO comparison described above (Table 1).

At 8 h p.i., most of the enriched BP terms in the MO-Bb versus MO comparison were associated with nutrient deprivation and metabolic processes. Regarding MF terms, enriched categories were related to molecular binding and transport, and for CC terms, intracellular membrane-bound organelles and Atg1/ULK1 and CHOP-ATF4 complexes were identified. KEGG pathway analysis only showed that the *Herpes simplex* virus 1 infection signalling pathway was enriched, with 41 genes being significantly regulated. Several type I interferon-stimulated genes (ISGs) were upregulated: *cGAS, IFIH1*, zinc-finger (ZNF) protein-encoding genes, *OAS* (oligo adenylate synthetase), *CCL2*, *caspase-3* and *TAB1*, among others (Fig. 2B, Fig. 5; Supplementary Table S3). In addition, heat-killed parasite internalization (MO-hkBb versus MO) did not lead to regulation of the *Herpes simplex* virus 1 infection pathway, but it did regulate other pathways such as ribosome biogenesis and RNA polymerase. Furthermore, the Atg1/ULK1 and CHOP-ATF4 complexes were also shown to be upregulated when gene expression between MO-Bb versus MO-hkBb was compared (Table 1).

### 3.3. Transcriptional regulation of apoptosis was validated by TUNEL assay

The results of the TUNEL assay showed an increase in apoptosis in MO-Bb cells at 8 h p.i. At 4 h p.i., there were no differences in the numbers of apoptotic cells among the groups (MO-Bb, MO-hkBb and MO). However, at 8 h p.i., a significant increase ($P < 0.05$) in TUNEL-positive cells was observed in the MO-Bb group (approximately 5–6%) compared with the MO-hkBb and MO groups (<1%) (Fig. 6A, B). Furthermore, in MO-Bb almost 100% of TUNEL-positive cells were uninfected cells at all time points in the study (Fig. 6C, D).

### 3.4. Relevant genes modulated in the in vitro model of *B. besnoiti* infection were also regulated in testicular parenchyma during natural infections

We selected genes that showed the most significant changes in the differential expression analysis and significant genes from the KEGG enrichment analysis (apoptosis and *Herpes simplex* virus 1 infection signalling pathways) to study their expression in samples from naturally infected animals. Analysis of the expression of several genes (Supplementary Table S4) revealed that four out of eight genes analysed were found to be modulated by *B. besnoiti* infection in the testicular parenchyma of naturally infected bulls (Fig. 7). *CHOP* gene was significantly upregulated in vitro in MO-Bb cells compared with MO cells at 4 h p.i. However, it was found to be downregulated in the testicular parenchyma of acutely and chronically infected bulls (Fig. 7A). Moreover, we found that several type-I interferon-stimulated genes (ISGs) were downregulated in vitro, including several oligoadenylate synthetase (*OAS*) and

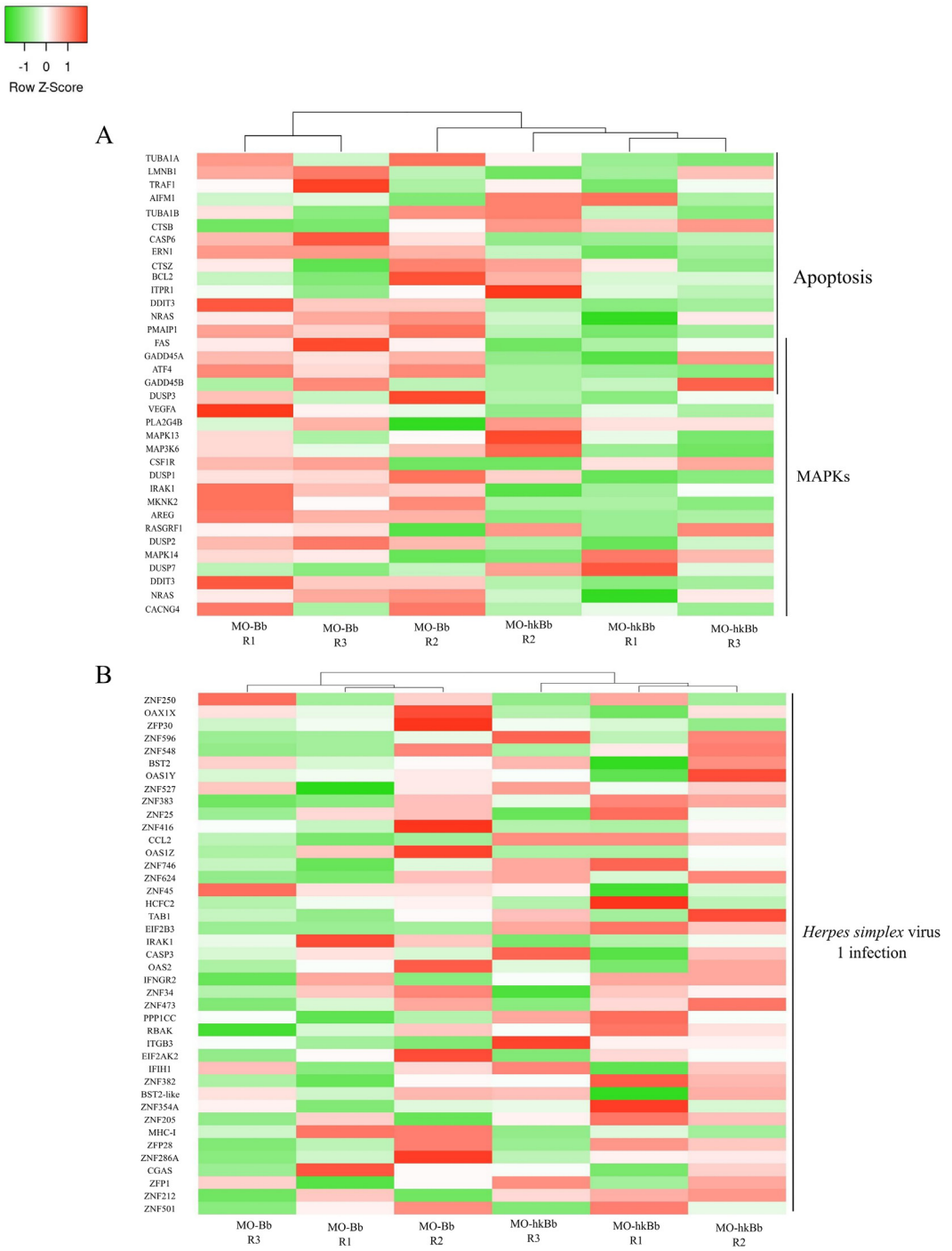


**Fig. 2.** Heatmaps of a selection of *Bos taurus* differentially expressed genes (DEGs). (A) A heatmap showing patterns of expression in a selection of *B. taurus* DEGs in macrophages infected with live tachyzoites (MO-Bb) and macrophages infected with heat-killed tachyzoites (MO-hkBb) at 4 h p.i. (B) A heatmap showing patterns of expression in a selection of *B. taurus* DEGs in macrophages infected with live tachyzoites (MO-Bb) and macrophages infected with heat-killed tachyzoites (MO-hkBb) at 8 h p.i.

cytosolic sensors, *MDA5* and *cGAS*. Interestingly, the type-I IFNα gene was significantly downregulated in acutely infected bulls (Fig. 7B). *Metallothioneins 1A* (*MET-1A*) and *1E* (*MET-1E*) showed very high FCs in vitro, and *MET-1A* was significantly upregulated in vivo in both acutely and chronically infected bulls, whilst *MMET-1E* was significantly upregulated in vivo in chronically infected bulls (Fig. 7C). The remaining analysed genes (*ATF*, *Bcl-2*, *IFNβ* and *OAS2*) did not show significant expression changes in vivo (Fig. 7).

### 3.5. *Besnoitia besnoiti* transcriptome profiling highlights strong regulation of invasion- and metabolism-related genes

A total of 538 *B. besnoiti* genes were differentially expressed between 4 and 8 h p.i. It was noted that 537 DEGs were upregulated versus only one downregulated gene at 8 h p.i. Unfortunately, 199 out of 538 DEGs corresponded to hypothetical proteins. Annotated DEGs for *B. besnoti* or its syntenic orthologous gene in *T. gondii* belonged mainly to two categories: invasion and metabolism

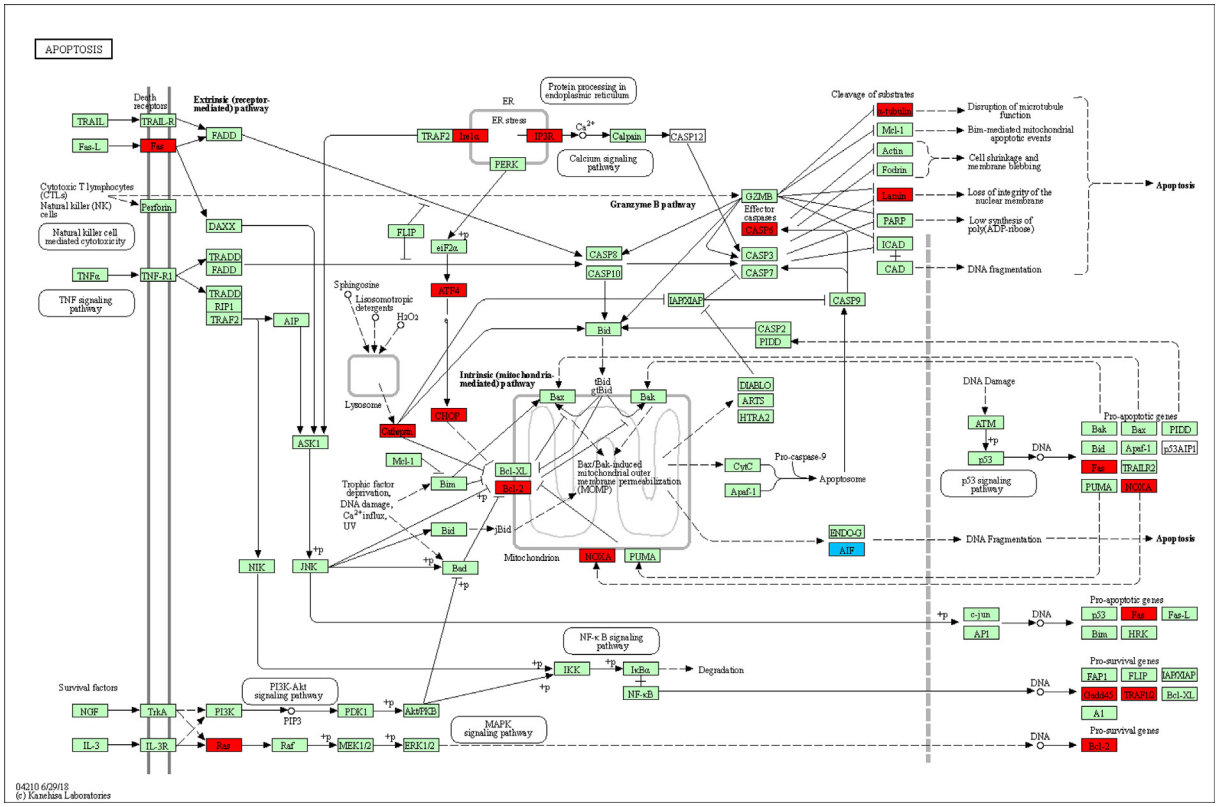


**Fig. 3.** The Kyoto Encyclopedia of Genes and Genomes (KEGG) pathway map (bta04210) represents the apoptosis pathway in which differentially expressed genes (DEGs) in bovine macrophages infected with *Besnoitia besnoiti* (MO-Bb) versus non-infected macrophages (MO) at 4 h p.i. are highlighted. Upregulated genes are represented in red, and downregulated genes are represented in blue. The results were obtained from three biological replicates for each condition.

(Table 2). Within the invasion category ($n$ = 31), genes coding for rhoptry proteins (*ROP6, ROP11, ROP23, ROP26, ROP31, ROP38, ROP40, rhoptry metalloprotease toxolysin (TLN1), RON1, RON2, RON3, RON4, RON5, RON6, RON8, RON9, RON10, RON12, RON14, RON15, RON17, RON18 and rhoptry protein (BESB_055810)*) were most numerous, followed by the components of the gliding machinery (*myosin light chain 1, myosin light chain 4*). However, only one surface antigen (*SRS49D*) and one microneme-like protein (BESB_067360) were upregulated in bovine macrophages at 8 h p.i. The next category with the highest number of upregulated genes was metabolism with genes ($n$ = 18) related to valine, leucine, isoleucine, and arginine metabolism; pantothenic acid and coenzyme A (CoA) synthesis and nitrogen metabolism. The only gene downregulated at 8 h p.i. when compared with 4 h p.i. was BESB_064630, which encodes a PAN/Apple domain-containing protein.

## 4. Discussion

In the present study, it was shown that *B. besnoiti* can survive and proliferate in a specialized phagocytic immune cell, the primary bovine monocyte-derived macrophage. Moreover, live parasites can modulate macrophages in a specific manner. Several host-cell enriched pathways and parasite effectors were identified upon infection.

*Besnoitia* parasites displayed a lytic cycle characterized by a high host cell invasion rate and morphological changes in invaded macrophages that differed from those induced by dead parasites (control of phagocytosis). An invasion rate higher than 50% was demonstrated at 36 h p.i., when only degraded dead tachyzoites were present in the control phagocytosis wells. Moreover, phagocytosis of *B. besnoiti* tachyzoites was completed at 12 h p.i., whereas active invasion progressively increased up to 36 h p.i. *Neospora caninum* showed a lower invasion rate at 36 h p.i. (García-Sanchez et al., 2019). Additional features showed that the *B. besnoiti* tachyzoite lytic cycle is slower than in the case of a virulent *Neospora* isolate: a higher dT is observed (15.13 h versus 13.15 h in *N. caninum*-infected macrophages), and egression continues at 72 h p.i. when it is already finished in macrophages infected with *N. caninum*. The asynchronous life cycle of *B. besnoiti* and delayed egression at 72 h p.i. were also observed in other primary bovine cells (BAECs and fibroblasts) (Jiménez-Meléndez et al., 2019) as well as in established cell lines (e.g. MARC-145 cells) (Frey et al., 2016). It has been hypothesized that this in vitro behaviour could be related to prolonged survival of extracellular *Besnoitia* tachyzoites to retain their infectivity for extended periods of time, which might favour mechanical vector-borne transmission. Moreover, at 36 h p.i. onwards, macrophages infected with live parasites showed a round cell shape and lacked cytoplasmic extensions compared with macrophages that phagocytosed dead parasites. The latter were elongated and presented several cytoplasmic extensions that are directly related to their phagocytic activity (McWhorter et al., 2013). These findings were already described in dendritic and microglial cells infected with *T. gondii* tachyzoites (Bhandage and Barragan, 2019) and monocyte-derived macrophages infected with *T. gondii* and *N. caninum* tachyzoites in vitro. In fact, macrophages infected with *T. gondii* and *N. caninum* tachyzoites exhibited a hypermigratory phenotype characterized by a hypermotility state accompanied by these morphological changes in the host cell (rounded shape, absence of podosomes and loss of filopodia) that contributed to parasite dissemination (Weidner et al., 2013; García-Sánchez et al., 2019). A similar cell morphology score (rounded cells, absence of podo-

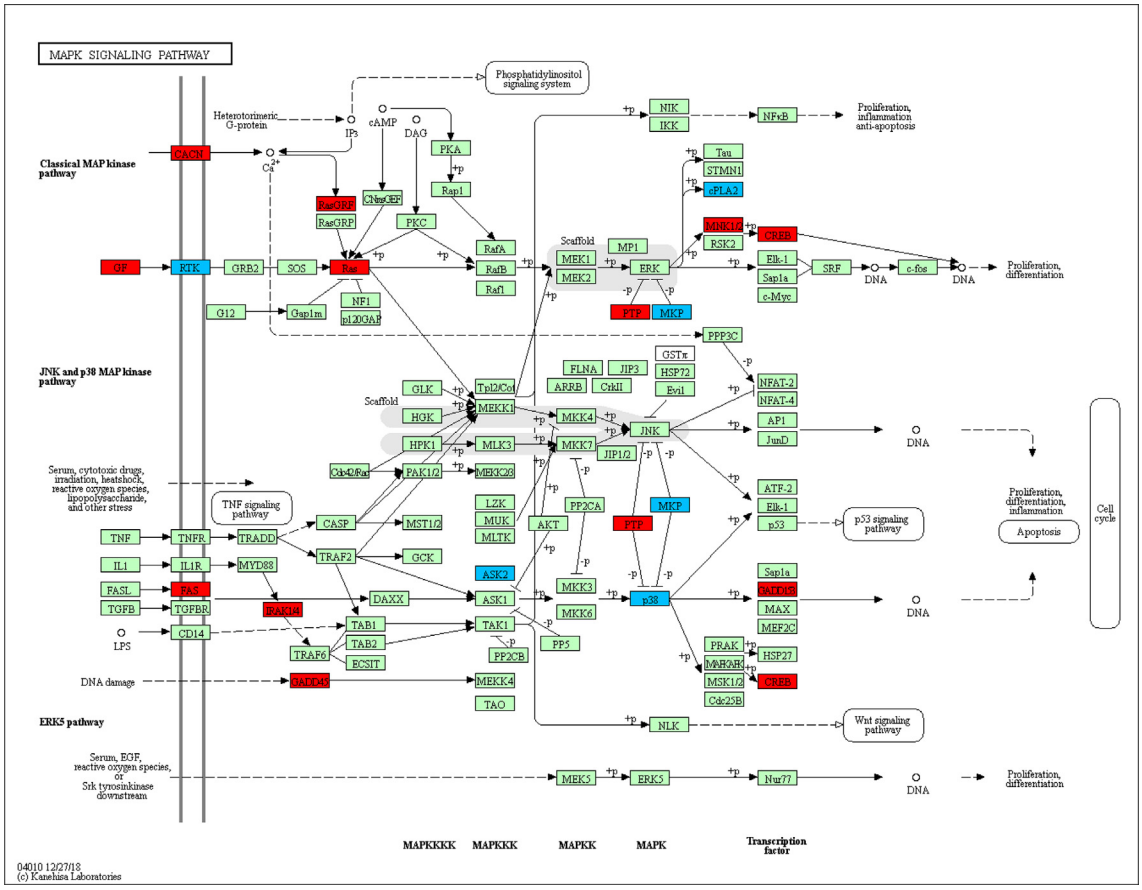


**Fig. 4.** The Kyoto Encyclopedia of Genes and Genomes (KEGG) pathway map (bta04010) represents the mitogen-activated protein kinase (MAPK) pathway in which differentially expressed genes (DEGs) in bovine macrophages infected with *Besnoitia besnoiti* (MO-Bb) versus non-infected macrophages (MO) at 4 h p.i. are highlighted. Upregulated genes are represented in red, and downregulated genes are represented in blue. The results were obtained from three biological replicates for each condition.

somes and presence of cell extensions, veils and ruffles) was observed in *B. besnoiti*-infected dendritic cells when compared with *N. caninum* and *T. gondii* infections (Pastor-Fernández et al., unpublished data) that could be compatible with a migratory phenotype. In this regard, further studies should attempt to obtain conclusive results in *B. besnoiti*-infected bovine macrophages.

The macrophage activation by live parasites shown by the morphological changes was also reflected at the transcriptomic level. The number of DEGs increased at 8 h p.i. and could reflect an intracellular environment more prone to favour parasite immune evasion and survival. This hypothesis is supported by a higher number of intracellular events present at 8 h p.i. The GO and KEGG terms showed that *B. besnoiti* infection predominantly modulates the apoptosis and MAPK pathways at 4 h p.i. versus the *Herpes simplex*virus 1 infection pathway at 8 h p.i., since these pathways were not enriched in macrophages that phagocytosed dead parasites when compared with non-infected cells.

The transcriptional response induced by live parasites revealed features of programmed cell death at 4 h p.i. A wide variety of DEGs, including death receptors and apoptosis regulators from both intrinsic (*FAS*, *ERN1*, *ITPR1*, *Caspase 6*, *Tubulin-α*, *Laminin b1*) and extrinsic pathways (*ATF4*, *CHOP*, *Bcl-2*, *Cathepsin Z*, *NRAS*, *GADD45*) were upregulated. Moreover, prolonged ER stress activates the apoptotic pathway (Galluzi et al., 2016), and significant upregulation of ER stress- and UPR-related genes was also observed (e.g. *IRE1α* and *ITPR1*). These results correlate with a significantly higher number of apoptotic cells visualized by IF at 8 h p.i. versus 4 h p.i. in macrophage cultures infected with live parasites. This asynchrony between transcriptomic and proteomic changes could be attributed to the fact that the regulation of transcription and translation contains a time-delayed component in eukaryote species (Maier et al., 2009; de Sousa Abreu et al., 2009; Wang et al., 2010). Remarkably, apoptotic cells were not infected by *B. besnoiti,* although apoptosis was likely induced by live parasites since these apoptotic cells were not present in non-infected macrophage control wells. Similar observations were reported in *T. gondii* infection, and it was hypothesized that the parasite might still protect the infected cell from apoptosis, while cell death is efficiently induced in non-infected cells (Mordue et al., 2001). Several studies have provided feasible explanations for how programmed cell death that is thought to promote efficient pathogen clearance can also contribute to parasite immune evasion (reviewed by Bosurgi and Rothlin, 2021). Indeed, apoptosis induction or inhibition by *Toxoplasma* is quite complex, and the mode of action is thought to be dependent on both parasite strain and host cell type. In this sense, a highly virulent type I Toxoplasma strain may induce apoptosis in lymphocytes and other immune cells, facilitating parasite immune evasion and virulence during the acute phase of infection (Gavrilescu et al., 2001, whereas type II strains can interfere with the host cell apoptosis machinery at different levels (Besteiro, 2015; Lima et al., 2019). The ability of *B. besnoiti* to prevent host cell apoptosis should also be considered, as it might facilitate parasite survival during the chronic phase of infection, similar to how other relevant tissue cyst-forming parasites act (Mammari et al., 2019; Rosenberg et al., 2021). In this regard, transcriptional changes such as the downregulation of *Caspase-3*, an apoptosis executioner caspase, and the modulation of *Herpes simplex* virus 1 infection at 8 h p.i., together with the

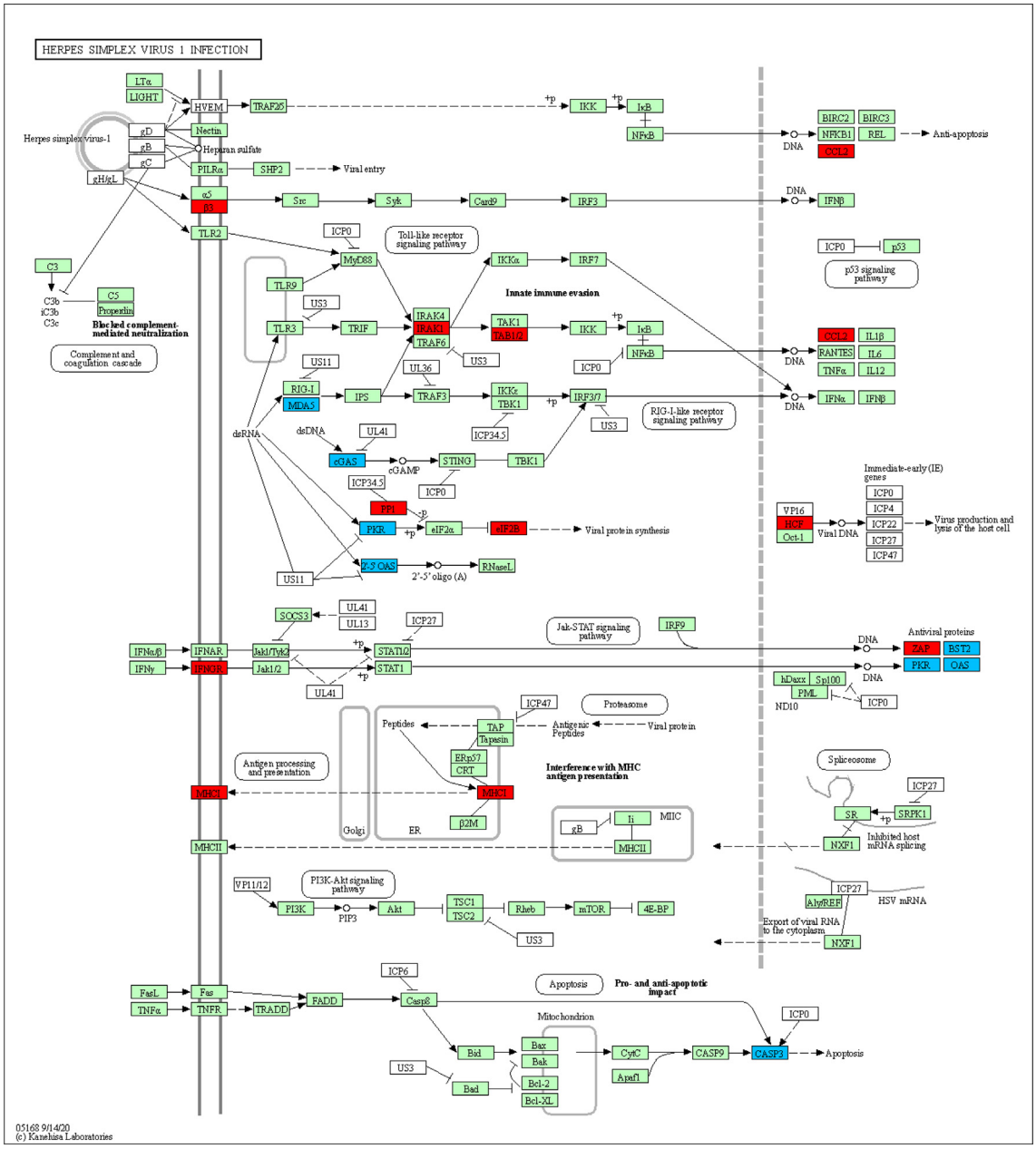


**Fig. 5.** The Kyoto Encyclopedia of Genes and Genomes (KEGG) pathway map (bta05168) represents the *Herpes simplex* virus 1 infection pathway in which differentially expressed genes (DEGs) in bovine macrophages infected with *Besnoitia besnoiti* (MO-Bb) versus non-infected macrophages (MO) at 8 h p.i. are highlighted. Upregulated genes are represented in red, and downregulated genes are represented in blue. Viral genes involved in viral interference are presented in white. The results were obtained from three biological replicates for each condition.

results obtained in the testicular parenchyma of naturally infected bulls, might serve as indications.

*Herpes simplex* virus 1 infection was the only pathway regulated by live parasites at 8 h p.i., which agrees with previous reports in *T. gondii* infection (Bougdour et al., 2013; Wang et al., 2019). It is known that during *Herpes simplex* virus 1 infection, the main immune evasion mechanism consists of dampening of type-I interferon production and its downstream signalling pathway (Su et al., 2016; Danastas et al., 2020). Several type-I ISG genes that participate in the immune response raised against *Herpes simplex* virus and are involved in apoptosis were downregulated (*OAS2*, *IFIH1* and *cGAS*) (Melchjorsen et al., 2010; Pierog et al., 2017; Zeng et al., 2022).

The modulation of these relevant pathways by the parasite in vivo was supported by the downregulation of *CHOP* and *IFNα* in the testicular parenchyma of infected bulls that could favour parasite persistence and tissue cyst formation. Upon infection by pathogens, effector proteins in ER are activated and further involved in regulation of apoptosis, whereas knockdown of the CHOP gene has been related with a defect in the cellular stress response pathway which attenuates ER stress-induced apoptosis (Hu et al., 2019). Moreover, it is known that *T. gondii* effector TgIST blocks type-I IFN signalling to promote infection (Matta et al., 2019).

Finally, type-I metallothioneins (*MT1A, MT1E*), that were regulated in infected macrophages, have been demonstrated to be

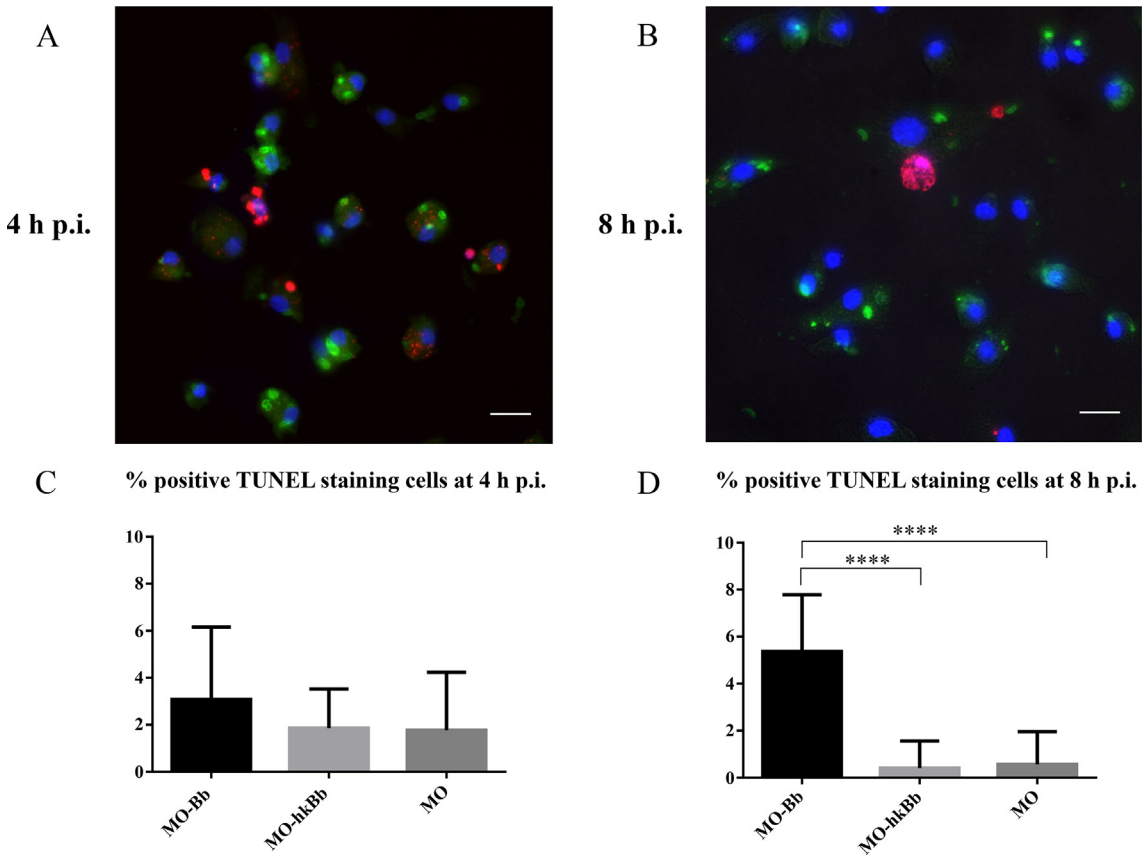


**Fig. 6.** Apoptosis visualization by terminal deoxynucleotidyl transferase-mediated dUTP nick-end labelling (TUNEL) assay. TUNEL assay in macrophages infected with live *Besnoitia besnoiti* tachyzoites at 4 h p.i. (A) and at 8 h p.i. (B) Percentage of macrophages undergoing apoptosis at 4 h (C) and 8 h p.i. (D). Apoptotic macrophages showed TUNEL-positive red-stained nuclei. Scale bars: 100 μm. MO-Bb, macrophages infected with live tachyzoites; MO-hkBb, macrophages infected with heat-killed tachyzoites; MO, non-infected macrophages. ****Adjusted *P* value less than 0.0001; as determined by Kruskal-Wallis test followed by Dunn's test.

essential stress proteins in maintaining physiological balance and regulating immune homeostasis. In particular, *MT1A* is a relevant marker of chronic inflammation and a leukocyte chemotactic protein that is synthesized in response to acute phase cytokines (Dai et al., 2021). Despite the undoubted value of these tissue samples, the correlation of transcriptomic results obtained in vitro and in vivo is hampered, as it is influenced by the complexity of the tissue composition and the time points p.i. In fact, gene expression of cells may differ in vitro and in vivo (Nilsson et al., 2020), and this could be because functional dynamic genetic effects on gene regulation are specific to particular cell types, but also due to environmental conditions (Findley et al., 2021).

Additional parasite survival strategies should be considered and investigated in future studies. Herein, the classical proinflammatory activation characterized by the induction of a predominantly M1 phenotype was not triggered at early infection, which could prevent the macrophage immune response to infection (Supplementary Fig. S4). On the other hand, the lysosome pathway was modulated by both live and dead parasites. However, live parasites exhibited a different regulation pattern, which might be related to the parasite's ability to reside in a parasitophorous vacuole and avoid lysosomal degradation. In addition, previous studies showed that the low virulence *N. caninum* isolate (NcSpain-1H) was able to regulate the lysosome pathway. However, none of the *N. caninum*-regulated genes, except for cathepsins, were regulated by *B. besnoitia,* which modulated other genes (García-Sánchez et al., 2020).

Transcriptomic analyses of *B. besnoiti* led us to identify a large set of putative parasite effectors that might be involved in macrophage activation. DEGs were categorized into two main groups: invasion and metabolism, which are critical processes for a pathogen to establish a niche within the host (Blume and Seeber, 2018).

The early invasion step associated with the higher number of intracellular events identified at 8 h p.i. was mainly represented by the upregulation of numerous rhoptry bulb (*ROP*s) and neck (*RON*s) protein encoding genes. In a previous study conducted in BAECs infected with *B. besnoiti,* the upregulation of *RON*s and *ROP*s also predominated during parasite proliferation. Several *ROP*s and *RON*s found herein corresponded to DEGs previously identified in infected BAECs (*ROP6*, *ROP11*, *ROP12*, *ROP18*, *ROP31*, *ROP32*, *ROP37*, *ROP40*, *RON3*, *RON4*, *RON5*, *RON6*, *RON8* and *RON10*), whereas other DEGs were identified for the first known time (*ROP14*, *ROP15*, *ROP17*, *ROP23*, *ROP26*, *ROP38*, *RON1*, *RON2* and *RON9*). These findings support the statement that rhoptries play a central role in invasion and the establishment of intracellular parasitism in *Besnoitia* infection, as proven for other apicomplexan parasites (Ben Chaabene et al., 2021). Whether some of these DEGs encode the main virulence factors responsible for manipulating the host transcriptome, as reported for *Toxoplasma* (Hakimi and Bougdour, 2015), should be further studied. ROP18 is an interesting target since the orthologous *Toxoplasma* virulence factor ROP18 inhibits type-I IFN production by interacting with the cGAS sensor (Melo et al., 2013; Wang et al., 2019; Chen et al., 2022), which is a pathway modulated by *Besnoitia,* as discussed above.

*Besnoitia besnoiti*, similar to other apicomplexan parasites, is an auxotrophic parasite that depends on the host for some essential nutrients. However, the strategies employed to acquire nutrients

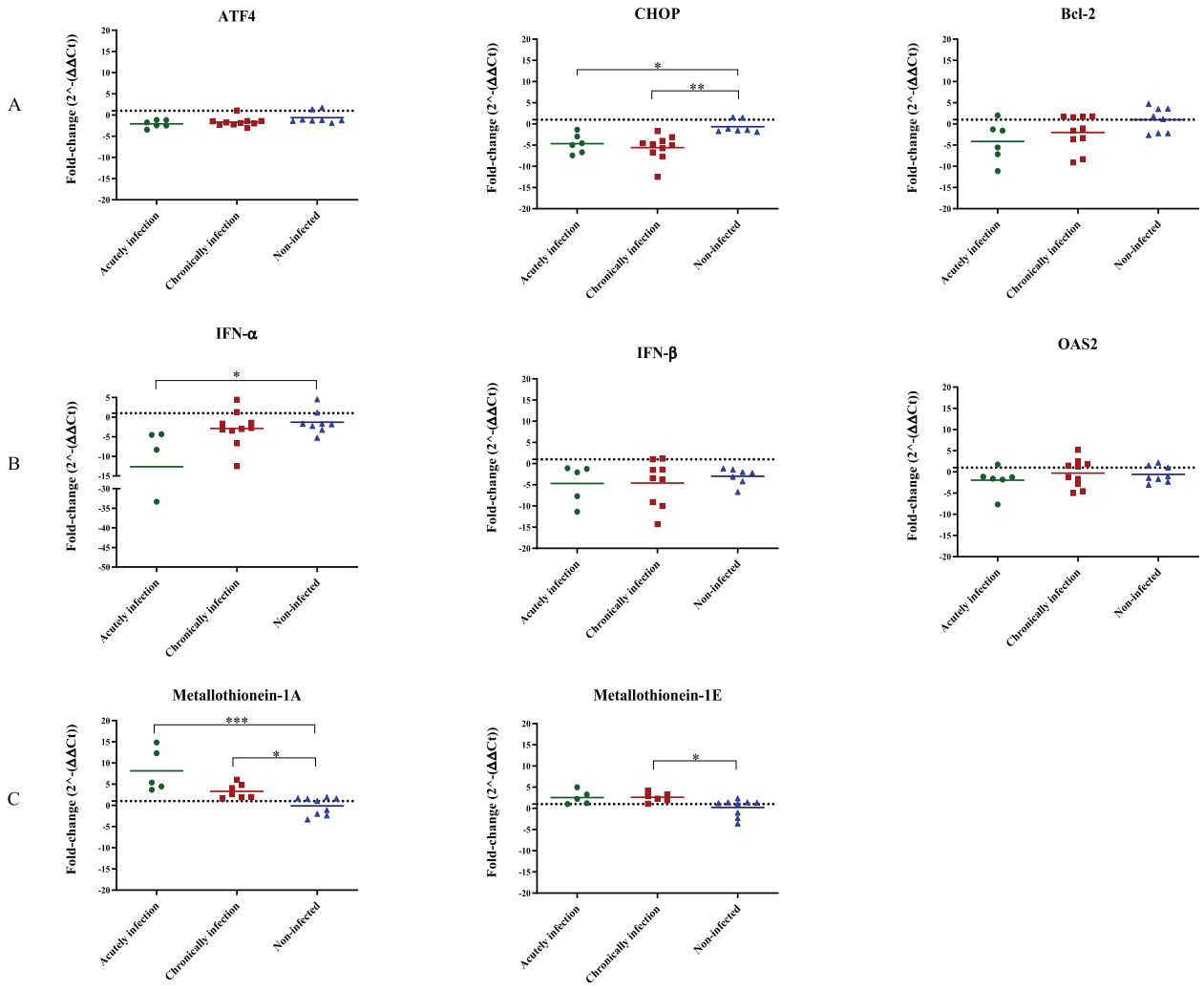


**Fig. 7.** Scatter plot graphs of relative mRNA expression levels derived from real-time quantitative reverse-transcription PCR (RT-qPCR) analysis across testicular parenchyma samples from naturally infected bulls. Each dot represents data obtained from one bull (acutely infected, chronically infected, non-infected), and the bar represents the average fold-change (FC) for each gene and condition. The genes analysed were those associated with the (A) apoptosis pathway (*ATF4, CHOP, Bcl-2*), (B) *Herpes simplex* pathway (*IFNα, IFNβ, OAS2*) and (C) *metallothionein 1A* and *metallothionein 1E,* which showed the highest FC in macrophages infected with live tachyzoites at 8 h p.i. The horizontal discontinuous line set at 1 indicates uninfected, the baseline for animals. *Adjusted *P* values between 0.01 and 0.05; **adjusted *P* values between 0.01 and 0.001; *** adjusted *P* values less than 0.001; as determined by Kruskal-Wallis test followed by Dunn's test.

from the host are unknown (Larrazabal et al., 2021). Transcriptomic analysis showed the relevance of valine, leucine, isoleucine, and arginine metabolism. These are essential amino acids that must be taken up by *Toxoplasma* and *Plasmodium* (reviewed by Krishnan et al., 2021). Moreover, *B. besnoiti* encodes various enzymes for pantothenic acid and CoA synthesis, and these pathways are essential for *T. gondii* acute and chronic infection (Lunghi et al., 2022). Our data indicate that *B. besnoiti* might also be capable of regulating nitrogen metabolism. *Toxoplasma gondii* acquires nitrate and nitrite from the host as sources of ammonia, which is required for the de novo synthesis of glutamine and glutamate, two non-essential amino acids (Krishnan et al., 2021). These results highlight the relevance of metabolism during *B. besnoiti* at early invasion and offer promising chemotherapy targets.

Furthermore, only one gene (BESB_064630) that encodes a PAN/Apple domain-containing protein was upregulated at 4 h p.i. This domain is believed to mediate interspecific interactions between proteins and carbohydrates, thereby providing a link between the host and parasite during *T. gondii* infection (Gong et al., 2012), and could also be involved in *B. besnoiti* adhesion to macrophages during the initial interaction (4 h p.i.). The results obtained herein, together with the comparative transcriptomic data of the tachyzoite and bradyzoite stages (Ramakrishnan et al., 2022), and the differences on the metabolomic level between *T. gondii*- and *B. besnoiti*-infected host cells (Kadesch et al., 2020), may serve to give a clue about putative drug targets.

In conclusion, we have demonstrated that *Besnoitia* tachyzoites can invade and proliferate in bovine primary monocyte-derived macrophages and modulate this host cell, inducing morphological as well as transcriptomic changes. This study represents the first known attempt to dissect *Besnoitia*-macrophage interactions by means of a dual RNA-Seq analysis during early parasite invasion. Apoptosis-, MAPK- and *Herpes simplex* virus 1 infection-enriched pathways could provide clues about the putative early evasion mechanisms induced by the parasite that could facilitate parasite replication and dissemination. Additionally, several biomarkers were associated with in vivo infection. Several parasite effectors, mainly involved in invasion and metabolism, that could be responsible for the altered host transcriptome were also identified for the first known time. Whether any host and parasite DEGs might represent valuable vaccine or drug targets should be investigated.

**Table 2**
Category, gene ID, gene description, *Toxoplasma gondii* orthology analysis results and fold-change (FC) of a selection of *Besnoitia besnoiti* differentially expressed genes (DEGs).

| | | Gene ID | Description | *Toxoplasma gondii* ortholog | FC MO-Bb at 8 h vs MO-Bb at 4 h p.i. |
|---|---|---|---|---|---|
| **Invasion** | **Rhoptries** | BESB_055810 | *Rhoptry protein, putative* | TGME49_315210 | 10.41 |
| | | BESB_079420 | *RON3* | TGME49_223920 | 6.98 |
| | | BESB_072910 | *RON5* | TGME49_311470 | 6.97 |
| | | BESB_071010 | *RON9* | TGME49_308810 | 6.56 |
| | | BESB_002170 | *RON10* | TGME49_261750 | 6.41 |
| | | BESB_040860 | *RON2* | TGME49_300100 | 6.40 |
| | | BESB_052840 | *Rhoptry metalloprotease toxolysin 1* | TGME49_269885 | 6.28 |
| | | BESB_063670 | *RON6* | TGME49_297960 | 6.26 |
| | | BESB_071470 | *RON1* | TGME49_310010 | 5.70 |
| | | BESB_018150 | *RON8* | TGME49_306060 | 5.68 |
| | | BESB_083570 | *RON4* | TGME49_229010 | 5.07 |
| | | BESB_010080 | *ROP37* | . | 17.15 |
| | | BESB_059140 | *ROP11* | TGME49_227810 | 11.85 |
| | | BESB_016430 | *ROP15* | TGME49_211290 | 11.30 |
| | | BESB_048880 | *ROP32* | . | 11.18 |
| | | BESB_019040 | *ROP40* | TGME49_291960 | 10.33 |
| | | BESB_055800 | *ROP14* | TGME49_315220 | 9.96 |
| | | BESB_016400 | *ROP26* | TGME49_211260 | 7.28 |
| | | BESB_082430 | *ROP23* | TGME49_239600 | 7.11 |
| | | BESB_002440 | *ROP31* | TGME49_258800 | 7.06 |
| | | BESB_084550 | *ROP6* | TGME49_258660 | 6.12 |
| | | BESB_065210 | *ROP12* | TGME49_203990 | 5.88 |
| | | BESB_084470 | *ROP17* | TGME49_258580 | 5.85 |
| | | BESB_013500 | *ROP18* | . | 5.31 |
| | | BESB_052840 | *Rhoptry metalloprotease toxolysin 1* | TGME49_269885 | 6.28 |
| | **Micronemes** | BESB_067360 | *Microneme-like protein* | TGME49_286740 | 3.18 |
| | **Surface proteins** | BESB_033430 | *SAG-related sequence SRS49D* | TGME49_207160 | 5.65 |
| | **Gliding motility** | BESB_072760 | *Myosin light chain 1* | TGME49_311260 | 5.19 |
| | | BESB_052960 | *Myosin-light-chain kinase* | TGME49_269730 | 4.70 |
| | | BESB_025840 | *Myosin light chain 4* | TGME49_294390 | 3.76 |
| **Metabolism** | **Valine, leucine, and isoleucine degradation** | BESB_072840 | *putative methylmalonate-semialdehyde dehydrogenase [acylating]* | TGME49_311370 | 10.81 |
| | | BESB_051790 | *putative hydroxymethylglutaryl-CoA lyase* | TGME49_204460 | 10.65 |
| | | BESB_007470 | *putative acetyl-CoA acyltransferase B* | TGME49_273740 | 8.33 |
| | | BESB_079590 | *enoyl-CoA hydratase/isomerase family protein* | TGME49_224090 | 6.59 |
| | | BESB_076350 | *pyruvate carboxylase* | TGME49_284190 | 6.02 |
| | | BESB_039920 | *AMP-binding enzyme domain-containing protein* | TGME49_219230 | 5.29 |
| | | BESB_000260 | *aldehyde dehydrogenase* | TGME49_264000 | 3.43 |
| | **Pantothenate and CoA biosynthesis** | BESB_069580 | *putative Acetyl-coenzyme A transporter* | TGME49_215940 | 5.51 |
| | | BESB_044550 | *deoxyribose-phosphate aldolase* | TGME49_318750 | 5.15 |
| | | BESB_046420 | *flavoprotein* | TGME49_242880 | 5.13 |
| | | BESB_052960 | *myosin-light-chain kinase* | TGME49_269730 | 4.70 |
| | | BESB_045210 | *Maf family protein* | TGME49_240450 | 4.52 |
| | | BESB_078080 | *uridine kinase* | TGME49_316700 | 4.10 |
| | | BESB_000260 | *aldehyde dehydrogenase* | TGME49_264000 | 3.43 |
| | **Nitrogen metabolism** | BESB_003210 | *carbonate dehydratase, eukaryotic-type domain-containing protein* | TGME49_259950 | 5.87 |
| | | BESB_071380 | *dynein heavy chain family protein* | TGME49_309980 | 4.48 |
| | | BESB_025910 | *dynein heavy chain* | TGME49_294550 | 3.05 |
| | **Arginine biosynthesis** | BESB_085430 | *ATP-binding cassette transporter ABC.B1* | TGME49_260310 | 6.18 |
| | | BESB_014390 | *peptidase M20D, amidohydrolase* | TGME49_213520 | 5.91 |
| | | BESB_071380 | *dynein heavy chain family protein* | TGME49_309980 | 4.48 |
| | | BESB_003190 | *Nitric-oxide synthase* | TGME49_259920 | 4.20 |
| | | BESB_025910 | *dynein heavy chain* | TGME49_294550 | 3.05 |

FC. fold change; MO-Bb, macrophages infected with live *B. besnoiti* tachyzoites; MO-hkBb, macrophages inoculated with heat-killed *B. besnoiti* tachyzoites.

## Acknowledgements

This work was financially supported through research projects from the Spanish Ministry of Economy and Competitiveness (Ref. AGL2016-75202-R and Ref. PID2019-103960RB-I00) and the Community of Madrid, Spain (Ref. P2018/BAA-4370 PLATESA2-CM). MF-A was supported by a grant from the Complutense University of Madrid (Ref- UCM 2018).

## Appendix A. Supplementary material

Supplementary data to this article can be found online at https://doi.org/10.1016/j.ijpara.2023.05.002.

## References

Álvarez-García, G., Frey, C.F., Ortega-Mora, L.M., Schares, G., 2013. A century of bovine besnoitiosis: An unknown disease re-emerging in Europe. Trends Parasitol. 29 (8), 407–415. https://doi.org/10.1016/j.pt.2013.06.002.

Álvarez-García, G., García-Lunar, P., Gutiérrez-Expósito, D., Shkap, V., Ortega-Mora, L.M., 2014. Dynamics of *Besnoitia besnoiti* infection in cattle. Parasitology 141 (11), 1419–1435. https://doi.org/10.1017/S0031182014000729.

Anders, S, Huber, W, 2010. Differential expression analysis for sequence count data. Genome Biol 11 (10), R106. https://doi.org/10.1186/gb-2010-11-10-r106.

Ben Chaabene, R., Lentini, G., Soldati-Favre, D., 2021. Biogenesis and discharge of the Rhoptries: Key organelles for entry and hijack of host cells by the Apicomplexa. Mol. Microbiol. 115 (3), 453–465. https://doi.org/10.1111/mmi.14674.

Benjamini, Y., Hochberg, Y., 1995. Controlling the false discovery rate: a practical and powerful approach to multiple testing. J. Roy. Stat. Soc. B Met. 57, 289–300. https://doi.org/10.1111/j.2517-6161.1995.tb02031.x.

Besteiro, S., 2015. *Toxoplasma* control of host apoptosis: The art of not biting too hard the hands that feeds you. Microbial Cell 2 (6), 178–181. https://doi.org/10.15698/mic2015.06.209.

Bhandage, A.K., Barragan, A., 2019. Calling in the cavalry—*Toxoplasma gondii* hijacks GABAergic signaling and voltage-dependent calcium channel signalling for trojan horse-mediated dissemination. Front. Cell. Infect. Microbiol. 9, 61. https://doi.org/10.3389/fcimb.2019.00061.

Blume, M., Seeber, F., 2018. Metabolic interactions between *Toxoplasma gondii* and its host. F1000 Res. 7, 1719. https://doi.org/10.12688/f1000research.16021.1.

Bosurgi, L., Rothlin, C.V., 2021. Management of cell death in parasitic infections. Sem. Immunopathol. 43 (4), 481–492. https://doi.org/10.1007/s00281-021-00875-8.

Bougdour, A., Durandau, E., Brenier-Pinchart, M.-P., Ortet, P., Barakat, M., Kieffer, S., Curt-Varesano, A., Curt-Bertini, R.-L., Bastien, O., Coute, Y., Pelloux, H., Hakimi, M.-A., 2013. Host cell subversion by *Toxoplasma* GRA16, an exported dense granule protein that targets the host cell nucleus and alters gene expression. Cell Host Microbe 13 (4), 489–500. https://doi.org/10.1016/j.chom.2013.03.002.

Chen, M., Yao, L., Zhou, L., Yang, P., Zou, W., Xu, L., Li, S., Peng, H., 2022. *Toxoplasma gondii* ROP18 inhibits host innate immunity through cGAS-STING signaling. FASEB J. 36 (2), e22171.

Dai, H., Wang, L., Li, L., Huang, Z., Ye, L., 2021. Metallothionein 1: a new spotlight on inflammatory diseases. Fronti. Immunol. 12,. https://doi.org/10.3389/fimmu.2021.739918 739918.

Danastas, K., Miranda-Saksena, M., Cunningham, A.L., 2020. *Herpes simplex* virus type 1 interactions with the interferon system. Int. J. Mol. Sci. 21 (14), 5150. https://doi.org/10.3390/ijms21145150.

de Sousa Abreu, R., Penalva, L.O., Marcotte, E.M., Vogel, C., 2009. Global signatures of protein and mRNA expression levels. Mol. BioSyst. 5 (12), 1512–1526. https://doi.org/10.1039/b908315d.

Diezma-Díaz, C., Jiménez-Meléndez, A., Re, M.T., Ferre, I., del Ferreras, M., Gutiérrez-Expósito, D., Rojo-Montejo, S., Román-Trufero, A., Benavides-Silván, J., García-Lunar, P., Calleja-Bueno, L., Blanco-Murcia, J., Osoro, K., Ortega-Mora, L.-M., Álvarez-García, G., 2018. Effect of parasite dose and host age on the infection with *Besnoitia besnoiti* tachyzoites in cattle. Transboundary Emerg. Dis. 65 (6), 1979–1990. https://doi.org/10.1111/tbed.12980.

Fernández-García, A., Álvarez-García, G., Risco-Castillo, V., Aguado-Martínez, A., Marugán-Hernández, V., Ortega-Mora, L.M., 2009. Pattern of recognition of *Besnoitia besnoiti* tachyzoite and bradyzoite antigens by naturally infected cattle. Vet. Parasitol. 164 (2–4), 104–110. https://doi.org/10.1016/j.vetpar.2009.06.020.

Findley, A.S., Monziani, A., Richards, A.L., Rhodes, K., Ward, M.C., Kalita, C.A., Alazizi, A., Pazokitoroudi, A., Sankararaman, S., Wen, X., Lanfear, D.E., Pique-Regi, R., Gilad, Y., Luca, F., 2021. Functional dynamic genetic effects on gene regulation are specific to particular cell types and environmental conditions. ELife 10, e67077.

Frey, C.F., Regidor-Cerrillo, J., Marreros, N., García-Lunar, P., Gutiérrez-Expósito, D., Schares, G., Dubey, J.P., Gentile, A., Jacquiet, P., Shkap, V., Cortes, H., Ortega-Mora, L.M., Álvarez-García, G., 2016. *Besnoitia besnoiti* lytic cycle *in vitro* and differences in invasion and intracellular proliferation among isolates. Parasites Vectors 9, 115. https://doi.org/10.1186/s13071-016-1405-9.

Galluzzi, L., Diotallevi, A., De Santi, M., Ceccarelli, M., Vitale, F., Brandi, G., Magnani, M., 2016. *Leishmania infantum* induces mild unfolded protein response in infected macrophages. PLOS ONE 11 (12), e0168339.

García-Lunar, P., Ortega-Mora, L.M., Schares, G., Gollnick, N.S., Jacquiet, P., Grisez, C., Prevot, F., Frey, C.F., Gottstein, B., Álvarez-García, G., 2012. An inter-laboratory comparative study of serological tools employed in the diagnosis of *Besnoitia besnoiti* infection in Bovines. Transboundary Emerg. Dis. 60 (1), 59–68. https://doi.org/10.1111/j.1865-1682.2012.01318.x.

García-Sánchez, M., Jiménez-Pelayo, L., Horcajo, P., Regidor-Cerrillo, J., Ólafsson, E.B., Bhandage, A.K., Barragan, A., Werling, D., Ortega-Mora, L.M., Collantes-Fernández, E., 2019. Differential responses of bovine monocyte-derived macrophages to infection by *Neospora caninum* isolates of high and low virulence. Frontiers Immunol. 10, 915. https://doi.org/10.3389/fimmu.2019.00915.

García-Sánchez, M., Jiménez-Pelayo, L., Horcajo, P., Collantes-Fernánez, E., Ortega-Moira, L.M., Regidor-Cerrillo, J., 2020. *Neospora caninum* infection induces an isolate virulence-dependent pro-inflammatory gene expression profile in bovine monocyte-derived macrophages. Parasites Vectors 13, 374. https://doi.org/10.1186/s13071-020-04239-3.

Gavrilescu, L.C., Denkers, E.Y., 2001. IFN-γ overproduction and high-level apoptosis are associated with high but not low virulence *Toxoplasma gondii* infection. J. Immunol. 167 (2), 902–909. https://doi.org/10.4049/jimmunol.167.2.902.

Gollnick, N.S., Scharr, J.C., Schares, G., Langenmayer, M.C., 2015. Natural *Besnoitia besnoiti* infections in cattle: Chronology of disease progression. BMC Vet. Res. 11. https://doi.org/10.1186/s12917-015-0344-6.

Gong, H., Kobayashi, K., Sugi, T., Takemae, H., Kurokawa, H., Horimoto, T., Akashi, H., Kato, K., 2012. A novel Pan/Apple Domain-containing protein from *Toxoplasma gondii*: Characterization and receptor identification. PLoS ONE 7 (1), e30169.

González-Barrio, D., Diezma-Díaz, C., Tabanera, E., Aguado-Criado, E., Pizarro, M., González-Huecas, M., Ferre, I., Jiménez-Meléndez, A., Criado, F., Gutiérrez-Expósito, D., Ortega-Mora, L.M., Álvarez-García, G., 2020. Vascular wall injury and inflammation are key pathogenic mechanisms responsible for early testicular degeneration during acute besnoitiosis in bulls. Parasites Vectors 13, 113. https://doi.org/10.1186/s13071-020-3959-9.

González-Barrio, D., Diezma-Díaz, C., Gutiérrez-Expósito, D., Tabanera, E., Jiménez-Meléndez, A., Pizarro, M., González-Huecas, M., Ferre, I., Ortega-Mora, L.M., Álvarez-García, G., 2021. Identification of molecular biomarkers associated with disease progression in the testis of bulls infected with *Besnoitia besnoiti*. Vet. Res. 52, 106. https://doi.org/10.1186/s13567-021-00974-2.

Gutiérrez-Expósito, D., Ortega-Mora, L.M., Gajadhar, A.A., García-Lunar, P., Dubey, J. P., Álvarez-García, G., 2012. Serological evidence of *Besnoitia* spp. infection in Canadian wild ruminants and strong cross-reaction between *Besnoitia besnoiti* and *Besnoitia tarandi*. Vet. Parasitol. 190 (1–2), 19–28. https://doi.org/10.1016/j.vetpar.2012.06.017.

Hakimi, M.-A., Bougdour, A., 2015. *Toxoplasma*'s ways of manipulating the host transcriptome via secreted effectors. Curr. Opin. Microbiol. 26, 24–31. https://doi.org/10.1016/j.mib.2015.04.003.

Hoffmann, B., Depner, K., Schirrmeier, H., Beer, M., 2006. A universal heterologous internal control system for duplex real-time RT-PCR assays used in a detection system for pestiviruses. J. Virolog. Methods 136 (1–2), 200–209. https://doi.org/10.1016/j.jviromet.2006.05.020.

Horcajo, P., Jiménez-Pelayo, L., García-Sánchez, M., Regidor-Cerrillo, J., Collantes-Fernández, E., Rozas, D., Hambruch, N., Pfarrer, C., Ortega-Mora, L.M., 2017. Transcriptome modulation of bovine trophoblast cells *in vitro* by *Neospora caninum*. Int. J. Parasitol. 47 (12), 791–799. https://doi.org/10.1016/j.ijpara.2017.08.007.

Hu, H., Tian, M., Ding, C., Yu, S., 2019. The C/EBP homologous protein (CHOP) transcription factor functions in endoplasmic reticulum stress-induced apoptosis and microbial infection. Front. Immunol. 9, 3083. https://doi.org/10.3389/fimmu.2018.03083.

Jiménez-Meléndez, A., Ojo, K.K., Wallace, A.M., Smith, T.R., Hemphill, A., Balmer, V., Regidor-Cerrillo, J., Ortega-Mora, L.M., Hehl, A.B., Fan, E., Maly, D.J., Van Voorhis, W.C., Álvarez-García, G., 2017. *In vitro* efficacy of bumped kinase inhibitors against *Besnoitia besnoiti* tachyzoites. Int. J. Parasitol. 47 (12), 811–821. https://doi.org/10.1016/j.ijpara.2017.08.005.

Jiménez-Meléndez, A., Fernández-Álvarez, M., Calle, A., Ramírez, M.Á., Diezma-Díaz, C., Vázquez-Arbaizar, P., Ortega-Mora, L.M., Álvarez-García, G., 2019. Lytic cycle of *Besnoitia besnoiti* tachyzoites displays similar features in primary bovine endothelial cells and fibroblasts. Parasites Vectors 12 (1), 517. https://doi.org/10.1186/s13071-019-3777-0.

Jiménez-Meléndez, A., Ramakrishnan, C., Hehl, A.B., Russo, G., Álvarez-García, G., 2020. RNA-seq analyses reveal that endothelial activation and fibrosis are induced early and progressively by *Besnoitia besnoiti* host cell invasion and proliferation. Front. Cell. Infect. Microbiol. 10, 218. https://doi.org/10.3389/fcimb.2020.00218.

Jiménez-Pelayo, L., García-Sánchez, M., Regidor-Cerrillo, J., Horcajo, P., Collantes-Fernández, E., Gómez-Bautista, M., Hambruch, N., Pfarrer, C., Ortega-Mora, L.M., 2017. Differential susceptibility of bovine caruncular and trophoblast cell lines to infection with high and low virulence isolates of *Neospora caninum*. Parasites Vectors 10 (1), 463. https://doi.org/10.1186/s13071-017-2409-9.

Jiménez-Pelayo, L., García-Sánchez, M., Collantes-Fernández, E., Regidor-Cerrillo, J., Horcajo, P., Gutiérrez-Expósito, D., Espinosa, J., Benavides, J., Osoro, K., Pfarrer, C., Ortega-Mora, L.M., 2020. Crosstalk between *Neospora caninum* and the bovine host at the maternal-foetal interface determines the outcome of infection. Vet. Res. 51 (1), 83. https://doi.org/10.1186/s13567-020-00803-y.

Jombart, T., 2008. Adegenet: A R package for the multivariate analysis of genetic markers. Bioinformatics 24 (11), 1403–1405. https://doi.org/10.1093/bioinformatics/btn129.

Kadesch, P., Hollubarsch, T., Gerbig, S., Schneider, L., Silva, L.M., Hermosilla, C., Taubert, A., Spengler, B., 2020. Intracellular Parasites *Toxoplasma gondii* and *Besnoitia besnoiti*, unveiled in single host cells using AP-SMALDI MS imaging. J. American Soc. Mass Spectrom. 31 (9), 1815–1824. https://doi.org/10.1021/jasms.0c00043.

Kim, D., Pertea, G., Trapnell, C., Pimentel, H., Kelley, R., Salzberg, S.L., 2013. Tophat2: accurate alignment of transcriptomes in the presence of insertions, deletions and Gene Fusions. Genome Biol. 14 (4), R36. https://doi.org/10.1186/gb-2013-14-4-r36.

Krishnan, A., Soldati-Favre, D., 2021. Amino acid metabolism in Apicomplexan parasites. Metabolites 11 (2), 61. https://doi.org/10.3390/metabo11020061.

Larrazabal, C., Silva, L.M., Hermosilla, C., Taubert, A., 2021. Ezetimibe blocks *Toxoplasma gondii*, *Neospora caninum* and *Besnoitia besnoiti* tachyzoite infectivity and replication in primary bovine endothelial host cells. Parasitology 148 (9), 1107–1115. https://doi.org/10.1017/s0031182021000822.

Lima, T.S., Lodoen, M.B., 2019. Mechanisms of human innate immune evasion by *Toxoplasma gondii*. Front. Cell. Infect. Microbiol. 9, 103. https://doi.org/10.3389/fcimb.2019.00103.

Livak, K.J., Schmittgen, T.D., 2001. Analysis of relative gene expression data using real-time quantitative PCR and the $2-\Delta\Delta CT$ method. Methods 25 (4), 402–408. https://doi.org/10.1006/meth.2001.1262.

Love, MI, Huber, W, Anders, S, 2014. Moderated estimation of fold change and dispersion for RNA-seq data with DESeq2. Genome Biol 15 (12), 550. https://doi.org/10.1186/s13059-014-0550-8.

Lunghi, M., Kloehn, J., Krishnan, A., Varesio, E., Vadas, O., Soldati-Favre, D., 2022. Pantothenate biosynthesis is critical for chronic infection by the neurotropic parasite *Toxoplasma gondii*. Nature Comm. 13 (1), 345. https://doi.org/10.1038/s41467-022-27996-4.

Maier, T., Güell, M., Serrano, L., 2009. Correlation of mRNA and protein in complex biological samples. FEBS Lett. 583 (24), 3966–3973. https://doi.org/10.1016/j.febslet.2009.10.036.

Maksimov, P., Hermosilla, C., Kleinertz, S., Hirzmann, J., Taubert, A., 2016. *Besnoitia besnoiti* infections activate primary bovine endothelial cells and promote PMN adhesion and net formation under physiological flow condition. Parasitol. Res. 115 (5), 1991–2001. https://doi.org/10.1007/s00436-016-4941-5.

Mammari, N., Halabi, M.A., Yaacoub, S., Chlala, H., Dardé, M.-L., Courtioux, B., 2019. *Toxoplasma gondii* modulates the host cell responses: An overview of apoptosis pathways. BioMed Res. Int. 2019, 1–10. https://doi.org/10.1155/2019/6152489.

Matta, S.K., Olias, P., Huang, Z., Wang, Q., Park, E., Yokoyama, W.M., Sibley, L.D., 2019. *Toxoplasma gondii* effector TgIST blocks type I interferon signaling to promote infection. Proc. Nat. Acad. Sci. 116 (35), 17480–17491. https://doi.org/10.1073/pnas.1904637116.

McCully, R.M., Basson, P.A., Van Niekerk, J.W., Bigalkie, R.D., 1966. Observations on *Besnoitia* cysts in the cardiovascular system of some wild antelopes and domestic cattle. Onderstepoort J. Vet. Res. 33 (2), 245–276.

McWhorter, F.Y., Wang, T., Nguyen, P., Chung, T., Liu, W.F., 2013. Modulation of macrophage phenotype by cell shape. Proc. Nat. Acad. Sci. 110 (43), 17253–17258. https://doi.org/10.1073/pnas.1308887110.

Melchjorsen, J., Rintahaka, J., Søby, S., Horan, K.A., Poltajainen, A., Østergaard, L., Paludan, S.R., Matikainen, S., 2010. Early innate recognition of *Herpes simplex* virus in human primary macrophages is mediated via the MDA5/mavs-dependent and MDA5/MAVS/RNA polymerase III-independent pathways. J. Virol. 84 (21), 11350–11358. https://doi.org/10.1128/jvi.01106-10.

Melo, M.B., Nguyen, Q.P., Cordeiro, C., Hassan, M.A., Yang, N., McKell, R., Rosowski, E. E., Julien, L., Butty, V., Dardé, M.-L., Ajzenberg, D., Fitzgerald, K., Young, L.H., Saeij, J.P., 2013. Transcriptional analysis of murine macrophages infected with different *Toxoplasma* strains identifies novel regulation of host signalling pathways. PLoS Pathog. 9 (12), e1003779. https://doi.org/10.1371/journal.ppat.1003779.

Mordue, D.G., Monroy, F., La Regina, M., Dinarello, C.A., Sibley, L.D., 2001. Acute toxoplasmosis leads to lethal overproduction of th1 cytokines. J. Immunol. 167 (8), 4574–4584. https://doi.org/10.4049/jimmunol.167.8.4574.

Muñoz Caro, T., Hermosilla, C., Silva, L.M., Cortes, H., Taubert, A., 2014. Neutrophil extracellular traps as innate immune reaction against the emerging apicomplexan parasite *Besnoitia besnoiti*. PLoS ONE 9 (3), e91415.

Nilsson, L.M., Castresana-Aguirre, M., Scott, L., Brismar, H., 2020. RNA-seq reveals altered gene expression levels in proximal tubular cell cultures compared to renal cortex but not during early glucotoxicity. Sci. Rep. 10 (1), 10390. https://doi.org/10.1038/s41598-020-67361-3.

Pierog, P.L., Zhao, Y., Singh, S., Dai, J., Yap, G.S., Fitzgerald-Bocarsly, P., 2017. *Toxoplasma gondii* inactivates human plasmacytoid dendritic cells by functional mimicry of IL-10. J. Immunol. 200 (1), 186–195. https://doi.org/10.4049/jimmunol.1701045.

Pols, J.W., 1960. Studies on bovine besnoitiosis with special reference to the aetiology. Onderstepoort J. Vet. Res. 28 (3), 265–356.

Puech, C., Dedieu, L., Chantal, I., Rodrigues, V., 2015. Design and evaluation of a unique SYBR green real-time RT-PCR assay for quantification of five major cytokines in cattle, sheep and goats. BMC Vet. Res. 11 (1), 65. https://doi.org/10.1186/s12917-015-0382-0.

Ramakrishnan, C., Krishnan, A., Francisco, S., Schmid, M.W., Russo, G., Leitão, A., Hemphill, A., Soldati-Favre, D., Hehl, A.B., 2022. Dissection of *Besnoitia besnoiti* intermediate host life cycle stages: from morphology to gene expression. PLOS Pathog. 18 (11), e1010955. https://doi.org/10.1371/journal.ppat.1010955.

Regidor-Cerrillo, J., Gómez-Bautista, M., Sodupe, I., Aduriz, G., Álvarez-García, G., Del Pozo, I., Ortega-Mora, L., 2011. *In vitro* invasion efficiency and intracellular proliferation rate comprise virulence-related phenotypic traits of *Neospora caninum*. Vet. Res. 42 (1), 41. https://doi.org/10.1186/1297-9716-42-41.

Rosenberg, A., Sibley, L.D., 2021. *Toxoplasma gondii* secreted effectors co-opt host repressor complexes to inhibit necroptosis. Cell Host Microbe 29 (7), 1186–1198.e8. https://doi.org/10.1016/j.chom.2021.04.016.

Schares, G., Basso, W., Majzoub, M., Cortes, H.C., Rostaher, A., Selmair, J., Hermanns, W., Conraths, F.J., Gollnick, N.S., 2009. First *in vitro* isolation of *Besnoitia besnoiti* from chronically infected cattle in Germany. Vet. Parasitol. 163 (4), 315–322. https://doi.org/10.1016/j.vetpar.2009.04.033.

Su, X., Yu, Y., Zhong, Y., Giannopoulou, E.G., Hu, X., Liu, H., Cross, J.R., Rätsch, G., Rice, C.M., Ivashkiv, L.B., 2015. Interferon-γ regulates cellular metabolism and mrna translation to potentiate macrophage activation. Nature Immunol. 16 (8), 838–849. https://doi.org/10.1038/ni.3205.

Su, C., Zhan, G., Zheng, C., 2016. Evasion of host antiviral innate immunity by HSV-1, an update. Virol. J. 13, 38. https://doi.org/10.1186/s12985-016-0495-5.

Velásquez, Z.D., Lopez-Osorio, S., Pervizaj-Oruqaj, L., Herold, S., Hermosilla, C., Taubert, A., 2020. *Besnoitia besnoiti*–driven endothelial host cell cycle alteration. Parasitol. Res. 119 (8), 2563–2577. https://doi.org/10.1007/s00436-020-06744-x.

Wang, P., Li, S., Zhao, Y., Zhang, B., Li, Y., Liu, S., Du, H., Cao, L., Ou, M., Ye, X., Li, P., Gao, X., Wang, P., Jing, C., Shao, F., Yang, G., You, F., 2019. The GRA15 protein from *Toxoplasma gondii* enhances host defense responses by activating the Interferon stimulator sting. J. Biol. Chem. 294 (45), 16494–16508. https://doi.org/10.1074/jbc.ra119.009172.

Wang, H., Wang, Q., Pape, U.J., Shen, B., Huang, J., Wu, B., Li, X., 2010. Systematic investigation of global coordination among mRNA and protein in Cellular Society. BMC Genomics 11 (1), 364. https://doi.org/10.1186/1471-2164-11-364.

Weidner, J.M., Kanatani, S., Hernández-Castañeda, M.A., Fuks, J.M., Rethi, B., Wallin, R.P., Barragan, A., 2013. Rapid cytoskeleton remodelling in dendritic cells following invasion by *Toxoplasma gondii* coincides with the onset of a hypermigratory phenotype. Cell. Microbiol. 15 (10), 1735–1752. https://doi.org/10.1111/cmi.12145.

Zheng, Z.-Q., Fu, Y.-Z., Wang, S.-Y., Xu, Z.-S., Zou, H.-M., Wang, Y.-Y., 2022. Herpes simplex virus protein UL56 inhibits cgas-mediated DNA sensing to evade antiviral immunity. Cell Insight 1, (2). https://doi.org/10.1016/j.cellin.2022.100014 100014.

*microorganisms*

MDPI

*Article*

# Transcriptomics of *Besnoitia besnoiti*-Infected Fibroblasts Reveals Hallmarks of Early Fibrosis and Cancer Progression

**María Fernández-Álvarez [1], Pilar Horcajo [1], Alejandro Jiménez-Meléndez [1], Pablo Angulo Lara [1], Ana Huertas-López [1,2], Francisco Huertas-López [3], Ignacio Ferre [1], Luis Miguel Ortega-Mora [1] and Gema Álvarez-García [1,*]**

[1] SALUVET, Animal Health Department, Faculty of Veterinary Sciences, Complutense University of Madrid, 28040 Madrid, Spain; marfer23@ucm.es (M.F.-Á.); phorcajo@ucm.es (P.H.); ajmelendez@ucm.es (A.J.-M.); pabang01@ucm.es (P.A.L.); ana.huertas@um.es (A.H.-L.); iferrepe@ucm.es (I.F.); luis.ortega@ucm.es (L.M.O.-M.)
[2] Animal Health Department, Faculty of Veterinary Sciences, University of Murcia—Regional Campus of International Excellence "Campus Mare Nostrum", 30100 Murcia, Spain
[3] Marbyt—Smart Solutions for Biotechnology, 30100 Murcia, Spain; francisco.huertas@marbyt.com
* Correspondence: gemaga@ucm.es; Tel.: +34-913944095

**Abstract:** Endothelial injury, inflammatory infiltrate and fibrosis are the predominant lesions in the testis of bulls with besnoitiosis that may result in sterility. Moreover, fibroblasts, which are key players in fibrosis, are parasite target cells in a *Besnoitia besnoiti* chronic infection. This study aimed to decipher the molecular basis that underlies a drift toward fibrosis during the disease progression. Transcriptomic analysis was developed at two times post-infection (p.i.), representative of invasion (12 h p.i.) and intracellular proliferation (32 h p.i.), in primary bovine aorta fibroblasts infected with *B. besnoiti* tachyzoites. Once the enriched host pathways were identified, we studied the expression of selected differentially expressed genes (DEGs) in the scrotal skin of sterile infected bulls. Functional enrichment analyses of DEGs revealed shared hallmarks of cancer and early fibrosis. Biomarkers of inflammation, angiogenesis, cancer, and MAPK signaling stood out at 12 h p.i. At 32 h p.i., again MAPK and cancer pathways were enriched together with the PI3K–AKT pathway related to cell proliferation. Some DEGs were also regulated in the skin samples of naturally infected bulls (*PLAUR*, *TGFβ1*, *FOSB*). We have identified potential biomarkers and host pathways regulated during fibrosis that may hold prognostic significance and could emerge as potential therapeutic targets.

**Keywords:** *Besnoitia besnoiti*; bovine aorta fibroblasts; RNA-Seq; early fibrosis; MAPK signaling; TGF$\beta$; cancer progression



**Citation:** Fernández-Álvarez, M.; Horcajo, P.; Jiménez-Meléndez, A.; Lara, P.A.; Huertas-López, A.; Huertas-López, F.; Ferre, I.; Ortega-Mora, L.M.; Álvarez-García, G. Transcriptomics of *Besnoitia besnoiti*-Infected Fibroblasts Reveals Hallmarks of Early Fibrosis and Cancer Progression. *Microorganisms* **2024**, *12*, 586. https://doi.org/10.3390/microorganisms12030586

Academic Editor: Graham H. Mitchell

Received: 29 January 2024
Revised: 28 February 2024
Accepted: 11 March 2024
Published: 15 March 2024



## 1. Introduction

*Besnoitia besnoiti* belongs to the Sarcocystidae family, together with the closely related apicomplexan parasites *Toxoplasma gondii* and *Neospora caninum*. It is the etiologic agent of bovine besnoitiosis, a relevant disease in cattle in Africa, Europe, the Middle East and Asia [1]. The clinical progression of bovine besnoitiosis occurs in a two-stage process. In the initial stage, there is a rapid replication of tachyzoites, which invade the endothelial cells and macrophages. First, infected cattle develop fever, depression and anorexia. Next, this febrile phase is followed by the anasarca stage, characterized by subcutaneous edema, nasal and ocular discharge, respiratory disorders and orchitis. In the scleroderma stage, the tachyzoites transform into slowly dividing bradyzoites that form tissue cysts within fibroblasts and myofibroblasts, primarily in subcutaneous tissues, gaining access to a protective niche capable of avoiding immune clearance. These cysts are commonly observed in chronically infected animals, causing skin lesions such as hyperkeratosis, folding, hair loss, nodules and scars. Additionally, visible cysts can be found in the conjunctiva and *vestibulum vaginae* [2,3]. This parasitic disease impairs reproductive parameters since

orchitis may result in sterility [4,5]. The severity of clinical signs and lesions can vary among affected animals. Most animals remain subclinically infected, while a small proportion develop pronounced clinical manifestations and lesions, which can ultimately lead to irreversible lesions and even mortality [3,6]. The unknown *B. besnoiti* complete life cycle, together with the complex pathogenesis of besnoitiosis, is a challenge for the development of effective treatment and control strategies. Therefore, nowadays, control programs are limited to management practices coupled with diagnostic tools to prevent new cases and disease dissemination [7].

To decipher the intricate interplay between the parasite and the host, it is essential to focus on the target cells involved in the infection process. Among other target cells, fibroblasts garner significant attention during *B. besnoiti* infection due to their diverse functions in tissue repair, remodeling and immune responses [8,9]. Moreover, fibroblasts are widely acknowledged as the primary cell type in connective tissue, known for their remarkable versatility in producing a diverse array of vital substances such as collagen proteoglycans, fibronectin, laminins, glycosaminoglycans, metalloproteinases and prostaglandins. Therefore, fibroblasts are responsible for synthesizing and reorganizing the extracellular matrix (ECM) [10]. Additionally, in the context of fibrosis, activated fibroblasts, also known as myofibroblasts, are the key players. These myofibroblasts exhibit enhanced contractile properties and increase the production of ECM components, particularly collagen. They also release profibrotic factors that stimulate further fibroblast activation and collagen deposition, perpetuating the fibrotic process. This leads to functional impairment and can ultimately result in organ failure in severe cases [11,12]. In bovine besnoitiosis, fibrosis is a prominent lesion observed in the scrotal skin of acutely and chronically infected bulls [4,5], and two fibrosis biomarkers (*ICAM-1* and *PLAT*) are upregulated in the testicular parenchyma, pampiniform plexus and scrotal skin of naturally chronically infected bulls [5]. Additionally, evidence of fibrosis occurrence in primary bovine aorta endothelial cells (BAEC) during *B. besnoiti* infection was demonstrated in vitro through RNA-Seq analysis [13].

Nevertheless, there is no available data regarding the molecular mechanisms underlying fibroblast infection and the progression of tissue fibrosis during bovine besnoitiosis. Herein, we analyzed the molecular mechanisms that govern *B. besnoiti* infection in bovine fibroblasts following a transcriptomic approach. RNA-Seq analysis of *B. besnoiti*-infected bovine fibroblasts was carried out at two different time points representing early invasion (12 h p.i.) and intracellular proliferation (32 h p.i.). Next, we analyzed the expression of some selected DEGs in the scrotal skin of naturally infected bulls.

## 2. Materials and Methods

### *2.1. Cell Line and Parasite Culture*

Primary bovine aorta fibroblasts [14] were cultured in T25 culture flasks with Dulbecco's Modified Eagle Medium containing 15% fetal bovine serum and 100 IU/mL of penicillin, 100 mg/mL of streptomycin and 0.25 µg/mL of amphotericin B. Low passage fibroblasts (passage 10) were passaged once a week using pre-mix trypsin EDTA (TrypLE Gibco, Thermo Fisher Scientific, Waltham, MA, USA).

Tachyzoites from the *B. besnoiti* Spain1 isolate (BbSp1) were maintained in African green monkey kidney epithelial cell line MARC-145 cells, following a previously described procedure [15]. Only low passage (10 to 21) tachyzoites were used to avoid changes associated with adaptation to long-term cell culture maintenance [16]. After three days of infection, when most parasites were still intracellular, the tachyzoites were scraped and purified using PD-10 columns. The number of viable tachyzoites was estimated using a trypan blue dye exclusion assay, and the viable tachyzoites were counted on a Neubauer chamber. Purified and viable tachyzoites were used to infect T25 flasks seeded with confluent fibroblasts monolayers ($2 \times 10^6$ cells) with a multiplicity of infection (MOI) of 10:1. The cell cultures were incubated at 37 °C with 5% $CO_2$ in a humidified incubator.

### *2.2. Transcriptome Analysis*

#### 2.2.1. Experimental Design and RNA Extraction

Samples were collected at 12 h p.i., when most of the parasites had already invaded the host cell and had not replicated yet (FI-Bb 12 h p.i.), and at 32 h p.i., when the parasites had replicated twice (FI-Bb 32 h p.i.) [14]. Extracellular parasites were eliminated by washing infected flasks with phosphate-buffered saline 1x before the cells were recovered at both time points. Non-infected fibroblasts (FI) were used as a control. The cells were recovered by gentle scraping, centrifuged at 1350× *g* for 10 min at 4 °C, and, once the supernatant was discharged, the pelleted cells were stored at −80 °C until RNA extraction. All the analyses were performed with three biological replicates.

Total RNA from the three independent biological replicates was purified by using a QIAGEN RNeasy Mini Kit (Qiagen, Hilden, Germany) following QIAshredder (Qiagen, Hilden, Germany) homogenization according to the manufacturer's instructions. RNA integrity was evaluated by 1% agarose gel electrophoresis with GelRed staining (Biotium, Fremont, CA, USA).

#### 2.2.2. Quality Control of Total RNA, Library Preparation and Sequencing

The total RNA's quality and quantity were assessed using Bioanalyzer 2100 (Agilent Biotek, Santa Clara, CA, USA) and a Qubit 2.0. B (Invitrogen, Carlsbad, CA, USA). Subsequently, the poly(A)+ mRNA fraction was extracted from the total RNA, and cDNA libraries were prepared following Illumina's guidelines [17]. The quantification of the libraries was performed by qPCR using a LightCycler 480 (Roche, Basel, Switzerland), and their quality was assessed using a Bioanalyzer 2100 (Agilent Biotek, Santa Clara, CA, USA). The sequencing of the equimolarly pooled cDNA libraries was performed by paired-end sequencing (100 bp × 2) using an Illumina HiSeq 2000 sequencer (Illumina, San Diego, CA, USA).

#### 2.2.3. Computational Analysis of RNA-Seq Data

The FastQC tool was used to assess the raw data quality, and any reads of low quality were removed through the utilization of Picard Tools software, version 1.129 (http://picard.sourceforge.net, accessed on 10 February 2023).

The raw paired-end reads were mapped against the *Bos taurus* genome, version UDM3.1 (NCBI:GCA_000003055.3), provided by the ENSEMBL/NCBI database (http://www.ensembl.org/, accessed on 10 February 2023) using the TopHat2 v2.1.1 algorithm [18]. Gene quantification was carried out using htseq_count 0.10 [19]. Differential expression between fibroblasts infected with tachyzoites of *B. besnoiti* (FI-Bb) at 12 h vs. uninfected fibroblasts (FI) and FI-Bb at 32 h vs. FI was studied using the algorithm proposed by DESeq2 [20], with a binomial negative distribution for determination of the statistical significance [21]. Genes were considered differentially expressed when they presented a fold change (FC) $\geq 1.5$ and a false discovery rate (FDR)-adjusted [22] *p*-value (p adj) less than 0.05, following previous studies [13,23].

Furthermore, to explore the correlation among all replicates, a principal component analysis (PCA) was performed using the prcomp function (centering and scaling data) from Stats R Package version 4.3.0, according to the expression level of genes, and plotted using ggplot2 R package version 3.4.2. The correlation among the samples was determined by using the adegenet library [24] of the statistical software package R (http://www.r-project.org, accessed on 1 January 2023) for their acceptance as biological replicates. Heatmaps were generated with a selection of bovine fibroblast DEGs in the pathways identified by using the heatmap.2 function from the gplots R package version 3.1.3.

#### 2.2.4. Functional Enrichment Analyses

The functional enrichment analyses to identify the enriched Gene Ontology (GO) terms (biological process (BP) and molecular function (MF)) and the Kyoto Encyclopedia of Genes and Genomes (KEGG) pathways were performed using the g:Profiler web server (https://biit.cs.

ut.ee/gprofiler/gost, accessed on 10 February 2023) [17]. The g:SCS significance threshold was employed, which is the default method within g:Profiler for correcting multiple testing for *p*-values obtained from GO and KEGG pathway enrichment analysis. This threshold corresponds to an experiment-wide significance level of a = 0.05. Adjusted *p*-values were calculated by multiplying the *p*-values of the query by the ratio of the approximate threshold and the initial experiment-wide threshold (a = 0.05).

### *2.3. Analysis of Gene Expression in the Scrotal Skin of Naturally Infected Bulls*

Scrotal skin samples obtained from naturally infected bulls were used to assess the expression of a set of genes chosen from the transcriptomic data. The scrotal skin was chosen due to the extensive occurrence of fibrosis in acutely and chronically infected bulls, as noted by González-Barrio et al. [4,5]. We selected genes that showed the most significant changes in the differential expression analysis and DEG representative of the main enriched KEGG pathways. The studied samples came from fifteen naturally infected breeding bulls from extensive beef herds (5 acutely infected bulls, 10 chronically infected bulls and 9 non-infected bulls). Acutely infected bulls showed fever and orchitis, and only one showed 2–3 tissue cysts per skin section [4]. Chronically infected bulls displayed skin lesions and were sterile, with testis atrophy with azoospermia [5]. Scrotal skin tissue samples were collected from each bull, and the samples were frozen at −80 °C until RNA extraction. Gene expression analyses were performed as previously explained [17]. Briefly, total RNA was purified by using a QIAGEN RNeasy Mini Kit (Qiagen, Hilden, Germany) following homogenization with a QIAshredder (Qiagen, Hilden, Germany). RNA concentration and purity were measured using a NanoPhotometer Classic (Implen, Munich, Germany), and RNA integrity was checked by agarose gel electrophoresis with GelRed staining (Biotium Inc., Fremont, CA, USA). Afterward, reverse transcription was performed using a SuperScript VILO cDNA Synthesis Kit (Invitrogen, Thermo Fisher Scientific, Waltham, MA, USA) and up to 2.5 µg of total RNA in a 20 µL reaction. Quantitative real-time PCRs were performed in 25 µL using 12.5 µL of Power SYBR PCR Master Mix (Applied Biosystems, Thermo Fisher Scientific, USA), 10 pmol of each primer and 5 µL of the diluted cDNA samples. The primers are listed in Supplementary Table S1. The reactions were performed in an ABI 7500 FAST Real-Time PCR System (Applied Biosystems, Foster City, MA, USA). Relative expression levels were calculated using the comparative method $2^{-\Delta\Delta Ct}$ [25] after normalization with the housekeeping gene *β-actin* [23,26]. For data analysis, the Kruskal–Wallis test followed by Dunn's test was used, and $p \leq 0.05$ was considered statistically significant.

## 3. Results

### *3.1. Quality Analysis and Mapping of RNA-Seq Data*

All the samples included in the RNA-Seq study passed the quality checks, ensuring their suitability for subsequent analyses. The RNA integrity number (RIN) varied between 9.6 and 10 in all the samples. The sequencing process accounted for approximately 1 billion reads between all the samples. After alignment, an average of 70% of the high-quality reads mapped to the reference *Bos taurus* (Supplementary Table S2). Furthermore, all replicates from the same condition clustered together according to PCA, shown in Supplementary Figure S1.

### *3.2. Transcriptional Responses of B. besnoiti-Infected Fibroblasts Highlight Key Cancer and Fibrosis Pathways*

Differential expression analysis revealed a higher number of DEGs in FI-Bb compared to FI at 12 h p.i. versus 32 h p.i, with a total of 479 DEGs (287 upregulated in infected cells and 192 downregulated) and 280 DEGs (172 upregulated and 108 downregulated DEGs), respectively. Among these DEGs, 91 were DEGs at both time points. To investigate the underlying mechanisms during *B. besnoiti* infection in bovine fibroblasts, we performed functional enrichment analysis for GO and KEGG annotations (Table 1). When FI-Bb

and FI were compared at both 12 and 32 h p.i., an enrichment in BP and MF related to cell proliferation and communication was revealed. Notably, the examination of KEGG pathways highlighted shared regulation at 12 and 32 h p.i. in several cancer-related pathways, namely "Proteoglycans in cancer", "Pathways in cancer", "Gastric cancer" and "MAPK signaling pathway" (Figure 1).

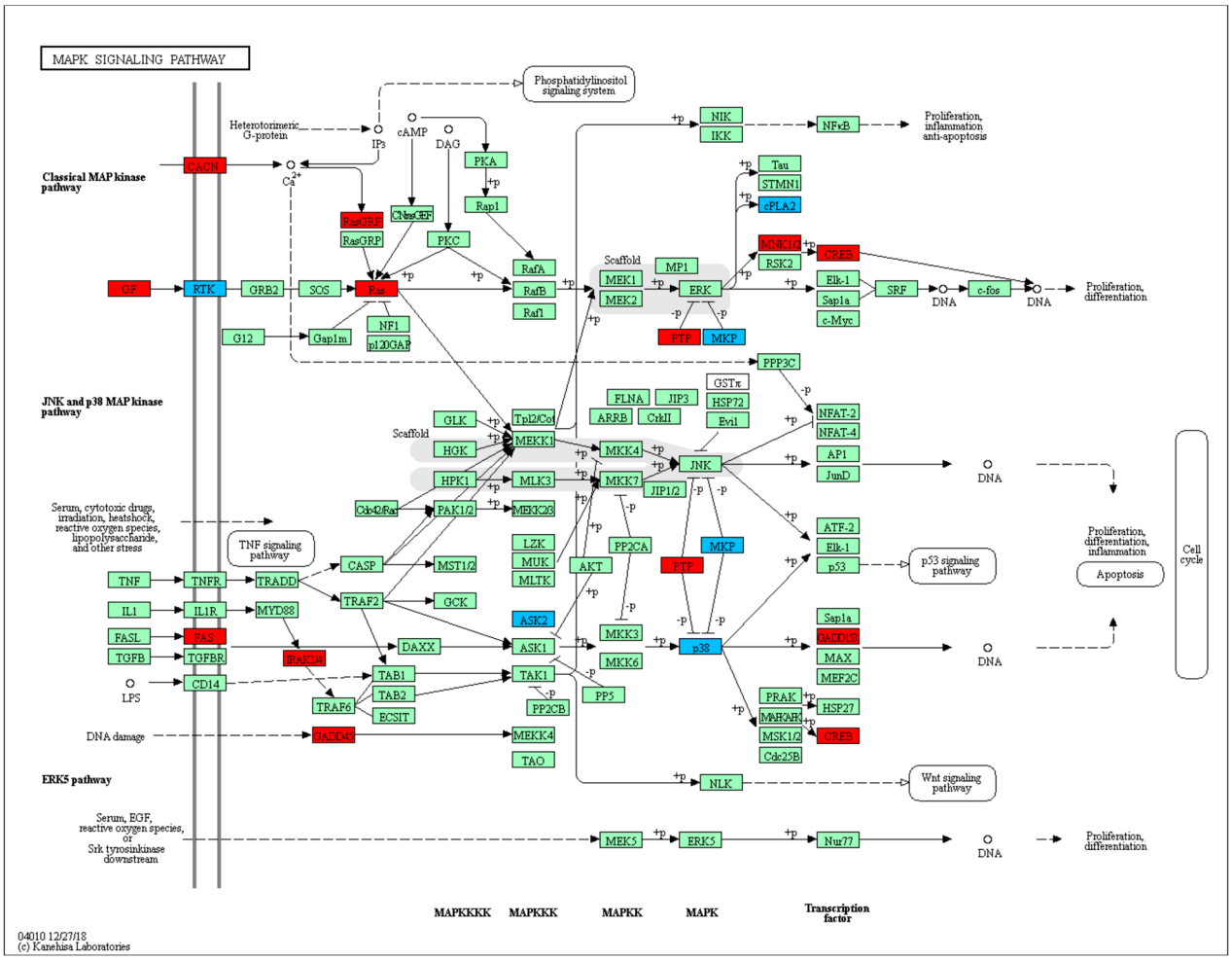


**Figure 1.** MAPK signaling pathway (KEGG: 04010) enriched in bovine fibroblasts infected with *B. besnoiti*. DEGs at 12 h p.i. is represented in blue and DEGs at 32 h p.i. in red.

Specifically, at 12 h p.i., the comparison between FI-Bb and FI demonstrated an enrichment of BP and MF associated with cytokines and growth factor activity. The KEGG pathway analysis identified several pathways, including "Cytokine–cytokine receptor interaction, the "AGE–RAGE signaling pathway" and "TNF signaling pathway". Notably, in infected cells, there was a significant upregulation of the cytokines and cytokine receptor (transforming growth factor β (TGFβ) family, TNF family, IFN family, chemokines family), vascular endothelial growth factors (*VEGFA*, *VEGFC*), the *fibroblast growth factor 1* (*FGF1*) and relevant genes associated to fibrosis such as *fibronectin type III domain-containing protein 3A* (*FNDC3A*), *collagen type VII A1* (*COL7A1*), *matrix metalloproteinase 9* (*MMP9*) transforming growth factor-beta factors (*TGFβ1*, *TGFβ3*) and *urokinase plasminogen activator surface receptor* (*PLAUR*). Other genes associated with cell proliferation and differentiation were also upregulated (e.g., *NOTCH1*, *FOFB*, a member of the Fos family of AP-1 transcription factors and *phosphatidylinositol-specific phospholipase C, X domain containing 1* (*PLCXD1*) (Figure 2).

**Table 1.** GO and KEGG enrichment analyses. The number of differentially expressed genes (DEGs) between fibroblasts infected with *Besnoitia besnoiti* tachyzoites (FI-Bb) and non-infected fibroblasts (FI) are shown together with the top 6 upregulated Gene Ontology (GO) terms, biological processes (BP) and molecular functions (MF), and top 5 upregulated Kyoto Encyclopedia of Genes and Genomes (KEGG) pathways).

| | No. DEGs | Upregulated DEGs | Downregulated DEGs | Biological Processes | | Molecular Function | | Pathway Enrichment | |
|---|---|---|---|---|---|---|---|---|---|
| | | | | GO Term | Adjusted *p*-Value | GO Term | Adjusted *p*-Value | KEGG Term | Adjusted *p*-Value |
| **FI-Bb vs. FI 12 h p.i.** | 479 | 287 | 192 | Positive regulation of biological process (GO:0048518) | $2.60 \times 10^{-18}$ | Molecular function regulator activity (GO:0098772) | $8.70 \times 10^{-8}$ | Cytokine–cytokine receptor interaction (KEGG:04060) | $3.92 \times 10^{-4}$ |
| | | | | Anatomical structure development (GO:48856) | $2.43 \times 10^{-17}$ | Molecular function activator activity (GO:0140677) | $9.15 \times 10^{-8}$ | Pathways in cancer (KEGG:05200) | $3.94 \times 10^{-4}$ |
| | | | | Anatomical structure morphogenesis (GO:0009653) | $6.64 \times 10^{-17}$ | Protein binding (GO:0005515) | $6.01 \times 10^{-6}$ | MAPK signaling pathway (KEGG:04010) | $1.32 \times 10^{-3}$ |
| | | | | Developmental process (GO:0032502) | $1.67 \times 10^{-16}$ | Signaling receptor regulator activity (GO:0030545) | $6.07 \times 10^{-5}$ | Proteoglycans in cancer (KEGG:05205) | $5.32 \times 10^{-3}$ |
| | | | | Positive regulation of cellular process (GO:0048522) | $6.89 \times 10^{-16}$ | Receptor ligand activity (GO:0048018) | $1.96 \times 10^{-4}$ | Axon guidance (KEGG:04360) | $3.13 \times 10^{-2}$ |
| | | | | Multicellular organism development (GO:0007275) | $9.70 \times 10^{-15}$ | Signaling receptor activator activity (GO:0030546) | $3.03 \times 10^{-4}$ | TNF signaling pathway | $3.43 \times 10^{-2}$ |

**Table 1.** *Cont.*

| | No. DEGs | Upregulated DEGs | Downregulated DEGs | Biological Processes | | Molecular Function | | Pathway Enrichment | |
|---|---|---|---|---|---|---|---|---|---|
| | | | | GO Term | Adjusted *p*-Value | GO Term | Adjusted *p*-Value | KEGG Term | Adjusted *p*-Value |
| **FI-Bb vs. FI 32 h p.i.** | 280 | 172 | 108 | Multicellular organism development (GO:0007275) | $1.28 \times 10^{-16}$ | Protein binding (GO:0005515) | $3.47 \times 10^{-6}$ | Proteoglycans in cancer (KEGG:05205) | $4.18 \times 10^{-5}$ |
| | | | | Anatomical structure development (GO:0048856) | $8.42 \times 10^{-15}$ | Identical protein binding (GO:0042802) | $7.88 \times 10^{-5}$ | Malaria (KEGG:05144) | $3.59 \times 10^{-3}$ |
| | | | | System development (GO:0048731) | $1.22 \times 10^{-14}$ | Signaling receptor binding (GO:000510) | $3.95 \times 10^{-4}$ | Focal adhesion (KEGG:04510) | $7.48 \times 10^{-3}$ |
| | | | | Developmental process (GO:0032502) | $1.88 \times 10^{-14}$ | Collagen binding (GO:0005518) | $1.55 \times 10^{-3}$ | Pathways in cancer (KEGG:05200) | $7.51 \times 10^{-3}$ |
| | | | | Anatomical structure morphogenesis (GO:0009653) | $4.38 \times 10^{-14}$ | Signaling receptor regulator activity (GO:0030545) | $3.63 \times 10^{-3}$ | MAPK signaling pathway (KEGG:04010) | $1.08 \times 10^{-2}$ |
| | | | | Multicellular organismal process (GO:0032501) | $1.99 \times 10^{-12}$ | Receptor ligand activity (GO:0048018) | $5.99 \times 10^{-3}$ | PI3K–AKT signaling pathway (KEGG: 04151) | $2.89 \times 10^{-2}$ |

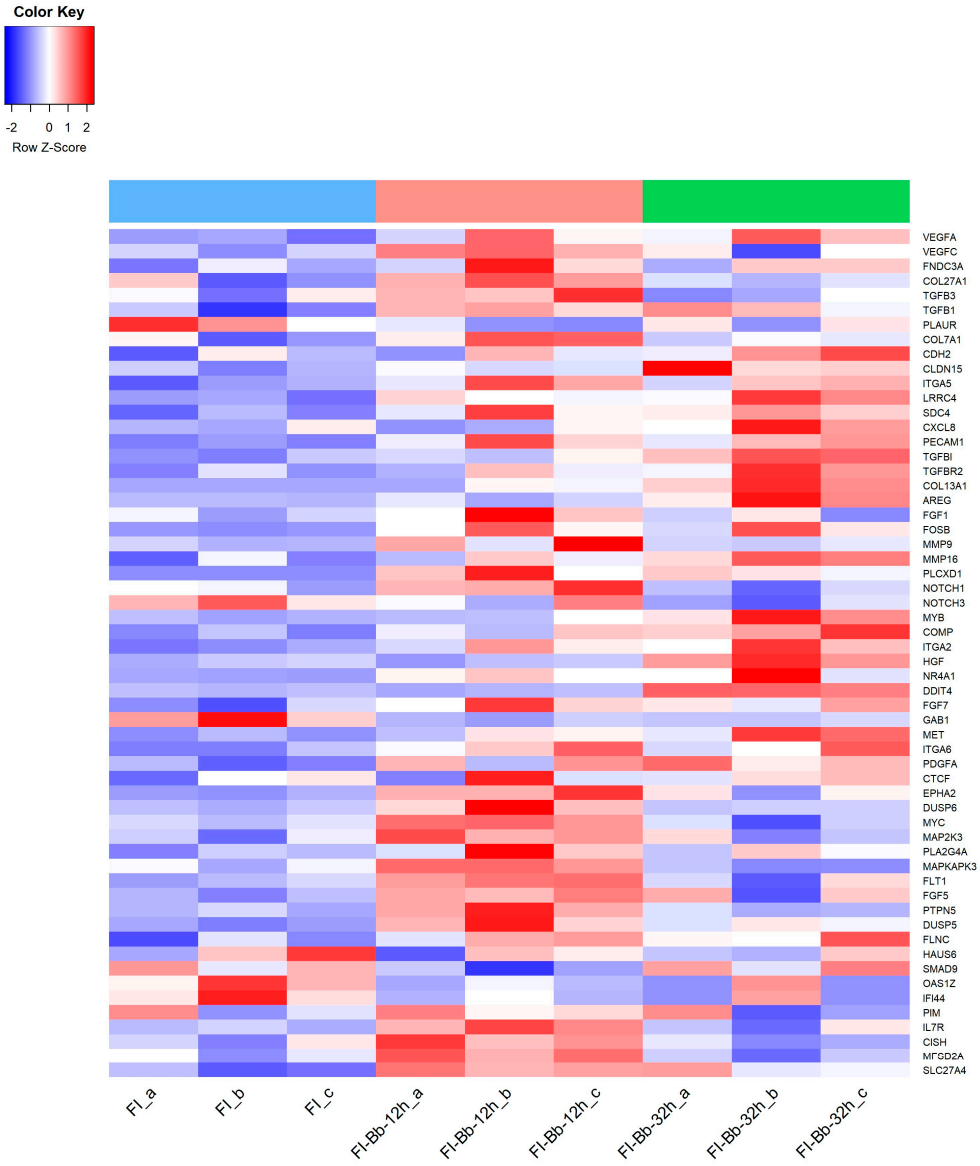


**Figure 2.** Heatmap of a selection of *Bos taurus* differentially expressed genes (DEGs) in fibroblasts infected with *B. besnoitia* tachyzoites (FI-Bb) at 12 (pink color) and 32 h p.i. (green color) and non-infected fibroblasts (FI) (blue color).

At 32 p.i., the comparison between FI-Bb and FI demonstrated an enrichment of processes related to cell adhesion. KEGG pathway analysis unveiled several pathways, including "Focal adhesion", "Cell adhesion molecules, "PI3K–AKT signaling pathway" and the "Malaria" (HGF–MET signaling pathway). Some upregulated genes were also upregulated at 12 h p.i (FOSB, *PLCXD1*, *TGFβ1*). Particularly at 32 h p.i, there was a significant upregulation of several adhesion molecules (*CDH2*, *CLDN15*, *ITGA2*, *ITGA5*, *ITGA6*, *LRRC4*, *SDC4*, *PECAM1*), genes associated with fibrosis (*TGFβ1*, *TGFβ3*, *transforming growth factor β receptor 2—TGFβR2—*, *PLAUR*, *collagen type XIII A1—COL13A1—*, *matrix metallopeptidase 16* (*MMP16*) and *cell proliferation* (*FOSB*, *Amphiregulin—AREG—*) (Figure 2).

### *3.3. PLAUR, TGFβ1 and FOSB as Potential Biomarkers of B. besnoiti Infection in Scrotal Skin of Naturally Infected Bulls*

The expression of a set of selected DEGs from the RNA-Seq data (*AREG*, *FGF1*, *FOSB*, *MMP9*, *MMP16*, *PLAUR*, *PLCXD1*, *TGFβ1*) was analyzed in scrotal skin samples from

naturally infected bulls [4]. Among the eight genes examined, three showed distinct regulatory patterns in the scrotal skin of naturally infected bulls. Specifically, *PLAUR* exhibited upregulation in both acutely and chronically infected bulls when compared to the non-infected group. Moreover, *TGFβ1* was found to be upregulated in chronically infected bulls compared to the non-infected group. In contrast, only *FOSB* showed downregulation in chronically infected bulls. Notably, the remaining assessed genes (*FGF1*, *FGF1*, *MMP9*, *MMP16*, *AREG*, *PLCXD1*) did not display significant expression changes when infected and non-infected animals were compared (Figure 3).

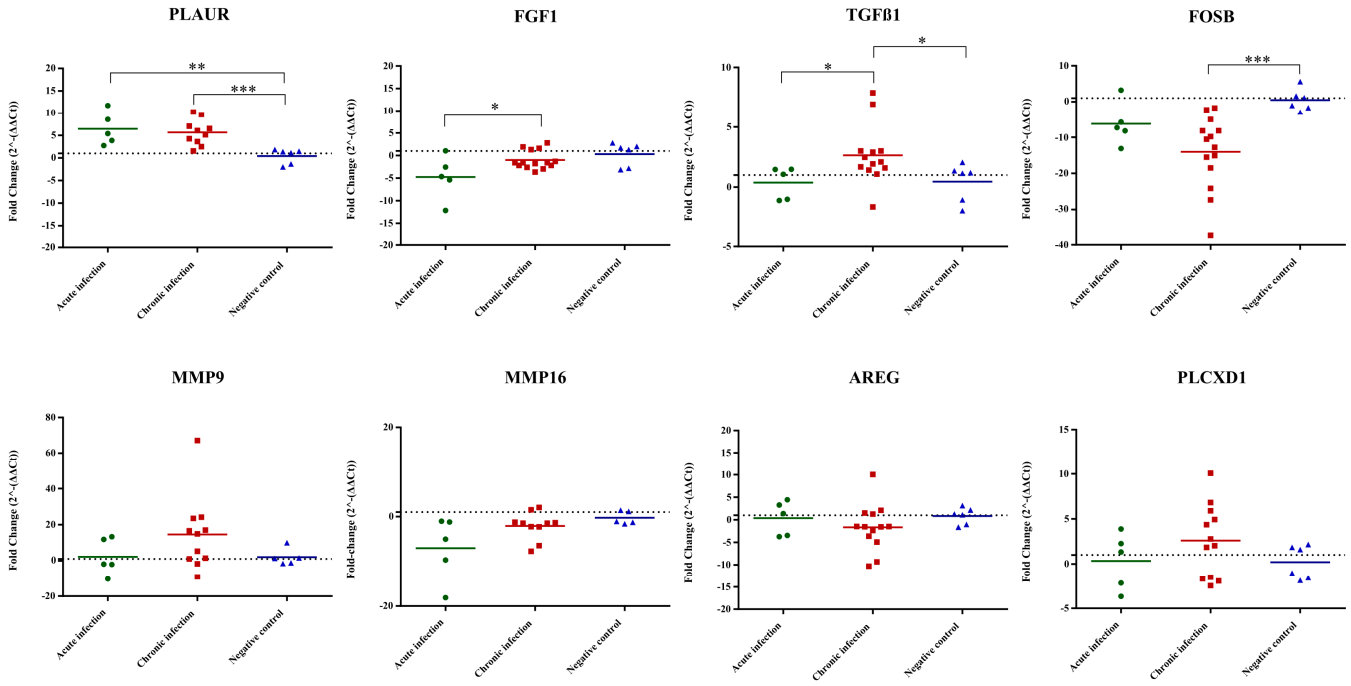


**Figure 3.** Relative mRNA expression levels of selected DEGs determined by quantitative real-time PCR (RT-qPCR) analysis of scrotal skin samples from naturally infected bulls. In the scatterplot graphs, each dot represents data obtained from one single bull, and the bar represents the average fold change (FC) for each gene and condition. The baseline for uninfected animals is set at 1 (horizontal line). One asterisk (*) corresponds to adjusted *p* values between 0.01 and 0.05; two asterisks (**) to adjusted *p* values between 0.01 and 0.001; and three asterisks (***) to adjusted *p* values less than 0.001 (determined by Kruskal–Wallis test followed by Dunn's test).

## 4. Discussion

Primary bovine aorta fibroblasts were chosen as the in vitro model for this study due to their relevance as target cells for the parasite, as well as their intrinsic roles as immune modulators and pivotal contributors to fibrosis processes. It is noteworthy, however, that transcriptomic profiles may exhibit variability across fibroblasts of different origins. Fibroblasts represent a heterogenous cell population with diverse functional capacities, as exemplified by studies focused on skin-derived fibroblasts [27,28]. Nonetheless, our in vitro model holds promise as a valuable tool for studying fibrosis in the context of *B. besnoiti* infection, supported by the upregulation of classic fibrotic markers such as *TGFβ1*, *FNDC3A* and COL7A1.

Under physiological conditions, myofibroblasts are relatively rare. However, following infection and injury, fibroblasts typically undergo a transformation into myofibroblasts, serving as key drivers in the wound-healing process [29]. In our study, the upregulation of *TGFβ1*, *VEGFs* and *NOTCH1*—all known promoters of this fibroblast-to-myofibroblast transformation—was observed.

However, it is worth noting that the full transition to a myofibroblast phenotype generally involves the expression of alpha-smooth muscle actin (α-SMA) [30], which was

not differentially expressed in *B. besnoiti*-infected fibroblasts. Therefore, it is possible that the observed changes represent an early step in myofibroblast transformation.

The differential expression analysis revealed a notably higher number of DEGs in FI-Bb vs. FI at 12 h p.i compared to 32 h p.i, suggesting an intensive early cellular reaction to the pathogen during invasion. However, the common core set of genes regulated at both time points showed initial steps of fibrosis, also observed at the host–tumor interface, evidenced by several enriched cancer-related pathways such as angiogenesis, apoptosis inhibition, cell proliferation and migration, which in turn related to innate immunity required for control and clearance of invading pathogens [31,32]. In addition, the MAPK pathway was upregulated at both times p.i., which is significant in relation to fibrosis, as it governs well-preserved cascades regulating cell proliferation, immune response, and inflammation [33].

Three phases are often presented sequentially during the fibrotic process: inflammation, proliferation and maturation [34]. Our transcriptomics findings suggest a gradual regulation of the fibrotic process. At 12 h p.i., pathways associated with the inflammatory response were enriched (e.g., "Cytokine–cytokine receptor interaction" "TNF signaling pathway" "AGE–RAGE signaling pathway"). Inflammation might facilitate the recruitment of immune cells, driven by the action of cytokines [35]. Nevertheless, inflammation could act as a double-edged sword; while it could effectively help to eliminate the invading parasite, prolonged activation could lead to tissue damage and, ultimately, fibrosis. Additionally, the upregulation of the "AGE–RAGE signaling pathway" could be contributing to this process by inducing oxidative stress and inflammation [36].

With parasite replication at 32 h p.i., the transcriptomic response evolves towards cell proliferation and ECM remodeling. The "PI3K–AKT signaling pathway" is well-known for its role in promoting cell survival and growth [37,38]. The process of tissue repair relies on fibroblasts' ability to anchor themselves to ECM, which in turn leads to cell migration and ECM contraction. In fact, upregulation of adhesion signaling pathways is a key phenotypic hallmark of fibrotic cells [39]. While adhesion serves as a central feature of the proliferation phase, its significance perseveres and even amplifies as the fibrotic process advances into the maturation phase, since cell adhesion molecules are involved in binding to the extracellular matrix [40,41]. Moreover, the upregulation of the "Malaria" pathway, and more specifically, the HGF–MET signaling axis within this pathway, might promote a favorable environment for parasite infection by the inhibition of cell apoptosis [42]. Additionally, previous investigations have elucidated the role of the HGF–MET signaling pathway in inducing a hypermigratory phenotype in dendritic cells infected with *T. gondii* [43].

All these findings led us to identify potential fibrosis markers that displayed upregulation exclusively at 12 h p.i. (*FNDC3A*, *COL7A1*, *MMP9*) [44,45], at 32 h p.i. (*TGFβR2*, *COL13A1*, *MMP16*) [46,47] or at both time points (*PLAUR*, *TGFβ1*, *TGFβ3*) [48–50]. Among a set of selected and highly regulated DEGs involved in the different stages of the fibrotic process, *PLAUR*, *TGFβ1* and *FOSB* evidenced their potential as relevant biomarkers of disease progression in the scrotal skin of naturally infected bulls. *PLAUR* is involved in fibroblast-to-myofibroblast differentiation and fibrosis [51,52] and was upregulated in both acutely and chronically infected bulls. *TGFβ1* is intricately linked to the pathogenesis of fibrosis [53] and has been correlated with the activation of MAPK activity in fibroblasts during the fibrosis progression [54]. Herein, chronically infected bulls exhibited upregulation of *TGFβ1*, and the MAPK pathway was upregulated at both time points. In contrast, *FOSB* expression did not correlate between the in vitro and in vivo assays. *FOSB* was downregulated in the scrotal skin of chronically infected bulls but was upregulated in vitro at both times p.i. Downregulated expression of *FOSB* has been associated with cell migration (metastasis) and advanced tumorigenic stages [55] whereas its upregulation is associated with regulation of ECM production. Consequently, tissue complexity and infection timing likely contributed to differences between the in vitro and in vivo models and to the variability observed in the mRNA expression levels in the chronically infected group.

It is not surprising that "Pathways in cancer" was enriched at both time points studied since cancer-associated fibrosis is a critical component of the tumor microenvironment that correlates with prognosis. Moreover, tumors are characterized by ECM deposition, remodeling and angiogenesis, which are fibrosis steps that are regulated by *B. besnoiti* [56]. Herein, we also found a relevant DEG at both time points studied that is a marker of angiogenesis, VEGFA. VEGF signaling results in the activation of several downstream pathways including the RAS/MAPK (ERK) pathway regulating cell proliferation and the PI3K–AKT pathway, regulating cell survival, among others, that also were found enriched in this work (Table 1). A functional in vitro study carried out with an ERK inhibitor demonstrated that ERK inhibition at 12 h p.i. may prevent endothelial sprouting by downregulating VEGFA expression (Supplementary Figure S2). It has also been reported that VEGF autoregulates ERK1/2 and p38 cascades enhancing the expression of DUSP phosphatases (MAPK phosphatases) [57]. Interestingly, DUSP5 and DUSP6 were also found to be upregulated at 12 h p.i. (Figure 2).

Similar transcriptomic studies have been developed in other primary bovine cell targets of *B. besnoiti* infection (bovine aorta endothelial cells (BAEC) and macrophages), and some regulated genes and pathways related to immune response and fibrosis were common to all the cell lines. Regarding the fibrotic process, the TGFβ signaling pathway was commonly upregulated. The antiviral immune response was represented by several DEGs (*OAS1Z*, *IFI44*, *PIM*, *IL7R*, *CISH*) and the JAK–STAT pathway. Although *OAS1Z* and *IFI44* are recognized for their roles in viral infections [58,59], they can also be induced in response to certain parasites [60–62]. In addition, the JAK–STAT pathway is known for orchestrating potent antiviral reactions by leading to the upregulation of numerous interferon-stimulated genes (ISGs), which can be also triggered by apicomplexan parasites as *T. gondii* [63] and *N. caninum* [64], and, indeed, the role of ISGs was demonstrated during *B. besnoiti* infection in primary bovine macrophages [17]. Moreover, genes associated with programmed cell death were also regulated in all bovine cells as well, which could favor the infection, as shown for *T. gondii* [65]. In addition, previous studies have described apoptosis as one of the main pathways regulated in primary bovine macrophages during early infection [64]. Additionally, there were also commonly regulated adhesion molecules that serve a crucial role in the host's defense against infections, facilitating processes such as pathogen recognition [66], pathogen internalization, cytoskeletal rearrangements, and even influencing gene expression events that ultimately impact the phenotype of the infected cell [67].

## 5. Conclusions

Our study sheds light on the molecular mechanisms governing fibroblast activation during infection, revealing a progressive modulation of fibrotic processes that share hallmarks with cancer progression. MAPK signaling arises as a key element together with other relevant pathways (e.g., TNF and cell adhesion) whose role in bovine pathogenesis remains to be dissected. Moreover, several potential biomarkers of the different phases of fibrosis, including *PLAUR*, *TGFβ1* and *FOSB*, which were also regulated in vivo, were identified. The DEGs and associated pathways identified in infected fibroblasts may serve as invaluable prognostic indicators and potential drug targets for combating fibrosis triggered by *B. besnoiti* infection (e.g., anti-angiogenic therapies [68–70]). This study represents a first attempt to identify putative biomarkers of fibrosis with the most appropriate samples currently available from bovines with besnoitiosis. These results should be further validated with complementary methodologies (e.g., Western blot or ELISA), which will also require additional samples from the field.

**Supplementary Materials:** The following supporting information can be downloaded at: https://www.mdpi.com/article/10.3390/microorganisms12030586/s1, Figure S1: Principal component analysis (PCA) plots representing the clustering of biological replicates based on gene expression levels of fibroblasts at 12 h (a) and 32 h p.i. (b); Figure S2: Scatterplot graphs of VEGFA relative mRNA expression levels derived from quantitative real-time PCR (RT-qPCR) analysis in human foreskin

fibroblasts (HFFs) infected with B. besnoiti tachyzoites at 12 h p.i. and treated with ERK inhibitor FR180204. Table S1: Sequences of primers used for quantitative real-time PCR (RT-qPCR) for *Bos taurus* genes; Table S2: Library sizes and mapping results for transcriptome sequencing from all samples (fibroblasts infected with *Besnoitia besnoiti* tachyzoites (FI-Bb), and non-infected macrophages (FI)) at 12 h and 32 h pi; References [17,23,25,26,71–77] are cited in the Supplementary Materials.

**Author Contributions:** G.Á.-G., I.F. and L.M.O.-M. conceived the study and acquired funding for the study; M.F.-Á., A.J.-M. and P.H. carried out the experimental assays; M.F.-Á., P.A.L., A.H.-L. and F.H.-L. performed the bioinformatic and statistical analyses and prepared the figures and tables. M.F.-Á., G.Á.-G. and P.H. drafted the original manuscript. All authors have read and agreed to the published version of the manuscript.

**Funding:** This research was funded by the Spanish Ministry of Economy and Competitiveness, project numbers AGL2016-75202-R and PID2019-103960RB-I00, and the Community of Madrid (Ref. P2018/BAA-4370 PLATESA2-CM). M.F.-Á. was supported by the Complutense University of Madrid, grant number UCM 2018. A.H.L. was supported by the University of Murcia through the Margarita Salas Program of Requalification of the Spanish University System (Spanish Ministry of Universities) financed by the European Union—NextGenerationEU, grant number R-1593/2022.

**Data Availability Statement:** The data are contained within the article or Supplementary Materials. Additionally, the RNA-Seq data reported in this study have been deposited in the NCBI database under accession number SUB14163821.

**Acknowledgments:** We would like to acknowledge Carlos Diezma Díaz for his excellent technical assistance.

**Conflicts of Interest:** Author Francisco Huertas-López was employed by the company Marbyt—Smart Solutions for Biotechnology (Murcia, Spain). The remaining authors declare that the research was conducted in the absence of any commercial or financial relationships that could be construed as a potential conflict of interest.

## References

1. European Food Safety Authority. Bovine Besnoitiosis: An emerging disease in Europe. *EFSA J.* **2010**, *8*, 1499. [CrossRef]
2. Álvarez-García, G.; García-Lunar, P.; Gutiérrez-Expósito, D.; Shkap, V.; Ortega-Mora, L.M. Dynamics of *Besnoitia besnoiti* infection in cattle. *Parasitology* **2014**, *141*, 1419–1435. [CrossRef]
3. Cortés, H.; Leitão, A.; Gottstein, B.; Hemphill, A. A review on bovine besnoitiosis: A disease with economic impact in herd health management, caused by *Besnoitia besnoiti* (Franco and Borges). *Parasitology* **2014**, *141*, 1406–1417. [CrossRef]
4. González-Barrio, D.; Diezma-Díaz, C.; Tabanera, E.; Aguado-Criado, E.; Pizarro, M.; González-Huecas, M.; Ferre, I.; Jiménez-Meléndez, A.; Criado, F.; Gutiérrez-Expósito, D.; et al. Vascular wall injury and inflammation are key pathogenic mechanisms responsible for early testicular degeneration during acute besnoitiosis in bulls. *Parasit. Vectors* **2020**, *13*, 113. [CrossRef]
5. González-Barrio, D.; Diezma-Díaz, C.; Gutiérrez-Expósito, D.; Tabanera, E.; Jiménez-Meléndez, A.; Pizarro, M.; González-Huecas, M.; Ferre, I.; Ortega-Mora, L.M.; Álvarez-García, G. Identification of molecular biomarkers associated with disease progression in the testis of bulls infected with *Besnoitia besnoiti*. *Vet. Res.* **2021**, *52*, 106. [CrossRef]
6. Álvarez-García, G.; Frey, C.F.; Ortega-Mora, L.M.; Schares, G. A century of bovine besnoitiosis: An unknown disease re-emerging in Europe. *Trends Parasitol.* **2013**, *29*, 407–415. [CrossRef]
7. Gutiérrez-Expósito, D.; Ferre, I.; Ortega-Mora, L.M.; Álvarez-García, G. Advances in the diagnosis of bovine besnoitiosis: Current options and applications for control. *Int. J. Parasitol.* **2017**, *47*, 737–751. [CrossRef]
8. Pakshir, P.; Alizadehgiashi, M.; Wong, B.; Coelho, N.M.; Chen, X.; Gong, Z.; Shenoy, V.B.; McCulloch, C.A.; Hinz, B. Dynamic fibroblast contractions attract remote macrophages in fibrillar collagen matrix. *Nat. Commun.* **2019**, *10*, 1850. [CrossRef]
9. Xuan, Y.; Chen, C.; Wen, Z.; Wang, D.W. The roles of cardiac fibroblasts and endothelial cells in myocarditis. *Front. Cardiovasc. Med.* **2022**, *9*, 882027. [CrossRef]
10. Tracy, L.E.; Minasian, R.A.; Caterson, E.J. Extracellular matrix and dermal fibroblast function in the healing wound. *Adv. Wound Care* **2016**, *5*, 119–136. [CrossRef]
11. McAnulty, R.J. Fibroblasts and myofibroblasts: Their source, function and role in disease. *Int. J. Biochem. Cell Biol.* **2007**, *39*, 666–671. [CrossRef]
12. Yao, L.; Rathnakar, B.H.; Kwon, H.R.; Sakashita, H.; Kim, J.H.; Rackley, A.; Tomasek, J.J.; Berry, W.L.; Olson, L.E. Temporal control of pdgfrα regulates the fibroblast-to-myofibroblast transition in wound healing. *Cell Rep.* **2022**, *40*, 111192. [CrossRef] [PubMed]
13. Jiménez-Meléndez, A.; Ramakrishnan, C.; Hehl, A.B.; Russo, G.; Álvarez-García, G. RNA-seq analyses reveal that endothelial activation and fibrosis are induced early and progressively by *Besnoitia besnoiti* host cell invasion and proliferation. *Front. Cell Infect.* **2020**, *10*, 218. [CrossRef]

14. Jiménez-Meléndez, A.; Fernández-Álvarez, M.; Calle, A.; Ramírez, M.Á.; Diezma-Díaz, C.; Vázquez-Arbaizar, P.; Ortega-Mora, L.M.; Álvarez-García, G. Lytic cycle of *Besnoitia besnoiti* tachyzoites displays similar features in primary bovine endothelial cells and fibroblasts. *Parasit. Vectors* **2019**, *12*, 517. [CrossRef] [PubMed]
15. Frey, C.F.; Regidor-Cerrillo, J.; Marreros, N.; García-Lunar, P.; Gutiérrez-Expósito, D.; Schares, G.; Dubey, J.P.; Gentile, A.; Jacquiet, P.; Shkap, V.; et al. *Besnoitia besnoiti* lytic cycle in vitro and differences in invasion and intracellular proliferation among isolates. *Parasit. Vectors* **2016**, *9*, 115. [CrossRef]
16. Pérez-Zaballos, F.J.; Ortega-Mora, L.M.; Álvarez-García, G.; Collantes-Fernández, E.; Navarro-Lozano, V.; García-Villada, L.; Costas, E. Adaptation of *Neospora caninum* isolates to cell-culture changes: An argument in favor of its clonal population structure. *J. Parasitol.* **2005**, *91*, 507–510. [CrossRef] [PubMed]
17. Fernández-Álvarez, M.; Horcajo, P.; Jiménez-Meléndez, A.; Diezma-Díaz, C.; Ferre, I.; Pastor-Fernández, I.; Ortega-Mora, L.M.; Álvarez-García, G. Transcriptional changes associated with apoptosis and type I IFN underlie the early interaction between *Besnoitia Besnoiti* tachyzoites and monocyte-derived macrophages. *Int. J. Parasitol.* **2023**, *53*, 505–521. [CrossRef]
18. Kim, D.; Pertea, G.; Trapnell, C.; Pimentel, H.; Ryan, K.S.; Salzberg, S.L. TopHat2: Accurate alignment of transcriptomes in the presence of insertions, deletions and gene fusions. *Genome Biol.* **2013**, *14*, R36. [CrossRef]
19. Anders, S.; Pyl, P.T.; Huber, W. HTSeq—A Python framework to work with high-throughput sequencing data. *Bioinformatics* **2015**, *31*, 166–169. [CrossRef]
20. Anders, S.; Huber, W. Differential expression analysis for sequence count data. *Genome Biol.* **2010**, *11*, R106. [CrossRef]
21. Love, M.I.; Huber, W.; Anders, S. Moderated estimation of fold change and dispersion for RNA-seq data with deseq2. *Genome Biol.* **2014**, *15*, 550. [CrossRef]
22. Benjamini, Y.; Hochberg, Y. Controlling the False Discovery Rate: A practical and powerful approach to multiple testing. *J. R. Stat. Soc. Ser. B Stat. Methodol.* **1995**, *57*, 289–300. [CrossRef]
23. Horcajo, P.; Jiménez-Pelayo, L.; García-Sánchez, M.; Regidor-Cerrillo, J.; Collantes-Fernández, E.; Rozas, D.; Hambruch, N.; Pfarrer, C.; Ortega-Mora, L.M. Transcriptome modulation of bovine trophoblast cells in vitro by *Neospora caninum*. *Int. J. Parasitol.* **2017**, *47*, 791–799. [CrossRef]
24. Jombart, T. *adegenet*: A R package for the multivariate analysis of genetic markers. *Bioinformatics* **2008**, *24*, 1403–1405. [CrossRef]
25. Livak, K.J.; Schmittgen, T.D. Analysis of relative gene expression data using real-time quantitative PCR and the 2(-Delta Delta C(T)) Method. *Methods* **2001**, *25*, 402–408. [CrossRef]
26. Puech, C.; Dedieu, L.; Chantal, I.; Rodrigues, V. Design and evaluation of a unique SYBR green real-time RT-PCR assay for quantification of five major cytokines in cattle, sheep and goats. *BMC Vet. Res.* **2015**, *11*, 65. [CrossRef]
27. Jelaska, A.; Strehlow, D.; Korn, J.H. Fibroblast heterogeneity in physiological conditions and fibrotic disease. *Springer Semin. Immunopathol.* **2000**, *21*, 385–395. [CrossRef]
28. Jiang, D.; Guo, R.; Machens, H.G.; Rinkevich, Y. Diversity of fibroblasts and their roles in wound healing. *Cold Spring Harb. Perspect. Biol.* **2022**, *15*, a041222. [CrossRef]
29. Coelho, L.L.; Pereira, I.R.; Pereira, M.C.; Mesquita, L.; Lannes-Vieira, J.; Adesse, D.; Garzoni, L.R. *Trypanosoma cruzi* activates mouse cardiac fibroblasts in vitro leading to fibroblast-myofibroblast transition and increase in expression of extracellular matrix proteins. *Parasit. Vectors* **2018**, *11*, 72. [CrossRef] [PubMed]
30. Sousa, A.M.; Liu, T.; Guevara, O.; Stevens, J.; Fanburg, B.L.; Gaestel, M.; Toksoz, D.; Kayyali, U.S. Smooth muscle α-actin expression and myofibroblast differentiation by tgfβ are dependent upon mk2. *J. Cell Biochem.* **2006**, *100*, 1581–1592. [CrossRef] [PubMed]
31. Osherov, N.; Ben-Ami, R. Modulation of host angiogenesis as a microbial survival strategy and therapeutic target. *PLoS Pathog.* **2016**, *12*, e100547. [CrossRef]
32. Mammari, N.; Halabi, M.A.; Yaacoub, S.; Chlala, H.; Dardé, M.L.; Courtioux, B. *Toxoplasma gondii* modulates the host cell responses: An overview of apoptosis pathways. *Biomed. Res. Int.* **2019**, *2019*, 1–10. [CrossRef] [PubMed]
33. Liu, Y.; Shepherd, E.G.; Nelin, L.D. MAPK phosphatases—Regulating the immune response. *Nat. Rev. Immunol.* **2007**, *7*, 202–212. [CrossRef] [PubMed]
34. Murtha, L.A.; Schuliga, M.J.; Mabotuwana, N.S.; Hardy, S.A.; Waters, D.W.; Burgess, J.K.; Knight, D.A.; Boyle, A.J. The processes and mechanisms of cardiac and pulmonary fibrosis. *Front. Physiol.* **2017**, *8*, 777. [CrossRef] [PubMed]
35. Kany, S.; Vollrath, J.T.; Relja, B. Cytokines in inflammatory disease. *Int. J. Mol. Sci.* **2019**, *20*, 6008. [CrossRef]
36. Corica, D.; Aversa, T.; Ruggeri, R.M.; Cristani, M.; Alibrandi, A.; Pepe, G.; De Luca, F.; Wasniewska, M. Could age/rage-related oxidative homeostasis dysregulation enhance susceptibility to pathogenesis of cardio-metabolic complications in childhood obesity? *Front. Endocrinol.* **2019**, *10*, 426. [CrossRef] [PubMed]
37. Zhang, X.L.; Xing, R.G.; Chen, L.; Liu, C.R.; Miao, Z.G. PI3K/Akt signaling is involved in the pathogenesis of bleomycin-induced pulmonary fibrosis via regulation of epithelial-mesenchymal transition. *Mol. Med. Rep.* **2000**, *14*, 5699–5706. [CrossRef] [PubMed]
38. Wang, J.; Hu, K.; Cai, X.; Yang, B.; He, Q.; Wang, J.; Weng, Q. Targeting PI3K/akt signaling for treatment of idiopathic pulmonary fibrosis. *Acta Pharm. Sin. B* **2022**, *12*, 18–32. [CrossRef]
39. Kennedy, L.; Shiwen, X.; Carter, D.; Abraham, D.; Leask, A. Fibroblast adhesion results in the induction of a matrix remodeling gene expression program. *Matrix Biol.* **2008**, *27*, 274–281. [CrossRef]
40. Wight, T.N.; Potter-Perigo, S. The extracellular matrix: An active or passive player in fibrosis? *Am. J. Physiol. Gastrointest. Liver Physiol.* **2011**, *301*, G950–G955. [CrossRef]

41. Zhao, X.; Chen, J.; Sun, H.; Zhang, Y.; Zou, D. New insights into fibrosis from the ECM degradation perspective: The macrophage-MMP-ECM interaction. *Cell Biosci.* **2022**, *12*, 117. [CrossRef]
42. Leirião, P.; Albuquerque, S.S.; Corso, S.; Van Gemert, G.J.; Sauerwein, R.W.; Rodriguez, A.; Giordano, S.; Mota, M.M. HGF/Met signalling protects plasmodium-infected host cells from apoptosis. *Cell Microbiol.* **2005**, *7*, 603–609. [CrossRef]
43. Ólafsson, E.B.; Barragan, A. The unicellular eukaryotic parasite *toxoplasma gondii* hijacks the migration machinery of mononuclear phagocytes to promote its dissemination. *Biol. Cell* **2020**, *112*, 239–250. [CrossRef]
44. Piccinini, A.M.; Midwood, K.S. Illustrating the interplay between the extracellular matrix and microRNAs. *Int. J. Exp. Pathol.* **2014**, *95*, 158–180. [CrossRef]
45. Walton, K.L.; Johnson, K.E.; Harrison, C.A. Targeting TGF-β mediated SMAD signaling for the prevention of fibrosis. *Front. Pharmacol.* **2017**, *8*, 461. [CrossRef]
46. Biernacka, A.; Dobaczewski, M.; Frangogiannis, N.G. TGF-β signaling in fibrosis. *Growth Factors* **2011**, *29*, 196–202. [CrossRef] [PubMed]
47. Zheng, K.X.; Yuan, S.L.; Dong, M.; Zhang, H.L.; Jiang, X.X.; Yan, C.L.; Ye, R.C.; Zhou, H.Q.; Chen, L.; Jiang, R.; et al. Dihydroergotamine ameliorates liver fibrosis by targeting transforming growth factor β type II receptor. *World J. Gastroenterol.* **2023**, *29*, 3103–3118. [CrossRef] [PubMed]
48. Shmakova, A.A.; Popov, V.S.; Romanov, I.P.; Khabibullin, N.R.; Sabitova, N.R.; Karpukhina, A.A.; Kozhevnikova, Y.A.; Kurilina, E.V.; Tsokolaeva, Z.I.; Klimovich, P.S.; et al. Urokinase system in pathogenesis of pulmonary fibrosis: A hidden threat of COVID-19. *Int. J. Mol. Sci.* **2023**, *24*, 1382. [CrossRef] [PubMed]
49. Kim, K.K.; Sheppard, D.; Chapman, H.A. TGF-β1 Signaling and Tissue Fibrosis. *Cold Spring Harb. Perspect. Biol.* **2018**, *10*, a022293. [CrossRef] [PubMed]
50. Guo, J.; Liu, W.; Zeng, Z.; Lin, J.; Zhang, X.; Chen, L. TGFB3 and MMP13 regulated the initiation of liver fibrosis progression as dynamic network biomarkers. *J. Cell Mol. Med.* **2020**, *25*, 867–879. [CrossRef]
51. Bernstein, A.M.; Twining, S.S.; Warejcka, D.J.; Tall, E.; Masur, S.K. Urokinase receptor cleavage: A crucial step in fibroblast-to-myofibroblast differentiation. *Mol. Biol. Cell* **2007**, *18*, 2716–2727. [CrossRef]
52. Schuliga, M.; Jaffar, J.; Harris, T.; Knight, D.A.; Westall, G.; Stewart, A.G. The fibrogenic actions of lung fibroblast-derived urokinase: A potential drug target in IPF. *Sci. Rep.* **2017**, *7*, 41770. [CrossRef]
53. Maroni, D.; Davis, J.S. Transforming growth factor beta 1 stimulates profibrotic activities of luteal fibroblasts in cows. *Biol. Reprod.* **2012**, *87*, 1–11. [CrossRef]
54. McKenzie, B.; Korfei, M.; Henneke, I.; Sibinska, Z.; Tian, X.; Hezel, S.; Dilai, S.; Wasnick, R.; Schneider, B.; Wilhelm, J.; et al. Increased FGF1-FGFRC expression in idiopathic pulmonary fibrosis. *Resp. Res.* **2015**, *16*, 83. [CrossRef]
55. Tan, C.; Jiang, Y.; Shao, W.; Shi, W.; Gao, X.; Qin, W.; Jiang, T.; Wang, F.; Feng, S. Abnormal expression of FOSB correlates with tumor progression and poor survival in patients with Gastric Cancer. *Int. J. Oncol.* **2016**, *49*, 1489–1496. [CrossRef]
56. Piersma, B.; Hayward, M.; Weaver, V.M. Fibrosis and cancer: A strained relationship. *Biochim. Biophys. Acta Rev. Cancer* **2020**, *1873*, 188356. [CrossRef] [PubMed]
57. Bellou, S.; Hink, M.A.; Bagli, E.; Panopoulou, E.; Bastiaens, P.I.H.; Murphy, C.; Fotsis, T. VEGF autoregulates its proliferative and migratory ERK1/2 and p38 cascades by enhancing the expression of DUSP1 and DUSP5 phosphatases in endothelial cells. *Am. J. Physiol. Cell Physiol.* **2009**, *297*, C1477–C1489. [CrossRef] [PubMed]
58. Pasieka, T.J.; Baas, T.; Carter, V.S.; Proll, S.C.; Katze, M.G.; Leib, D.A. Functional genomic analysis of Herpes Simplex Virus Type 1 counteraction of the host innate response. *J. Virol.* **2006**, *80*, 7600–7612. [CrossRef] [PubMed]
59. Sánchez, R.; Mohr, I. Inhibition of cellular 2′-5′ oligoadenylate synthetase by the Herpes Simplex Virus Type 1 US11 protein. *J. Virol.* **2007**, *81*, 3455–3464. [CrossRef] [PubMed]
60. Carneiro, M.W.; Fukutani, K.F.; Andrade, B.B.; Curvelo, R.P.; Cristal, J.R.; Carvalho, A.M.; Barral, A.; Van Weyenbergh, J.; Barral-Netto, M.; de Oliveira, C.I. Gene expression profile of high IFN-γ producers stimulated with *Leishmania braziliensis* identifies genes associated with cutaneous leishmaniasis. *PLoS Negl. Trop. Dis.* **2016**, *10*, e0005116. [CrossRef]
61. Pierog, P.L.; Zhao, Y.; Singh, S.; Dai, J.; Yap, G.S.; Fitzgerald-Bocarsly, P. *Toxoplasma gondii* inactivates human plasmacytoid dendritic cells by functional mimicry of IL-10. *J. Immunol.* **2018**, *200*, 186–195. [CrossRef] [PubMed]
62. Menard, K.L.; Bu, L.; Denkers, E.Y. Transcriptomics analysis of *Toxoplasma gondii*-infected mouse macrophages reveals coding and noncoding signatures in the presence and absence of MyD88. *BMC Genom.* **2021**, *22*, 130. [CrossRef]
63. Schneider, A.G.; Abi Abdallah, D.S.; Butcher, B.A.; Denkers, E.Y. *Toxoplasma gondii* triggers phosphorylation and nuclear translocation of dendritic cell STAT1 while simultaneously blocking IFNΓ-induced STAT1 transcriptional activity. *PLoS ONE* **2013**, *8*, e60215. [CrossRef] [PubMed]
64. Fereig, R.M.; Nishikawa, Y. From signaling pathways to distinct immune responses: Key factors for establishing or combating *Neospora caninum* infection in different susceptible hosts. *Pathogens* **2020**, *9*, 384. [CrossRef] [PubMed]
65. Besteiro, S. *Toxoplasma* control of host apoptosis: The art of not biting too hard the hands that feeds you. *Microb. Cell* **2015**, *2*, 178–181. [CrossRef] [PubMed]
66. Harjunpää, H.; Llort Asens, M.; Guenther, C.; Fagerholm, S.C. Cell adhesion molecules and their roles and regulation in the immune and tumor microenvironment. *Front. Immunol.* **2019**, *10*, 1078. [CrossRef]
67. Hauck, C.R.; Agerer, F.; Muenzner, P.; Schmitter, T. Cellular adhesion molecules as targets for bacterial infection. *Eur. J. Cell Biol.* **2006**, *85*, 235–242. [CrossRef]

68. Chen, D. Dually efficacious medicine against fibrosis and cancer. *Med. Sci.* **2019**, *7*, 41. [CrossRef]
69. Elpek, G.Ö. Angiogenesis and liver fibrosis. *World J. Hepatol.* **2015**, *7*, 377. [CrossRef]
70. Lopes-Coelho, F.; Martins, F.; Pereira, S.A.; Serpa, J. Anti-angiogenic therapy: Current challenges and future perspectives. *Int. J. Mol. Sci.* **2021**, *22*, 3765. [CrossRef]
71. Kizaki, K.; Ushizawa, K.; Takahashi, T.; Yamada, O.; Todoroki, J.; Sato, T.; Ito, A.; Hashizume, K. Gelatinase (MMP-2 and -9) expression profiles during gestation in the bovine endometrium. *Reprod. Biol. Endocrinol.* **2008**, *6*, 66. [CrossRef]
72. Milner, J.M.; Rowan, A.D.; Cawston, T.E.; Young, D.A. Metalloproteinase and inhibitor expression profiling of resorbing cartilage reveals pro-collagenase activation as a critical step for collagenolysis. *Arthritis Res. Ther.* **2006**, *8*, R142. [CrossRef]
73. García, D.C.; Miceli, D.C.; Valdecantos, P.A.; García, E.V.; Roldán-Olarte, M. Expression of urokinase type plasminogen activator receptor (uPAR) in the bovine oviduct: Relationship with uPA effect on oviductal epithelial cells. *Res. Vet. Sci.* **2014**, *97*, 118–123. [CrossRef]
74. Berisha, B.; Welter, H.; Shimizu, T.; Miyamoto, A.; Meyer, H.H.; Schams, D. Expression of fibroblast growth factor 1 (FGF1) and FGF7 in mature follicles during the periovulatory period after GnRH in the cow. *J. Reprod. Dev.* **2006**, *52*, 307–313. [CrossRef]
75. Sugawara, K.; Kizaki, K.; Herath, C.B.; Hasegawa, Y.; Hashizume, K. Transforming growth factor beta family expression at the bovine feto-maternal interface. *Reprod. Biol. Endocrinol.* **2010**, *8*, 120. [CrossRef] [PubMed]
76. Shrestha, K.; Lukasik, K.; Baufeld, A.; Vanselow, J.; Moallem, U.; Meidan, R. Regulation of ovulatory genes in bovine granulosa cells: Lessons from siRNA silencing of PTGS2. *Reproduction* **2015**, *149*, 21–29. [CrossRef] [PubMed]
77. Lagrée, A.; Fasani, F.; Rouxel, C.; Pivet, M.; Pourcelot, M.; Fablet, A.; Romey, A.; Caignard, G.; Vitour, D.; Blaise-Boisseau, S.; et al. Bovine organospecific microvascular endothelial cell lines as new and relevant in vitro models to study viral infections. *Int. J. Mol. Sci.* **2020**, *21*, 5249. [CrossRef] [PubMed]